A Parallel Plate Model of Fractured Permeable Media

By

David Tunison Snow

A.B. (Harvard University) 1951
M.A. (University of California) 1957

DISSERTATION

Submitted in partial satisfaction of the requirements for the degree of

DOCTOR OF PHILOSOPHY

in

Engineering Science

in the

GRADUATE DIVISION

of the

UNIVERSITY OF CALIFORNIA, BERKELEY

Approved:

Irving Fatt ....

Paul A. Witherspoon ....

John Verhoogen ....

Committee in Charge

102.8

Degree conferred..
Date

TABLE OF CONTENTS

LIST OF FIGURES

LIST OF PLATES

LIST OF TABLES

ABSTRACT

In current practice the permeability of fractured media can be modelled adequately for two extreme cases seldom realized in nature: one, 1) when individual planar conductors, such as joints in rock, are so independent and infrequent that each may be analyzed asaseparate channel, or, 2) when aggregates of fractures, as in fault breccia, so resemble sedimentary pores that the medium is assumed to be a continuum. The object of this study is to model a wide variety of fractured media, especially jointed rock, whose geometry is between the above extremes. These media have planar conductors varying in frequency, dispersed in orientation, and distributed in aperture. Parallel-plate openings are used to simulate real fractures. With this idealization, if there is flow along intersecting conductors, the discharge of each is proportional to the cube of its aperture and to the projection of a field gradient generally parallel to no conductor. For a given gradient, one may add discharge components of intersecting plane conductors or intergranular conductive bodies between them. The discharge of one planar conductor or any set can be represented by a second-rank tensor. A tensor therefore describes the permeability of a continuous medium giving the same discharge as fractured medium under the same hydraulic gradients in laminar, incompressible flow situations.

Special cases of one, two, and three joint sets are modelled by applying Monte Carlo sampling methods that pair Fisher distributions of orientations and skewed distributions of apertures. New statistics of the orientation of principal axes and of principal permeabilities are developed. The model shows the causes of anisotropy and its variations.

A field method for measuring anisotropic permeability is

proposed. It is derived from a general solution to the discharge from cylindrical cavities arbitrarily oriented in saturated, infinite anisotropic media, utilizing pressure-discharge measurements in drill holes coinciding with principal axes predetermined by analysis of joint orientation data.

The statistics of pressure-test data from seven damsites on crystalline rock indicate that the number of effective conductors intercepted at depth by a drill-hole is distributed as a Poisson variate, much smaller than the number that would be expected from surface exposures of joints. The mean and variance of the number of conductors crossing a given length of drill hole can be estimated from the frequency of zero discharges encountered. The computer model successfully duplicates the shape of field discharge frequency curves once the sample-size is made to vary as a Poisson. Aperture distributions cannot be determined from permeability data but evidence suggests log normal or exponential distributions to be most likely.

In spite of indeterminate apertures, fracture porosity can be determined from anisotropic permeability within a range of about 10 percent of the true value, once the mean frequency of conductors of each joint set has been determined.

Many flow and potential distributions in civil and petroleum engineering or groundwater hydrology can be solved ultimately if fractured rock is evaluated as an anisotropic permeable medium with heterogeneities reflected in statistically-distributed measures.

SCOPE, OBJECTIVES AND METHODS OF STUDY

This investigation of basic aspects of fluid flow in fractured media was prompted by the writer's inability to comprehend how geological structures influence seepage and uplift of dams on rock, or drainage to tunnels. In each case, the lack of quantitative tools to assess the influence of joint orientations, apertures, and spacings led to the conclusion that conventional ground water hydrology could not advance our knowledge of the permeability of fractured media until a model was devised to combine statistically, the independent variables governing directional permeability.

The salient precursors to this work were papers by Versluys (1915) and Childs (1957). Versluys proved that any number of capillary tubes of arbitrary orientation can be replaced by three mutually orthogonal tubes giving the same vectorial discharge. In this thesis, the writer has replaced the tubes with parallel plates and streamlined the mathematics with tensorial notation. Childs investigated the directional permeability of uniform, parallel sets of fissures in soil. The present model fulfills the need for orientational generality, and provides flexibility to include other parameters.

Many unsolved aspects of this broad, almost untouched subject of fractured media have been treated here only heuristically, in the hope of stimulating studies sequel to this thesis.

The object of this study is to develop an understanding of the role of some of the geometrical variables controlling fluid flow in fractured media. The variables include dispersion of conduit orientations and apertures, the spacing of aggregates of conduits, and sample size. Since directional permeability is an attribute of fractured media, the theory of flow in anisotropic continua is reviewed. When there is established a basis for determining the properties of a continuum having statistical equivalence to a fractured discontinuum, then established methods of solving boundary problems can be applied to jointed rock, and the errors evaluated.

A method of measuring anisotropism is required before boundary problems can be solved. The problem of steady discharge from an arbitrarily-oriented cylindrical cavity in an infinite, anisotropic saturated medium is solved, and applied to pressure-testing of jointed rock to determine the three principal permeabilities.

The reason that anisotropy exists in fractured media and an approach to its prediction are investigated with a mathematical model, evaluated by computer programs. The model describes directional permeability as a second-rank tensor, or by its equivalent principal axes and permeabilities. Individual conductors are like the openings between smooth parallel plates, uniformly separated throughout their infinite extent, but oriented in arbitrary sets dispersed at random about mean directions. Apertures are distributed according to various density functions. A parameter to describe spacing or fracture density is devised. Since water flow problems are the main interest, incompressible Poiseuille flow is assumed. Some aspects of random inhomogeneity are considered, but not the effects of systematic inhomogeneity. Some variables not studied include those of anisotropy or discontinuity of individual conductors, compressibility, non-linear friction, or multi-phase flow.

Ground-water, engineering, and mining literature is reviewed for pertinent information describing the occurence of water in joints, faults, cleavage and schistosity, and to describe their geometry.

Permeability distributions in real jointed rock media are investigated by re-analysis of pressure-test data obtained largely by others in exploratory drill-holes at seven damsites on crystalline rocks of California. The results indicated need for an additional variable in the model; namely, a distribution of joint densities, and showed the dominating effect of small numbers of conductors.

On the basis of known average joint densities and known geometry, acceptable approximations to secondary porosity may be computed from measured principal permeabilities. It is shown to be impossible to establish from permeability data the distribution of apertures or a precise measure of porosity.

Applicability of theoretical and model study results to several practical problems in engineering is discussed.

ACKNOWLEDGMENTS

The late Dr. Parker D. Trask encouraged this undertaking. The writer is grateful for the supervision and counsel of Dr. Irving Fatt. Dr. Elizabeth Scott advised the writer on statistical methods. The advice and assistance of many faculty members and colleagues at the University of California, especially Dr. Richard E. Goodman and Mr. Wilson Blake, is acknowledged with appreciation.

Drs. John A. Verhoogen and Paul A. Witherspoon provided consultation and critical review of the manuscript. Mrs. Gloria Pelatowski drafted all figures except those produced by the Cal-Comp, computer-driven plotter. The University of California furnished office and laboratory space, equipment, machine shop facilities and 20 hours of IBM 7090 computer time. Financial support for this work, spanning full- and part-time periods between 1961 and the present, is largely due to my wife, Nancy, whose devoted encouragement and patience made the work possible. During 1961-62, the writer was supported by the Ford Foundation through the Special Pre-Doctoral Engineering Fellowship program, and during the Fall, 1964, through their loan program. The American Cyanamid Company is to be thanked for a generous grant in support of this work during 1964.

Chapter 1
GENERAL DISCUSSION OF ANISOTROPIC PERMEABLE MEDIA

Since this investigation of seepage through fractured media will lead ultimately to means of solving practical boundary problems, a survey of pertinent literature on anisotropic continua will provide perspective to the succeeding chapters.

Force-Flow Relationships

In the following treatment, potential is defined as the work done on a unit mass of fluid in moving it to its position and pressure from some reference condition. Childs (1957, pp. 39-44) discusses definitions. Darcy's law defines for isotropic media the proportionality between a discharge vector and a parallel potential gradient vector,

$$q_i = \frac{-k}{\mu} \frac{\partial \phi}{\partial x_i} . \qquad (1\text{-}1)$$

The vectors represented in equation (1-1) are directional quantities having no directional distribution. As first order tensors, such vectors are invarient to rotation in the medium. In other words, when there exists the condition known as isotropy, the proportionality coefficient, k, is a scalar, having the same value for all directions.

More general equations have been derived for anisotropic media, wherein the velocity and gradient vectors are non-parallel. If a medium has directional properties, the coefficient relating discharge to gradient varies with orientation. A vector operator defining such directional properties for all orientations of a medium is a second rank tensor. Examples of some properties that may be anisotropic are: thermal, electrical or fluid conductivity, dielectric constants, elastic or thermal-expansion coefficients.

The general form of Darcy's law for fluid permeability

$$v_i = K_{ij} \frac{\partial \phi}{\partial x_j} \qquad \text{(Ferrandon, 1948, p. 24)} \qquad (1\text{-}2)$$

degenerates to the familiar isotropic form when

$$K_{ij} = \frac{k}{\mu} \delta_{ij}$$

where δ_{ij} is the identity, unit, or isotropic tensor.

Historical Development

The notion of anistropy is old. Duhammel (1832) studied anisotropic thermal conductivity by measuring the elliptic shape of the melting front around a small heat source imbedded in crystals coated with paraffin. Munjal (1964) has recently applied the method to rocks.

Versluys (1915) was first to explain anisotropic permeability by modelling the conductors as arbitrarily-oriented bundles of tubes. He proved that any four arbitrary sets may be replaced by three mutually orthogonal sets of conductivity K_x, K_y, K_z, such that the continuity equation leads to the generalization :

$$K_x \frac{\partial^2 \phi}{\partial x^2} + K_y \frac{\partial^2 \phi}{\partial y^2} + K_z \frac{\partial^2 \phi}{\partial z^2} = 0 \qquad (1\text{-}3)$$

Versluys showed that four sets may be reduced to three (by solving 6 simultaneous equations) so any number, taken four at a time, may be reduced to three. The coefficients, K_s are the principal permeabilities of the system, associated with the three mutually orthogonal principal axes.

Ferrandon (1948) derived the tensor form (Equation 1-2) from the bundle of tubes model. The following treatment differs little from Ferrandon's and the summaries given by Scheidegger (1954) and Childs (1957).

The contribution to the flow q_n, through a unit area normal to n_i, due to tubes oriented along m_i, is proportional to the potential gradient along the tubes (Figure 1-1).

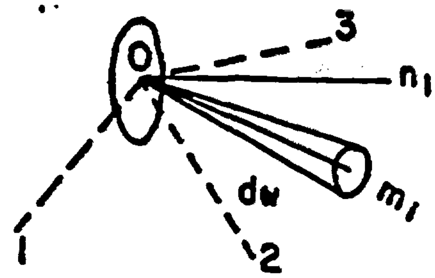

Figure 1-1. Definitions for Ferrandon's bundles - of tubes model of anisotropic media.

The cross-sectional area of tubes per unit area cutting across solid and fluid phases of a porous medium is equal to the solid angle $d\omega$ at unit distance from some arbitrary point times a proportionality coefficient, γ pertaining to that set of tubes. In the following discussion, subscripts $_i$ and $_j$ indicate 3 vector components, subscripts $_n$ and $_m$ signify designated scalars. Repeated indexes signify summation.

When the gradient is arbitrary, the component along the tubes is

$$\frac{\partial\phi}{\partial m} = \frac{\partial\phi}{\partial x_j} m_j .$$

The m-direction discharge of one bundle of tubes is

$$dq_m = \frac{k}{\mu} \frac{\partial\phi}{\partial x_j} m_j \gamma \, d\omega ,$$

where k is a conductivity coefficient and μ is the viscosity of the fluid. The component of this flow in the n_i-direction is proportional to the cosine of the angle $n_i m_i$, thus

$$dq_n = \frac{k}{\mu} n_i m_i \frac{\partial\phi}{\partial x_j} m_j \gamma \, d\omega .$$

The discharge of an aggregate of dispersed tubes is obtained by summation, each tube with its peculiar direction cosines m_i, and coefficients k and γ depending on the tube diameters and frequency. We may define a new coefficient,

$$k_{ij} = (k\gamma) m_i m_j \, d\omega ,$$

a second order symmetric tensor that operates on the gradient vector to give the discharge per unit of area normal to the velocity.

$$q_i = \frac{k_{ij}}{\mu} \frac{\partial p}{\partial x_j} \quad , \qquad (1\text{-}2)$$

or the discharge through an area normal to n_i,

$$q_n = n_i \frac{k_{ij}}{\mu} \frac{\partial p}{\partial x_j} \quad . \qquad (1\text{-}4)$$

The discharge coefficient of each tube or tube-set is a symmetric tensor in an arbitrary coordinate system, and if all coefficients are referred to the same system, the sum of symmetric tensors is another symmetric tensor.

Directional Permeability

An immediate consequence of the finding that permeability is a second rank tensor is that velocity is parallel to the gradient only along three mutually orthogonal axes, the principal axes or eigenvectors of the tensor, while elsewhere, velocity is nonparallel to the gradient. The eigenvalues of the tensor are the principal permeabilities, k_{11}, k_{22}, k_{33}.

Two alternative definitions of directional permeability have been offered by Scheidegger (1954). In one case, seepage is confined to a direction n, by cutting from the medium a thin, pencil-shaped, encased specimen, much more elongate than the drill-cores employed by Johnson and Hughes (1948) and Johnson and Breston (1951) to establish anisotropy of sandstones. With such boundaries, the gradient is unknown, for equipotentials are generally oblique to the core axis and to the principal planes of permeability.

The gradient along the axis is

$$\frac{\partial p}{\partial n} = n_i \frac{\partial p}{\partial x_i} ,$$

but in this case it is the gradient that is dependent upon the velocity.

$$\frac{\partial p}{\partial x_j} = \mu k_{ij}^{-1} q_i$$

$$\frac{\partial p}{\partial n} = \mu n_j k_{ij}^{-1} n_i q_n ,$$

where k_{ij}^{-1} is the inverse tensot $(k_{ij} k_{jk}^{-1} = \delta_{ik})$.

The proportionality constant between the discharge and the gradient in the flow direction is Scheidegger's first definition of directional permeability:

$$k_n = \mu q_n / \frac{\partial p}{\partial n} = 1/n_j k_{ij}^{-1} n_i . \qquad (1-5)$$

A second definition of directional permeability is derived for the flow through a specimen that is very wide compared to its thickness, like a pancake, with constant potentials at the broad surfaces. The gradient is fixed, while the velocity is generally oblique to the equipotentials and inclined to the principal axes of permeability.

Designating n_i the direction normal to the equipotential surfaces, and q_n the discharge (per unit area) through it, it is clear that the scalar discharge is

$$q_n = n_i q_i$$

where q_i is the vector discharge (per unit area) through the interior of the specimen. Scheidegger (p. 77) applies equation (1-2) for q, which gives

$$k_n = \mu n_i q_i \Big/ \frac{\partial p}{\partial x_n}$$

$$= \mu n_i \frac{k_{ij}}{\mu} \frac{\partial p}{\partial x_j} \Big/ \frac{\partial p}{\partial x_n} \qquad (1\text{-}6)$$

$$= n_i k_{ij} n_j \, .$$

Scheidogger concluded that the two definitions, 5) and 6) are identical, because

$$n_i k_{ij} n_j n_i k_{ij}^{-1} n_j = n_i k_{ij} k_{ij}^{-1} n_j = n_i \delta_{ij} n_j = 1 \, ,$$

so

$$n_i k_{ij} n_j = 1 / n_i k_{ij}^{-1} n_j$$

implying that the extra path length across the flat specimen is compensated by decreased resistance.

Marcus and Evanson (1961, 1962) investigated the two-dimensional aspects of anisotropy, concluding that the two definitions of Scheidegger lead to different values of directional permeability.

When the direction of flow is known (at an angle δ), the directional permeability at a general angle ϕ is

$$K_\phi = \frac{\cos\delta \cos\phi + \sin\delta \sin\phi}{\dfrac{\cos\delta \cos\phi}{K_x} + \dfrac{\sin\delta \sin\phi}{K_y}} \qquad (1\text{-}7)$$

where the angles are defined by figure [redacted] 1-2.

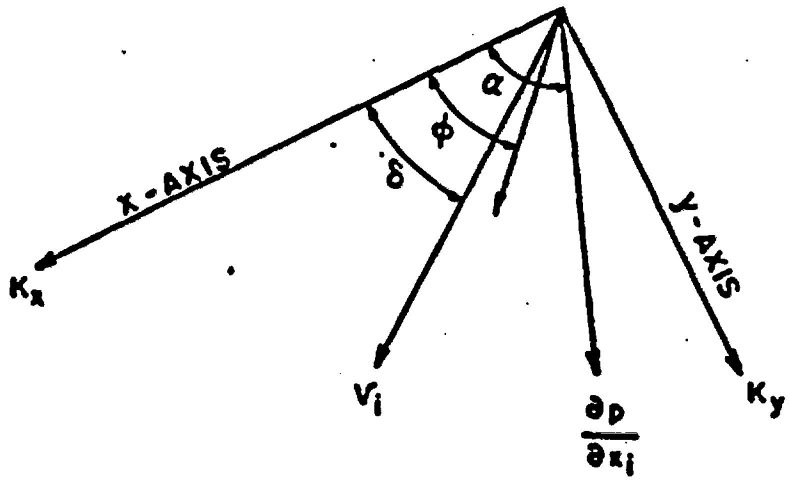

Figure δ-2. General flow conditions in anisotropic porous media (after Marcus and Evanson, 1961)

When $\phi = \delta$, directional permeability K_δ is measured in the flow direction, as in the case of Scheidegger's pencil-shaped boundaries. The equation

$$\frac{1}{K_\delta} = \frac{\cos^2\delta}{K_x} + \frac{\sin^2\delta}{K_y} \quad , \qquad (1\text{-}8)$$

is a centered ellipse with radius $\sqrt{K_\delta}$, and semi-axes $\sqrt{K_x}$ and $\sqrt{K_y}$.

When the direction of the gradient is known (at an angle α from the x-axis), the directional permeability at a general angle ϕ is

$$K_\phi = \frac{K_x \cos\alpha \cos\phi + K_y \sin\alpha \sin\phi}{\cos\alpha \cos\phi + \sin\alpha \sin\phi} \quad . \qquad (1\text{-}9)$$

When $\phi = \alpha$, directional permeability K_α is measured in the direction of the gradient, as with Scheidegger's pancake boundaries,

$$K_\alpha = K_x \cos^2\alpha + K_y \sin^2\alpha \quad , \qquad (1\text{-}10)$$

the equation of a centered ellipse with the radius $1/\sqrt{K_\alpha}$, and semi-axes $1/\sqrt{K_x}$ and $1/\sqrt{K_y}$.

Marcus and Evanson show that $K_\alpha \geq K_f$. For the same gradient along the axis of test specimens, there will be a greater discharge per unit area with the pancake boundaries than with the pencil-shaped boundaries. Flow takes the path of least resistance in the former case, some other in the latter. The difference between directional permeabilities defined by the flow and gradient directions exceeds 10 percent if $K_y / K_x < 0.5$, and if the flow or gradient is inclined greater than 15 degrees from a principal axis. Errors increase towards infinity for greater anisotropy.

Measurement errors were reported for various angles and anisotropies studied by electrical resistivity models having boundaries of various width-to-length ratios intermediate between the extremes posed by Scheidegger. Such studies are appropriate because conventional permeability tests are performed on nearly equant samples. Flow within the sample interior is non-parallel to the boundaries. It was concluded that the measurements of Johnson, et. al. (1948, 1951) were correct for the wrong reason: boundary conditions were ignored, but since the greatest anisotropy was $K_y/K_x = 0.75$, the errors were negligible.

Marcus and Evanson's two-dimensional expressions, and Scheidegger's tensor expressions should be consistant, since the two-dimensional equations correspond to flow along the principal plane z = a constant. A published explanation of the discrepancy has not been found, nor is the reason readily apparent. The problem is most pertinent to analysis of laboratory test data, as influenced by rectangular sample boundaries. Resolution of the inconsistancy will not be pursued further here because for field problems, directional permeability may be considered synonymous with anisotropic permeability. Where the phrase is used in this text, it implies only that there exist in the medium three principal permeabilities corresponding to three orthogonal principal axes.

Potential and Stream Functions

All problems of slow, steady, incompressible fluid flow in previous media depend on the applicability of the Laplace equation

$$\frac{\partial^2 \phi}{\partial x^2} + \frac{\partial^2 \phi}{\partial y^2} = 0 \qquad (1\text{-}11)$$

where hydraulic potential

$$\phi = (k'/g/\mu)(P/\rho g + z) = kh \qquad (1\text{-}12)$$

k' is the absolute permeability of the medium, as used by Muskat (1937),

μ is the viscosity of water,

ρ is its density,

g is the acceleration of gravity, and

p is the pressure at a point at

z elevation, all in consistent units.

k and h are lumped variables defined by the bracketed coefficients. Solutions to the differential equation (1-11) form an orthogonal network of curves

ϕ = a constant, with lines ψ = a constant that are solutions to

$$\frac{\partial^2 \psi}{\partial x \partial y} + \frac{\partial^2 \psi}{\partial y \partial x} = 0 \qquad (1\text{-}13)$$

Stream potential ψ is related to ϕ by the Cauchy-Rieman equations:

$$\frac{\partial \phi}{\partial x} = \frac{\partial \psi}{\partial y} \quad \text{and} \quad \frac{\partial \phi}{\partial y} = -\frac{\partial \psi}{\partial x} .$$

The two types of potentials were devised to express for every position (x, y) the proportion ϕ of hydraulic potential lost in flowing to that point as well as the proportion of the flux ψ lying to one side of the stream line passing through that point. The four variables are combined in the complex plane $(z = x + iy)$, $(\omega = \phi + i\psi)$. The two orthogonal families of lines constitute a flow net, a tool of great utility for visualizing and measuring the distribution and gradients of hydraulic potential, the quantities and directions of flow. Methods are available for obtaining flow nets by analytical means (Muscat, 1937; Collins, 1961; Long, 1961), by graphical techniques (Richardson, 1910; Forsheimer, 1930; Samsioe, 1931; Dachler, 1936; Casagrande, 1937; Twelker, 1958), by analogue studies (Lee, 1948; Hanson, 1952; Opsal, 1955; Todd, 1954, 1959) and by relaxation (Chien, 1952; Warren, Dougherty and Price, 1960; Dusinberre, 1961; Schenck, 1963), to mention a few.

Computations of discharge depend on the validity of Darcy's law to establish the proportionality with the gradients obtained by solving the Laplace equation. Darcy's law is applicable to water flow in most soils, but also mass air flow at low gradients (Muscat, 1937, p. 128, Carman, 1956). The simplest use of a flow net is to get total discharge.

$$Q = k\,\Delta\phi\left(\frac{\text{number of flow channels}}{\text{number of equal potential drops}}\right)$$

where k is hydraulic conductivity, (LT^{-1}), and

$\Delta\phi$ is the total head drop (L) between boundaries and

Q is the volume per unit slice width per unit time $(L^3L^{-1}T^{-1})$.

For anisotropic media, the Laplace equation must be rederived (Forsheimer, 1930, Maasland, 1957). Substituting

$$v_x = k_x \frac{\partial \phi}{\partial x}, \quad v_y = k_y \frac{\partial \phi}{\partial y} \text{ and } v_z = k_z \frac{\partial \phi}{\partial z}$$

into the continuity equation for steady flow

$$\frac{\partial v_x}{\partial x} + \frac{\partial v_y}{\partial y} + \frac{\partial v_z}{\partial z} = 0$$

gives

$$k_x \frac{\partial^2 \phi}{\partial x^2} + k_y \frac{\partial^2 \phi}{\partial y^2} + k_z \frac{\partial^2 \phi}{\partial z^2} = 0 . \qquad (1\text{-}3)$$

This reduces to the Laplace equation upon substitution of

$$x' = (k_0/k_x)^{1/2} x, \quad y' = (k_0/k_y)^{1/2} y, \quad z' = (k_0/k_z)^{1/2} z \qquad (1\text{-}14)$$

(k_o is an arbitrary constant), giving

$$\frac{\partial^2 \phi}{\partial x'^2} + \frac{\partial^2 \phi}{\partial y'^2} + \frac{\partial^2 \phi}{\partial z'^2} = 0 , \qquad (1\text{-}13)$$

the Laplace equation for isotropic flow in transformed anisotropic media. It is necessary only to transform the geometry of problem boundaries by applying equations (14), whereupon the new figure can be treated by any of the available isotropic methods. The coordinate expansions or contractions must be made along the principal axes. Upon completing the flow net solution, the net, as well as the boundaries, may be retransformed to the original system, thereby mapping the potentials throughout. In general, the lines are non-orthogonal solutions to (1-3).

The isotropic permeability used for computing discharge through transformed media is:

$$k = (k_x k_y k_z / k_0)^{1/2} .$$

This version is Maasland's (1957) modification of findings by Samsioe (1931); Vreedenburgh (1936); and Muscat (1937).

Application of the foregoing theory to fractured media was not the intention of the authors cited, with the exception of Childs (1957). If Darcy's-law coefficients may be found that give the same macroscopic discharges as do aggregates of fractures, then the numerous methods of problem-solving in common use for intergranular media may be applied also to fractured rock.

This thesis, therefore, attempts to determine how the geometrical parameters govern the orientation and magnitudes of principal permeabilities in fractured media. For a given field problem, principal axes may be estimated by the orientations of the planar conductors (Chapter 5), but the magnitude of principal permeabilities must be measured.

Chapter 2

STEADY FLOW FROM CYLINDRICAL CAVITIES IN SATURATED, INFINITE ANISOTROPIC MEDIA

Introduction

Development of a method of pressure-testing jointed rock to determine its anisotropic permeability is the object of this chapter. Continuum fluid mechanics are used here to establish properties of media that are distinctly discontinuous. Current practices of analyzing tests neglect anisotropy and heterogeneity. Solutions to boundary-value problems, to establish flow or pressure distribution in jointed rock, have thus far been attempted by methods designed for isotropic, intergranular, conducting media. Notable examples include Stuart's (1955) draw-down tests for predicting shaft drainage, Thayer's (1962) analysis of Oroville pump-test data and Yokota's (1963) study of potential in the Kurobe IV dam-site. No rational basis of justifying the assumed isotropy has been advanced, though close correspondence between measured and theoretical potential or discharge values is sometimes found.

More commonly we observe anomalous uplift pressures beneath masonry dams (Richardson's 1948 report, p. 16, on Hoover dam, for instance), wildly erratic pressure-test discharges (Lyon's 1962 report of Oroville tests), or sporadic tunnel infiltration (Wahlstrom and Hornback's 1962 report on the Harold D. Roberts tunnel, Colorado). These are expressions of the heterogeneity characteristic of jointed rock. As opposed to the systematic depth-varying inhomogeneity demonstrated by Turk (1963), and applied to water-well design by Davis and Turk (1964), heterogeneous permeability encountered in jointed rock is believed due to the process of sampling a few elements out of a large population having great dispersion of conductivity. It is better to attempt statistical interpretation of jointed-rock permeability values than it is to accept the pessimism of Terzaghi (1962), who said:

> "Water levels in observation wells located in jointed rock can vary over short distances by important amounts and the effect that filling the reservoir will have on the pore water pressures in the gouge seams cannot even be estimated in advance...the pattern of seepage is likely to be erratic...one cannot tell which ones (joints) are continuous over a large area."

Few field studies have demonstrated anisotropy for jointed rock, due to lack of methods to measure it. Interactions between wells indicated a preferred direction (in plan only) of permeability of the Spraberry oilfield (Elkins and Skov, 1960). Sweep efficiency has been proposed as a means of determining anisotropy (Landrum and Crawford, 1960). Contours on a piezometric surface for water conducted in fractures of the crystalline basement at the Nevada Test Site indicate high permeability in the direction of streamline convergence (Davis, 1963).

Improved resolution should prove anisotropy a general attribute of fractured rocks, by reason of the orientations of planar conductors. Diamond-drill explorations can be designed to facilitate measurement of principal permeabilities that can then be treated statistically to establish medians, means, and dispersions of the three heterogeneous measures. For these purposes, drill-holes should be oriented to nearly coincide with principal permeability axes, predetermined from study of joint orientations by methods given in Chapter 5.

To describe the orientation of three mutually orthogonal axes requires three independent parameters, and to describe the corresponding permeabilities, three additional. Since as many measures as unknowns are required for a unique solution, observable orientation data is relied upon for axial predictions, while three orthogonal drill-holes are employed to measure the principal permeabilities. Three orthogonal pressure-test holes can define the principal permeabilities because the discharge from each long cylindrical cavity depends largely upon the permeabilities in directions normal to the axis of the cavity, and but weakly upon the permeability parallel to the axis.

<u>Theoretical Development</u>

Theory developed by Maasland (1957, pp. 218-284) for piezometer tests in anisotropic soil is amplified and generalized here for arbitrary packer test-hole orientations in anisotropic media.

The three components of macroscopic velocity coinciding with the principal axes of an anisotropic medium may be expressed by Darcy's law:

$$v_i = -k_{ij} \frac{\partial \phi}{\partial x_j} ,$$

where the repeated index signifies summation and the k_{ij} are the terms of the hydraulic conductivity tensor, cm/sec.,

ϕ is the head, cm., and

x_i are the coordinates.

When substituted into the continuity equation, for steady state or uncomprehensible flow,

$$\frac{\partial v_i}{\partial x_i} = 0 ,$$

there results

$$k_{ii} \frac{\partial^2 \phi}{\partial x_i^2} = 0 .$$

Maasland introduces an arbitrary constant, k_o, into the equations transforming the original Cartesian coordinates to a system identified by primes:

$$x_i' = (k_o / k_{ii})^{1/2} x_i \quad \text{(after Samsioe, 1931).} \quad (2\text{-}1)$$

This substitution results in the Laplace equation,

$$\nabla^2 \phi = 0.$$

When boundary conditions are expanded or contracted by equations (2-1) then potential theory for isotropic media applies. The hydraulic conductivity of this equivalent but fictitious transformed medium,

$$k = (k_{11} k_{22} k_{33} / k_0)^{1/2} \qquad (2\text{-}2)$$

was derived by Vreedenburg (1936) and modified to the above form by Maasland. Kirkham (1945) gives a general equation for flow from cavities below the water table:

$$Q = k\,Sy \qquad (2\text{-}3)$$

where Q is the flow rate, say in gallons per day,

k is the hydraulic conductivity, feet per day,

y is the net hydraulic head, feet, and

S is a coefficient of length units dependent upon the geometry of the cavity, and the boundaries. Figure 2-1 (b) identifies the boundaries and variables.

Maasland gives derivations and electric analogue results leading to S-values for various shapes. Dachler (1936) called this coefficient the "Formfaktor"; Hvorslev (1951), the "shape factor"; and Zanger (1953) calls S/2 the "effective hemispherical radius". S is a constant for piezometers having unchanging boundaries, and a variable for auger-holes because the boundaries change with the water-level. In piezometer testing of agricultural soils, the hole is cased to a certain level, leaving open a cylindrical cavity of length w below. In rock pumping tests, water is conducted through drill rods to a section of hole isolated by packers. Thus, the customary use of S-factors derived for cased holes whose walls above and below the pumping cavity are streamlines (e.g., Thayer, 1962, p. 6) is at best an approximation of the actual conditions. The piezometer test could be more faithfully duplicated if, at least, tests were confined to the bottom of the hole, one packer only applied at various stages of completion of hole-drilling. Better still, the unneeded upper part of the hole might be grouted closed above a drillable obstructor. Heavy drilling mud might suffice to fill the hole above the cavity and around the drill rods.

No rigorous solution is known or expected for packer tests as they are currently practiced, because the hole above the cavity is either an equal-pressure surface if air-filled, equipotential if water-filled, or part one and part the other. Water levels within the hole are not customarily measured during tests. In Figure (2-1 (a), schematically illustrating these tests, potentials 1 and 3 differ from the cavity potential 2, according to the length and conductivity of fracture paths short-circuiting the packers through the rock. The performance of tests sometimes discloses leaking packers.

Figure 2-1 (b) portrays the assumed geometry that is used to analyze packer tests. It corresponds to piezometer tests described in the literature. The walls of the hole are no-flow boundaries except at the cavity. It is further assumed that the quantities of water injected are so small that the water-table remains unchanged.

The packer test currently gives empirical measures of discharge, believed useful as criteria for grouting needs and grout take estimation (Talobre, 1957, p. 153; Grant, 1964; de Mello, 1960, p. 703), but the test gives a low-confidence measure of

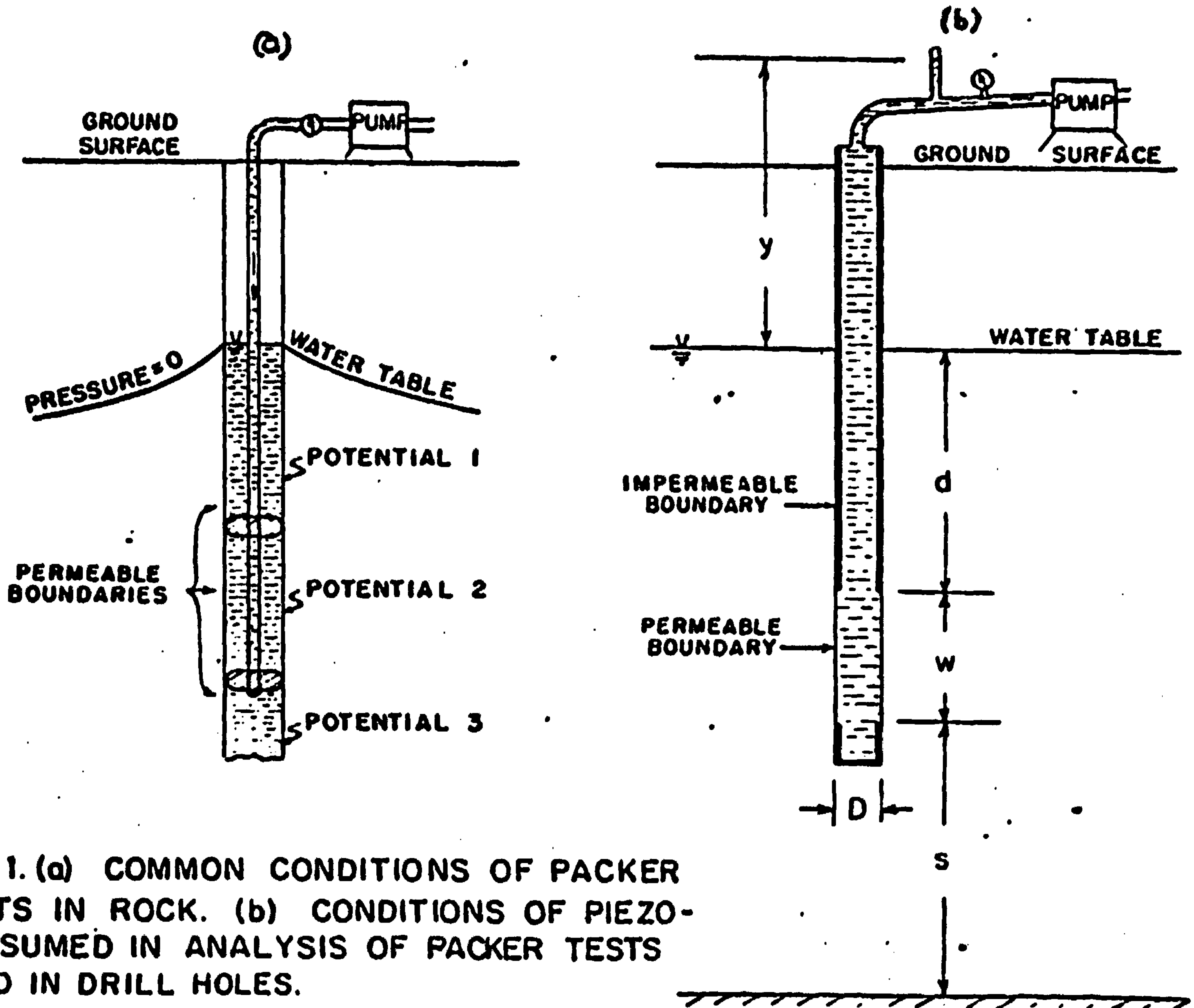

FIGURE 2-1. (a) COMMON CONDITIONS OF PACKER PUMP TESTS IN ROCK. (b) CONDITIONS OF PIEZOMETER ASSUMED IN ANALYSIS OF PACKER TESTS CONDUCTED IN DRILL HOLES.

permeability. This is due, in part, to the assumptions discussed above, and in part, to the great variability of permeability found in most rock bodies. Improvement of methods and confidence is one object of this work.

The dimensionless variables describing the cavity geometry and determining the shape factor are expressed by:

$$S/D = f\,(d/D\,,\ w/D\,,\ s/D\,). \qquad (2\text{-}4)$$

Frevert and Kirkham (1948) have established by electrical analogues that there is very little effect of lowered water table until d is less than one diameter, D, from the top of the cavity. The depth to an impermeable barrier, s, is seldom known in exploration, but can usually be assumed large in comparison to D. S/D is an insensitive to s/D as it is to d/D (Childs, 1952, p. 533). Thus, piezometer or packer tests are best analyzed as though in an infinite medium, provided that they are located below the water table. In such cases,

$$S/D = f\,(w/D)\,. \qquad (2\text{-}5)$$

In particular, if the cavity is long (w/D > 8)

$$S/D = \frac{2\pi\, w/D}{\ln(2w/D)} \quad \text{(Glover, reported by Zanger, 1946).*} \qquad (2\text{-}6)$$

Since the derivations of Dachler, Samsioe and Glover assume a line source, they fail to satisfy the condition of uniform potential over the surface of a cylinder. Maasland has provided, as alternative, the shape factors for ellipsoids.

Evans and Kirkham (1950) pointed out the analogy of the shape factor to the electrostatic capacity about an ellipsoid in an infinite medium:

*Zanger (1953) reports the derivation by Cornwell, but attributes the equation to R. E. Glover.

$$S = 4\pi C .$$

Smythe (1939) shows that

$$2/C = \int_0^\infty d\theta / [(\alpha^2+\theta)(\beta^2+\theta)(\gamma^2+\theta)]^{1/2} ,$$

where θ is a variable of integration and α, β, and γ are the semi-axes of an ellipsoid. For the ellipsoid inscribed in the cavity of a packer cavity, $\alpha = \gamma$ and $\beta > \alpha$, giving:

$$S = 8\pi(\beta^2-\alpha^2)^{1/2} / \ln\left(\frac{\beta+(\beta^2-\alpha^2)^{1/2}}{\beta-(\beta^2-\alpha^2)^{1/2}}\right) ,$$

which becomes

$$S = 4\pi[(w/D)^2-1]^{1/2} / \ln\left(\frac{w/D+[(w/D)^2-1]^{1/2}}{w/D-[(w/D)^2-1]^{1/2}}\right) \qquad (2\text{-}7)$$

upon substitution of

$$\alpha = D/2 \quad , \quad \beta = w/2 .$$

Shape factors computed by equation (2-7) differ by less than 3 percent from those computed by equations (2-6) if $w/D > 3.0$. As Maasland has noted (p. 273), neither of these equations are correct for a circular cylinder, though they are asymptotic to these values for large cavity lengths.

When a piezometer coincides with the extraordinary axis of a two-dimensional anisotropic medium (Maasland, pp. 275-280), then

$$k_h = k_1 = k_2 \quad \text{and} \quad k_v = k_3 .$$

The transformation equations are

$$x_1' = x_1 \quad , \quad x_2' = x_2 \quad , \quad x_3' = m x_3 ,$$

m being $(k_h/k_v)^{1/2}$. Circular sections remain circular in the fictitious transformed medium, and the isotropic hydraulic conductivity is

$$k = (k_h k_v)^{1/2} .$$

Thus, the discharge is:

$$Q = (k_h k_v)^{1/2} S_2 y , \qquad (2\text{-}8)$$

where y is the net head and

S_a is the anisotropic shape factor,

$S_a/D = f(mw/D)$,

found by equations (2-6) or (2-7).

Maasland reports equations for shapes other than the long cylindrical cavities considered here. It is noteworthy that the principal conductivities of a two-dimensional anisotropic soil can be found if the principal directions are known to coincide with the axes of two differently-shaped piezometers. The combination of a long cylindrical cavity for one, and an open-ended disk source (no cavity) for the other, is efficient for soil (Maasland, p. 279) but is inadequate for rock because too few joint conductors (too small a sample) would communicate with the end of a drill hole. Child's two-well system does not readily lend itself to rock testing because large potential differences cannot be introduced by gravity.

Maasland also developed a means of analyzing three-dimensional anisotropy. His work served as a guide to the following but is not repeated here because we do not assume the axis of the piezometer to coincide with a (vertical) principal axis of conductivity.

A rotation of the coordinate system is first necessary when the piezometer has an arbitrary orientation with respect to the principal axes of conductivity. Assume a drill-hole with orientation B_i, the direction cosines of its axis with respect to a right-handed geographic system (south = x_1, east = x_2, up = x_3), and three principal axes of conductivity U_{ij}, similarly referenced.

Figure 2-2 is a diagram of the unit vectors of three coordinate systems, two of them labelled with their direction cosines relative to the geographic axes x_i. In representing these, the superscript ^{o} signifies one of many possible coordinate systems

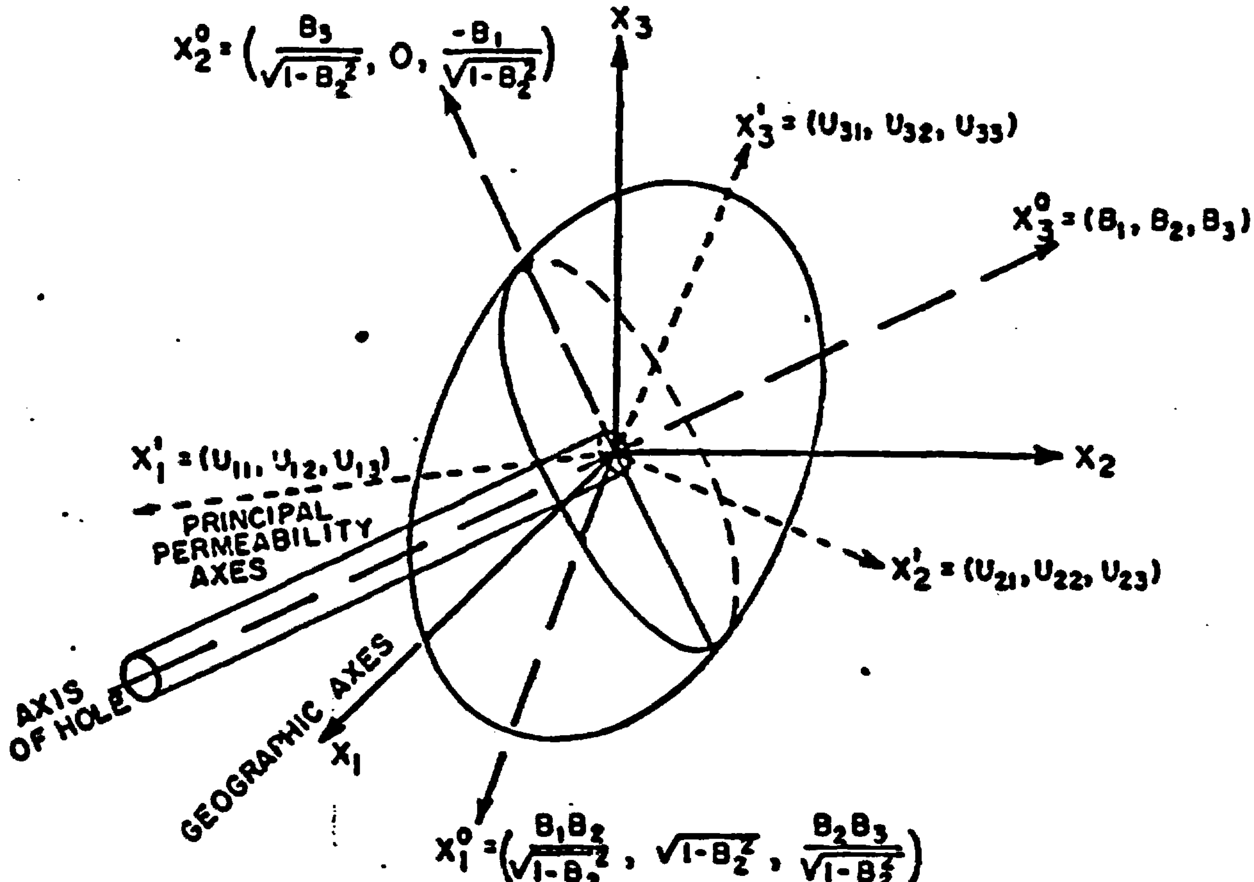

FIGURE 2-2 COORDINATE SYSTEMS FOR PACKER TESTS IN ANISOTROPIC MEDIA.

having an axis along the cylinder; it has B_i as x_3^0 and x_2^0 is in the x_2-plane. The x_i' system coincides with the principal conductivity axes, Uij, themselves being direction cosines in the x_i system. The origin is centered on the upper packer.

The equation of a right-circular cylinder with axis along the x_3^0 coordinate axis is:

$$x_1^{0\,2} + x_2^{0\,2} = r^2 \;, \quad r = D/2 \qquad (2\text{-}9)$$

and the test section is limited to

$$0 \geq x_3^0 \geq -w .$$

The equation for the cylinder must be rotated from the x_i^0 system to the x_i' system. Each position vector is related, one system to the other, by a transformation

$$x_i^0 = a_{ij}\, x_j' \qquad (2\text{-}10)$$

whose matrix is defined as

$$a_{ij} = \begin{vmatrix} \cos(1^0, 1') & \cos(1^0, 2') & \cos(1^0, 3') \\ \cos(2^0, 1') & \cos(2^0, 2') & \cos(2^0, 3') \\ \cos(3^0, 1') & \cos(3^0, 2') & \cos(3^0, 3') \end{vmatrix}$$

Inspection of Figure 2-2 will verify that the elements of the transformation are: $a_{ij} =$

$$\begin{vmatrix} \left[\frac{U_{11}B_1B_2}{\sqrt{1-B_2^2}} - U_{12}\sqrt{1-B_2^2} + \frac{U_{13}B_2B_3}{\sqrt{1-B_2^2}}\right] & \left[\frac{U_{21}B_1B_2}{\sqrt{1-B_2^2}} - U_{22}\sqrt{1-B_2^2} + \frac{U_{22}B_2B_3}{\sqrt{1-B_2^2}}\right] & \left[\frac{U_{31}B_1B_2}{\sqrt{1-B_2^2}} - U_{32}\sqrt{1-B_2^2} + \frac{U_{33}B_2B_3}{\sqrt{1-B_2^2}}\right] \\ \left[\frac{U_{11}B_3}{\sqrt{1-B_2^2}} - \frac{U_{13}B_1}{\sqrt{1-B_2^2}}\right] & \left[\frac{U_{21}B_3}{\sqrt{1-B_2^2}} - \frac{U_{23}B_1}{\sqrt{1-B_2^2}}\right] & \left[\frac{U_{31}B_3}{\sqrt{1-B_2^2}} - \frac{U_{33}B_1}{\sqrt{1-B_2^2}}\right] \\ \left[U_{11}B_1 + U_{12}B_2 + U_{13}B_3\right] & \left[U_{21}B_1 + U_{22}B_2 + U_{23}B_3\right] & \left[U_{31}B_1 + U_{32}B_2 + U_{33}B_3\right] \end{vmatrix} \qquad (2\text{-}11)$$

The matrix multiplication of equation (2-10) gives the original components of a position vector in terms of the primed coordinates. Equation (2-9) for the cylinder in the coordinate system parallel to principal axes of the anisotropic medium becomes

$$(a_{11}x_1' + a_{12}x_2' + a_{13}x_3')^2 + (a_{21}x_1' + a_{22}x_2' + a_{23}x_3')^2 = r^2 \qquad (2\text{-}12)$$

To replace the medium by an imaginary isotropic one, we must transform linearly to a third coordinate system according to:

$$\begin{aligned} x_1'' &= (k_0/k_{11})^{1/2}\, x_1' \\ x_2'' &= (k_0/k_{22})^{1/2}\, x_2' \\ x_3'' &= (k_0/k_{33})^{1/2}\, x_3' \end{aligned} \qquad (2\text{-}13)$$

where again, k_o is an arbitrary constant. The k_{ii} are principal hydraulic conductivity coefficients, proportional to the principal permeabilities K_{ii}, and one of the factors listed in Table 2-1.

Table 2-1

CONVERSION FACTORS, PERMEABILITY TO HYDRAULIC CONDUCTIVITY

To obtain conductivity in: NAME	UNITS	Multiply absolute cgs units (cm^2) by: FACTOR	
Darcys	cm^2	1.0132×10^8	
Meinzer, K_s	gal/day/ft^2 water @ 60°F	1.844×10^9	
Field Units K_f	gal/day/ft^2 water @ f°	$1.844 \times 10^9 \times$	
	ft/year water @ 60°F	0.9053×10^{11}	
	cm/sec water @ 20.2°C	0.9772×10^5	
	meters/day water @ 20.2°C	0.861×10^8	
Lugeon Units	l/min/m hole/Atmos over 10 min.	0.6×10^{10}	(R. E. Goodman, personal communication)

One possible definition of the arbitrary constant is

$$k_o = (k_{11} k_{22})^{1/2} , \qquad (2\text{-}14)$$

which makes

$$\left.\begin{aligned} x_1' &= (k_{11}/k_{22})^{1/4} x_1^{''} \\ x_2' &= (k_{22}/k_{11})^{1/4} x_2^{''} \\ x_3' &= [k_{33}^{1/2}/(k_{11} k_{22})^{1/4}]\, x_3^{''} . \end{aligned}\right\} \qquad (2\text{-}15)$$

To find how the length of the cavity is changed by the transformation, identify the center of the distal end by the vector y_1, originally at

$$y_1^0 = y_2^0 = 0 \quad , \quad y_3^0 = -w \; ,$$

then rotated to

$$y_1' = a_{31}\, y_3^0 \quad , \quad y_2' = a_{32}\, y_3^0 \quad , \quad y_3' = a_{33}\, y_3^0 \quad ,$$

and transformed to isotropy by substitution equations 2-15 and $y_3^0 = -w$.

$$y_1'' = (k_{22}/k_{11})^{1/4}\, a_{31}\, w$$

$$y_2'' = (k_{11}/k_{22})^{1/4}\, a_{32}\, w$$

$$y_3'' = [(k_{11}\, k_{22})^{1/4}/k_{33}^{1/2}]\, a_{33}\, w$$

The cavity length in the fictitious system is found from

$$\ell^2 = y_i''\, y_i'' \quad ,$$

which gives:

$$\ell = [(k_{22}/k_{11})^{1/2} a_{31}^2 + (k_{11}/k_{22})^{1/2} a_{32}^2 + \{(k_{11} k_{22})^{1/2}/k_{33}\}\, a_{33}^2]^{1/2}\, w \quad (2\text{-}16)$$

Direction cosines of the axis of the cylinder are:

$$\gamma_i = y_i''/\ell \, .$$

The general equation for the cylindrical cavity in the isotropic system is obtained by substituting equation 2-15 into 2-12, changing it to an oblique elliptic cylinder:

$$\begin{aligned} &[(k_{11}/k_{22})^{1/4} a_{11} x_1'' + (k_{22}/k_{11})^{1/4} a_{12} x_2'' + \{k_{33}^{1/2}/(k_{11} k_{22})^{1/4}\}\, a_{13} x_3'']^2 + \\ &[(k_{11}/k_{22})^{1/4} a_{21} x_1'' + (k_{22}/k_{11})^{1/4} a_{22} x_2'' + \{k_{33}^{1/2}/(k_{11} k_{22})^{1/4}\}\, a_{23} x_3'']^2 = r^2 \end{aligned} \quad (2\text{-}17)$$

A cross-section normal to its axis is also an ellipse, defining the new cavity shape by its semi-axes. To find them, we first solve the oblique section, equation 2-17, for its semi-axes, then project them to the plane normal to the cylinder axis. The expanded form of 2-17 is:

$$\begin{aligned} &\frac{(k_{11}/k_{22})^{1/2}(a_{11}^2 + a_{21}^2)}{r^2} x_1''^2 + \frac{2(a_{11}a_{12} + a_{21}a_{22})}{r^2} x_1'' x_2'' + \frac{2(k_{33}/k_{22})^{1/2}(a_{11}a_{13} + a_{21}a_{23})}{r^2} x_1'' x_3'' \\ &+ \frac{(k_{22}/k_{11})^{1/2}(a_{12}^2 + a_{22}^2)}{r^2} x_2''^2 + \frac{2(k_{33}/k_{11})^{1/2}(a_{12}a_{13} + a_{22}a_{23})}{r^2} x_2'' x_3'' \\ &+ \frac{\{k_{33}/(k_{11} k_{22})^{1/2}\}(a_{13}^2 + a_{23}^2)}{r^2} x_3''^2 = 1 \end{aligned} \quad (2\text{-}18)$$

The coefficients of x_ix_j, as arranged here, define a symmetric matrix after first dividing off-diagonal ($i \neq j$) elements by 2. Diagonalization transforms the equation of the oblique elliptic section to a coordinate system parallel to the axis of that ellipse.

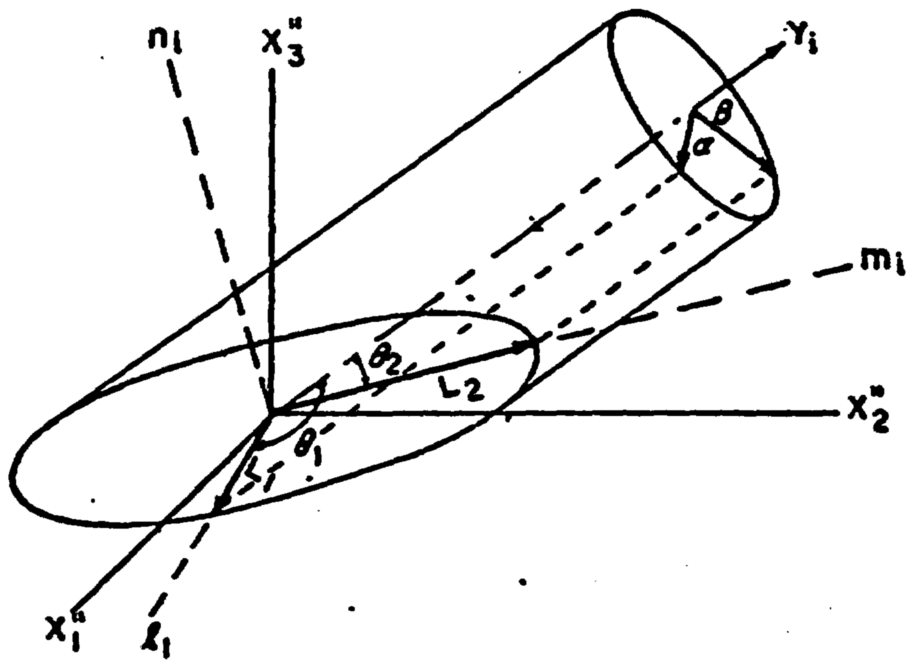

Figure 2-3. The originally circular directrix of a cylinder is an oblique ellipse after transformation. The true directrix is found by projection along the axis Y_1.

The diagonal matrix:
$$\begin{vmatrix} A & 0 & 0 \\ 0 & B & 0 \\ 0 & 0 & C \end{vmatrix}$$

will contain only two non-zero terms, A and B, B and C, or A and C, which are coefficients of the ellipse

$$A x_1'^2 + B x_2'^2 + C x_3'^2 = 1 .$$

The semi-axes are, then, two of the following:

$$L_1 = (1/A)^{1/2} , \; L_2 = (1/B)^{1/2} , \; L_3 = (1/C)^{1/2} .$$

The eigenvectors must next be determined, to define the orientations of the above semi-axes of the oblique elliptic section in terms of the transformed (isotropic) coordinate system. Call these axes l_i, m_i, and n_i, corresponding to the A, B, and C eigenvalues. Figure 2-3 illustrates the simple projection of these eigenvalues to the plane normal to the cylinder axis:

$$\alpha = L_1[1-(\gamma_i l_i)^2]^{1/2}$$
$$\beta = L_2[1-(\gamma_i m_i)^2]^{1/2}$$
$$\gamma = L_3[1-(\gamma_i m_i)^2]^{1/2},$$

whichever two are pertinent.

The greatest possible ellipticity would arise if the circular section in the original anisotropic medium coincided with the plane of k_{11} and k_{33}. Then

$$\alpha/\beta = (k_{33}/k_{11})^{1/2}.$$

We have described the elliptic cylinder in the fictitious isotropic medium by the length l and semi-axes, say α and β, corresponding to the length w and the radius D/2 of a right circular cylinder test section in an anisotropic medium. The ends of the cylinder are non-orthogonal after transformation. This will influence the shape factor when $w < D$, but may be neglected for pumping tests where w is invariably many times D.

The shape factor has been reduced to:

$$S/D = f\left[k_{11}, k_{22}, k_{33}, \left\{(k_{33}/k_{11})^{1/2} a_{13}^2 + (k_{33}/k_{22})^{1/2} a_{23}^2 + \{(k_{11}k_{22})^{1/2}/k_{33}\} a_{33}^2\right\}^{1/2} w/D\right]. \quad (2\text{-}19)$$

Maasland has studied the relation between ellipticity and the shape factor (1957, p. 244). Rather than evaluate the integral for electrostatic capacity for $\alpha \neq \beta \neq \gamma$, he employed electric analogues. He found little influence, provided that $w/D > 5$ and $1/3 < \alpha/\beta < 3$. Thus,

$$S_a \cong f(l/D)$$

alone. Sa is determinable by equation (2-6) with less than 4 percent error.

The limitation that k_{11}/k_{33} be less than 9 is serious only when a single, near-parallel joint set is present or dominant, because the orientation studies have indicated no cases of such strong anisotropy when more than one set of joints, in adequate samples, is present in the medium. The circular-cylinder form factor approximation is acceptable for two or three-set systems, unless, for instance, one set consists of large parallel faults, and the other conductors are tight joints. In some cases of strong anisotropy, problems may be solved by reducing to two dimensions on the plane of symmetry.

D should be the diameter of a circle having the same area as the elliptic section in the fictitious isotropic medium (Maasland, p. 284).

$$D = 2(\alpha\beta)^{1/2} \qquad (2\text{-}20)$$

The Glover-Cornwell equation for the shape factor of long cavities in an infinite medium is suitable for packer tests in rock, provided that w is computed by equation (2-16), and D by equation (2-20). The conductivity must be determined by equation (2-2) and (2-14). Then equation (2-3) for the discharge is

$$Q = [(k_{11} k_{22})^{1/2}/k_{33}]^{1/2} S_a \, y \qquad (2\text{-}21)$$

A computation of discharge for one hypothetical packer test will exemplify the method. Suppose that the diagonalized permeability tensor is

$$K_{ij} = \begin{vmatrix} 27.9 & 0 & 0 \\ 0 & 7.1 & 0 \\ 0 & 0 & 4.6 \end{vmatrix} \times 10^{-6} \text{ cgs units}$$

and the matrix of direction cosines of the principal axes is

$$U_{ij} = \begin{vmatrix} .632 & -.770 & .081 \\ .564 & .386 & -.730 \\ .531 & .507 & .678 \end{vmatrix}$$

Suppose a 200-foot NX (D in equation 3-6 = 0.25 ft.) drill hole is inclined 45 degrees east (B_i = 0.0, .7071, - .7071) with one packer set 50 feet from the bottom (w = 50). The static water table is 40 feet below ground and the temperature 60°F. Gage pressure is 75 psi (y = 40 + 75 (2.31) = 231 ft.).

Hydraulic conductivities are obtained by applying a factor from Table 2-1.

$$k_{ii} = K_{ii} (1.84 \times 10^{9}) \text{ gallons/day/ft}^2$$

$$k_{11} = 5.15 \times 10^4, \quad k_{22} = 1.31 \times 10^4, \quad k_{33} = 0.84 \times 10^4$$

Next, we compute the transformation matrix (equation 2-11), that will rotate the drill hole B_i to coordinates parallel to the principal conductivities.

$$a_{ij} = \begin{vmatrix} a_{11} & a_{12} & a_{13} \\ a_{21} & a_{22} & a_{23} \\ a_{31} & a_{32} & a_{33} \end{vmatrix} = \begin{vmatrix} .478 & .243 & -.837 \\ -.632 & -.564 & -.531 \\ -.601 & .789 & -.121 \end{vmatrix}$$

The transformed test length has components

$$y_1^* = -(k_{22}/k_{11})^{1/4} a_{31} w = .504(.601)50.0 = 21.7 \text{ ft.}$$

and similarly

$$y_2^* = -(k_{11}/k_{22})^{1/4} a_{32} w = \quad -55.6$$

$$y_3^* = -[(k_{11} k_{22})^{1/4}/k_{33}^{1/2}] a_{33} w = \quad 10.6 .$$

Direction cosines are

$$Y_i = .358, \ -.919, \ .175$$

The test length in the isotropic medium is given by equation (2-16).

$$l = [(.254)^{1/2}(-.602)^2 + (3.93)^{1/2}(.789)^2 + \{(5.15)^{1/2}(1.31)^{1/2}/0.84\}(-.121)^2]^{1/2}(50.0) = 60.5 \text{ ft.}$$

The matrix of the cross-sectional ellipse is found by equation (2-18)

$$64.0\begin{vmatrix} 1.263 & .475 & -.058 \\ .475 & .190 & .039 \\ -.058 & .039 & .391 \end{vmatrix}$$

Upon diagonalization (see Long, 1961, p. 23), to slide-rule precision,

$$\begin{vmatrix} A & 0 & 0 \\ 0 & B & 0 \\ 0 & 0 & C \end{vmatrix} = \begin{vmatrix} 0.0 & 0.0 & 0.0 \\ 0.0 & 92.4 & 0.0 \\ 0.0 & 0.0 & 21.1 \end{vmatrix} .$$

The oblique elliptic section has the equation,

$$92.4\,\bar{X}_2^2 + 21.1\,\bar{X}_3^2 = 1 ,$$

with semi-axes:

$$L_2 = .104,\ L_3 = .218 \text{ feet} .$$

To project those semi-axes to the plane normal to the axis of the cylinder, Y_1, the coefficient matrix eigenvectors must be determined. Those are the directions of L_1, L_2, and L_3. For each eigenvalue, B and C, there are four simultaneous equations to satisfy:

$$\begin{aligned} (1.263 - A/64.0)\,\ell_1 + .475\,\ell_2 - .058\,\ell_3 &= 0 \\ .475\,\ell_1 + (.190 - A/64)\,\ell_2 + .039\,\ell_3 &= 0 \\ -.058\,\ell_1 + .039\,\ell_2 + (.391 - A/64)\,\ell_3 &= 0 \\ \ell_1^2 + \ell_2^2 + \ell_3^2 &= 1 . \end{aligned}$$

The solutions are direction cosines, the pertinent ones in this case being

B: $m_i = .167,\ .354,\ .920$

C: $n_i = 0.0,\ 0.0,\ .999$.

The cylinder axis Y_1 makes angles with the semi-axes of the oblique ellipse having cosines

$$Y_i\ m_i = (.358)(.167) + (-.019)(.354) + (.175)(.920) = -.105$$

$$Y_i\ n_i = (.175)(.999) \qquad = .175$$

The projection of the semi-axis, L_i, onto the plane normal to Y_i, gives the semi-axes of the directrix of the transformed cylinder:

$$\beta = .104(1-.105^2)^{1/2} = .103 \text{ ft.}$$

$$\gamma = .218(1-.175^2)^{1/2} = .215$$

and $\beta/\gamma = .478$. Were the test oriented to attain the maximum ellipticity, then it would have been

$$\beta/\gamma = (k_{33}/k_{11})^{1/2} = .405 \ .$$

Since $1/3 < \beta/\gamma < 3$, a circular cylinder will give a good approximation to the shape factor, if the circle diameter is taken to be:

$$D = 2(\beta\gamma)^{1/2} = .298 \ .$$

Now we apply Glover's formula (2-6) for the shape factor of a long cylinder:

$$S_a = \frac{2\pi \ell}{\ln(2\ell/D)} = \frac{2\pi\, 60.5}{\ln[2(60.5)/.298]} = 146.$$

The hydraulic conductivity of the fictitious isotropic medium is

$$k = (k_{11}\,k_{22}\,k_{33}/k_o)^{1/2} = (k_o\,k_{22})^{1/4} k_{33}^{1/2} = 1.48 \times 10^4 \text{ gal./d./ft.}^2$$

Then the discharge,

$$Q = k\, S_a\, \mathcal{J}$$

$$= 1.48\,(146.)\,213.$$

$$= 45900 \text{ gal./day}$$

or $\qquad = 32 \text{ gpm}.$

<u>Three-hole pump test for anisotropic media</u>

If a piezometer or packer test hole is oriented parallel to one of the principal conductivity axes, the special case discussed by Maasland (p. 283) leads to equation 2-21.

The shape factor depends upon which axis is followed by the hole, and cannot be determined at the outset since the conductivities are unknown. Maasland's method for determining the unknown is adequate when the plane normal to the axis of the hole is one of isotropy, the hole following the unique axis. A more general method is presented below, for the case of three different principal conductivities of known direction.

To replace the real anisotropic system with a fictitious isotropic one, a linear transformation only is required, since the hole already coincides with an axis. By equations similar to (2-13), we transform

$$x_1' = (k_0/k_{11})^{1/2} x_1$$
$$x_2' = (k_0/k_{22})^{1/2} x_2 \qquad (2\text{-}22)$$
$$x_3' = (k_0/k_{33})^{1/2} x_3$$

where the constant $k_0 = (k_{11}k_{22})^{1/2}$. The circular cross-section becomes an ellipse with axial ratios

$$\beta/\gamma = (k_{33}/k_{22})^{1/2}, \quad \alpha/\gamma = (k_{33}/k_{11})^{1/2} \quad \text{or} \quad \alpha/\beta = (k_{22}/k_{11})^{1/2},$$

depending upon which axis coincides with the hole, 1, 2, or 3, respectively. Before generalizing, let us attend to an i-axis hole. Label this the z-axis, with x and y normal to the hole and $k_0 = (k_x k_y)^{1/2}$. Then the semi-axes of the elliptic section in the transformed medium are

$$a = (k_0/k_x)^{1/2} D/2 \quad \text{and} \quad b = (k_0/k_y)^{1/2} D/2.$$

The circular section having the same area as the ellipse has diameter

$$D' = 2(ab)^{1/2} = D \qquad (2\text{-}23)$$

The cavity length w' in the fictitious isotropic medium is

$$w' = (k_0/k_z)^{1/2} w = \{(k_x k_y)^{1/4}/k_z\} w. \qquad (2\text{-}24)$$

The shape factor defined by Glover's equation for a long cylindrical cavity gives a good approximation to that of an elliptical cylinder cavity if $1/3 < a/b < 3$.

$$S_a/D' = \frac{2\pi w'/D'}{\ln(2w'/D')}$$

$$S_a/D = \frac{2\pi (k_0/k_z)^{1/2} w/D}{\ln\left[\frac{2[(k_x k_y)^{1/4}/k_z^{1/2}] w}{D}\right]} \qquad (2\text{-}25)$$

$$S_a = \frac{2\pi w (k_x k_y)^{1/4}/k_z^{1/2}}{\ln\left[\frac{2w(k_x k_y)^{1/4}/k_z^{1/2}}{D}\right]}$$

The discharge of such a piezometer or packer test in an aniso- tropic medium under head y is

$$Q = (k_x k_y k_z/k_0)^{1/2} S_a y = \frac{2\pi w y (k_x k_y)^{1/2}}{\ln\left[\frac{2w}{D}(k_x k_y)^{1/4}/k_z^{1/2}\right]} \qquad (2\text{-}26)$$

Interpreting field data, one can only assume isotropy and compute an apparent conductivity, k_a, by

$$Q = k_a S y ,$$

where the shape factor is given by equation (2-6). Thus

$$Q = k_a \frac{2\pi w}{\ln(2w/D)} y . \qquad (2\text{-}27)$$

Equating 2-26 to 2-27,

$$k_a \frac{2\pi w}{\ln(2w/D)} y = \frac{2\pi w y (k_x k_y)^{1/2}}{\ln\left[\frac{2w}{D}(k_x k_y)^{1/4}/k_z^{1/2}\right]}$$

$$\frac{(k_x k_y)^{1/2}}{k_a} = \frac{\ln(2w/D) + \ln[(k_x k_y)^{1/4}/k_z^{1/2}]}{\ln(2w/D)} \qquad (2\text{-}28)$$

$$k_a(1+e) = (k_x k_y)^{1/2} \; ; \; e = \frac{\ln[(k_x k_y)^{1/4}/k_z^{1/2}]}{\ln(2w/D)} .$$

The error term e tends to zero for such large w/D as apply to most packer tests in rock. Thus, an apparent conductivity, computed on the assumption of isotropy, approximates the geometric mean of the principal conductivities in directions normal to the hole. Reeve and Kirkham (1951) have already observed that the apparent conductivity depends largely upon the conductivity normal to the piezometer.

Table 2-2 gives values of the error e for $10 \leq w/D \leq 500$, $1 \leq k_x/k_y \leq 10$, and $0.1 \leq k_z/k_y \leq 10$. Inspection shows that for all w/D, k_a underestimates $(k_x k_y)^{1/2}$, i.e. $e > o$, if the hole is drilled along a minimum conductivity axis, and overestimates it if drilled along a maximum conductivity axis. If we limit consideration to media having $k_x/k_y < 9$, then the elliptical cavities can be adequately analyzed as equivalent circular cylinders, and we will be within the range of Table 2-2.

We can return to the notation of the x_i coordinate system, and label k_{a1}, k_{a2}, and k_{a3} the apparent hydraulic conductivities determined by three orthogonal piezometers or packer tests, each drilled parallel to a principal axis, 1, 2, or 3. As a first approximation:

$$k_{a1}^2 = k_{22} k_{33} \quad , \quad k_{a2}^2 = k_{11} k_{33} \quad , \quad k_{a3}^2 = k_{11} k_{22} \; .$$

Solved simultaneously,

$$k_{11} = k_{a2} k_{a3}/k_{a1} \; , \quad k_{22} = k_{a1} k_{a3}/k_{a2} \; , \quad k_{33} = k_{a1} k_{a2}/k_{a3} \; .$$

With these estimates, it is easy to find in Table 2-2 the errors made in assuming k_{a1}, k_{a2} or k_{a3} to equal the geometric means of conductivities normal to each test hole. Corrected values of k_a yield improved principal conductivities by equations (2-29). Two or three consecutive corrections will converge on the true values.

A truly general in-situ piezometer test is yet to be devised. The present methods, as well as those of Frevert and Kirkham (1948), Luthin and Kirkham (1949), Reeve and Kirkham (1951), Childs (1952) and Maasland (1957) require independent knowledge or assumptions of the principal directions of hydraulic conductivity. The assumed uniqueness of the horizontal plane is usually justifiable for agricultural soils or certain stratified, unconsolidated deposits (Childs, 1952, p. 527; Maasland, 1957, p. 228), but even Child's two-well system requires trial field arrangements to find maximum and minimum conductivity directions in the horizontal plane.

In the general case of anisotropy, there are six independent unknowns, three to define the orientation of axes, and three to define principal conductivities. A single determinative test for these variables would, in all likelihood, be too complex for practical use. It is thought better to continue use of other criteria for recognition of principal axes before applying tests for the three conductivities. If discharge is all that is measured in a flow test, three tests are necessary to solve for the three unknowns.

Such a test is the three-hole arrangement described above, also the two-well and short piezometer combination of Childs (1952). In practice, a test with three holes uniquely oriented will often prove inconvenient because of terrain limitations. Furthermore, exploratory holes drilled primarily for purposes other than pump-testing, oriented for convenience or economy between principal axes, would not be useful for analyses of this sort. Usually, some latitude of choice exists, because diamond-drill explorations are somewhat arbitrary in design, especially in preliminary stages. For purposes of permeability testing, they could be better oriented than is customary, concurrently disclosing other geological unknowns. When seepage or potential distribution is the prime problem, the entire layout should be oriented according to predetermined conductivity directions.

The geometry of the system of joint sets, faults, shears, foliation and bedding determined from surface exposures provides the only initial indication of the orientation of principal directions. A stereonet plot of joint normals offers the best tool for visualizing the symmetry of systems, and for measuring average directions. The orientation studies illustrated in Plates 1 through 15 of Chapter 5 can be put to direct application in an important qualitative way. Models of cases where there are one, two, or three joint sets of equal or different properties, will find their approximate counterparts in prototype situations. Principal axes follow intersections of planes of orthogonal systems. A plane of isotropy lies normal to sets of a conjugate system, or the approximate angle of a principal axis between two unequal sets may be indicated by their relative spacing, orientation dispersion, surface texture or continuity. Progressive analysis of tests during the drilling program should normally give improved definition of axes to improve hole orientations.

As an example of anisotropic testing procedure, consider a foundation rock whose surface expression of jointing reveals a pattern such as is displayed in the stereonet plot of normals, Figure 2-4. Three orthogonal but unequal sets are apparent. A plot of β-lineations (Billings, 1942, p. 336) measured on all surfaces would yield a similar pattern. NX diamond-drill holes are then oriented 45 degrees northwest and southeast, and horizontally, NE - SW, so that each coincides most faithfully with the central tendency of a joint set. Pumping tests with packers are then performed as drilling progresses. For each test, discharge, static water level and gage pressure are measured, packers set at intervals of about 25 feet. Hydraulic conductivity is computed for each test, assuming isotropic conditions, and the results for each orientation are averaged. Let these be:

$$k_{a1} = 1.6 \times 10^{4};\ k_{a2} = 2.1 \times 10^{4};\ k_{a3} = 3.3 \times 10^{4} \text{ gal./d./ft}^2,$$

where subscript 1 refers to holes trending NW, 2 for holes trend-

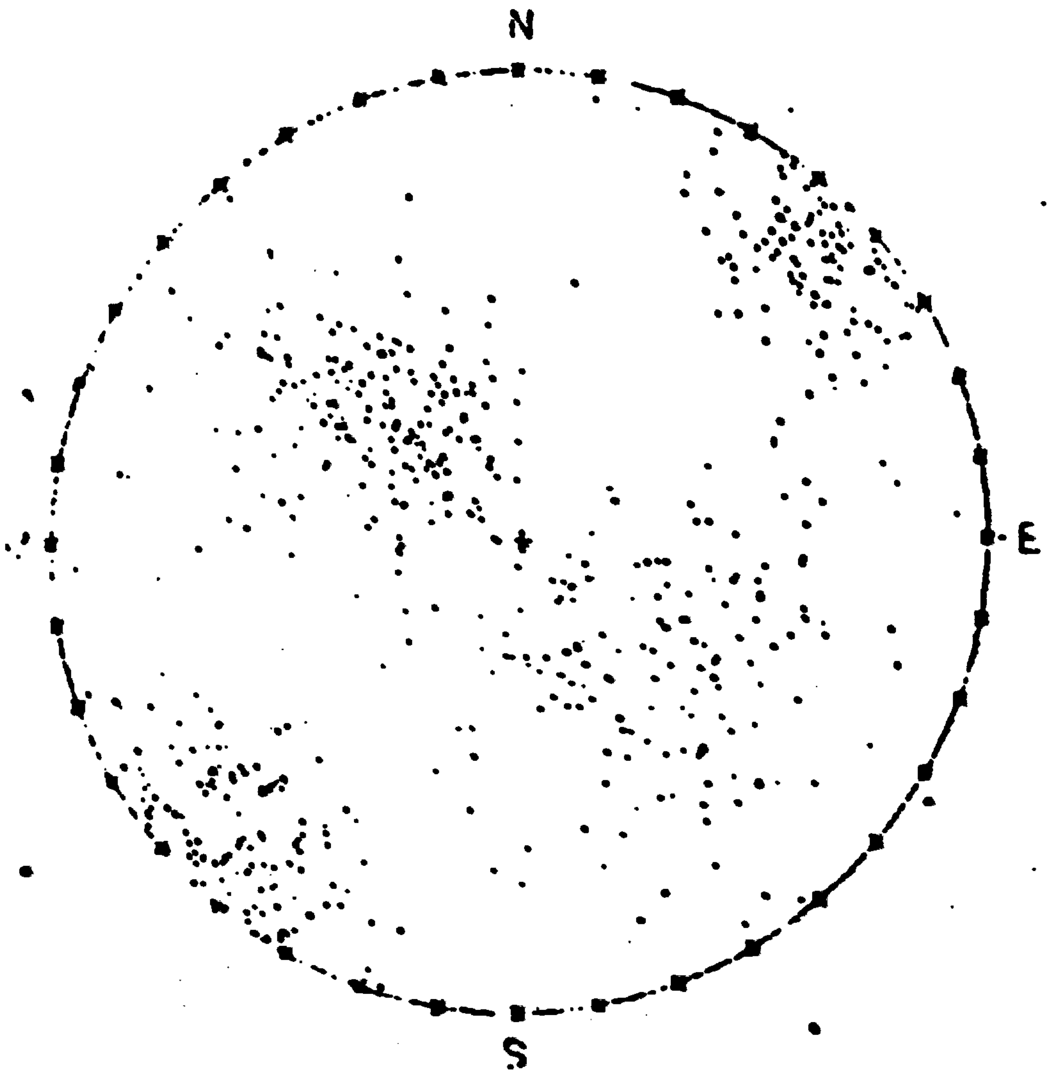

FIGURE 24.
STEREOGRAPHIC PROJECTION. UPPER HEMISPHERE
3 NORMAL JOINT SETS WITH SAME SPACING. DIFFERENT DISPERSIONS $K_f = 6$, DIP 45 DEG SE; $K_f = 15$ DIP 45 DEG NW AND $K_f = 30$ DIP 90 DEG SW

ing SE, and 3, horizontal. According to equations (2-29),

$k_{11} = k_{a2} k_{a3} / k_{a1} = 4.3$; $k_{22} = k_{a1} k_{a3} / k_{a2} = 2.5$; $k_{33} = k_{a1} k_{a2} / k_{a3} = 1.0 \times 10^4$

Clearly, the direction dipping 45 degrees NW is most conductive, as might be guessed from the large number of joints parallel to this direction, and the horizontal, NE-SW direction is least conductive, since fewest joints trend or intersect along this line.

Now, we can enter Table 2-2 with w/D = 25 / 0.25 = 100 and the above estimates.

$(k_x/k_y)_1 = 2.5 / 1.0 = 2.5$; $(k_z/k_y)_1 = 4.3 / 1.0 = 4.3$

$(k_x/k_y)_2 = 4.3 / 1.0 = 4.3$; $(k_z/k_y)_2 = 2.5 / 1.0 = 2.5$

$(k_x/k_y)_3 = 4.3 / 2.5 = 1.7$; $(k_z/k_y)_3 = 1.0 / 2.5 = 0.4$

The errors that apply to the equation

$$k_a (1 + e) = (k_x k_y)^{1/2}$$

are obtained by interpolation:

$e_1 = -.095$; $e_2 = -.016$; $e_3 = .109$

Thus corrected, harmonic means of conductivities normal to each hole alignment are:

$$k_{a1}' = k_{a1} (1 + e_1) = 1.6 (1 - .095) = 1.40 \times 10^4$$

$$k_{a2}' = k_{a2} (1 + e_2) = 2.1 (1 - .016) = 2.0 \times 10^4$$

$$k_{a3}' = k_{a3} (1 + e_3) = 3.3 (1 + .109) = 3.6 \times 10^4,$$

and by equations (2-29):

$k_{11} = 5.2 \times 10^4$; $k_{22} = 2.6 \times 10^4$; $k_{33} = 0.82 \times 10^4$.

Again obtaining anisotrophies, errors, corrected geometric means, and principal conductivities, we find:

$k_{11} = 5.5 \times 10^4$; $k_{22} = 2.6 \times 10^4$; $k_{33} = 0.77 \times 10^4$.

Another re-estimate gives

$k_{11} = 5.6 \times 10^4$; $k_{22} = 2.6 \times 10^4$; $k_{33} = 0.75 \times 10^4$,

which is adequate for most purposes, being close to the asymptotes of the principal conductivities.

Chapter 3

PLANAR GEOLOGIC STRUCTURES AND THE OCCURRENCE OF WATER IN FRACTURED ROCKS

Introduction

Chapter 1 reviewed theory for homogeneous, continuous anisotropic permeable media, and Chapter 2 presented a method of measuring anisotropic permeability in any medium. Such idealized media are distinctly different from fractured rock with its occasional conductive openings. Before we develop in Chapter 4 an analytical method of relating such discontiua to equivalent continuous media, it is desirable to scrutinize the literature for definition of all types of planar features of rock, to review their geometrical character and interrelationships, and particularly, to seek indications of their hydraulic conductivity.

Much work remains before we can define comprehensively the hydraulic characteristics of all types of planar structural elements of sedimentary, igneous, and metamorphic rocks. In the analysis of data employed in Chapter 6, namely, water-pressure tests from damsites on crystalline (metamorphic and granitic) rocks, it has been found impossible to discriminate between coexisting features, for instance foliation, faulting and jointing in the same rock body. Such features might be lumped under the heading of "rock defects", or simply called fractures, since their origins are not clearly understood. (Terzaghi, 1946). Full description of each fracture type awaits refined methods of isolating and measuring properties of coexisting structural features.

Yet the observations in this chapter, treating all types and aggregates of conductors, reveal certain fundamental differences between types. When several are present, the large-scale properties of the medium reflect only the major openings. For instance, when joints having apertures of hundreds of microns cut folia having openings of tens of microns, the permeability is due to the jointing, since, under a given potential gradient, the discharge of each depends on the cube of its aperture (Chapter 4). There is no evidence for fluid flow in intact cleavage, foliation or, as will be shown in chapter 6, in most of the joints that are confined by overburden loads. Faults and shear zones may be greater or lesser conductors than joints, depending on the lithology of the wall-rock or other factors. Lacking flow data to establish criteria that characterize faults as aquifers or aquicludes relative to their country rock, we can only infer fault characteristics from such observations as mineralization. While for engineering purposes a strong conductivity contrast between different types justifies the neglect of all but the major openings in a rock body, the mechanical, chemical and electrical properties may depend upon the continuity of fluids filling all classes of opening.

Since there is interest in all types of planar fluid conductors in rock, whether or not they exist as the only, or dominant type in a given body, a classification and summary of the literature on planar features is appropriate. Such texts as Billings (1942) and de Sitter (1956) describe some aspects of all types.

Cleavage

Fracture cleavages are fine planes of dislocation, 1 to 10 per millimeter, oriented essentially parallel to the axial planes of folds in metamorphic rock. Best developed in argillites, fracture cleavage is either absent, less close-spaced, or less continuous in arenaceous beds of the same sequence, or occasionally present only at the axis of folds. When cleavage of this orientation is found to cut through beds of any lithology, it is called slaty cleavage. In both classes, weak recrystallization develops smooth mica-covered surfaces. When coarser crystals form and the bedding becomes indistinct, it is called flow cleavage. de Sitter reports (p. 98) cleavages that extend great distances in limestones, sandstones and shales, but spaced several millimeters apart. Slaty cleavage is best developed in meta-shales, less perfectly in meta-sandstones, but if pyroclastics, conglomerates, chert, marl, lavas, talc or even serpentine are present, they too may show slaty cleavage. Sometimes there are two sets of fracture cleavage planes intersecting at a small angle and parallel to fold axes. The above types are believed formed always normal to the major compressive stress, and accompanied by minute lateral displacements, expressed as shear folds in the original strata. Schistosity is cleavage with clearly recrystallized micas and quartz, both along fracture planes and throughout the rock. The original bedding is usually obscured. Breakage planes extend across all rock types, individual surfaces following and alternating between innumerable intercrystalline boundaries. The origin of schistosity is mechanical (Goguel, 1945), like cleavage but more intense, and augmented by growth of flat mineral grains. Gneissic structure in granite rocks may be of similar compressional origin. Foliation is a descriptive name that avoids the distinction between shear, cleavage and schistosity. Most cleavage and schistosity is near-vertical in orientation, though horizontal schistosity exists that may be genetically related to so-called concentric slip along bedding-planes (de Sitter, p. 104). Concentric shear surfaces, with mica, gouge or slickensides, are consequences of the bending of successive laminae to different curvatures.

Fluid conductivity in cleavage

Cleavage does not conduct water in quantities of engineering significance, but whether or under what circumstances does cleavage contain continuous fluid-filled openings capable of transmitting changes in hydraulic potential remains an important unknown. Pressure tests in metamorphic rock at Oroville damsite on the Feather River, and McSwain damsite on the Merced River, California, have each demonstrated (Chapter 6) a sufficient proportion of zero-water-take records that the ubiquitious cleavage crossed by the drill holes cannot be significantly conductive when in fresh, hard rock under overburden load. On exposure, however, a few surfaces open, accommodating strain such as accompanies decompression around a tunnel. On prolonged weathering, clays transported into or developed in the cleavages expand seasonally to extend and widen the openings, or to initiate other fractures nearby. Innumerable folia open in the zone of gravitational movement, especially when there in creep. The surficial system of fractures, at least in crystalline rock, differs greatly from the system in buried, intact rock. Some foliation breaks in fresh rock at a tunnel heading are distinctly water-wet though not draining. This water probably does not exist there prior to stress relief, but rather, is imbibed by capillarity in certain openings connected to other fractures having sufficient storage capacity or transmissibility.

Joints

Billings (1942, p. 111) defines a joint as a divisional plane or surface that divides rocks, and along which there has been no visible movement parallel to the plane or surface. de Sitter (1959, p. 122) suggests that all transitions exist, from shear joints with no lateral movement, through joints with small movement, to small and then large faults. It seems likely that some, namely, the tension joints, fit the no-movement category, while others have moved so minutely that reference marks on opposite sides seem undisturbed.

Genetic classifications of joints have been advanced but none satisfactorily explain all complexities found in nature. It is usually assumed that joints and faults are closely related by a common origin in formation by orogenic stresses. Joints sometimes do, and other times don't, have orientations the same as faults in the same body. Another unresolved aspect is the remarkably uniform spacing often observed in joints. This has suggested tidal strain (Holmes, 1964) or earthquakes as propagating or triggering mechanisms for failure of a stressed crust.

Classifications are also possible on the basis of the orientation of a joint with respect to other joints, and with respect to fold axes or fault planes. It is widely recognized that shear joints sometimes come in conjugate pairs, the planes of a pair intersecting along a line parallel to the intermediate of three principal stresses, and the bisector of the smallest angle between the pair parallel to the major stress. The angle formed by a pair varies from 15 to 90 degrees, qualitatively agreeing with Mohr's failure theory, and depending, among other things, on rock type. Pincus (1951, p. 116) found no such variation between gneiss and sediments. Siegel (1950, p. 617) thinks anisotropy of fabric explains the common absence of one set of a conjugate pair (C. Meyer, personal communication, 1956). Figure 3-1, taken from de Sitter (p. 124), interprets a 90 degree change in the orientation of conjugate shear joints as a result of anticlinal tension and synclinal compression across the axes, while the stress

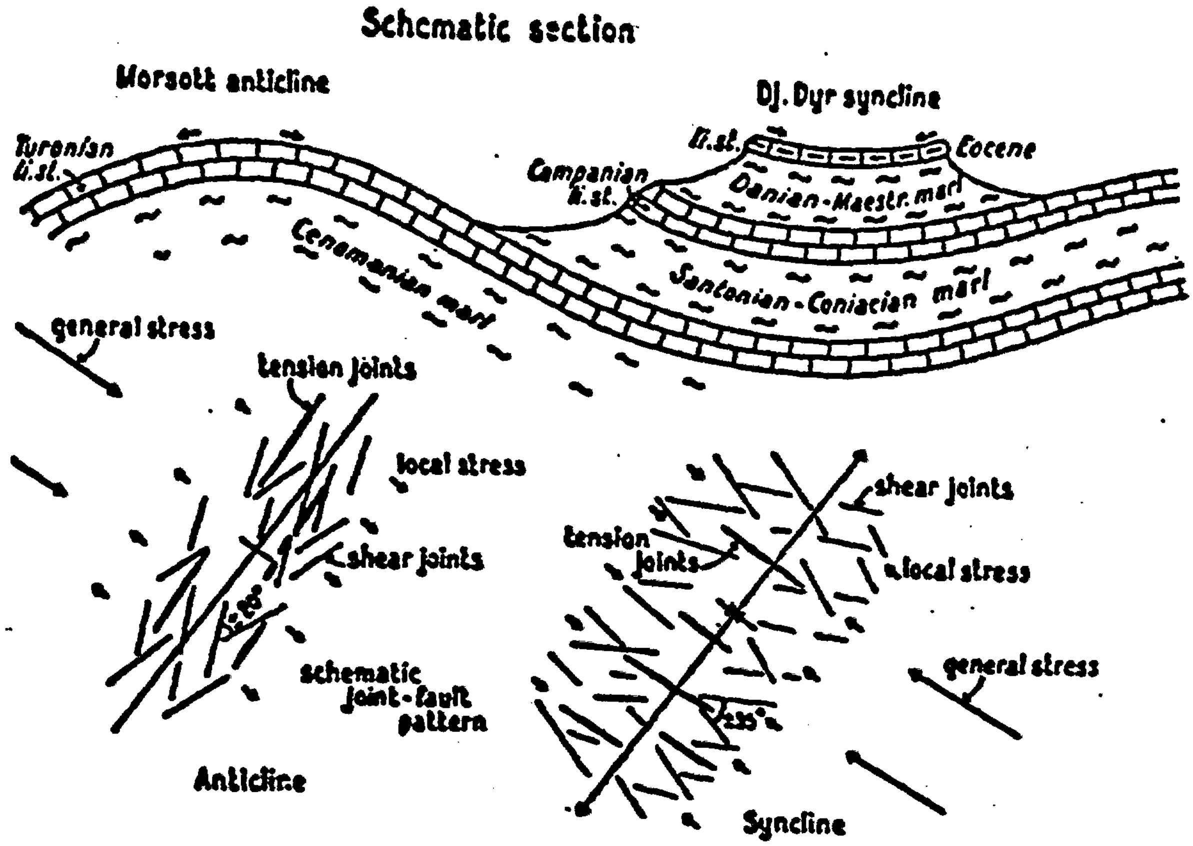

Figure 3-1. Plan and section of adjoining synclinal and anticlinal folds, SE Algeria, showing exchange of orientation of major and minor stresses according to the sense of flexural stresses (after de Sitter, 1956, p. 124, and by permission, McGraw-Hill Book Co.).

parallel to the fold axes remained relatively unchanged from one position to another.

Melton (1929) and Pincus (1951) each found that the directions of joint normals bear a more consistent relationship to bedding than to geographic axes. The directions of joints are not related to foliation (Pincus, 1951, p. 115). King (1948, p. 114) described an orthogonal joint system in sediments of the Guadalupe mountains. One set strikes parallel to the normal faults but rotates to maintain dips normal to the bedding. The set normal to the strike remains essentially vertical, normal to the bedding. King found the frequency of joints to be greatest near the faults.

In simply-folded regions, very persistent geographic directions are sometimes maintained. Figure 3-2, from Parker's (1942) study of joints in New York and Pennsylvania, shows the strike of paired shear joints (Set I) shifting slowly from NW to ENE as one traces fold axes eastward across the map. The joint directions change consistently with a reorientation of fold axes, but independent of local fold orientations.

de Sitter (1956) cites cases from the literature demonstrating parallelinity of joints to fault systems (Wölk, 1937) as in Figure 3-3, and others where they are clearly unrelated (Kwantes, 1946). It is sometimes important to differentiate sets of conductors according to relative age, for jointing in some cases preceeds and parallels faulting in the same stress field, while subsequent jointing or faulting may be inconsistent with the earlier. Joints may be classified in Anderson's (1951) scheme of fault types: normal, thrust and wrench, according to the orientation of principal stresses. Reoriented stress fields between faults, as indicated by higher-order fault systems described by Moody and

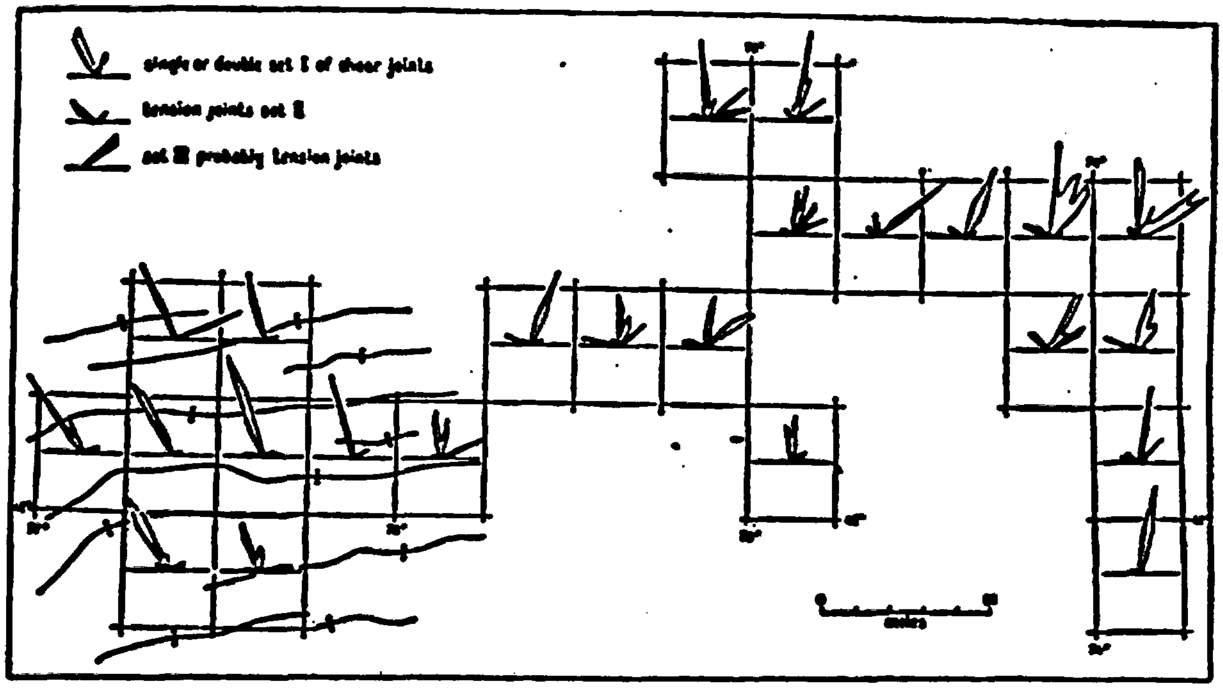

Figure 3-2. Map of portions of New York and Pennsylvania, showing joint strikes reorienting as the fold axes change direction (after Parker, 1942, and by permission, McGraw-Hill Book Co.).

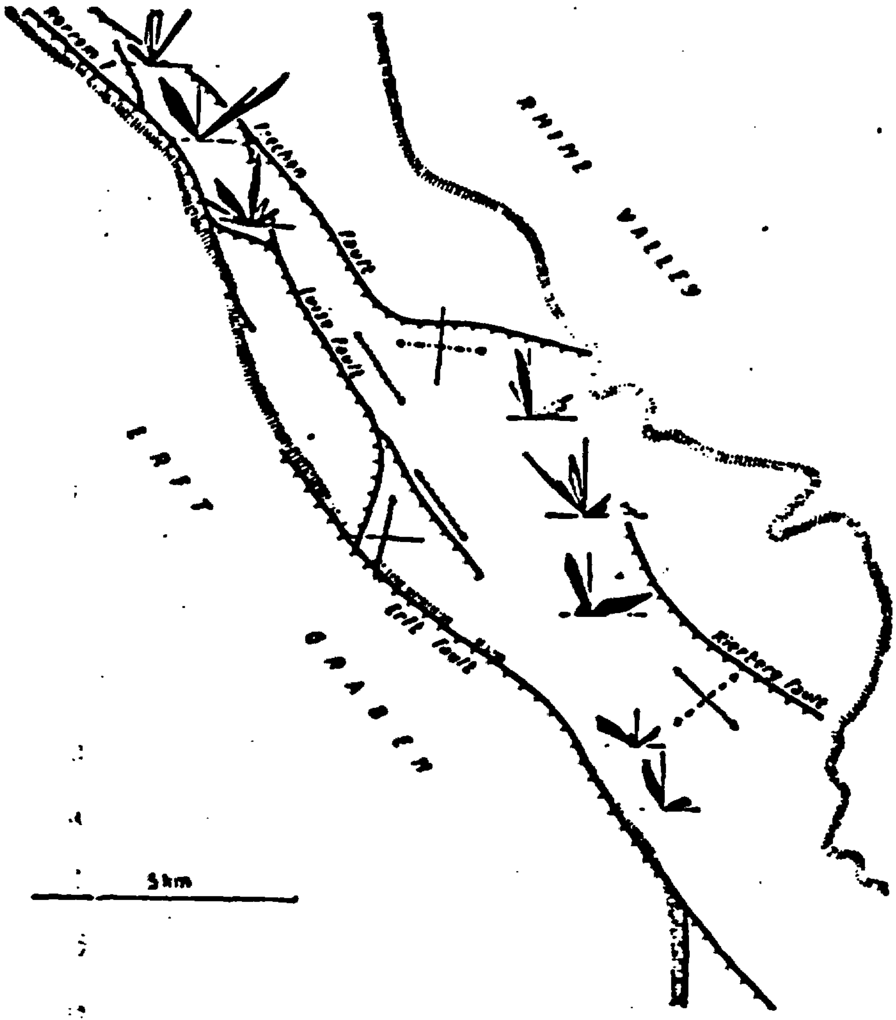

Figure 3-3. Map of the Villar lignite field near Cologne, Germany, showing joint strikes maintaining paralleinity to normal faults (after Wölk, 1937).

Hill (1956) are cause for the observed multiplicity and disper-
sion of joint sets, together with differences in rock strength and changes of stress over geologic time.

So-called tension joints are oriented either normal to the minor principal stress, or normal to the direction that has acted as major principal stress in forming shear joints. Tension joints are either vertical or horizontal, seldom inclined. Siegel (1950, p. 613) expressed the opinion that horizontal tension joints were impossible because the overburden would always insure vertical compression. If sheeting is not a tension phenomenon, it is caused by column bending moments under compression tangential to the ground surface. In Figure 3-1 are tension joints disposed normal to the minor stress, parallel to the anticlinal axis and normal to the synclinal axis.

Hodgson's work (1961B) on jointing in gently folded sediments of the Colorado Plateau is so thorough that it warrants summarization as a definition of the occurrence of joints in sedimentary rocks. Prominent bedding-plane discontinuities between tabular rock bodies distinguish sediments from crystalline rocks. Shear joints are apparently absent in sediments. Hodgson's analysis of sedimentary joint structures must be translated to other environments only with care.

His concept of a "structural rock unit" is important in visualizing boundaries of homogeneous joint systems: it is a "body of rock behaving nearly uniformly throughout its extent under like stress". It may be a formation or units of greater or lesser volume.

New and established terminology applied by Hodgson is wholly descriptive. It will therefore require no modification when the genesis of jointing is ultimately established. A joint is a fracture that traverses a rock and is not accompanied by any discernable displacement of one face of the feature relative to the other" (p. 12).

Systematic joints occur in sets, parallel or subparallel in plan but not necessarily showing similar relations in section. Systematic joints cross joints of other sets. They have straight or gently sigmoidal traces, a few inches to 400 feet in length. The traces become irregular at the ends, curving towards a neighboring joint, which it may join at right angles. These termini are non-systematic (unoriented), often bifurcating. The surface area of a systematic joint may be a few square inches, up to hundreds of square feet. Surfaces appear to be nearly equidimensional in thick rock units, may be wholly contained in the unit, or elongated if the unit is thin, but many individual thin beds may be cut by a single joint. Some systematic joints cross boundaries between very different rock units, such as massive sandstone and thin-bedded shale, but the joint spacing changes at the boundary: wider in coarser, thicker bodies, closer in fine-grained, thin bodies. Parallelism depends on constancy of lithology, most perfectly developed in massive sandstones and some limestones. The orientations of planes are more dispersed in siltstones or flaggy shales, increasingly so in lenticular, coarse-grained, poorly-bedded units. A systematic joint set occupies a demonstrably limited geographic area of a few square miles, often overlapping areas occupied by other sets. Angles of intersection between sets are fairly constant when viewed in plan, but dip orientations may vary up to 25 degrees from the normal to bedding, so that one set cannot be differentiated from another set if viewed in section. The writer believes that joints should be identified according to sets after plotting their poles in stereographic projection, not in plan or sectional view. Hodgson reports no mutual interference or dislocation at intersections of two systematic joints.

Non-systematic joints abut normal to systematic joints, but have variable angles of intersection with other non-systematic joints. They are curved in plan, and either curved or straight in section, depending on the thickness of the rock unit they cut. Though they attain great dimensions in units, they are seldom observed in outcrop, for they weather and open by weathering less readily than systematic joints. Cross-joints are a planar variety of non-systematic joints, also terminating at bedding or systematic joint surfaces. It might be inferred from Hodgson's description of non-systematic joints, that they have imperfect hydraulic continuity since they are tighter. Yet they are more rough and irregular than systematic joints, so may provide important continuity in single-set systems. A significant continuity notion is the "joint zone". Seen in plan, parallel systematic joints often occupy a narrow belt wherein individual joints are slightly offset from one another (en echelon). The frequency of interruptions along a zone is nearly a constant for a structural unit, increasing with the thickness of the unit. The individual joints terminate irregularly, sometimes hooked into and normal to each other. Joint zones are separated by a predominant spacing characteristic of the set.

Joint sets have great aerial persistance and regularity in plan and spacing. Up to six sets occur at any one place. Where Hodgson studied them, systematic joints extend vertically through Paleozoic and Mesozoic formations. The sets are unrelated to fold axes except by rotation about those axes.

Origin of Jointing

The geometry of several co-existing sets cannot be explained by conventional tectonic shear or tensional origin. Hodgson detected no slickensided shear surfaces. He cites evidence that joints form very early in the depositional history of a sediment: Jointing may exist in young unconsolidated soils, such as Lake Bonneville claybeds, "wet" Miocene claybeds in Maryland, or lignite beds among soft sands. His hypothesis is that joints are upward extensions of pre-existing fractures, formed as soon as the rock is sufficiently brittle to fail by tidal fatigue. Plafker (1964) gives further evidence of the extension of joints maintaining basement orientations, propagated upwards through unconsolidated alluvium to control rectangular drainage and lake shores in eastern Bolivia.

The role of pore pressure as a contributing cause of jointing has been neglected. The existence of high pore pressures approaching the total overburden load at depth has been established from oilwell experience (Hubbert and Ruby, 1959). While pore pressures are insufficient cause for jointing, isotropic excess fluid pressure (Terzaghi, 1925) results in low effective or intergranular rock pressures. Pore pressures are applied throughout long periods of time, even in crystalline rocks of very low primary permeability. Other stress sources, tectonic, tidal or thermal, can therefore more readily trigger either shear or tensile failure. Total stress must be compressional in all directions, but need only fall below the pore pressure by an amount equal to the tensile strength for failure to occur. The marl aquicludes shown in figure 3-1 would promote high fluid pressures under heavy overburden, making the limestones sensitive to flectural reorientation of principal stresses. The so-called tension joints oriented normal to the axis of greatest stress are called release, or extention joints. In figure 3-2, the E-W joints are of this type, thought to originate upon elastic release of compression. One cannot invoke isotropic remanent pore pressures as their cause, because as the major stress declines, tension would arise in the direction of also-declining minor stress. The origin of steep-dipping "extension" joints remains enigmatic.

Tension cracking was modeled mathematically by Lachenbruch (1961, p. 4286), who concluded that the common physical properties of rock should preclude tension joints below depths of about 900 feet. Yet, there is field evidence, cited in this chapter, to indicate openings to thousands of feet, or more if the brines described by Smith (1958) and White, Anderson and Grubbs (1963) are indeed partly magmatic in origin. Pore pressure is possibly the mechanism accounting for propagation and preservation of such openings to great depths.

When failure takes place, there would be an immediate drop in pore pressure along a fracture, thus an increase (not a release) of effective compression across a tension joint. Joint faces do not separate upon rupture, as they would if tension existed in the solid phase. With correspondingly low fracture conductivity, fluid pressure-drops would be slowly transmitted along a fracture. Adjacent rock masses would have unaltered neutral and effective stresses for some time, during which succeeding fractures form. Hodgson (1961) noted that the spacing of systematic joints is uniform within a structural unit and varies directly with coarseness of sediment grain-size. Spacing may logically be related to rock permeability, manifested by grain-size, for when intergranular permeability exceeds fracture conductivity in transmitting a failure pressure-drop, the distance to adjacent joints may be governed by the transient. Failure is unlikely in the region of relieved pore pressure, extending laterally at a rate proportional to permeability and inversely to porosity.

The suggested role of pore pressure in joint formation has yet to be fully explored, but its inclusion as a component of tectonic and gravitational forces may suggest a theory of jointing consistent with such field evidence as Hodgson (1961) has collected.

Microscopic features of joint surfaces

Surface texture can be used in some cases to distinguish tension from shear joints. When both types are present one can often, but not invariably, show that the tension joints are rough and irregular pull-aparts, while shear joints have relatively smooth, sometimes fluted and polished, tight contacts. Chlorite, sericite or epidote coatings are sometimes found on shear joints (Moye, 1959, p. 26; Lyons, 1960). The textural contrast may depend upon confinement at rupture, since many joints of shear orientation are rough and wholly lacking in evidence of lateral movement (King, 1948). D. G. Moye (personal communication, 1963, 1959, p. 26) has noted a hydraulic distinction between the two types, tension joints being the more conductive. Granular debris is produced on both fracture types in laboratory rock tests, but the debris is coarser in tension breaks than shear breaks. The writer has observed that on rough surfaces of tension joints opened in the laboratory, there are dislocated but attached grains as well as free particles. Thus the faces never reseat within less than one thousandth of an inch, as measured by micrometers attached before separation. Griggs, (1936, p. 555) envisions laboratory fractures as an integration of minute shear and tensile fractures, thus having variable aperture. Brace (1963, pp. 2-38, 39) reports that oblique shear failure of confined specimens develops first a milkiness along an oblique zone, then little en echelon

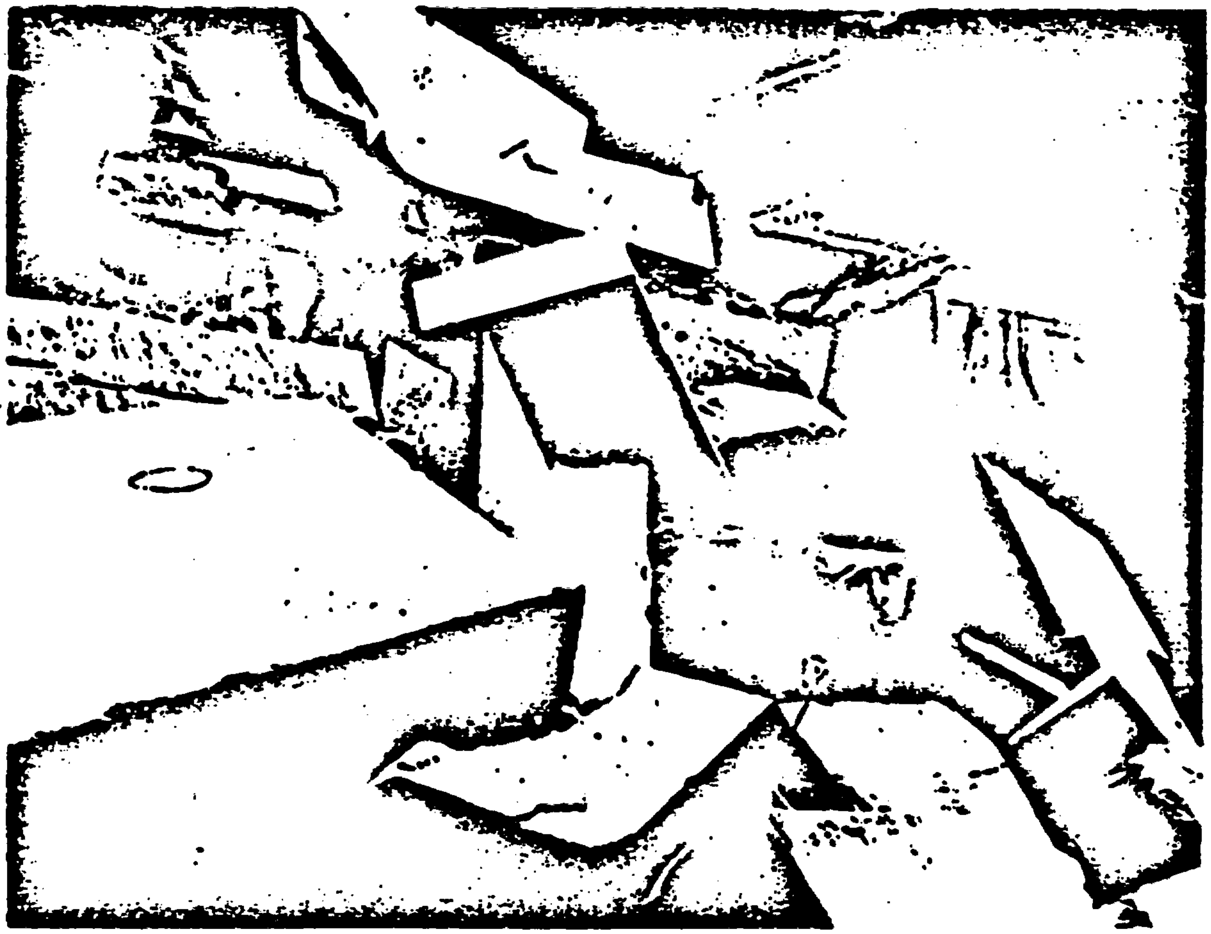

Figure 3-4. An orthogonal system of continuous fractures in massive sandstone: Smooth continuous (horizontal) bedding planes, rough, plumose tension joints (facing viewer's right) and smooth shear joints (von Engeln, 1961, by permission, The Cornell Univ. Press).

grain boundary cracks that coalesce to form the rupture surface. Fine pulverized grains can be brushed from the surfaces. The size of such detritis, or of dislocated grains attached between the en echelon cracks, probably determines the minimum apertures. Greater apertures may result from wedge action on the surface irregularities. Figure 3-4, taken in the western area of Parker's map, shows the perfection and extensiveness of planar joints found in some rocks and the textural contrast between smooth shear and rough, feathered tension joints.

Plumose surface structures consist of low-relief joint markings similar to the pattern made by two feathers in line, with their butt ends joined. Woodworth (1897) called it feather fracture, Parker (1942) called the features "plumes". Radiating features are described also, by Woodworth (p. 166), Raggatt (1954) and Hodgson (1961A, 1961B, p. 20). The plume structures might be described as sharp, irregular ridges of amplitude and wave length on the order of a few grain diameters arranged in conjugate families of hyperbolas having a common directrix parallel to, and superimposed on the long axis of elliptical, concoidal ridges of greater amplitude, longer wave length and smoother wave form. (See Hodgson, 1961B, Figure 25). The directrix or long central axis of the structure is usually parallel, but sometimes normal, to the boundaries (bedding) of a structural unit. Opposite fracture faces are tight-fitting until disturbed, and show no evidence of transcurrent movement. Similar tension and fatigue failure surfaces have been observed in metals. The extremities of the elliptic pattern are coarser textured, terminating in en echelon, oblique "terminal offset faces" (Hodgson, 1961B, p. 21). The scale of the texture is proportional to the size of the joint surface, and thus to the thickness of the structural unit. The pattern is usually, but not always, centered in the unit, for joints normal to the bedding. Hodgson does not substantiate the idea that the center of the structure is the point where failure began. The writer feels that the en echelon offsets at the periphery are consistent with Brace's (1963) observations on failure, and that the plumes grow inward from the discontinuities.

Miscellaneous geometrical types of joints

Joints with thrust fault orientations intersect bedding along lines parallel to fold axes but at acute angles to the bedding planes, since the major compressive stress tends to follow the dip of the beds. Moderate-dipping conjugate joint sets in granite rocks may also be of this sort, arising when the overburden pressure is the minor stress. Whether or not they are actually shear joints is questionable, for they are usually planar, rough and lacking lineation. de Sitter has plotted all the possible joint directions relative to a fold axis. His stereonet is reproduced here as Figure 3-5.

Short joints, normal to competent beds of a hard-soft alternating sequence, are called rotational joints, and are believed due to the bedding plane shear developed on the limbs of folds. Normal faults and tension joints are also found at the necks of boudinaged competent beds.

Concentric stress systems developed around isolated intrusions are superimposed on horizontal regional stress systems. The doming process (Wisser, 1960) results in radial and tangential tensile stresses, expressed in apical grabens, cone-sheets and radial fractures or dikes (Billings, 1943; Anderson and Jeffreys, 1936) over plutons or salt domes (Hanna, 1934). The details of such structures are important guides to ores (Newhouse, 1942) because experience has shown that mineral veins often form

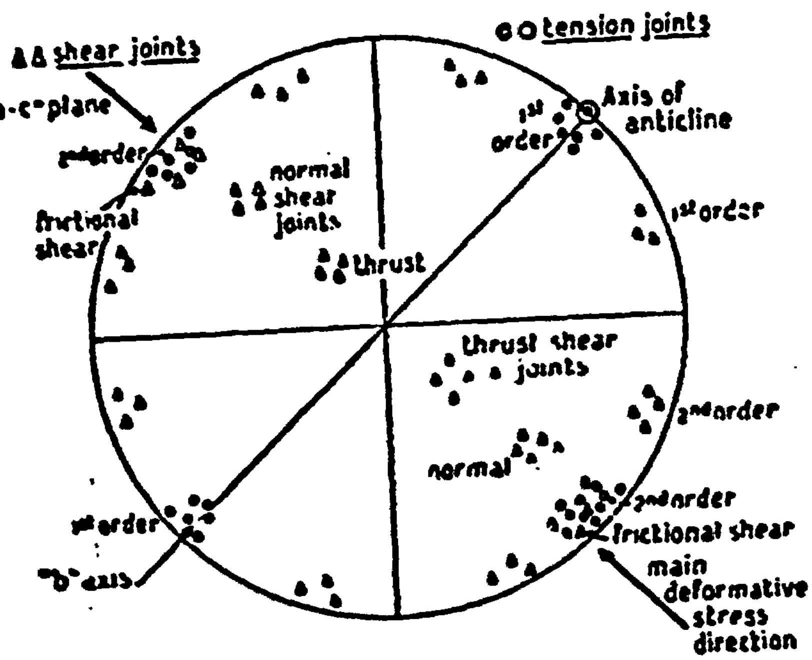

Figure 3-5. Stereographic projection of the normals to joint-plane orientations genetically related to tectonic stresses (after de Sitter, 1956, by permission McGraw-Hill Book Co.).

normal to tensile directions. An analysis of domical structures for their unique arrangement of conducting fractures would help mineral exploration, since ores are fluid-borne. Work on this problem may be stimulated soon by the need to engineer the production of steam and brine from similar structures.

Columnar contraction joints of regular pattern are common in basaltic lava flows, and more crudely formed in breccia flows and welded tuffs (Gilbert, 1938). The model of permeable jointed media (Chapter 6) is not designed for such discontinuous conductors.

Sheeting is an important joint class, dominating the occurrence of water in some areas. These are extensive, flat to gently curved or undulating seams or partings found in massive rocks, especially granite (Jahns, 1943), but also in quartzite, limestone, and probably in some metamorphic rocks. Sheeting is most conspicuously developed near the ground surface, conforming generally to hills and valleys alike (Gilbert, 1904). Frequency decreases with depth, for sheeting is seldom found below 300 feet. The lateral extent is generally hundreds of feet, where they abutt older steep joints or faults, or where they feather out as neighboring fractures converge. The fractures cut indiscriminately across all primary structures, dikes, contacts, country rock, etc. The sheets of unjointed rock between seams are under compression parallel to their extent, as evidenced by "popping" (Terzaghi, 1946), or by sudden splitting or lateral movement into quarry excavations. Watson (1910, p. 24) has observed polished and striated joint surfaces in granite, possibly due to translation upon surficial release of stress. Whatever the deep-seated cause of stress, the sheet-structures are believed the result of relief from confinement by erosion of overburden, as suggested by Gilbert (1904), Matthes (1930), and Jahns (1943). Bending of sheets under column loading accounts for sheet joint openings of several inches (Matthes, 1930, p. 114). Some very deep horizontal cracks are permeable, for mineralization has been seen on them (Farmin, 1937, p. 626). Highly conductive, flat undulatory joints in slate, metavolcanic and a serpentine complex at the Merced River damsite, are probably of the same origin as the more obvious sheet structures in massive rocks. In the Southern States are extensive horizontal joints (Watson, 1910, p. 24) through granitic and metamorphic rock, to which LeGrand, (1949) attributes most of the fracture permeability of the region.

Terzaghi (1946), has listed as guides some joint characteristics associated with different rock types. The more brittle rocks tend to have closer joint spacing than ductile rocks. For example, rhyolite shows more frequent, irregular jointing than basalt. Massive rocks tend to have less continuous joints than tubular rocks. Sediments usually have three sets: the bedding, and two others normal to the bedding. Joints in limestone and sandstone are commonly several feet apart, shale much closer, down to fractions of an inch. Rebound in shale produces slickensiding on minute, conchoidal fractures. No water could be found below 500 feet in jointed Triassic shales of New Jersey (New Jersey, date unknown).

Spacing of fractures has attracted little attention of field geologists. King (1948) found that spacing is closest for rocks of greatest deformation, but the more brittle rocks have closer spacing under like circumstances. Pincus (1951, p. 92) found no correlation with degree of deformation in pre-Cambrian and Paleozoic rocks of New Jersey. Hodgson's observations (1961B) are described above. Changes of spacing with depth have been surmised by Tolman (1937), King (1948), Müller (1933), and Pincus (1951). The consensus is that weathering opens pre-existing weaknesses. King, (1948, p. 114) noted vertical joints extending as much as 1100 feet, in the vertical sense, down cliff faces. Appleby (1942) found that the pattern of fractures on dynamited faces corresponds closely to natural patterns. The writer's belief, based on analysis of pump-test data in chapter 6, is that porosity increases towards any free face, both by increase of fracture apertures and frequencies. The rock around the drill-hole is more akin to the undisturbed state than that exposed in mines, tunnels, or quarries.

Evidence of fluid conductivity of joints and faults

Joints are the most important class of conducting fractures. This is because one type or another, or several types at once, are present in practically all consolidated rock types. Faults are so infrequent within the boundaries of most problem areas that they can seldom be treated statistically. Cleavage is confined to metamorphics.

Tolman (1937, pp. 291 to 313) differentiates deep-seated fractures (faults and some shear joints) from superficial ones opened by weathering. He believed that the water table limits the zone of weathering. In Turk's (1963) study of well yield variation with depth, a weathered zone was assumed to act as an infiltration and storage bed just as Tolman suggested, but the continuously varying well-discharge measures did not support the notion of a demarkation. Rather, a continuous variation of permeability with depth was shown. Lewis and Borgy (1964) conducted well-pumping tests in jointed phyllite. Plots of the draw down - log time relationship proved never to be linear in the way indicated by theory and experience in unconsolidated aquifers. A continuous decrease in permeability with depth is suggested by the continuous curvature of their plots. The statistics of pump tests reported in Chapter 6 has proved that the preponderance of joints visible at the surface are insignificant as conductors at depth.

The few conductors existing below the water table, Tolman considered largely unconnected. It is the writer's belief, from some experience in dam-site exploration, that isolated water bodies are more likely in the weathered zone where clay deposits plug some parts of wide openings, and leave other parts open. Drill holes at McSwain damsite, Merced River, California, penetrated many weathered joints, often filled with an inch or so of red clay. Instantaneous bit advance, sudden loss of drilling water, high pump test discharge and crystal-covered joint surfaces on recovered core ends indicated large open joints, connected to the rest of the system. In other joints, apparently unfilled, no water flow developed, suggesting localized clay fillings.

There are a few cases described in the literature (Townsend, 1962; Thayer, 1962; Moye, 1959; and Stewart, 1955), for example, where drawdown at a line sink produced recognizable cones of depression, or other indications of continuity. These cases support the assumption made in designing a mathematical model (Chapter 6) having wholly continuous intersecting plane conductors. A worthy topic of further research would be to ascertain at what length-to-spacing ratio do discontinuities become important to the overall permeability of such a model.

The report of E. J. Daniel (1954) on the Persian Gulf oil fields contains some of the best available subsurface data on fractured limestone. The Ain Zalah field produces wholly from fractures without solution enlargements, so continuous and interconnected that a few suitably placed wells could drain the entire reservoir. Oil moves as much as 2 miles distant from a well, and bottom-hole pressure recovery is rapid upon shutin. There is hydraulic connection between the First Pay and Second Pay, though separated by 2000 feet of non-productive fine sediments (p. 778). Open fractures without solution enlargements must extend over 3000 feet in depth. Joints and bedding-planes are infrequent but vital conduits, most of the production being in calcite-veined, highly fractured (6-12 per foot) bodies of rock. It is not known how much fracture permeability is due to fractures that were never recrystallized, versus fractures reopened by recurrent tectonism. The more brittle, cherty limestones are more intensely fractured. Similar vein-frequency, water permeability relationships are recorded in mining districts (See below). The permeability in the Ain Zalah structure is not restricted to tension joint openings, for there have been observed oil films on hair-thin breaks, stylolites, slickensided fractures, and faces of calcite crystals. Some undisturbed (?) joints cutting cores have openings of 0.1 to 0.2 mm., carrying oil films.

The Kirkuk field produces from super-capillary openings so continuous that the entire field acts as a single pressure sink. The maximum water-edge rise is 25 miles away. Permeability is so high that a single well can produce 30,000 bbl. per day with only 3 to 4 psi drawdown. Caverns (up to 14 feet), residual dolomite sand and solution-opened planes provide storage (up to 30 percent porosity), but joints and a few faults provide the interconnections. Even the tight, slickensided faults have oil films. Joints are spaced 1-1/2 to 3 feet, essentially orthogonal, with "intact" (?) openings of 0.1 to 0.2 mm. Surface textures accord with grain size: rough in coarse rocks, smooth if porcelainous rocks.

Large joint openings at great depth are not peculiar to limestones, but may be encountered in igneous and metamorphic rocks also. T. Gross (personal communication, 1964) drilled horizontal holes for water in the pre-Cambrian crystalline complex west of Colorado Springs, attaining 50 gal. per minute discharge and almost instantaneous pressure recovery on shutin. Production may be from one or more large openings (1 mm. or so) of great extent (thousands of feet).

One of the richest mines of structural data pertinent to the occurrence of water in consolidated rocks is Newhouse's (1942) treatise on guides to ore. Interrelations of faults, folds, joints and rock type have been investigated more thoroughly for vein deposits than would ever be economically justified for water occurrence. The preservation of structural detail by mineralization in openings, once fluid-filled, is more advantageous for present purposes than would ever be a like investigation of fluid-filled openings that are sensitive to disturbance. Progressive opening of mineral veins upon successive refilling invalidates any quantitative measures that might be made on them. "Book" quartz veins indicate progressive enlargement. Yet the contention that ores take great spans of time to form from dilute solutions is refuted by the recent discovery of hot brine at Nyland, California, containing up to 300,000 ppm total dissolved solids, including remarkable metal concentrations (White, Anderson and Grubb, 1963). An 8-inch well discharge pipe at the surface closed to 3 inches by encrustation in 3 months of free flow. Thus, veins could form quickly, as reckoned by geologic time, and their thickness could resemble the fluid-filled apertures. Caution dictates the assumption that openings are formed progressively, no matter how rapid, for Newhouse, (1942), Wisser (1960), and other authorities have demonstrated that veins form concurrent with orogenic movement. Structural guides to ore are valuable guides to meteoric water occurrence whether or not mineralization has taken place. Mine waters tend to follow paths of prior mineralization, as observed by the writer at Cerro de Pasco, Peru. (D. T. Snow, private report, 1958) The best water well prospects in the California Mother Lode rocks, metamorphics of very low permeability, are the quartz veins that have been refractured by post-mineralization deformations.

If vein deposits are qualitative indicators of water-conduit geometry, it must be concluded that a model composed of uniformly-spaced, parallel-plate conductors only approximates the irregular, pinching and swelling, discontinuous features seen in mines. Fractured media must have extreme inhomogeneity if the conductors are as capricious as vein deposits.

Mineral veins indicate open conduits at some time past. Hot springs, with or without accompanying zones of hydrothermal alteration, are the surface expressions of similar modern permeable structures. Since communication to heat and mineral sources is accidental, it is inferred that meteoric water occurs in innumerable regions of high permeability just like the ore districts. Ore guides from Newhouse (1942) therefore constitute pertinent guides to groundwater, summarized here for fractures and faults:

Veins form along fractures where normal compression is low compared to other orientations or positions. Those showing no relative movement parallel to the plane of the break are conventionally called tension fractures. These may form part of a pattern, some of which are fractures and some faults. Isolated tension fracture fillings prove that the shear breaks must also be permeable to a lesser degree, otherwise the tension veins could not fill. Tension fractures may cross from one side of a fault to the other, extending into one or the other of the walls. "Feather" fractures are inclined to a fault plane, intersecting along a line normal to the slip and making an acute angle pointing in the direction of relative motion (Billings, 1942, p. 124). Wisser (1939, p. 301, 318) says that tension fractures are located along portions of a fault where the greatest, rather than the least compression acts normal to the walls of the fault. Varying contact pressures result from the ill fit upon dislocation of irregular fault surfaces, high friction there resulting in high tensile stresses in a direction oblique to the fault. Figure 3-6 illustrates the location of feather fractures at fault deflections. Gouge is more apt to form than breccia on faults subject to high normal stress. Thus feathers are often associated with gouge in fault zones.

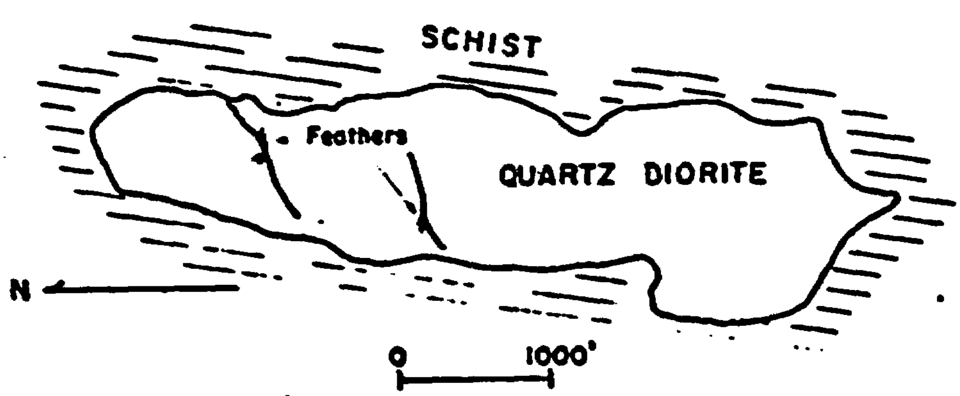

Figure 3-6. Deviations on shear faults cause feather fractures at loaded contacts, Hog Mountain Mine, Alabama (after Wisser, 1939).

If a dip-slip fault changes dip with dip, feather fractures strike parallel to the fault. If a dip-slip fault changes strike with dip, feather fractures strike parallel to the dip. They are more prevalent in the hanging wall, perhaps due to unsupported spans.

There are guides for locating changes in the orientation of faults, and therefore, permeable wall-rock, but these criteria are reserved for the paragraphs on fluid conductivity in faults. The importance of faults in predicting regions of high permeability has long been recognized because joint frequency often increases towards faults (Terzaghi, 1946; King, 1948).

The parallel-plate model for fractured media was not intended for fault systems, solution-enlarged joint systems in limestone, or for primary openings in lavas, but attempts to so apply it may be better than nothing. The scope of this summary does not include all environments, but of the three just mentioned, faults will be discussed further because of their close relationships to joints.

Hydrologically significant features of faulting

Faults "are often open to a greater or less degree...In many instances where a fault zone is developed with many subparallel and sometimes branching and anastomosing fissures, especially in harder and more brittle rocks, large quantities of water may be transmitted..." (Louderback, 1950, p. 129). We may look to Newhouse (1942) for the more detailed criteria for detecting where and what faults will be aquifers or aquicludes. Completely mineralized faults are aquicludes but even these are subject to reopening upon reactivation of tectonism.

More often than not, faults are tabular zones of crushed rock rather than distinct single breaks. If uniform in character throughout their extent, they could be replaced by single openings that would conduct the same fluid discharge at the same sub-critical gradient. Deviations from uniformity are believed more serious in the case of faults than of joints, for the granularity or gouge-content of faults is notably variable, the main conducting fractures forming an anastomosing pattern within a zone of variable thickness and gouge content. Faults are best characterized as inhomogeneous-anisotropic planar conductors, but in the absence of specific or general research on the properties of faults, it can only be assumed that they are homogeneous and isotropic.

Portions of faults locally deviate in orientation towards the plane of minimum compression, so certain portions tend to open upon fault displacement. In the case of deflected joints, they may open wider due to fluid pressure acting against lesser rock pressure. The cause of deviations is usually a contrast in rock deformability. In geological parlance, one rock is more "competent" than another if its strength or rigidity is greater, failing more brittle than ductile. Just as laboratory compression tests show failure at angles more acute to the applied deviator stress as the Mohr's failure envelope steepens, so too do faults refract towards the normal upon passing from incompetent to competent rock. Subsequent relative movements along the ill-fitting surfaces result in load concentration on some areas, and voids elsewhere. Figures 1 to 14 of Newhouse (1943) illustrate general and specific cases. If the geometry of the fault surface and the net slip are known from exploration, the open portions may be predicted. Table 3-1 lists the circumstances possible. Definitions of the terms may be found in the AGI glossary (Howell, 1960) or Billings (1942).

Table 3-1

Fault Permeability due to Relative Movement of Irregular Surfaces (abstracted from Newhouse, 1943)

Circumstances	Where openings form
I. Dip Slip Faults	
a. Change of angle of dip along the line of dip.	
1. Normal faults	Where fault steepens, competent formations if flat contacts; incompetent formations if steep contacts.
2. Reverse faults	Where the fault flattens; incompetent formations if flat contacts; competent formations if steep contacts.
b. Change of angle of dip along the line of strike.	
1. Normal faults	Where fault steepens; competent formations if flat contacts; incompetent formations if steep contacts.
2. Reverse faults	Where fault flattens; incompetent formations if flat contacts; competent formations if steep contacts.
c. Change of strike along the line of dip.	
1. Normal faults 2. Reverse faults	Where changes favorable to openings, various possibilities due to deflections towards normal to contacts with more competent rocks, openings on parts oriented more normal to slip direction.
d. Change of strike along the line of strike.	No tendency to produce openings.
e. Combinations of a., b., c., and d.	Most common cases.
II. Strike Slip Faults	
a. Change of dip along the line of dip.	No tendency to produce openings.

Circumstances	Where openings form
b. Change of dip along the line of strike.	Where a portion of a fault is out of the general plane of bearing surface: flatter dipping hanging wall moving over steep dipping footwall, or steeper dipping hanging wall moving over flat footwall.
c. Change of strike along the line of dip.	Where a portion of a fault is deflected out of the general plane of bearing surface: bearing pressure on portions most normal to slip direction, openings on portions parallel or away from slip direction.
d. Change of strike along strike.	Same as c.: fault crossing steep contact, openings in competent or incompetent formations depending on angle of incidence, and if right or left-lateral slip.

Surface areas of high and low bearing pressure can be discriminated on the basis of subtle changes in fault attitude near contacts, and knowledge of slip direction. *Figure 3-7 illustrates case IId.* Evidence from mines favors openings on faults of small displacement, for if throw is great, areas of misfit configuration are overpassed or gouge-filled. Loading patterns also localize subsidiary faults, fractures and brecciation in the wall rock at positions of high stress, thus, wall rock permeability is apt to be high adjacent to fault segments having low permeability. Exceptions are found in positions where bridging is conducive to wall fracturing in tension. Wall rock fractures associated with dip slip faults tend to be parallel to the strike if the fault changes dip along the dip, and conversely, fractures tend to be parallel to the dip if the fault changes strike down the dip. As will be seen, (Chapter 5) if fracture orientations are known, principal axes of permeability may be predicted.

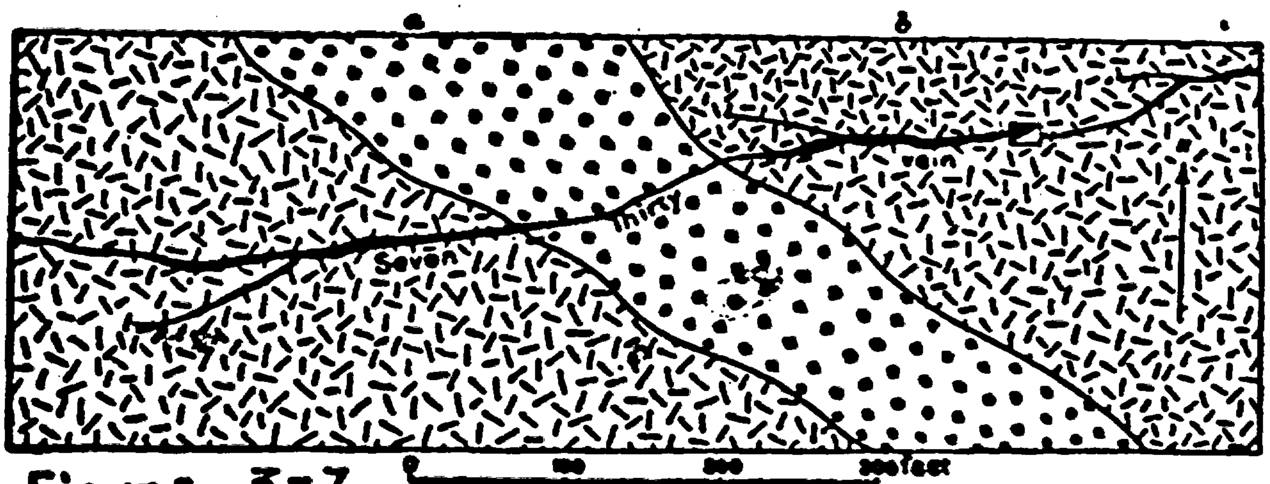

Figure 3-7

Fault deflection. Seven Thirty Mine, Silver Plume District, Colorado. (a) Quartz monzonite porphyry; (b) granite. (Spurr. U.S.G.S. Prof. Paper 63. Fig. 48)

Gouge in faults renders them relatively impermeable. The presence of aluminous rocks favors development of gouge, so formations having platy minerals, small grain size, low strength or high state of alteration tend to have relatively low fracture permeability. Gouge is prevalent in faults developed under high normal compression, such as flat, normal faults, steep reverse faults, or in faults of great displacement.

There is a debatable relationship between fracture permeability, (or rather, ore occurrence) and position with respect to folds. The biased data of ore occurrence suggest that anticlines are more broken and open than synclines. There is quite definitely greater fracturing near the crest of folds than near the flanks. Fault deflections are more prevalent near fold axes.

The rock type is an indicator of comparative fracture permeability. Lacking permeability measures, one may be guided by the occurrence of vein ores (Table 3-2) in contrasting rock types. "Favorable" and "unfavorable" rocks are equated, respectively, to relatively high and low permeability in the tabulation (Newhouse, 1943, pp. 41-43). For the most part the favorable rocks are the competent ones, thus, the table is also a guide to fault deflections.

Table 3-2

The influence of rock type in localizing vein deposits, an indicator of comparative fracture permeability.

Place	Favorable Rocks	Unfavorable Rocks	Significant features remarked by contributors
Oatman & Katherine Districts, Arizona	Rhyolite-Andesite	Trachyte	Brittleness or ability to shatter was important factor.
Georgia Gold Deposits	Hard brittle rocks	Soft rocks	Ore shoots are in hard brittle rocks; the surrounding rocks are soft and flow readily without fracturing.
London Mtn. Area, Colorado.	Porphyry sills, brittle limestones & quartzite	Shales	Shales deformed plastically; other rocks were brittle.
Silver Islet, Ontario	Diabase or other brittle rock		
Edwards-Balmat Mines, New York	Brittle silicated bands in limestone		The brittle silicated bands in the limestone were brecciated during flowage of the limestone. Some ore shoots related to these bands.
Siscoe Mine, Quebec	Granodiorite	Schistose lava flows	Granodiorite more brittle and hence more fractured.
McWatters Mine, Quebec	Conglomerate	Fine grained tuffs	Conglomerate more competent and under stress yielded by fracturing more than did the tuff.
Cadillac Township, Quebec	Competent rocks	Soft schists	Ore bodies are in persistent fissures in the competent strata adjoining the main shear zone. The soft schists were too incompetent to maintain

Place	Favorable Rocks	Unfavorable Rocks	Significant features remarked by contributors
			large or persistent openings for vein formation. However at the Lapa Cadillac mine pipe-like ore bodies containing little quartz but much disseminated sulphide occur in a wide zone of schist.
Porcupine, Ontario	Competent rocks, massive andesite or dacite. Conglomerate thick beds graywacke & porphyry bodies	Incompetent rocks. Tuffs, slates, soapstone, pillow lavas, chlorite carbonate schists	Veins in competent rocks. (A) Single vein fractures usually pinch out when they pass with divergence of strike into an adjoining incompetent horizon. (B) The multiple fracture zones may be in a competent member between relatively incompetent members, or in a competent member adjoining an incompetent member.
Brittania, British Columbia	Competent volcanics	Incompetent slaty tuffs	The competent volcanic rocks were brecciated and fractured giving channel-ways for solutions. The incompetent slaty tuffs in the foot wall were a good lubricant and facilated brecciation in the competent volcanics.
Mother Lode, California	Competent or rigid rocks (greenstone, graywacke) in hanging wall, with	Slate	Ore tends to be localized under a hanging wall of the more competent or rigid rocks where the foot wall

Place	Favorable Rocks	Unfavorable Rocks	Significant features remarked by contributors
	slate foot wall		of the vein is of plastic and easily fractured slate.
Little Long Lac Gold Mine, Ontario	Arkose or feldspathic quartzite	Graywacke	The graywackes above and below the arkose were rendered schistose by shearing and offered fewer and less continuous openings.
Thunder Bay, Ontario	(1) Weak beds	Competent beds	Fracturing may take place in weak beds, more competent beds being unfractured.
General Two Cases	(2) Competent beds	Weak beds	Under more extreme conditions shear zones develop in competent beds and zones of schistosity in weak beds. Thunder Bay gold veins in this group.
Breckenridge, Colorado	Quartzite	Shales	More open fissures in the relatively competent quartzites and consequently ore deposits are in these rocks.
Front Range, Colorado	Quartzite Porphyry	Porphyry Shale	Competence of quartzite much greater than that of schists and shales.
	Porphyry Granite Aplite	Schist Porphyry Coarse grained Boulder Creek granite	
	Diabase	Boulder Creek granite	
	Granite with layers of the less competent metamorphic rocks	Large masses of granite free from schist xenoliths	
	Granite	Schist	
	Aplite	Schist	

Place	Favorable Rocks	Unfavorable Rocks	Significant features remarked by contributors
Questa, New Mexico	Albite granite	Schist and metamorphosed sedimentary rocks	The weak schist and sedimentary rocks could not maintain openings.
Hot Springs, Barite District, North Carolina	Massive rocks Granite Quartzite		Barite in fracture and breccia zones along faults in massive rocks. The other rocks were made schistose.
Sheep Creek, British Columbia	Quartzite and hard argillaceous quartzites	Limestone, schist	The smaller fractures disappear on approaching the limestone or schist. Stress was taken up in these rocks by deformation (flowage) rather than by fracturing.
Takatama Mine, Japan	Tuff and breccia	Shale	Veins pinch out in shale which overlies the tuff and breccia.
Southwest Arkansas Quicksilver	Sandstone	Shale	Shales flowed while the sandstones were fractured and brecciated.
Granada Mine, Quebec	Conglomerate	Syenite porphyry	Quartz vein in both rocks. Gold negligible where vein is the more competent, porphyry due to lack of post quartz fracturing before gold introduction.
Copper Mountain, British Columbia	Andesitic volcanic breccia	Massive andesite or fine-grained augite andesite	Fracturing and schistosity in the volcanic breccia cease at the contact with the massive andesite or diorite.

Place	Favorable Rocks	Unfavorable Rocks	Significant features remarked by contributors
Erongo Area S. W. Africa Pegmatites	Schist	Quartzite and limestone	Pegmatites numerous in schists but are rare in the abundant quartzites and crystalline limestones.
Arakawa Mine, Japan	Shale Tuff	Liparite (Rhyolitic rock)	Copper veins in faults thin out in liparite.
Beatson Mine, Alaska	Graywacke, slate, flint rock, chlorite schist		Host rocks exerted little control. All rocks contain ore but richer shipping ore confined to chlorite schist.
Boise Basin, Idaho	Granodiorite	Dikes of rhyolite porphyry	Ore in well defined and continuous fissure lodes in granodiorite. In rhyolite porphyry the lode breaks up into minor seams and stringers commercially worthless.
	Dikes of rhyolite porphyry	Granodiorite	Ore in oblique sets of tension fractures related to horizontal shearing stresses in rhyolite porphyry. The fissures are tight where they pass into granitic rock__ generally no commercial ore.
Barkerville, British Columbia	Interbedded quartzite and argillite 600 ft. thick	Fissile calcareous quartzite 1,000 ft. thick. Massive argillite 800 ft. thick	The ore bearing member heterogeneous and frangible, and next to a unit that flowed, failed by thousands of short fractures.

Table 3-2 (Continued)

Place	Favorable Rocks	Unfavorable Rocks	Significant features remarked by contributors
Cobalt, Ontario	Cobalt Series, conglomerate, graywacke, arkose	Quartzite, Keewatin—Mostly basaltic lava flows, schists, a little graywacke, slate & cherty iron formation	In places veins pinch or values stop on going from the Cobalt Series into the Keewatin but good veins occur in Keewatin. Quartzites unfavorable.
Woods Point, Austrailia	Diorite dike	Slates	Productive veins confined to dike, they split and disperse in slate.
O.K. Mountain, Rossland, British Columbia	Altered andesitic & basic volcanics	Stock of serpentine	Fissures in volcanic rocks either die out completely on entering the serpentine or continue as shear zones of crushed rock and gouge.
Libby Quadrangle, Montana	Sedimentary rocks, sandstone, argillite, shale	Metadiorite dikes	The faults and veins are shorter metadiorite dikes than in the more brittle sedimentary rocks.
Gunnar Mine, Manitoba	Unsheared ellipsoidal andesite	Coarse grained andesite	Shear zones passing from ellipsoidal, fine grained andesites to massive coarse grained andesites generally die out in the latter rock.
Sulphide Replacements in Western Quebec	Permeable lavas, tuffs, flow breccias	Impermeable rocks, diorite, andesite, syenite porphyry	Faults are closely associated with most of the deposits.

Table 3-2 (Continued)

Place	Favorable Rocks	Unfavorable Rocks	Significant features remarked by contributors
Chanarcillo, Chile	Pure limestone	Tuff and impure limestone	Veins narrow and with little silver in tuff and impure limestone but widen in pure limestone and appreciable quantities of base metals and silver minerals appear.
Kennecott, Alaska	Lower 300 ft. of dolomitic limestone beds above basal limestone		Favorable due to physical and chemical properties. Fissures are the dominant localizers within the favorable dolomite beds.
Upper Miss. Valley Pb-Zn Deposits	Ore in dolomites and limestones related to but not in shaly layers		More fracturing of the dolomites and limestones near the shaly layers.
Tombstone, Arizona	Competent rocks	Incompetent rocks	The Paleozoic limestone and the "novaculite" or silicified shale, with conglomerate and quartzite at the base of the Bisbee group together with the Blue limestone are competent rocks that fractured readily to facilitate the migration of ore bearing solutions. The incompetent sandstones, shales and limestones of the upper part of the Bisbee group tended to close openings.

Table 3-2 (Continued)

Place	Favorable Rocks	Unfavorable Rocks	Significant features remarked by contributors
Tri-State Zinc and Lead District	Incompetent relatively thin-bedded strata, containing numerous stylolite partings.	Competent beds usually massive	In many cases the visible shearing is confined to the incompetent beds, its trace in the competent beds above and below being nearly imperceptible.
Bisbee, Arizona	Thick-bedded limestones	Shaly limestone (Middle Martin)	The shaly Middle Martin was probably an important factor in intensifying the fracturing in the overlying and underlying important ore horizons.
Central or Santa Rita Mining District, New Mexico	Hanover limestone & Middle Blue limestone		Hanover limestone is pure, the Middle Blue has minor shaly impurity. These limestones are separated by a bed of shale.
Combination Mine	Pure limestone beds	Shale, Shaly limestone & sills	
Cornwall, Pennsylvania	The more shaly beds of limestone	Non-shaly beds of limestone	Chemical control.
Gold Hill, Utah	A single mineralized limestone bed between other beds that are only slightly altered		Believed to be related to bedding plane faults.
Nickel Plate Mine, Hedley, British Columbia			Beds of certain composition, impure limestones, especially, exerted a further control.

The intersections or junctions of faults are often mentioned in the literature as the locus of ore deposition, but there are other cases where intersections are barren while ore is found elsewhere on the faults. Still, a tendency to greater brecciation and more openings due to deflection of one of the intersecting faults apparently favors these places as regions of high fracture permeability.

Impermeable barriers are also studied in mining districts. These include shales, gouge, and unfractured intrusive dikes, sills and plutons. Vein deposits themselves are aquicludes if no further fault movement has occurred. During periods of tectonic quiescence when no new fractures are formed, channelling may take place because hydrothermal alteration of the country rock probably closes small fractures, while large conduits are progressively enlarged.

From such sources as drill logs and tunnel or mine records come many reports of large natural openings underground, but their identity as joints or faults is seldom reported. Furthermore, the head is seldom known, much less the transient decline in head, so quantitative measures of fracture conductivity cannot be made from study of the literature. Only a few cases are mentioned here to indicate some extreme conditions.

Tolman (1937, p. 312) reports flows from mineralized fissures at the Ojuela Mine, Durango, Mexico. A steady pumped discharge of 7500 gallons per minute from a drainage tunnel crossing several fissures produced only 3 inches of drawdown in 20 months. Yet the fissures are so remotely inter-connected, probably via the overlying alluvium, that the mine has been stoped out eleven hundred feet below the water table simply by following only one fissure at a time, pumping from the workings to an unused fissure.

The water table is so little effected that only 10 percent is estimated to return. Gignoux and Barbier (1955, p. 126) report vertical tension grottos at Castillon dam, France, 20 meters high and up to 4 meters in aperture, opened along the axial plane of a limestone anticline. The surfaces are slickensided, not dissolved, nor is there evident any stratigraphic throw. P. H. Jones (lecture, University of California, 1962) photographed a 3 inch planar opening in gneiss. The writer has drilled weathered flat joints in slate having openings of about one inch. At Spitallamm dam on glaciated granite (Gignoux and Barbier, 1955, p. 291), one grout hole took 11 percent of the grout injected into 81 holes. Similar sheeting fractures plagued the construction of Mammoth pool dam, California (R. Spellman, address to Association of Eng. Geol., 1963), where openings up to 15 inches were encountered (Terzaghi, 1962). Ground movement on slopes is often the cause of large openings such as the six-inch joints found in shale as much as 100 feet behind the abutments of Mt. Morris Dam (Burwell and Moneymaker, 1950, p. 23). Usually, only the extreme flows or openings are reported, distorting expectations. Unpublished data accumulated by the California Dept. of Water Resources (R. C. Richter, personal communication, 1963) is one exception. They have collected many case histories of tunnels cutting faults of high and low water production. Other sources of information include many engineering works: Stini (1950); Louderback (1950); Gignoux and Barbier (1955); Calif. Dept. of Water Resources (1959), with references to 99 tunnels; and (1962), a bibliography on methods of determining transmissibility and storage capacity, Krynine and Judd (1957); Terzaghi (1946); Sanborn (1950); Talobre (1957); Leggett (1962); Richardson and Mayo (1941); and Ries and Watson

(1947). Pertinent ground water studies include Bryan (1919); Ellis (1906); Meinzer (1923), (1927); Johnson (1947); Rowe (1943); Smith (1958); plus innumerable leads in a host of U. S. Geological Survey Water Supply papers. There are scattered reports in the mining literature: Newhouse's references (1946), Stuart (1955), McKinstry (1948, p. 520). An accumulation of published and unpublished reports of water-bearing faults or fissures remains an interesting project only, until there is developed a uniformly sound method of translating the observations into measures of transmissibility.

Since the thickness of an opening, sheared zone, fault seam, breccia zone, etc., is seldom known, conductivity units like transmissibility, Kb, independent of thickness, should be used, that relates the discharge per unit <u>length</u> to the gradient. The discharge per unit cross-sectional area of a fracture, as used by Muskat, (1937, p. 409) and Amyx, Bass and Whiting (1960, p. 85) does not help assess the overall permeability of a volume cut by planar conduits, since what matters is the total discharge of individuals and the gross cross-section transected.

The conclusion reached on even a cursory inspection of the literature is that openings in excess of a millimeter are common features of crystalline and some sedimentary rocks. These occur not only in the weathered region, but contrary to philosophical (Crosby, 1881) and theoretical treatments (Lachenbruch, 1961) of the maximum depth of fracturing, large openings are also at depths to several thousand feet. Flows in such large channels may exceed the limits of laminar flow near concentrated sinks or sources, such as in tunnel drainage applications or close to producing wells.

For basement rock circulation under low natural gradients, (a few ft. per mile) laminar flow is still a good assumption, even with large openings.

There is clearly no explanation for anisotropic permeability to be found in the literature describing fractured rock, thus it is desirable to show how anisotropy is dependent upon the orientations, spacing and apertures of fractures. The mathematics of a model that combines the effects of those three independent variables is found in the next chapter. How the additional, unevaluated variables, such as discontinuity, variable apertures and anisotropy of individual plane conductors effect the ideality of the model, must be left largely for future research.

Chapter 4

THEORY OF A PARALLEL-PLATE MODEL FOR AGGREGATES OF INTERSECTING PLANAR CONDUCTORS

Introduction

It is conceivable that all the geometrical aspects of real fractured rock media may be described quantitatively, but to include all variables in some analysis of the dependent permeability of real media is an objective improbable of success.

This chapter treats the problem of predicting anisotropy from geometry of conduits in a medium, or conversely, of estimating conduit geometry from measured anisotropy. Conduits are assumed to have smooth parallel plane walls of indefinite extent, with arbitrary orientations and variable spacing. The aperture between conduit walls is also arbitrary. It is assumed that orientations and apertures are distributed variables. Before we proceed to the task of finding the combined influence of these idealized properties with their distributed values, the conductivity of a single parallel-plate opening must be known, then parallel sets, orientation-dispersed sets with the same apertures, and finally sets with dispersed orientations and apertures. Appendix B contains excerpts from the literature on rough fractures.

Parallel-plate flow

The Navier-Stokes equations (Lamb, 1932, p. 577, Muskat, 1937, p. 126) for slow, non-turbulent flow of an incompressible, Newtonian fluid saturating a medium may be abbreviated with indicial notation (Jeffreys and Jeffreys, 1956):

$$\text{grad}\,(p + u) = \nu \nabla^2 v \,, \tag{4-1}$$

where p is the pressure,

u is the gravitational potential,

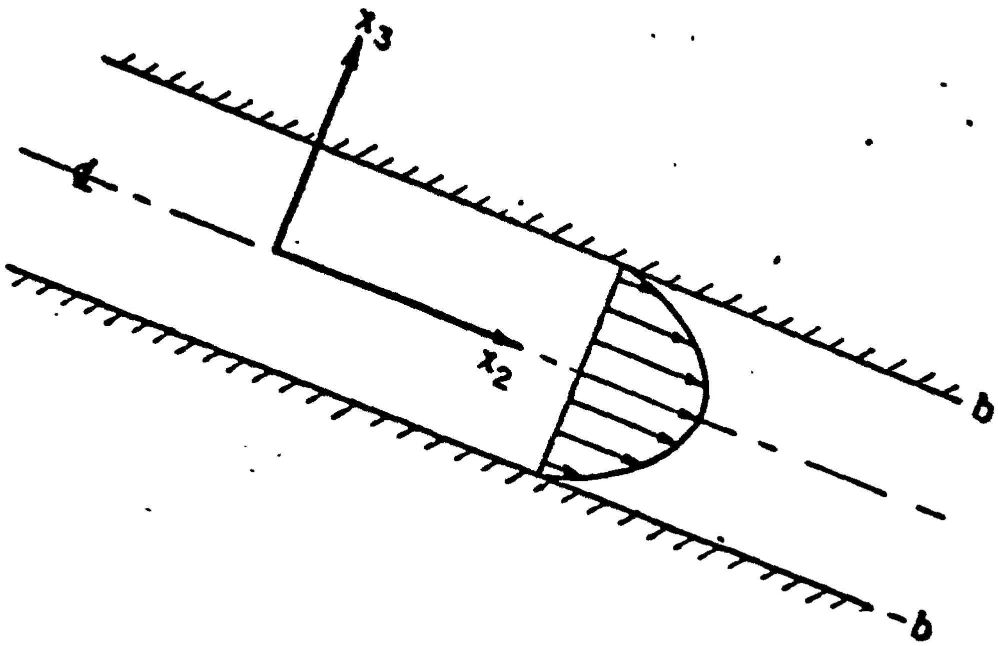

Figure 4-1. Fluid flowing slowly between parallel plates. Section normal to boundaries and parallel to streamlines.

ν is kinematic viscosity and

$\bar{v}$ is the velocity vector. (4-1 Cont.)

By substituting the hydraulic potential, as defined in Chapter 1, for the pressure and gravitational potential

$$\phi = p + u \ ,$$

we reduce equation (4-1) to the three equations:

$$\frac{\partial \phi}{\partial x_k} = \nu \nabla^2 v_k \qquad (4\text{-}2)$$

Expanding to matrix form, with subscripts referring to the Cartesian axes of Figure 4-1, we obtain

$$\begin{vmatrix} \frac{\partial \phi}{\partial x_1} \\ \\ \frac{\partial \phi}{\partial x_2} \\ \\ \frac{\partial \phi}{\partial x_3} \end{vmatrix} = \nu \begin{vmatrix} \frac{\partial^2 v_1}{\partial x_1^2} & \frac{\partial^2 v_1}{\partial x_2^2} & \frac{\partial^2 v_1}{\partial x_3^2} \\ \\ \frac{\partial^2 v_2}{\partial x_1^2} & \frac{\partial^2 v_2}{\partial x_2^2} & \frac{\partial^2 v_2}{\partial x_3^2} \\ \\ \frac{\partial^2 v_3}{\partial x_1^2} & \frac{\partial^2 v_3}{\partial x_2^2} & \frac{\partial^2 v_3}{\partial x_3^2} \end{vmatrix}$$

In the case of lamellar flow with coordinates as shown in Figure 4-1,

$$v_1 = v_3 = 0$$

and

$$\frac{\partial v_2}{\partial x_2} = 0$$

because of incompressible continuity. The x_1 plane is a plane of symmetry, across which there can be no shear, so

$$\frac{\partial v_2}{\partial x_1} = 0$$

The matrix thus reduces to

$$\begin{vmatrix} \frac{\partial \phi}{\partial x_1} \\ \frac{\partial \phi}{\partial x_2} \\ \frac{\partial \phi}{\partial x_3} \end{vmatrix} = \nu \begin{vmatrix} 0 & 0 & 0 \\ 0 & 0 & \frac{\partial^2 v_2}{\partial x_3^2} \\ 0 & 0 & 0 \end{vmatrix}.$$

Hydraulic potential is seen to be constant along lines normal to the flow, while the gradient in the flow direction is proportional to the rate of change of shear, or the velocity gradient, as one moves normal to the boundary.

$$\frac{\partial \phi}{\partial x_2} = \nu \frac{\partial^2 v_2}{\partial x_3^2} \qquad (4\text{-}3)$$

Since ϕ is independent of x_1 and x_3, the left and right-hand terms depend on different variables, and each must equal a non-zero constant, -K.

$$\frac{\partial \phi}{\partial x_2} = -K$$

and

$$\frac{\partial^2 v_2}{\partial x_3^2} = -\frac{K}{\nu}.$$

Two successive integrations of this last, with boundary conditions

$$\frac{\partial v_2}{\partial x_3} = 0 \text{ when } x_3 = 0$$

and $v_2 = 0$ when $x_3 = b$

give

$$v_2 = \frac{K}{2\nu}(b^2 - x_3^2), \qquad (4\text{-}4)$$

showing that velocity distribution may be represented by a parabolic cylinder whose generators are parallel to the boundaries and normal to the flow. A third integration between boundaries gives the discharge per unit conduit width,

$$q = \frac{2}{3}\frac{K}{\nu}b^3,$$

and the average velocity,

$$\bar{v}_2 = \frac{1}{3}\frac{K}{\nu}b^2, \qquad (4\text{-}5)$$

is two-thirds the central velocity.

Substituting the potential gradient for $-K$ and dropping the now unnecessary subscripts, we obtain

$$\bar{v} = -\frac{b^2}{3\nu}\frac{\partial \phi}{\partial x} \;;\quad q = -\frac{2}{3}\frac{b^3}{\nu}\frac{\partial \phi}{\partial x} \qquad (4\text{-}6)$$

per unit width along x_1.

These classic equations for parallel-plate flow are given in various forms in many texts (Hele-Shaw, 1898; Lamb, 1932, p. 583; Long, 1961, pp. 135-137; Borg, 1963, p. 246). It is desirable to put the hydraulic potential gradient into dimensionless form of cm (fluid column) per cm by redefining the potential on a unit weight basis.

Then $$\bar{v} = \frac{b^2}{3}\frac{g}{\nu} I$$

and $$q = \frac{2}{3} b^3 \frac{g}{\nu} I, \qquad (4\text{-}7)$$

per unit width of a single, plane, smooth conduit

Superposition of flows

It will be proved here that there can be no mutual interference of flows at the intersection of two or more planar conduits, provided that they are not dislocated, interrupted, or otherwise changed at the intersection. Even if there is additional friction at an intersection, it seems a good assumption that the local energy losses cannot be more than a few percent of the losses between intersections. If there is no interference between conductors then the discharge components of each may be added. Secondly, it will be shown that the driving force acting on the fluid in joints of various orientations may be represented by a gradient field vector not necessarily lying within the conduits but generally crossing the solid, whether or not there be continuous pore-fluid connection within the solid.

Figure 4-2a shows a uniform isotropic conduit plane with normal n_a crossing an impervious solid medium. There is assumed to be an arbitrary gradient vector I acting in the plane, and on another plane, n_b, shown in Figure 4-2b, a gradient vector I_b, generally not parallel to I_a. There is a unique vector I having I_a and I_b as projections, elsewise along an intersection of the two planes, such as in Figure 4-2c, there would be a different gradient on each joint. The prismatic volume elements are drawn with their shortest axes parallel to I. The sides of the elements are not boundaries.

On each conduit, we can draw evenly-spaced equipotential lines normal to the gradient vectors, I_a and I_b. If the elements are small enough, the equipotentials will be parallel and the

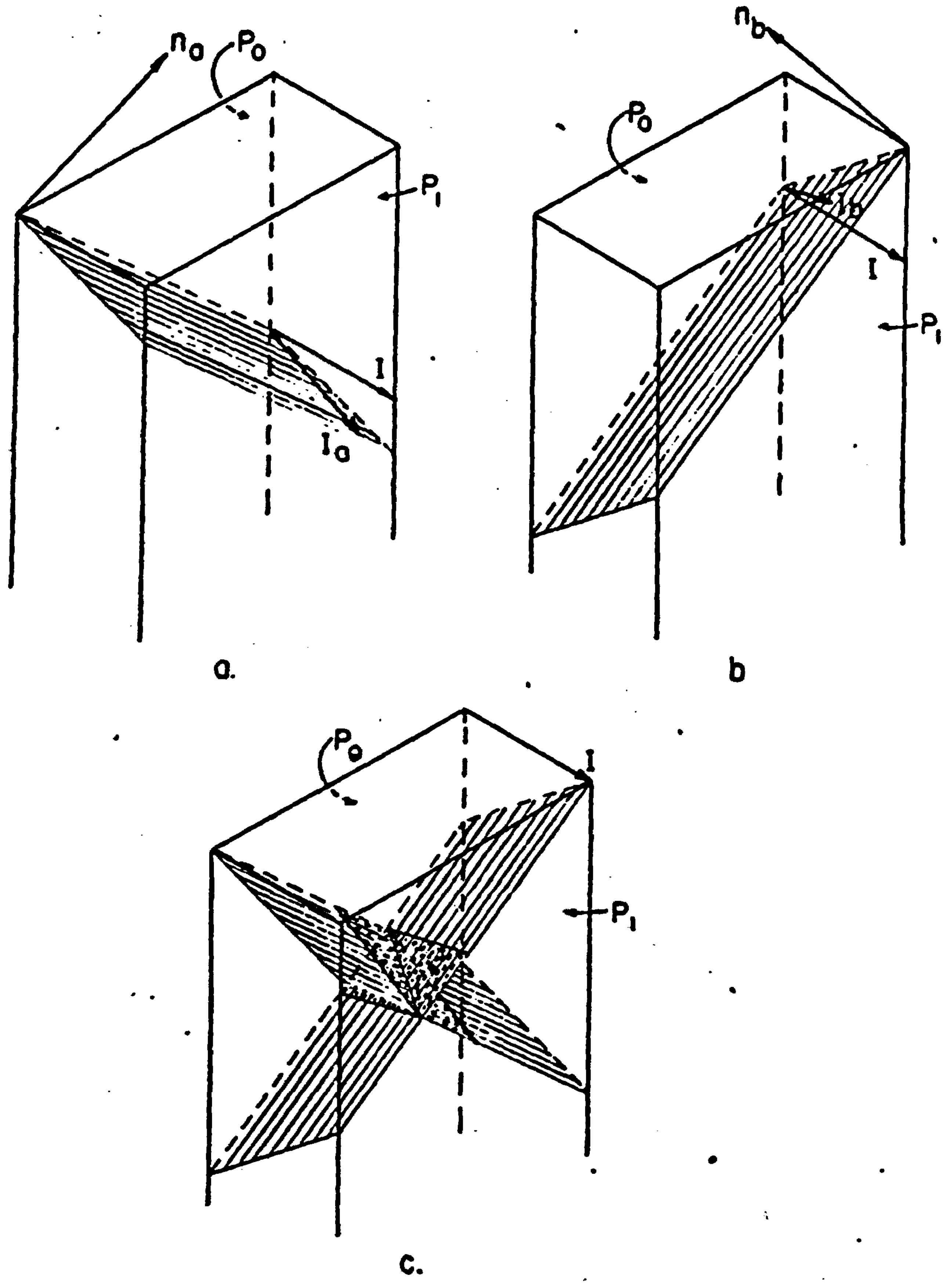

FIGURE 4-2 GRADIENTS ON INTERSECTING JOINTS THAT CUT A SOLID VOLUME.

gradients constant. Corresponding equipotential lines on the two conduits, shown intersecting in Figure 4-2c, may be imagined connected by surfaces crossing the solid phase of the medium. These will approach planar shape as the dimensions of an element decrease and must be normal to the vector I. The broad faces of the elements drawn in Figure 4-2, and all intermediate planes parallel to them, may be considered equipotentials. I is the field gradient. If the solid between joints were pervious granular rock, the same gradient would cause intergranular flow. In his two-dimensional model of fissured soil, Childs (1957, p. 50) has similarly treated gradients as projections.

The element drawn in Figure 4-2c is but one of an infinite number of identical ones situated on the infinitely extensive intersection of the two planes. If there is an increase or decrease of the gradients at or adjacent to the intersection, by reason of some mutual effect, then the same expansion or contraction of equipotential surfaces must apply throughout the extent of the intersection. This is impossible, for then successive equipotentials would become increasingly non-planar and dissimilar.

Nor can there be a variation of gradients within any one element. The flow lines on any individual conductor will, in general, be inclined to the line of intersection, as shown in Figure 4-2c. The flow enters and leaves the intersection via the shaded surfaces, flow lines remaining orthogonal to equipotentials if they are isotropic. Suppose, for example, that the gradient were increased on the portion of a conductor lying upstream of the intersection. Since potential must be equal at coincident points, so too must the gradient increase on the upstream portion of the other conductor. Gradients must then decrease on the downstream portions if the total drop across the element is to remain unchanged. But this is impossible because more fluid would enter the intersection than would leave it.

It is concluded that gradients remain unaltered, either in magnitude or direction, at intersections with other conductors, provided that the intersections are not obstructed or enlarged. Similar reasoning would show that no perturbations of gradients arise where three conduits intersect. If the conduits are anisotropic, flows will not generally parallel the gradients, but in the same manner, we are assured by necessity of flow and potential continuity that there is no perturbation.

An imaginary field gradient of arbitrary orientation may be imposed across any mass transected by arbitrarily-oriented, uniform continuous conductors. Real gradients on the conductors may be computed as projections of the field gradient. The flow on each may then be computed according to its geometry, and since no mutual interference takes place, the total flow through the medium is the vector sum of the contributions of individual conductors.

The foregoing does not say that the flow in a joint is independent of all others when boundary conditions are specified, for the addition of a joint will alter the directional permeability of the medium, and therefore the local field gradient and the flow. Rather, it says that if one is given a certain field gradient, on each joint there will act a projected gradient independent of gradients on its neighbors. To establish properties of a jointed rock medium, especially the property of directional permeability, one must start with either force or flow to be the independent variable, then find the relation between them to establish the unknown. Since in most applications the boundary potentials are known, force has been chosen independent in this work, and velocity dependent, related through the three-dimensional anisotropic Darcy's Law:

$$v_j = K_{ij} \frac{\partial}{\partial} I_i \qquad (4\text{-}8)$$

where I_i is the gradient vector, v_j the velocity vector, and K_{ij} is the linking coefficient, the directional permeability tensor. Versions of this formula have been published by Vreedenburg (1936), Scheidegger (1954), Long (1960) and Childs (1957, p. 54).

Parallel-plate flow under a general field gradient

Figure 4-3 illustrates an arbitrarily-oriented plane conductor in a Cartesian coordinate system, x_1, x_2, x_3. The orientation of the conductor is defined by its normal, with direction cosines n_i, or by two unit vectors in the plane, g_i and l_i, the latter being the directions of greatest and least conductivity. An arbitrary hydraulic gradient, represented by I_i, is imposed on the medium. Flow along the conductor is proportional to the projection of I onto the plane, either J_j, the normal projection, or the two orthogonal components $(I_i g_i) g_j$ and $(I_i l_i) l_j$, as shown. The magnitudes of these orthogonal components are given by the dot-products, in parentheses, and directions by the unit axial vectors, g_j and l_j. The indicial notation of Jeffreys and Jeffreys (1956) is used here, wherein the repeated subscript indicates summation. For clarity we resort occasionally to matrix display (Wylie, 1960, pp. 13-37 and Borg, 1963).

Discharge components are

$$G_j = \bar{k}(I_i g_i) g_j$$

and $\quad L_j = \underline{k}(I_i l_i) l_j \quad$ per unit width.

The maximum and minimum discharge coefficients of the opening are $\bar{k}$ and $\underline{k}$ respectively. These may differ from the value $2b^3/3$

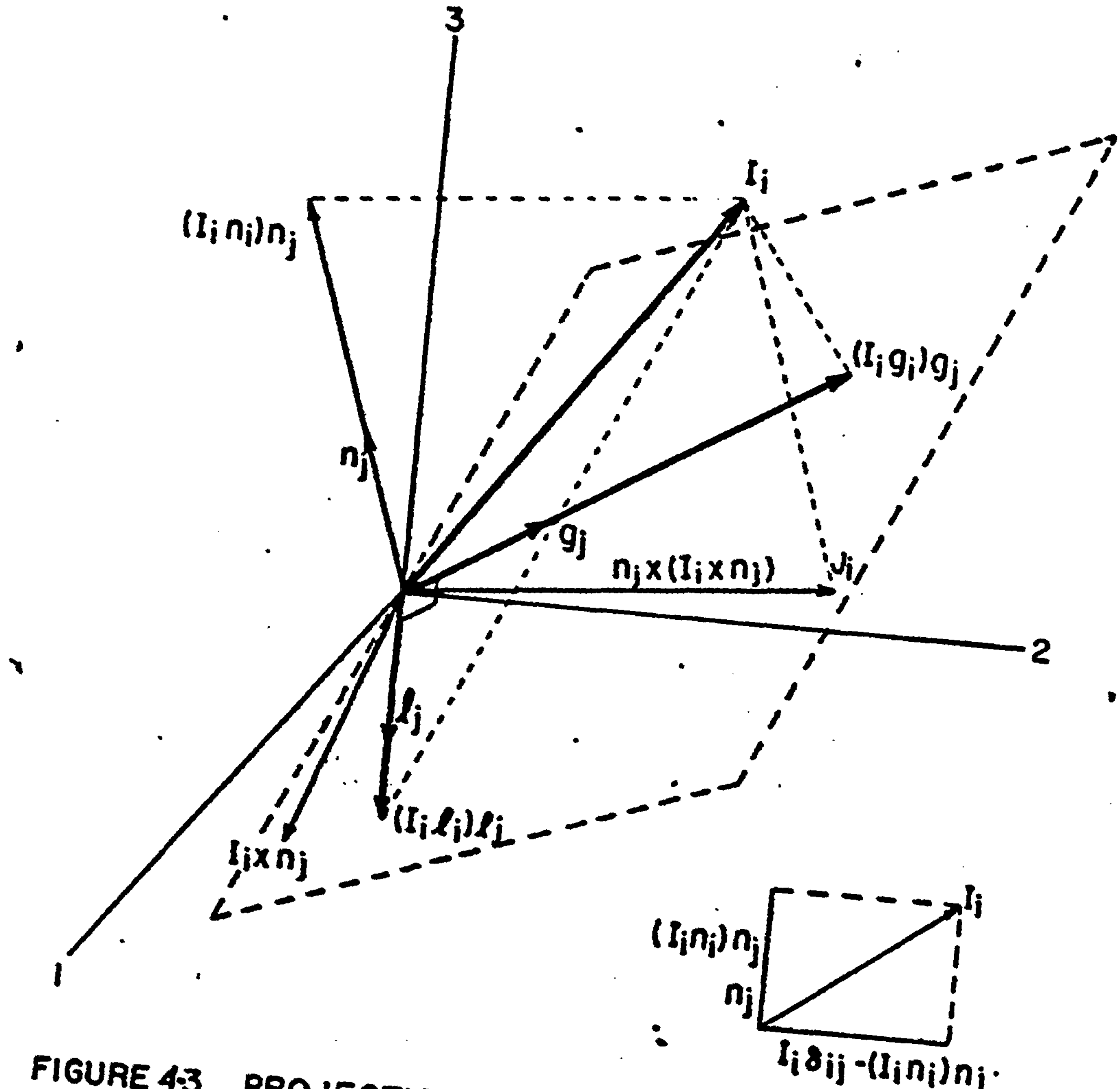

FIGURE 4-3. PROJECTIONS OF AN ARBITRARY GRADIENT ONTO A PLANAR CONDUIT AND (INSET), PROJECTIONS OF THE GRADIENT ON THE PLANE OF THE GRADIENT AND THE CONDUIT NORMAL.

derived above, by reason of directional roughness properties of the surfaces. The resultant discharge is

$$Q_j = G_j + L_j$$
$$Q_j = [\bar{k}\, g_i g_j + \underline{k}\, \ell_i \ell_j]\, I_i \qquad (4\text{-}9)$$

The bracketed term is a symmetric tensor of second rank, relating the discharge to the gradient. It defines the discharge per unit length, by components, for a unit gradient in any direction. The tensor may be abbreviated

$$T_{ij} = \bar{k}\, p_{ij} + \underline{k}\, \ell_{ij}$$

where

$$p_{ij} = g_i g_j \quad \text{and} \quad \ell_{ij} = \ell_i \ell_j .$$

Represented in matrix form (Borg, 1963, p. 56), this is:

$$T_{ij} = \bar{k} \begin{vmatrix} g_1 g_1 & g_1 g_2 & g_1 g_3 \\ g_2 g_1 & g_2 g_2 & g_2 g_3 \\ g_3 g_1 & g_3 g_2 & g_3 g_1 \end{vmatrix} + \underline{k} \begin{vmatrix} \ell_1 \ell_1 & \ell_1 \ell_2 & \ell_1 \ell_3 \\ \ell_2 \ell_1 & \ell_2 \ell_2 & \ell_2 \ell_3 \\ \ell_3 \ell_1 & \ell_3 \ell_2 & \ell_3 \ell_3 \end{vmatrix} .$$

A simpler equation can be deduced for discharge of an isotropic conductor. If $\underline{k} = \bar{k} = k$ in equation (4-9), then,

$$Q_j = k\,[(I_i g_i) g_j + (I_i \ell_i) \ell_j] . \qquad (4\text{-}10)$$

Since the coefficient k is defined for all directions of an isotropic conduit, any pair of orthogonal projections, or their resultant, J_j, will determine the discharge. If the vectors acting in the plane containing n_j, I_i, and J_j are considered it becomes evident that J_j is the vector difference (Inset, Figure 4-3):

$$J_j = I_i\, \delta_{ij} - (I_i n_i)\, n_j$$

δ_{ij} is the Kroneker delta, vanishing when $i \neq j$ and unity when $i = j$. Velocity components are proportional to the gradient components acting in the conductor plane,

$$v_i = \frac{b^2}{3} \frac{g}{\nu} J_i ,$$

according to the equation given on page . This expands to

$$\begin{vmatrix} v_1 \\ v_2 \\ v_3 \end{vmatrix} = \frac{b^2}{3} \frac{g}{\nu} \begin{vmatrix} (1-m_{11}) & -m_{12} & -m_{13} \\ -m_{21} & (1-m_{22}) & -m_{23} \\ -m_{31} & -m_{32} & (1-m_{33}) \end{vmatrix} \begin{vmatrix} I_1 \\ I_2 \\ I_3 \end{vmatrix} \qquad (4\text{-}11)$$

where $m_{ij} = n_i n_j$.

The coefficient common to all terms of this matrix equation may be considered to be the hydraulic conductivity for a unit width of opening, but not for the jointed medium until it is modified by applying it to an area across which the conduit discharges. It is not useful to pursue the line of reasoning (Muskat, 1937, p. 246; Amyx, Bass and Whiting, 1960, p. 84) that the permeability of a fracture is the discharge divided by the aperture, for such a procedure neglects the influence of spacing between conductors.

Parallel Jointed Media

The permeability of a non-conducting solid cut by smooth parallel openings is readily calculated. The discharge of each is

$$q_{x_1} = - \frac{b^2}{3} \frac{g}{\nu} W (2b) \frac{\partial \phi}{\partial x_1}$$

The x_2 component is similarly expressed, while q_{x_3} vanishes. Figure 4-4 defines the dimensions.

The total discharge of N equal joints is

$$Q_{x_1} = - \frac{2}{3} b^3 \frac{g}{\nu} N W \frac{\partial \phi}{\partial x_1} ,$$

provided that the aperture $2b$, of each conductor, and the spacing between conductor planes are constants throughout the medium. If aperture differs, joint to joint, but remains constant in all directions along each joint,

$$Q_{x_1} = -\frac{2}{3}\frac{g}{\nu} W \frac{\partial \phi}{\partial x_1} \sum b^3. \tag{4-12}$$

The flow through an equivalent continuous medium is given by Darcy's Law:

$$Q_{x_1} = -K \frac{g}{\nu} W^2 \frac{\partial \phi}{\partial x_1}. \tag{4-13}$$

Equating (4-12) and (4-13) gives

$$K = \frac{2}{3}\frac{1}{W}\sum b^3.$$

This coefficient is called the intrinsic permeability, to be consistent with the recommendations of the Committee on Termino-

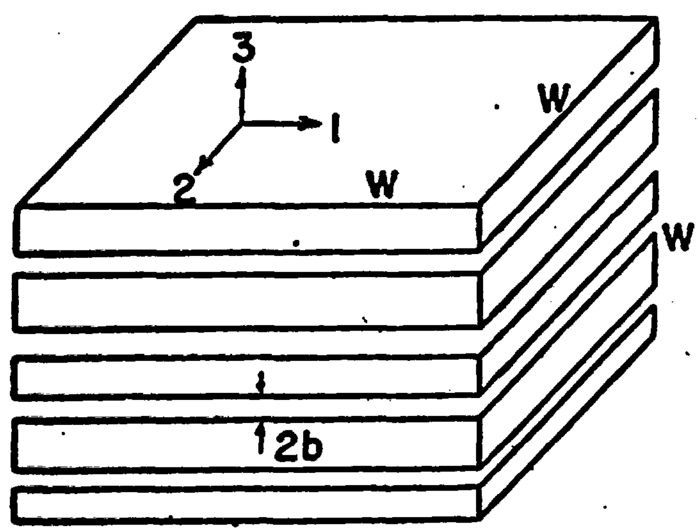

Figure 4-4. A solid volume of dimensions W cut by parallel plane conduits.

logy of the Soil Science Society of America (Richards, 1952). When this variable is applied to a physical problem, intrinsic permeability units (cm^2) may be converted to practical units by multiplying by one or another of the factors tabulated in Chapter 2.

Intrinsic permeability, expressed by K_{ij} in equation (4-8) will be used in a mathematical model for flow in jointed media, but with full cognizance that there is assumed no influence of the fluid properties other than that due to viscosity. Childs (1957, p. 49) has pointed out the invalidity of this assumption for soils containing colloidal or organic matter, since the soil structure is strongly influenced by clay-water chemistry. Clay coatings and partial fillings are common in weathered near-surface joints. These are observed in fine as well as large-aperture openings in crystalline rocks, or in any fractures argillaceous rocks. Therefore, the same objections to the use of intrinsic permeability apply to jointed media as to soils. Since interactions between the fluid and solid phases are not the subject of investigation by the mathematical model developed here, intrinsic permeability will be retained to describe a property of model media, keeping in mind that in application to practical problems, corrections may be necessary. It may be advisable, for example, to perform pumping tests on dam abutments using reservoir water if it differs chemically from the ground water or local supply. There has been no known research done to assess the unsteady chemical processes that may accompany conventional pump-in tests.

The simple parallel-conductor model of Figure 4-4 has other properties that we can characterize. Porosity is

$$\Theta = \frac{W^2 \sum 2b}{W^3}$$

and

$$W = \frac{\sum 2b}{\Theta}.$$

Then

$$K = \frac{\Theta}{3} \frac{\sum b^3}{\sum b}. \tag{4-14}$$

Under these special circumstances of two-dimensionally isotropic jointed media, a determination of permeability and the average spacing Δ yields a measure of the average aperture cubed, or vice-versa. If apertures were identical, porosity would be

$$\Theta = (3K)^{1/3}(2/\Delta)^{2/3}. \tag{4-15}$$

It is shown later that permeability can be used as an indicator of porosity but not precisely, for there is no method of determining $\sum b^3/\sum b$. Specific surface for this simple model is

$$S = \frac{2NW^2}{W^3}, \quad W = \frac{2N}{S},$$

but the average spacing $\Delta = W/N$, so

$$S = \frac{2}{\Delta}.$$

and

$$W = N\Delta.$$

Accordingly,

$$K = \frac{2}{3} \frac{1}{\Delta} \frac{\sum b^3}{N}. \tag{4-16}$$

<u>Dispersed Jointed Media</u>

The more general case of joints dispersed in orientation and position, requires a different approach. Unlike parallel joints, which are characterized by a unique repetition unit, the average spacing, there is no obvious unit describing the frequency of dispersed joints. It is shown below how specific surface is a frequency measure that serves the same purpose as does spacing for parallel systems.

One possible method of measuring joint orientations and positions in the field would entail bore-hole photography (Haddock, 1931) throughout a length of hole D. Each joint may be assigned to a set with the aid of a stereonet plot of normals. Preferably, a set would be included within a cone of 120° or less, and the axis of the bore-hole inclined no more than 30° from the central tendency of the "average" normal of any set. Otherwise inadequate sampling may result. Sampling procedures and discussion of orientation parameters are in Chapter 5.

A sample hole oriented within the above limits may be imagined surrounded by a cylindrical volume of unit base area and much larger height D. Then essentially all joint planes intersected will slice across the volume, cutting all generators of the cylinder. The specific surface of the set of joints is

$$S = \frac{2}{D} \sum_{i=1}^{m} \frac{1}{n_i} ,$$

where n is the cosine of the angle between the axis of the hole and the normal to each of the m planes. The coefficient 2 is used if both surfaces of joints are counted, as is conventionally done for porous media. S has units of 1/L, and serves the same role describing density of joints as does Δ for parallel joints.

Conversely, a joint set characterized by its specific surface and the orientations of all its members is associated with

$$D = \frac{2}{S} \sum_{i=1}^{m} \frac{1}{n_i} , \qquad (4\text{-}17)$$

a length depending only upon the dispersion and size of sample. If a jointed rock mass is drilled to a depth D, and all joints crossed are included in the sample, then logically the repetition unit is of dimensions similar to the volume occupied by the sample. The best that can be said about the unsampled rock beyond the hole is that it has the same distribution of joints as the part traversed.

Figure 4-5 shows a sampled conducting joint and an identical, parallel joint (both shaded). The second is located at a distance, D, as measured along the line of the central tendency (D is not the spacing). If a uniform potential gradient field is given, the direction of fluid flow can be computed. Let each joint lie on the bisector of a cubic element whose faces are: parallel to the joint, parallel to v and normal to v, respectively. The dimensions of the cube element W depend upon D and the absolute value of the cosine of the angle between the central tendency and the normal:

$$W = D\left| n \cdot CT \right|$$

The edges of the cubic element form a second coordinate system, designated below by primed variables. Components of discharge from a joint are:

$$\begin{vmatrix} q_1' \\ q_2' \\ q_3' \end{vmatrix} = \begin{vmatrix} a_1 V_1' \\ a_2 V_2' \\ a_3 V_3' \end{vmatrix} ,$$

where a is the area available for flow through each face. Since $a_1 = a_2 = 2bW$, $a_3 = 0$ and $V_3' = 0$,

$$\begin{vmatrix} q_1' \\ q_2' \\ q_3' \end{vmatrix} = 2bD\left| n \cdot CT \right| \begin{vmatrix} V_1' \\ V_2' \\ 0 \end{vmatrix} .$$

The same volume element can be evaluated as a continuum by Darcy's law, using the most general form of the coefficient, the conductivity tensor in the primed system:

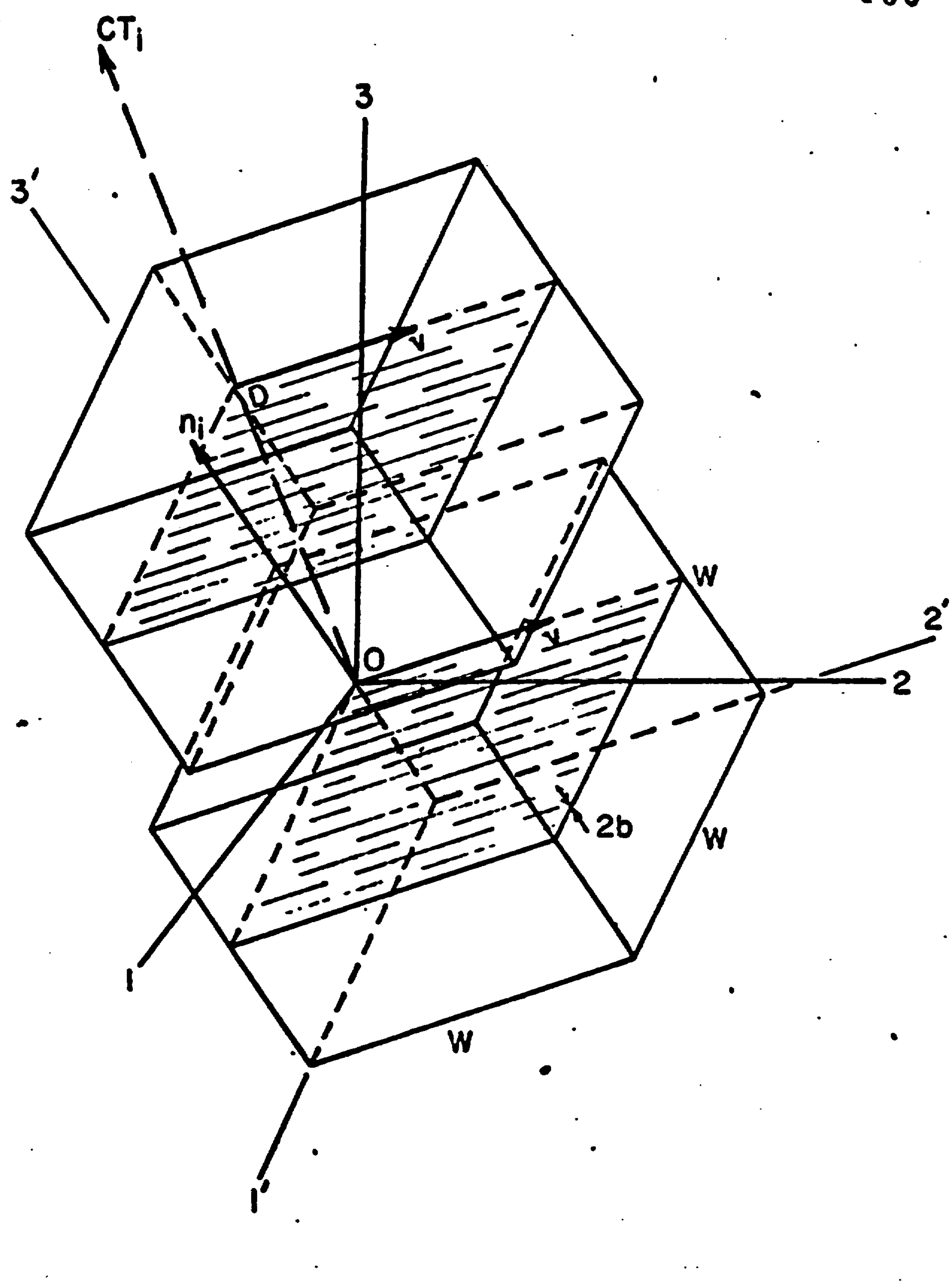

Figure 4-5. A joint conductor with normal n_i and its image distant D, the sampling length along a fixed sample line CT_i. Each conductor makes the enclosing cube a permeable medium.

$$\begin{vmatrix} \xi'_1 \\ \xi'_2 \\ \xi'_3 \end{vmatrix} = W^2 \frac{g}{\nu} \begin{vmatrix} K'_{11} & K'_{12} & K'_{13} \\ K'_{21} & K'_{22} & K'_{23} \\ K'_{31} & K'_{32} & K'_{33} \end{vmatrix} \begin{vmatrix} I'_1 \\ I'_2 \\ I'_3 \end{vmatrix} .$$

I' is the potential gradient in the primed system. The right-hand sides of the above two equations may be equated, then transformed to the unprimed system, common to all joint conduits. A is a transformation matrix.

$$\begin{vmatrix} V'_1 \\ V'_2 \\ V'_3 \end{vmatrix} = \frac{[D|m \cdot CT|]^2}{2bD|m \cdot CT|} \frac{g}{\nu} \begin{vmatrix} K'_{11} & K'_{12} & K'_{13} \\ K'_{21} & K'_{22} & K'_{23} \\ K'_{31} & K'_{32} & K'_{33} \end{vmatrix} \begin{vmatrix} I'_1 \\ I'_2 \\ I'_3 \end{vmatrix}$$

$$A \begin{Vmatrix} V'_1 \\ V'_2 \\ V'_3 \end{Vmatrix} = \frac{D|m \cdot CT|}{2b} \frac{g}{\nu} \left(A \begin{Vmatrix} K'_{11} & K'_{12} & K'_{13} \\ K'_{21} & K'_{22} & K'_{23} \\ K'_{31} & K'_{32} & K'_{33} \end{Vmatrix} A^{-1} \right) \left(A \begin{Vmatrix} I'_1 \\ I'_2 \\ I'_3 \end{Vmatrix} \right)$$

$$\begin{vmatrix} V_1 \\ V_2 \\ V_3 \end{vmatrix} = \frac{D|m \cdot CT|}{2b} \frac{g}{\nu} \begin{vmatrix} K_{11} & K_{12} & K_{13} \\ K_{21} & K_{22} & K_{23} \\ K_{31} & K_{32} & K_{33} \end{vmatrix} \begin{vmatrix} I_1 \\ I_2 \\ I_3 \end{vmatrix} . \qquad (4\text{-}18)$$

This matrix equation leads to an expression of directional permeability more general than that derived by Childs (1957). It gives principal permeabilities and axes for any arbitrary system of dispersed planar conduits having apertures uniform over their areas. We can now substitute the velocity vector derived previously, namely,

$$V_i = \frac{1}{3} b^2 \frac{g}{\nu} (\delta_{ij} - m_{ij}) I_i \quad , \tag{4-11}$$

so that

$$\frac{2}{3} b^3 \begin{vmatrix} (1-m_{11}) & -m_{12} & -m_{13} \\ -m_{21} & (1-m_{22}) & -m_{23} \\ -m_{31} & -m_{31} & (1-m_{33}) \end{vmatrix} \begin{vmatrix} I_1 \\ I_2 \\ I_3 \end{vmatrix} = D|n \cdot CT| \begin{vmatrix} k_{11} & k_{12} & k_{13} \\ k_{21} & k_{22} & k_{23} \\ k_{31} & k_{32} & k_{33} \end{vmatrix} \begin{vmatrix} I_1 \\ I_2 \\ I_3 \end{vmatrix} .$$

Clearly, the conductivity tensor for each joint is symmetric:

$$\begin{vmatrix} k_{11} & k_{12} & k_{13} \\ k_{21} & k_{22} & k_{23} \\ k_{31} & k_{32} & k_{33} \end{vmatrix} = \frac{2b^3}{3D|n \cdot CT|} \begin{vmatrix} (1-m_{11}) & -m_{12} & -m_{13} \\ -m_{21} & (1-m_{22}) & -m_{23} \\ -m_{31} & -m_{32} & (1-m_{33}) \end{vmatrix} . \tag{4-19}$$

The facial area of the repetition cube for a given joint, as illustrated in Figure 4-5, will differ from that of other joints having different orientations, the dimensions being proportional to the cosine of the angle defined. This poses no problem, since discharge has been translated into permeability, a property independent of the area of a cross-section through a continuum. Thus the tensor permeability contributions of all joints may be added to find the total. Each one is weighted by $1/|n \cdot CT|$, the absolute value of the inverse cosine of their inclinations from the average orientation. The unimportance of intersection of joints has already been established, and justification made for superposing flows. The location of any specific member of a joint set is ignored for present purposes, the presumption being that inhomogeneities within the sample are duplicated in successive samples and averaged out over the region within problem boundaries distant several D.

We may arrive at equation (4-19) without assuming homogeneity. If, in Figure 4-5, each conductor is unique in orientation, no second similar cubic element may be drawn. A cube of the same dimension,

$$W = D|n \cdot CT|$$

may be drawn containing the conductor parallel to a face at a position other than the bisector. This describes the cross-sectional area, W^2 to which the conductor contributes.

More than one set of joints may exist in our model. We cannot consider all joints to cross the same cylindrical volume about a single sampling line D. Rather, separate lines D_1, D_2, etc., each within 30 degrees of the expected central tendency, should be drilled to obtain adequate samples of all sets. A different length sampling line for each set ensures proportionately different numbers of joint set members, compensated in equation (4-19) by the coefficient 1/D. Permeability contributions of individual joints of several sets, related to sampling lines of different length and orientation, can therefore be added to obtain the permeability of the medium. It is convenient to use the central tendency of each set as a sampling line, and to further simplify the problem by using D the same for each set. The number of joints in each, combined for computation of directional permeability, must then be proportioned according to the assigned specific surface and orientation dispersion coefficient (Fisher's K_f, see Chapter 5).

$$D_1 : D_2 : D_3 = \frac{2}{S_1}\sum_{i=1}^{m_1}\frac{1}{m_i} : \frac{2}{S_2}\sum_{i=1}^{m_2}\frac{1}{m_i} : \frac{2}{S_3}\sum_{i=1}^{m_3}\frac{1}{m_i} .$$

If $D_1=D_2=D_3$, $\frac{2}{S_1} m_1 \left(\frac{1}{m}\right)_{av_1} = \frac{2}{S_2}\left(\frac{1}{m}\right)_{av_2} = \frac{2}{S_3}\left(\frac{1}{m}\right)_{av_3}$. (4-20)

The bracketed coefficient, average inverse cosine of the angles between normals and central tendency, is readily computed for any given joint set:

$$c = \left(\frac{1}{m}\right)_{av_j} = \frac{1}{m}\sum_{i=1}^{m}(1/\cos\theta)_i ,$$

where m is the total flux or number of joints in the j th set, given by Fisher's dispersion of errors on a sphere (1953).

$$m = -\frac{2\pi}{K_f}\left(e^{K_f} - e^{-K_f}\right) \qquad (4\text{-}21)$$

In an element d (cos θ) about the central tendency, there are

$$dF = -2\pi e^{K_f \cos\theta} d(\cos\theta)$$

members, so

$$c = \frac{1}{m}\int_0^{\pi} dF \frac{1}{\cos\theta}$$

or

$$c = \frac{-\int_{-1}^{1} 2\pi e^{K_f\cos\theta}\frac{1}{\cos\theta}d(\cos\theta)}{-\frac{2\pi}{K_f}\left(e^{K_f} - e^{-K_f}\right)} \qquad (4\text{-}22)$$

Unlike the vectors of Fisher's distribution, the normals to planes in space are two-headed. Within the region $\frac{\pi}{2} < \theta < \pi$, we choose to represent any vector by its negative, directed into the region $0 < \theta < \frac{\pi}{2}$. If a significant portion of a Fisher distribution lies outside the hemisphere having the central tendency as vertex, an abnormal flux concentration would lie near $\theta = \pi/2$. Most natural joint sets are reasonably concentrated (Fisher's $K_f > 10$, see Plates 2 and 3 of Chapter 5), and if joints lie outside of $\theta = \pi/2$, they would be identified with another set. The probability of a vector lying in the region $\theta > \pi/2$ is only .00067 for dispersions of $K_f = 5.0$. If we limit the definition of a joint set to members lying within a 120-degree cone ($\theta = \pi/3$), we find a maximum probability of .006 that a vector generated by Fisher's equation will lie outside those limits if $K_f = 5.0$ or greater.

The improper integral given above can therefore be evaluated over a practical range $1 > \cos\theta > 1/2$ for all values of $K_f > 5.0$:

$$C = \frac{K_f}{e^{K_f} - e^{-K_f}} \left[\ln\cos\theta + \frac{K_f\cos\theta}{1} + \frac{K_f^2\cos^2\theta}{2(2!)} + \frac{K_f^3\cos^3\theta}{3(3!)} + \ldots \right]_{1/2}^{1}.$$

The results of a short computer program to evaluate the integral are graphed in Figure 4-6.

Once D or the number of elements appropriate to a given joint set is established, the tensor permeability contribution of each can be determined by equation (4-19). Similar tensors for each of the other joints may be added term by term, since we have already ascertained that no mutual interference takes place. The accumulated tensors of all joint sets are then added to define the permeability tensor for the jointed rock medium,

$$K_{ij} = \sum k_{ij} . \qquad (4\text{-}22A)$$

Then any boundary problem may be treated as a homogeneous anisotropic medium with flow components given by

$$Q_j = K_{ij} A \frac{g}{\nu} I_i . \qquad (4\text{-}23)$$

In some cases where boundary transformations are inconvenient, for instance if two or more adjoining regions have different permeability tensors, the fully expanded form may be required for each region, and the problem solved in its original coordinate system:

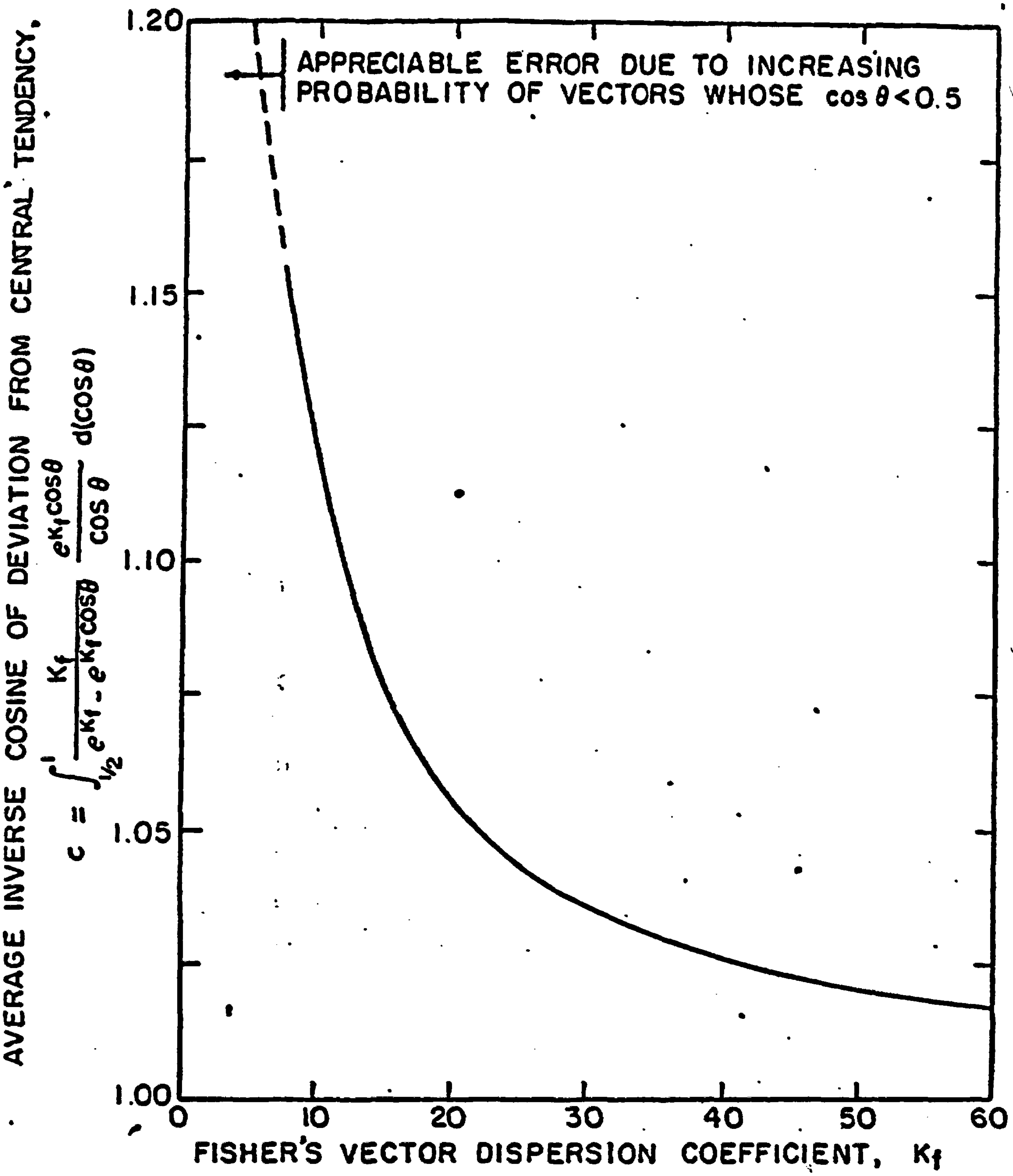

FIG. 4-6 THE AVERAGE RECIPROCAL OF THE COSINE OF ANGLE BETWEEN JOINT PLANE NORMALS AND THEIR CENTRAL TENDENCY, AS A FUNCTION OF DISPERSION. USED FOR PROPORTIONING SIZE OF SETS AND DETERMINING REPETITION LENGTH: $m_1 : m_2 : m_3 = S_1/ : S_2/ : S_3/$, DELTA = 2/S (m)C.

$$\begin{vmatrix} Q_1 \\ Q_2 \\ Q_3 \end{vmatrix} = A\frac{g}{\nu}\begin{vmatrix} K_{11} & K_{12} & K_{13} \\ K_{21} & K_{22} & K_{23} \\ K_{31} & K_{32} & K_{33} \end{vmatrix}\begin{vmatrix} I_1 \\ I_2 \\ I_3 \end{vmatrix} . \qquad (4\text{-}24)$$

All nine terms, six of which are different, are required for reference to an arbitrary coordinate system.

Computer relaxation programs, such as developed by Warren, Dougherty and Price (1960) to solve transient boundary problems in isotropic media, could be revised to satisfy continuity of flow through a cubical, or radial volume element when each discharge component is a function of all three gradient components, i.e.

$$Q_1 = A\frac{g}{\nu}\left[K_{11} I_1 + K_{12} I_2 + K_{13} I_3\right] \quad \text{, etc.}$$

More commonly, problems are solved isotropically after transforming coordinates. To obtain the transformation factors and the effective conductivity of the fictitious medium (discussed in Chapter 1), principal axes and permeabilities are required. To obtain these, it remains only to diagonalize the summary tensor of equation (4-24), finding the principal axes as eigenvectors, and principal permeabilities as eigenvalues.

Equation (4-24) then becomes

$$\begin{vmatrix} Q'_1 \\ Q'_2 \\ Q'_3 \end{vmatrix} = A\frac{g}{\nu}\begin{vmatrix} K'_{11} & 0 & 0 \\ 0 & K'_{22} & 0 \\ 0 & 0 & K'_{33} \end{vmatrix}\begin{vmatrix} I'_1 \\ I'_2 \\ I'_3 \end{vmatrix} , \qquad (4\text{-}25)$$

the primes signifying reference to a coordinate system parallel to the principal axes of the tensor. Equation (4-25) is equivalent to the familiar equations

$$Q_x = A \frac{g}{\nu} K_x \frac{\partial \phi}{\partial x}$$

$$Q_y = A \frac{g}{\nu} K_y \frac{\partial \phi}{\partial y}$$

$$Q_z = A \frac{g}{\nu} K_z \frac{\partial \phi}{\partial z} \quad ,$$

given by Muskat (1927, p. 226), Childs (1957, p. 63), and others.

It has been noted already that intergranular flow may be superposed upon model fracture flow, so that the permeability of jointed, granular-porous media may be determined. If the solid of the medium has permeability K_s, this value may be added to each of the principal permeabilities determined for the joint system. If the solid is itself anisotropic, described by

$$V_i = \frac{g}{\nu} K_{ij} I_i \quad ,$$

then one may transform its tensor to the coordinate system used to orient the joints, add each term to the tensor for the joint system referred to the same coordinates, then diagonalize the tensor sum.

It can be demonstrated that the tensor form reduces to the equation given for parallel joint sets. When all joints have the same orientation n_i,

$$\begin{vmatrix} K_{11} & K_{12} & K_{13} \\ K_{21} & K_{22} & K_{23} \\ K_{31} & K_{32} & K_{33} \end{vmatrix} = \frac{2}{3D} \Sigma b^3 \begin{vmatrix} (1-m_{11}) & -m_{12} & -m_{13} \\ -m_{21} & (1-m_{22}) & -m_{23} \\ -m_{31} & -m_{32} & (1-m_{33}) \end{vmatrix} .$$

If further, n_i is also a coordinate axis, say the 3-axis,

$$n_1 = n_2 = 0 \quad \text{and} \quad n_3 = 1 \quad ,$$

so,

$$\begin{vmatrix} K_{11} & K_{12} & K_{13} \\ K_{21} & K_{22} & K_{23} \\ K_{31} & K_{32} & K_{33} \end{vmatrix} = \frac{2}{3D} \sum b^3 \begin{vmatrix} 1 & 0 & 0 \\ 0 & 1 & 0 \\ 0 & 0 & 0 \end{vmatrix} , \qquad (4\text{-}26)$$

or

$$K_{11} = K_{22} = \frac{2}{3D} \sum b^3 \quad , \quad K_{33} = 0 \; ,$$

as previously derived (p. 103).

Porosity Estimation

It is possible to work in reverse, to obtain from permeability and geometry measurements, an approximate value for porosity that is better than the first estimate shown on page , because it includes the influence of orientation of the conduits. Field tests have been developed to establish for a site the principal permeabilities (Chapter 2) when principal axes have been determined from the geometry of the joint system (Chapter 5). These axes should be taken as a new coordinate system. Joint orientations, obtained with reference to geographical coordinates (or other), should be transformed to the new axes. If apertures were also known, the measured directional permeability could be compared to the values computed by the present model, thereby justifying use of the model as a substitute for tests.

Determination of pore-size distribution from flow data obtained from intergranular porous media requires assumptions of pore geometry to interpret such tests as the capillary-pressure, water-saturation curve. Bundles of tubes and networks (Fatt, 1956, pp. 152-153) have been assumed. The macroscopic nature of fractured media permits better definition of the geometry of its conductors, but there remains ambiguity because we cannot currently determine either the pairing of apertures and orientation, nor the distribution of apertures alone. We must be content, at this time, to assume all apertures alike in magnitude. In a later chapter the errors of porosity estimation, made on the assumption of average apertures throughout, are assessed by calculation of porosity from dispersed model media containing normal, log-normal and exponential aperture distributions.

Let the permeability tensor for a jointed rock medium be known, as well as the orientation dispersion for, say, three sets of joints, but assume no dispersions of apertures. The summary tensor is composed of sub-tensors arising from each set (superscripts 1, 2, and 3):

$$\begin{vmatrix} K_{11} & 0 & 0 \\ 0 & K_{22} & 0 \\ 0 & 0 & K_{33} \end{vmatrix} = \begin{vmatrix} k^1_{11} & k^1_{12} & k^1_{13} \\ k^1_{21} & k^1_{22} & k^1_{23} \\ k^1_{31} & k^1_{32} & k^1_{33} \end{vmatrix} + \begin{vmatrix} k^2_{11} & k^2_{12} & k^2_{13} \\ k^2_{21} & k^2_{22} & k^2_{23} \\ k^2_{31} & k^2_{32} & k^2_{33} \end{vmatrix} + \begin{vmatrix} k^3_{11} & k^3_{12} & k^3_{13} \\ k^3_{21} & k^3_{22} & k^3_{23} \\ k^3_{31} & k^3_{32} & k^3_{33} \end{vmatrix} . \qquad (4\text{-}27)$$

We cannot solve for the eighteen unknowns on the right (each matrix is symmetric), since we can write but six different simultaneous equations from the above. The matrices must first be simplified.

A set of joints symmetrically dispersed (say by Fisher's equation) about a central tendency can be replaced by a parallel set of planar conduits plus a tubular set parallel to the central tendency of joint normals. The ratio of permeability of the tube set to the plane set depends on the anisotropy characteristic of the dispersion. It will be shown in Chapter 5 that the anisotropy of a dispersed set depends more strongly upon the orientation dispersion than on the dispersion of apertures in the set.

Further, it will be shown that the tensor for a single dispersed set has negative uniaxial symmetry, that the extraordinary permeability, k min, is always less than the ordinary permeability, k max (to borrow terminology from petrography), the ordinary being radially symmetric about the central tendency of the set. In other words, the geometrical interpretation of the permeability tensor for single dispersed sets is an oblate spheroid.

Thus k_{max} and k_{min} can be expressed as proportions of the permeability, k_p, of a parallel set of joints having the same specific surface and aperture dispersion:

$$k_{max} = c_1 k_p \quad , \quad k_{min} = c_2 k_p .$$

A single joint or a set of parallel joints is mathematically equivalent to an isotropic continuum plus a tube with negative conductivity lying along the normal to the plane. This fact is employed in the first matrix on the right of the following equation, where the isotropic (δ_{ij}) and normal (m_{ij}) components are resolved,

$$\begin{vmatrix} k_{11} & k_{12} & k_{13} \\ k_{21} & k_{22} & k_{23} \\ k_{31} & k_{32} & k_{33} \end{vmatrix} = c_1 \frac{2}{3D} \sum b^3 \begin{vmatrix} (1-m_{11}) & -m_{12} & -m_{13} \\ -m_{21} & (1-m_{22}) & -m_{23} \\ -m_{31} & -m_{32} & (1-m_{33}) \end{vmatrix} + c_2 \frac{2}{3D} \sum b^3 \begin{vmatrix} m_{11} & m_{12} & m_{13} \\ m_{21} & m_{22} & m_{23} \\ m_{31} & m_{32} & m_{33} \end{vmatrix} .$$

The unique tube sets arising from the two replacement steps are parallel, thus additive as shown below,

$$\begin{vmatrix} k_{11} & k_{12} & k_{13} \\ k_{21} & k_{22} & k_{23} \\ k_{31} & k_{32} & k_{33} \end{vmatrix} = \frac{2}{3D} \sum b^3 \left\{ \begin{vmatrix} c_1 & 0 & 0 \\ 0 & c_1 & 0 \\ 0 & 0 & c_1 \end{vmatrix} + (c_2 - c_1) \begin{vmatrix} m_{11} & m_{12} & m_{13} \\ m_{21} & m_{22} & m_{23} \\ m_{31} & m_{32} & m_{33} \end{vmatrix} \right\} .$$

In this equation, $n_{ij} = n_i n_j$, where n_i is the central tendency of one of the sets. Since there is an equation of this sort for each joint set, and their sum is given by equation (4-27), we may let

$$\overset{\ell}{k}_p = \frac{2}{30} \sum^{\ell} b^3 .$$

Now we are ready to sum components:

$$K_{11} = [\overset{1}{c}_1 + (\overset{1}{c}_2 - \overset{1}{c}_1)\overset{1}{m}_{11}]\overset{1}{k}_p + [\overset{2}{c}_1 + (\overset{2}{c}_2 - \overset{2}{c}_1)\overset{2}{m}_{11}]\overset{2}{k}_p + [\overset{3}{c}_1 + (\overset{3}{c}_2 - \overset{3}{c}_1)\overset{3}{m}_{11}]\overset{3}{k}_p \tag{4-28}$$

$$K_{22} = [\overset{1}{c}_1 + (\overset{1}{c}_2 - \overset{1}{c}_1)\overset{1}{m}_{22}]\overset{1}{k}_p + [\overset{2}{c}_1 + (\overset{2}{c}_2 - \overset{2}{c}_1)\overset{2}{m}_{22}]\overset{2}{k}_p + [\overset{3}{c}_1 + (\overset{3}{c}_2 - \overset{3}{c}_1)\overset{3}{m}_{22}]\overset{3}{k}_p$$

$$K_{33} = [\overset{1}{c}_1 + (\overset{1}{c}_2 - \overset{1}{c}_1)\overset{1}{m}_{33}]\overset{1}{k}_p + [\overset{2}{c}_1 + (\overset{2}{c}_2 - \overset{2}{c}_1)m_{33}]\overset{2}{k}_p + [\overset{3}{c}_1 + (\overset{3}{c}_2 - \overset{3}{c}_1)m_{33}]\overset{3}{k}_p .$$

These are three of the six possible equations in the three unknowns $\overset{1}{k}_p$, $\overset{2}{k}_p$, $\overset{3}{k}_p$. A unique solution for as many as six sets is possible.

It should be clear after seeing in Chapter 5 how anisotropy varies with orientation dispersion, how the coefficients c_1 and c_2 can be determined. By computing numerous dispersions of both orientation and aperture, forming each time the ratios of k_{max} and k_{min}, respectively, to the permeability of a similar parallel set, k_p, there were obtained the relationships graphed in Figure 4-7.

If it is assumed that all conductors are identical in aperture, 2b, then that aperture can be computed from k_p, the permeability of the parallel set. Porosity can be computed from the first, single-valued estimate, but such estimated porosity, or any other derived porosity, will differ from the true values according to the actual distribution of apertures. The purpose of Chapter 7 is to find the magnitude of these errors, by comparison of the identical-aperture value and certain distributed-

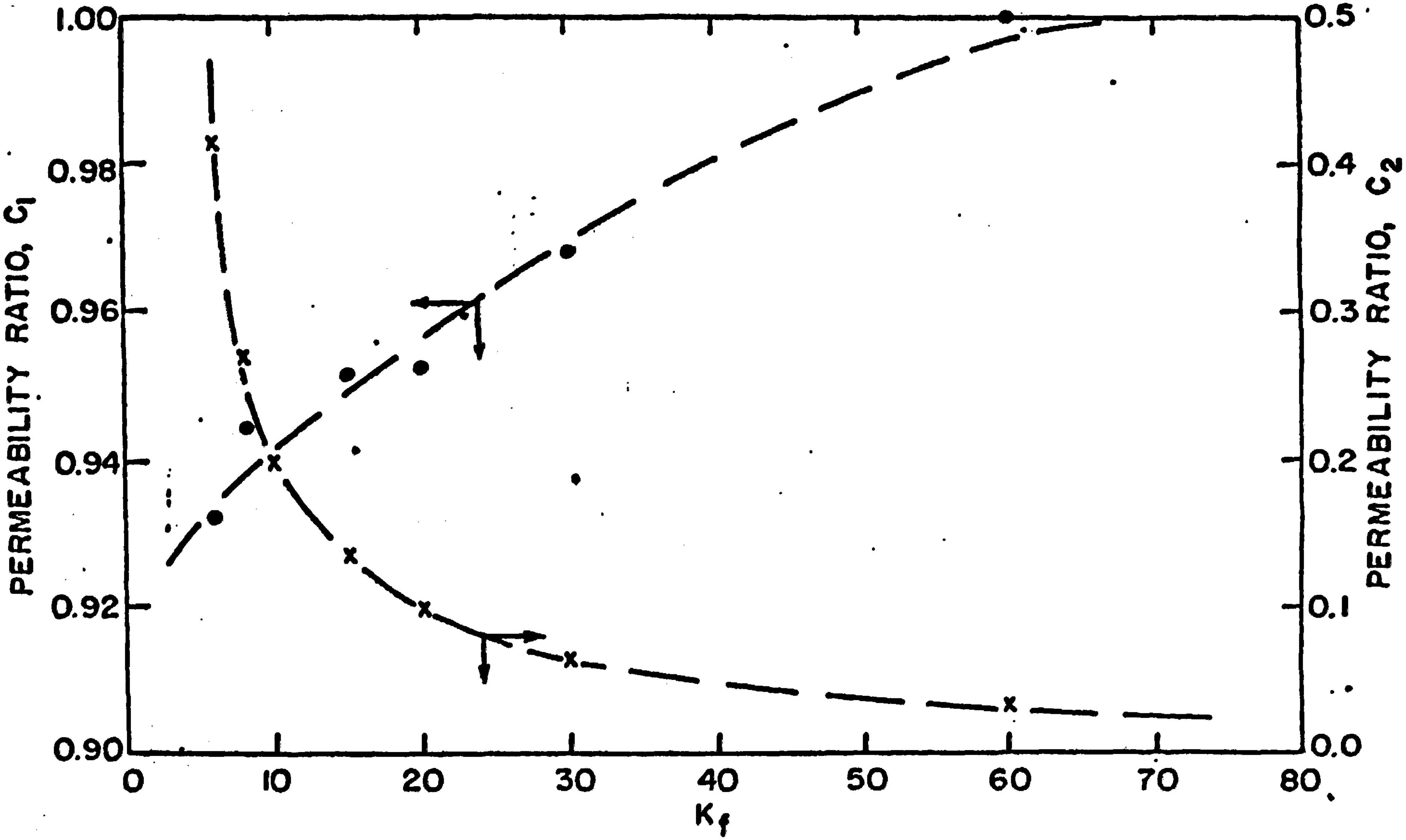

FIGURE 4-7 PERMEABILITY RATIOS AS A FUNCTION OF DISPERSION, K_f: ISOTROPIC PLANE, C_1, AND CENTRAL AXIS, C_2, OF A DISPERSED SET, TO THAT OF A PARALLEL SET.

aperture values. For all distribution of aperture,

$$k_p = \frac{2}{3D} \sum b^3 ,$$

while for a unique constant aperture b_0,

$$k_p = \frac{2N}{3D} b_0^3 ,$$

thus

$$b_0 = \left(\frac{3 k_p D}{2N}\right)^{1/3} . \qquad (4\text{-}29)$$

An aperture estimate can be made for each set whose representative permeability k_p has been determined. It is a function of the number of dispersed conductors traversed by a sampling line of length D following the central tendency (D is the same for each set of the system), and k_p. Secondary joint porosity in rock can be better estimated by equation (4-30) than by equation (4-15),

$$\Theta \doteq c\,(3 k_p)^{1/3} (2N/D)^{2/3} , \qquad (4\text{-}30)$$

where

$$c = \frac{1}{N} \sum \frac{1}{|m \cdot CT|} ,$$

the constant dependent on the orientation dispersion of a set, graphed in Figure 4-6. The estimated total porosity is the sum of the porosities of the sets.

Dead-end pore space (Fatt, 1961) is not included in equation (4-30) since permeability does not reflect stagnant voids. Displaceable porosity is desired for such purposes as grouting, but omission of dead-end volume may be detrimental for electrical conductivity studies or for flow of compressible fluids.

<u>Combined dispersion of orientation and aperture</u>

By letting both orientations and apertures vary in their values, we have introduced a complicating difficulty, for it is usually impossible to determine analytically the distribution of a variable dependent upon two or more distributed variables. There are many engineering problems of this sort that can only be solved by iterative techniques, and most handily on computers. Fatt (1952) reported a statistical analysis of multiple independent variables in electric log determination of formation saturation. Later he determined saturation-capillary pressure relationships (1956) for distributions of pore radius in random network locations. Discrete pore-size distributions facilitated step-wise computation of saturations corresponding to the extent of invasion of a phase boundary upon increase of pressure. Different pairings of pore sizes and pore locations gave negligible dispersion of results. Had the procedure yielded significantly different results each time, a statistical analysis of the distributed results would have been necessary. Warren and Price (1961) reported sampling of various permeability distributions to characterize individual volume elements occupying random positions in a heterogeneous permeable medium. From a finite number of computer runs, the most likely overall permeability and moments of the distribution of permeabilities were obtained. Other applications have been described by Meyer (1956).

Like the applications cited, the present model of jointed media employs a general technique called Monte-Carlo sampling (U. S. Nat. Bur. Standards, 1951). The proper method of obtaining dependent distributed properties is to compute successive solutions in batches, each run in a batch having random input data sampled from large discrete or continuous populations of independent variables. When batches are large in number of runs, the central limit theorem (Mood and Graybill, 1963, pp. 149 and 403) justifies the application of normal error statistics for analyzing the resulting distributions of answers. The theorem states that if the sample size n (number of runs, in a batch) is increased without limit, the distribution of sampling means (average of a batch) approaches normal with mean equal to the population mean (average of an infinitely large batch of runs), and with variance (of batch averages) equal to 1/n times the population variance. If, instead, a batch consists of only one run (samples of size n=1), the batch answer is the one-run answer and Monte Carlo sampling will generate a population that need not be normal, nor need the mean or variance equal the population parameters sought. For this reason, batches of 49 runs have been employed in this study, so that a batch may be nearly exactly reproduced. In Figure 4-8 are graphic results of directional permeability determinations (described more fully later). In this figure, two separate batches are superimposed, each of which is a full computation of principal permeabilities from the same populations of orientations, apertures, and spacings, but with data re-arranged to assure generation of different random numbers. The batch median of each curve falls well within the computed 95 percent confidence range of the corresponding re-run curve. This eliminates the need for multiple batches, since we can calculate the precision of measures of a single batch, reducing computer running time to reasonable values.

In the frequency plots of Chapter 5, (bottom row of Plates 1-15), each run value has been represented by a point on each curve. These runs are samples of size n = 1 (as opposed to the average of more runs than one). The curves represent the desired frequency distribution of a population of permeabilities. More or less runs than 49 will not greatly alter the distribution, but will effect the reliability.

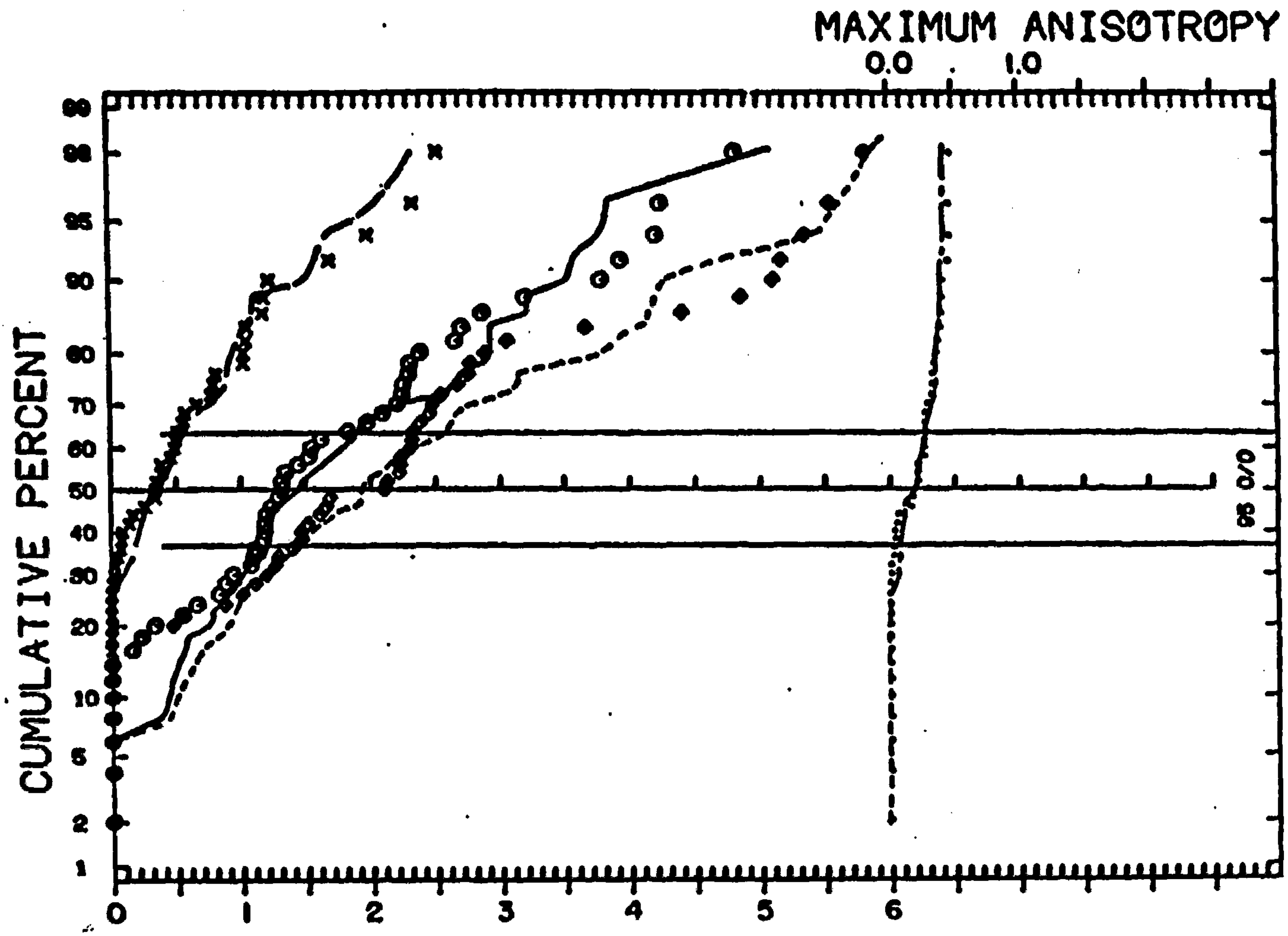

FIGURE 4-8. PRINCIPAL PERMEABILITIES, X 10^9 CGS UNITS
MEAN NUMBER OF 1/2 JOINT ON SE SET, 1 ON NW SET
NORMAL APERTURE DISTRIBUTION, CENTEN=.005, STD=.001,DELTA=112
REPRODUCEABILITY IS SHOWN BY TRACES OF A DIFFERENTLY ORDERED BATCH OF SOLUTIONS HAVING THE SAME PARAMETERS.

However, the central limit theorem operates on a lower level here also, for each run is a process of averaging the contributions m conductors make to the sample permeability. If m were infinitely large, all permeabilities computed from a population of orientations, etc, would be the same. If m is small, only a few random conductors are included and the permeabilities are scattered. One object is to study parameters of this scatter as a function of m, thus evaluating requirements of sample size for replacement of discontinuous media by equivalent continua. The speed at which the distribution of means approaches normalcy as m increases depends on the shape of the distribution of the population sampled. It approaches more rapidly near the mean than near the tails. Figure 4-9 is reproduced from Mood and Graybill (1963, p. 152) to illustrate the changes of the distribution of means as sample size increases. If a normal curve is not demonstrated, normal error theory cannot be used to evaluate parameters of the population. The permeability curves developed by the model are estimates of the population of permeabilities, but the parent form of the population is unknown, approaching normal only in the limit of large samples. The reliability of the parameters of a curve of unknown shape can only be found by applying non-parametric methods (Mood and Graybill, pp. 403-422), so called because with these methods the functional form of the parent distribution (described by the mean and variance) does not occur in the analysis. The basis of these methods is a property of ordered statistics: n values, ranked in ascending order of magnitude, divide the distribution into 1/ (n+1) areas, which, on the average, are equal. Thus, the 25th smallest solution, out of 49, estimates the median permeability. Confidence intervals on the median can be calculated from the

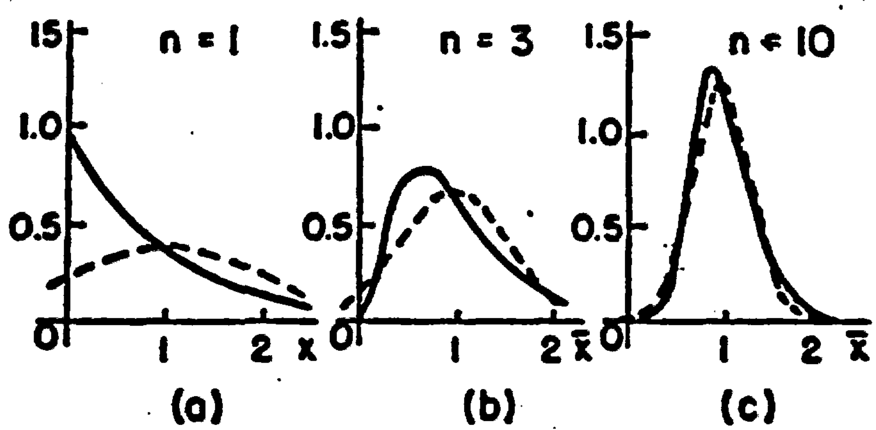

Figure 4-9. Illustration of the central limit theorem, showing the distribution of sampling means. (a) The means of samples of size n = 1 is the population sampled (exponential in this case). (b) Skewness decreases for n = 3, and (c) normalcy is approached for n = 10. (After Mood and Graybill, 1963, p. 152).

binomial distribution, since the probability of an observation falling above or below the median is 1/2 in each case. The normal approximation to the binomial is good for samples as large as 49. The Harvard binomial tables (Aitken, 1955) locate the 95 percent confidence interval about the median of 49 measures within 7 observations to either side, as does the normal approximation, $1.96 \sqrt{n}/2$. If successive batches of 49 runs are executed, and the 95 percent interval laid off about each median, 95 percent of these internals would include the median of the population of batches.

If batches of runs are made with smaller and smaller numbers of conductors, their distributions are something closely resembling the distribution of apertures cubed. Almost any distribution cubed is highly skewed to the right, thus, any distribution of means of small samples is also skewed. If the sample size differs, from batch to batch, every batch of 49 runs is an estimate of a separate population. Intuitively, the permeability of a 10-foot cube of jointed rock should model the same as a statistically homogeneous 100-foot cube containing it, yet it is proven to be not so. Changes in median values of directional permeability with change of sample size or volume are important aspects of this study, for they indicate the trend of values that should be applied to boundary problems of different dimensions.

The reader interested in the mechanics of the computer programs built to implement this model will find a brief description accompanying the programs in Appendix A. The first version of the computer model listed there (several versions, not shown, preceded this one) was meant solely to investigate anisotropy variations upon changes of the orientation and spacing parameters. That is the subject of Chapter 5. Additional subroutines were added to make the second version listed, a tool for investigating aperture distributions, pressure-test discharges and porosity, the subjects of Chapter 6 and Chapter 7.

There has been shown a need for a model study that will guide the field worker to appropriate identification of principal axes of any given geometrical system of joints, faults or other planar conductors. The three-hole pressure-test arrangement proposed in Chapter 2 was predicated on fore-knowledge of the principal axes, without which principal permeabilities cannot be measured. While the 14 model joint systems reported in Chapter 5 may not fit any real system exactly, the variety of special cases covered should serve as guides to define, by comparison, the approximate orientations of axes for nearly all cases.

The model results are significant evidence that fractured media are generally anisotropic, even more so if real conductors are individually anisotropic.

Chapter 5

THE INFLUENCE OF JOINT ORIENTATION ON DIRECTIONAL PERMEABILITY

Introduction

One of the more useful results to come from the parallel-plate model is knowledge of the influence on flow behavior of the spacing and orientation of conductor planes transecting an impervious solid.

The formula for the permeability tensor elements

$$K_{ij} = \frac{2}{3}\,\frac{b^3}{D|m \cdot CT|}\left(\delta_{ij} - m_{ij}\right) \qquad (4\text{-}19)$$

for a single uniform planar conduit of aperture 2b and orientation n_i can be applied to as many conduits as one wishes to include in a model of intersecting elements. A selected set of apertures, paired with orientations, may be envisioned as a sample from some jointed rock medium. The directional permeability of the model, or an approximation to the directional permeability of a real jointed medium, can be obtained by diagonalizing the tensor found of the sum of all 9 elements contributed by each planar conductor.

In the abstract, it is immaterial whether the conductors are faults, joints, foliation, sand seams, or saw cuts. Let us call them joints, since joints are the most likely conductors encountered. In Chapter 3, it was pointed out that to assume a conductor to be uniform and isotropic throughout an infinite extent is to depart considerably from reality. Still, the model set up in Chapter 4, leading to equation (4-19) and the superposition of flows, here finds utility in defining the principal permeability axes of a medium, in relation to the geometry of its joints. Though the assumptions need refinement, improvements made by future workers will probably not change the qualitative findings of this part of the study.

Models of planar conductors, each of which is uniform, isotropic and continuous, may be characterized: (1) by parameters specifying orientations, (2) by parameters specifying the frequency of occurrence in a volume, and (3) by parameters describing the variation of the apertures of conductors. The desired insight into the properties of real jointed media can be obtained through study of these three classes of geometric variables alone, before further complicating parameters are introduced in the future to describe continuity, non-uniformity or anisotropy of individual conductivity.

If for every conductor, spacially defined in position and orientation, there is assigned a particular aperture, then there would be for the aggregate of conductors one unique permeability tensor. The addition of other conductors to the system would alter the tensor in magnitude and direction. An arbitrary gradient is implied in computing the directional permeability of the model, and the field gradient is assumed uniform over the dimensions of the model (D in equation 4-19).

Only one distribution of apertures will be used in the following discussion, but the effect of a variation in the distribution of apertures on porosity will be considered in Chapter 7. It is assumed that the aperture distributions are continuous for all rock types; within the range of apertures represented, any given value may be found by increasing the sample size sufficiently.

Though it may be possible to measure and associate an aperture with each joint orientation observed in the field, the practical difficulties of attaining undisturbed conditions suggests that it will never be done on a routine basis. Rather, aperture distributions will probably be approximated by indirect means analogous to those used to estimate intergranular pore size distributions (Purcell, 1949; Burdine, et.al., 1950; Ritter and Drake, 1945).

Orientation Distributions

An orderly natural grouping of rock joint orientations has been demonstrated by innumerable field geologists (see references in Chapter 3). One subparallel group is called a set, and the several sets at a site, a system. Individuals of a set are dispersed around a central or "average" orientation. Orientation distribution is best envisioned by first translating all planes of a set to intersect at a point in space, then erect a vector normal to each plane. Let the points where these vectors pierce a unit sphere represent the orientation distribution. The resultant of unit vectors representing a set of planes is the central tendency. Joint normals are dispersed about the central tendency, as illustrated by stereonet plots of real systems in Plate 16, and for synthetic systems in Figures 1 of Plates 1 to 15. The theory, techniques and applications of stereographic representation of vectors in space have been presented by Sänder (1948), Donn (1958) and Goodman (1963). Real systems commonly show imperfect radial symmetry about a central tendency, whereas the computer-generated synthetic systems are symmetric.

The generated synthetic vectorial data are used as sets of planer conductors that may exist or be approximated in nature. Generated data has the advantage over natural dispersions for parameter studies, because a vector frequency distribution can be reproduced quickly and consistently by association with a dispersion coefficient. Real joint orientations can be used in the same manner as synthetic ones, by randomizing the elements in digital form, but the answers derived from them cannot be related to well-defined dispersion coefficients.

A mathematical formulation of vector dispersions devised by Fisher (1953), has been used to generate synthetic joint sets. Other formulations, with or without significance tests, have been published by Arnold (1941), Greenwood and Durand (1955a and 1955b), Watson (1956a and 1956b), and Watson and Williams (1956), but these are not used here.

The frequency at any point of a Fisher distribution is proportional to $e^{K_f \cos\theta}$, where K_f is called Fisher's coefficient, and θ is the central angle between that point and the central tendency. By varying K_f from 0 to infinity, the dispersion may be changed from uniform over the entire sphere, to concentrated at the central tendency. Synthetic joint sets with axial symmetry can therefore be generated as desired, either dispersed or aligned in orientation, by varying K_f and specifying the orientation of the central tendency. A ring of width $d\theta$ at θ from the central tendency includes an area of the unit sphere that is

$$dA = -2\pi\, d(\cos\theta)$$

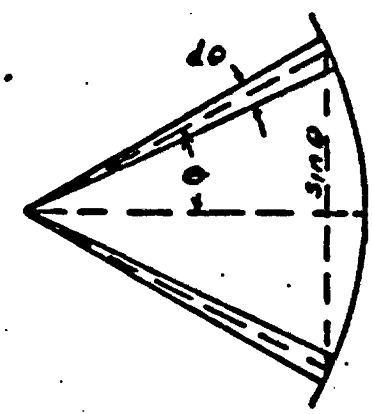

so the number of vectors through the ring is proportional to

$$dF = -2\pi e^{K_f \cos\theta} d(\cos\theta).$$

The total through the sphere is proportional to

$$F = -2\pi \int_{-1}^{1} e^{K_f \cos\theta} d(\cos\theta)$$

$$F = -2\pi \frac{1}{K_f} \left(e^{K_f} - e^{-K_f}\right) \tag{5-1}$$

$$= -\frac{4\pi \sinh K_f}{K_f} .$$

The frequency is therefore

$$df = \frac{dF}{F} = \frac{K_f}{2 \sinh K_f} e^{K_f \cos\theta} d(\cos\theta) \tag{5-2}$$

The flux through a cone of half-angle θ about the central tendency is proportional to

$$-2\pi \int_{\cos\theta}^{1} e^{K_f \cos\theta} d(\cos\theta) = -\frac{2\pi}{K_f}\left(e^{K_f} - e^{K_f \cos\theta}\right). \tag{5-3}$$

Fisher's equations were designed as an error law, for if the vectors are random, the probability that one lies within an angle θ is the ratio of expressions (5-3) to (5-1):

$$P(\theta) = \frac{e^{K_f} - e^{K_f \cos\theta}}{e^{K_f} - e^{-K_f}} . \tag{5-4}$$

All the synthetic joint normal dispersions shown in plates 1 to 15 were produced by taking probabilities between 0 and 1 from a random uniform number generator, equated as in equation (5-4) and solved for θ. Appendix A contains computer programs VECGEN and VECTOR, that use this algebra.

Real joint dispersions can also be described by a central tendency orientation, and the dispersion coefficient best fitting the set. The centroid of a set of points on a stereonet can be easily obtained algebraically if the set is not split between two hemispheres. A general method is contained in subroutine JDATA (Appendix A), whereby all elements of a set are transformed to orientations dispersed in their original relative positions, but around an estimated central tendency, shifted to the zenith of the plot. The computed orientations are indicated in [redacted] Figures 1 through 4 of Plate 16. Fisher dispersion coefficients can be estimated by comparing a plot directly to the sequence of synthetic plots in Plates 2 and 3. If the set is irregular or assymetric, an approximate K_f can be obtained by calculating the vector strength (Arnold, 1941; Pincus, 1953) and entering a graph (Figure 5-0) relating K_f to the strength. Vector strength is defined as the average component of vectors taken in the direction of the central tendency:

$$(STR) = \frac{1}{N} \sum_{j=1}^{N} (\cos\theta)_j \quad (5\text{-}5)$$

The relationship of vector strength to K_f was obtained as follows: The total number of elements in a Fisher distribution is

$$N = -\frac{2\pi}{K_f}\left(e^{K_f} - e^{-K_f}\right),$$

and in an element $d(\cos\theta)$ there are

$$df = -2\pi e^{K_f \cos\theta} d(\cos\theta)$$

members. So

$$(STR) = \frac{1}{N}\int df \cos\theta$$

$$= \frac{K_f}{e^{K_f} - e^{-K_f}} \int_{-1}^{1} e^{K_f \cos\theta} \cos\theta \, d(\cos\theta).$$

Integration by parts gives

$$(STR) = \frac{K_f}{e^{K_f} - e^{-K_f}}\left[\frac{1}{K_f}\cos\theta \, e^{K_f\cos\theta} - \frac{1}{K_f^2} e^{K_f\cos\theta}\right]_{-1}^{1}$$

$$= \frac{\left(1 - \frac{1}{K_f}\right)e^{K_f} + \left(1 + \frac{1}{K_f}\right)e^{-K_f}}{e^{K_f} - e^{-K_f}}.$$

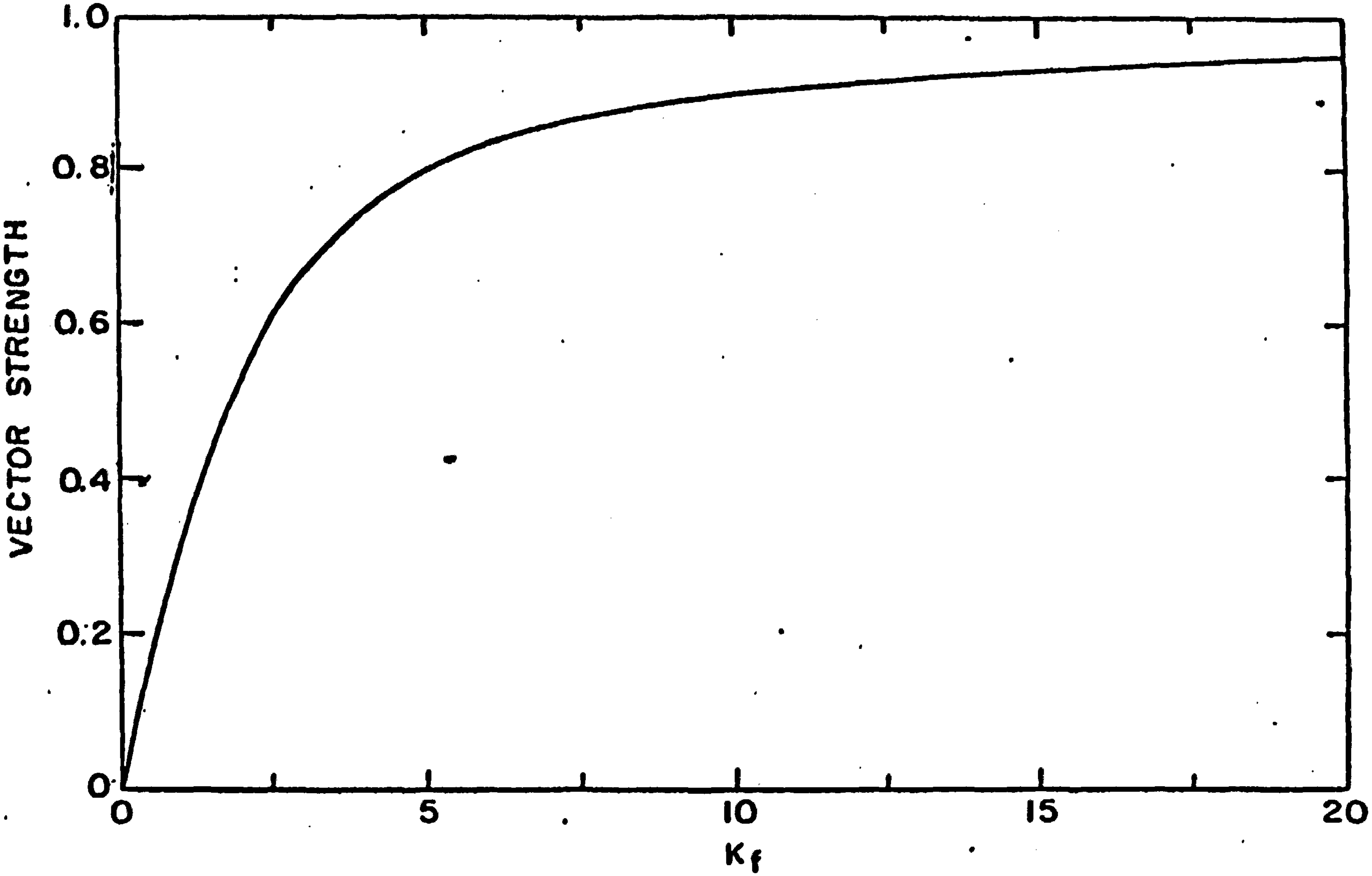

FIG. 5-0. RELATIONSHIP BETWEEN VECTOR STRENGTH, $\frac{1}{m}\sum_{i=1}^{m} n_i$, AND FISHER'S VECTOR DISPERSION COEFFICIENT.

this simplifies to

$$(STR) = \frac{e^{K_f} + e^{-K_f}}{e^{K_f} - e^{-K_f}} - \frac{1}{K_f} \qquad (5\text{-}6)$$

the function graphed in Figure 5-0.

<u>Orientation of principal axes and distribution of principal permeabilities for various joint systems</u>

Lacking indications that there is any relationship between joint aperture and its orientation relative to the whole set, it is assumed that the elements of an aperture distribution are wholly independent of the elements of the orientation distribution. This necessitates statistical evaluation of a few sample combinations out of the infinite possible combinations of two independent continuous distributions.

The computer program designed to implement equations (4-19) and (4-22A) is in Appendix A, together with a description. Examples of graphical output serving to abbreviate the voluminous results of computations are in Plates 1 to 15. Once the task of programming is complete, these machine-made plots save enough interpretation time to permit inclusion of an additional dimension in parameter studies. More numerous configurations of spacing, orientation and aperture distribution have been studied than were possible by manual processing of computer output. The plots reproduced here, but a portion of the total number executed, include 2646 separate determinations of directional permeability. Each conductor, numbering 20 to 2000 for each solution, requires a solution of equation (4-19), aggregating about 14,000. Each sample of 49 solutions, leading to a complete print-out of matrices and derived parameters, as illustrated in Appendix A, plus a pair of plots, requires about 2 minutes of IBM 7090 computer time. Development of the program required about 10 computer hours in progressive compilation and debugging over a span of a year.

Plates 1 through 15 illustrate most of the special cases of joint system geometries that might be met or approached in nature. The systems modeled include up to three sets. Plate 1 shows the effect of sample size for a single set with a given dispersion. Plates 2 and 3 show in sequence the effect of decreasing orientation dispersion, from Fisher's K_f = 6 to 60. Plate 4 treats two equal, orthogonal sets, followed in order by other plates illustrating two orthogonal sets of different dispersion, two orthogonal sets of different spacing, two non-orthogonal (45 degrees between central tendencies) sets of equal dispersion, two non-orthogonal, different sets, three orthogonal sets of equal dispersion, three orthogonal sets, one of which has different spacing than the other two, three orthogonal sets, one of which has different dispersion, three orthogonal sets, each with different dispersion, three orthogonal sets, each with different spacing, two orthogonal sets and one non-orthogonal with equal dispersions, and last, Plate 15, three non-orthogonal sets with equal dispersion.

Common to all computer solutions illustrated here is a fixed-parameter distribution of apertures. It was chosen somewhat arbitrarily on the knowledge only that permeabilities measured in many places in a jointed medium give skewed distributions with frequencies much higher in the low ranges than in the high. Later work showed this distribution to be imperfect, a finite frequency at zero apertures being impossible. This is not a vital error. The answers are not seriously affected by the distribution of the small elements because permeability contributions depend on the cube of aperture. Figure 1 of Plate 2 and Figure 2 of all other plates describe the assumed aperture distribution, plotted as a density distribution for 1 micron classes of half apertures, and as a cumulative percent curve. The computed arithmetic, geometric, and harmonic means are shown; also the median.

Figure 1 of all but Plate 2 is an upper hemisphere stereographic projection of the normals to joints forming the population sampled. Computer programs VECGEN and STEREO (Appendix A) were used to put a large number of these orientations into digital form, the direction cosines of individual elements of a Fisher distribution of normal errors on a sphere (1953) and to plot them as points on a stereogram. Samples of these populations, usually smaller in number than represented on the stereonets were used to compute directional permeabilities. The caption of each plot identifies the spatial orientation of the central tendency of the vector distribution, obvious also by the center of gravity of the points. This efficient representation of vectors is not only a great labor and spacing-saving device, but also facilitates mental grasp of complicated aggregates of numbers. Each plot of 500 vectors required about 1 minute on the IBM 7090, after appropriate programming and debugging, as opposed to 10 hours hand-plotting for 500 points. Such a study as this would have been impractical a few years ago, since the enormous volume of data handled could not be processed by one man in years. The sequence of plots, Figures 3, 6 and 9 of Plate 2, and Figures 1, 4, 7 and 10 of Plate 3, offers a visual comparison tool for estimating the dispersion coefficient of similarly displayed orientation data obtained in the field. Any one of the Figures 1 of Plates 4 through 15 may be used as reference approximations of patterns of field data involving one, two or three sets. Principal permeability axes may be oriented approximately with the aid of these idealized solutions. The need for this was demonstrated in Chapter 3, where a 3-hole pumping test was designed on the assumption that axes could be predicted from joint data.

The second row of figures on each plate displays in stereographic projection the principal axes corresponding to the given orientation, dispersion, and spacing parameters. In each figure there appear orthogonal triplets of diamonds, circles and crosses, corresponding to maximum, intermediate and minimum permeability axes. There are 49 such triplets, each a separate solution computed from an independent random sampling of the given population(s) of joint orientations and apertures. In this way the range of possible solutions can be portrayed, for each sampling contains differently oriented conduits, paired with different apertures. With so many solutions plotted together, unique triplets cannot be identified easily, but it is the whole range and concentration of solutions that is of interest. The scatter of axial orientations indicated by the model reflect the variations in principal axes that would exist from one place to another in a jointed medium having geometrical distributions like the model. Each sampling of conductors leads to the directional permeability of a medium having those specific conduits, repeated over and over throughout the infinite space. There is introduced a random error because in prototype rocks, adjacent volumes have different conduits, but the directional permeability error decreases as a mean value is approached upon increase of sample size or volume. Since part of our interest is in the dispersion of the permeability statistics, our purposes would be defeated by considering only mean values and large samples. One of the purposes of this parameter study is to ascertain the size of sample required to get good representation of a medium, and to estimate the errors involved if small samples are used.

To this end, principal permeabilities are plotted in the bottom row of figures. Again, we use diamonds, circles and crosses to maintain correspondence of permeabilities and axes. The data generated by the computer program is seen to consist of three principal axes and three principal permeabilities for each solution, the former plotted in stereonet form, the latter in distribution curves. Cumulative frequency is plotted on a probability scale, to bring out departures from normalcy. Since the permeability data for each axis must be ranked before plotting, correspondence of axes and magnitudes is lost, but a statistical description of variable quantities is obtained. Only one of the principal permeabilities could be plotted cumulatively if mutual identity between direction and permeability were maintained. If two principal conductivities are nearly the same each time, then their axial orientations are sensitive to changes in the samples. Since any two equal orthogonal vectors define a plane of isotropy, we expect and find in this case that successive solutions scatter orientations throughout a great circle of the stereonet. The equatorial plane of Figures 4, 6 and 8 of Plate 1 is an example. The zenith, normal to the plane of isotropy, is the only unique principal axis. Curves of principal conductivities on the isotropic plane, for example, Figures 5, 7 and 9 of Plate 1, show slight separations, indicating that individual solutions are slightly anisotropic. While slight anisotropy exists on the plane for each sample, the intermingling of diamonds and circles on the girdle indicates statistical isotropy over a

[illegible]

large volume. Subroutine HD13 (Mervin, 1959) emphasizes any such bias. This program computes the eigenvectors and eigenvalues, always labeling the major axis, 1; the intermediate, 2; and minor, 3. These labels determine the use of diamonds, circles, or crosses plotted in the figures. Thus, in cases of near-isotropy on a plane, the curve of major permeabilities for example, shown by diamonds, is actually a series of values for various axes on the plane, not for a unique axis. The separation of the curves vaniches for larger samples.

Another consequence of cumulative plotting of three permeabilities is loss of identity of particular solution triplets. A line parallel to the abcissa does not intercept three principal permeabilities of a single solution. So to preserve the individual relationships, there has been plotted also the maximum anisotrop ies. These data are recorded by dots in the lower row of figures, representing the ratio of minimum permeability to maximum permeability. As this property varies with the magnitudes computed, a cumulative distribution is generated.

Different sample sizes or volumes have been used to evaluate changes in dispersion of principal axes and permeabilities. The lower two rows of figures should be read in pairs, a stereonet plot of axes and a cumulative frequency plot of permeabilities describing all solutions for samples of a size stated in the captions to the frequency plots. The size of samples increases from left to right, sharpening the definition of answers. From left to right on each plate, (except 2 and 3), there is also shown a decrease of dispersion as sample size increases. These results are summarized in Figure 2 of Plate 2 and Figure 3 of Plates 1 and 4 through 15. The heavy solid line connects computed values of the median permeability for various sample dimensions or conduit numbers, and by light or dashed lines, the 95 percent confidence ranges about the medians.

Plate 1 introduces the computation technique with the simplest geometry, a single, symmetrical dispersion of planar conduits, (Figure 1). Apertures are dispersed according to the absolute value of a normal distribution with mean, .025 cm, and standard deviation, .035 cm (Figure 2). By changing the sign of improper negative apertures, a skewed distribution is formed with higher arithmetic mean and median, and lower geometric mean than pertains to the non-transposed normal distribution. The first problem solved (illustrated by solutions in Figures 4 and 5) was to find the distribution of possible orientations of principal axes of this jointed medium when only 25 conductors are present in a 270-cm cube, and to find the principal permeabilities that correspond to these axes. The Monte Carlo sampling mechanism involves the pairing of a random orientation from the population of Figure 1, and a random aperture from Figure 2. Its conductive contribution is stored as 9 terms of a symmetric permeability tensor referred to the axes of Figure 1. The sampling proceeds with the pairing and computing of terms, each time adding them to the tensor. After 25 samplings, the general tensor is complete except for a scale correction to account for joint spacing. The tensor is then diagonalized to yield three scalar principal permeabilities and three vectors as principal axes. These are stored for the moment, while 25 more conductors are sampled, giving a new tensor solution of permeabilities and axes, somewhat different than before since different joints are included in the second sample of 25 than were included in the first 25. In this manner, 49 independent solutions of 25 conductors each are generated and stored. Subroutine STEREO then computes, as instructions to the Cal-Comp plotter, the x-y coordinates of the poles of vectors (the principal axes) in stereographic projection. One axis at a time is marked by appropriate symbols. In one of the stereograms, Figure 4, a concentration of x's lies at the center, orienting the minimum principal permeability and displaying its dispersion. It is approximately similar to the plot of poles of conductor planes (Figure 1), since only small flow components take the direction of the average joint normal. The axes of intermediate and major permeabilities are plotted in turn, as circles and diamonds, forming a girdle along the equator, dispersed 10° to 15° to either side. One orientation on such a plane of statistical isotropy is as likely as another, though an individual solution possesses slight anisotropy. The same statement may apply to natural jointed media. Note that aberrant orientations are possible, as illustrated by the intermediate axis (circle) oriented N78°W, 30° from the vertical. One large opening at an extreme orientation within the population will dominate the directional permeability just as an open or brecciated fault will dominate the flow in jointed rock.

For the set of 49 solutions, there is produced also a frequency plot of principal permeabilities, Figure 5. The curve of smallest magnitude corresponds to the direction normal to the set of conduit planes. The skewness of this curve is so slight that one may consider the interval marked between the 16th and 84th percentiles to approximate two standard deviations from the mean permeability. In general, however, the form of a permeability distribution is unknown, therefore only non-parametric methods of interpretation are justified. The median value of a ranked statistic (the 25th out of 49 in this case) is a useful measure because half the time, values will be greater, and half the time, smaller than this value. In effect, what has been done is to generate 49 solutions to assess the entire range of possible solutions under the given input parameters. Only a finite number of solutions are possible, even with a modern computer. So a method of assessing the reliability is required. Confidence intervals about the median have been computed on the basis of the normal approximation to the binomial distribution, justified for samples of size 49 (Mood and Graybill, 1963, p. 408), and including 7 observations on either side of the median at the 95 percent level. Under the caption to the corresponding stereonet plot (Figure 4), there has been printed the median principal permeabilities and the confidence ranges for all axes.

The median and its range are useful for predicting an individual value, say the permeability prediction for a single test hole in a large formation. On the other hand, the arithmetic mean, not shown in these figures, would be desirable for estimation of the most representative average permeability that will be encountered by individual drill holes in many parts of the formation. Means are often inadequate for special purposes, for instance where extremes govern design. For example, dam foundation treatment is usually undertaken simply out of fear that local erosion and progressive deterioration may occur at places where extreme permeabilities occur, even though the water loss is economically acceptable. If we had data of such quality as in these synthetic media, the extremes could be estimated from the distribution curves, because the percentage points of ranked statistics are themselves estimates of the probability of obtaining a given value. Figure 5 of Plate 1 indicates a 2 percent chance of exceeding a principal permeability of 14.6×10^{-6} cgs units for a sample of 25 conductors with the given parameters.

Confidence intervals may be computed on this estimate by applying the binomial distribution.

Dispersion of principal permeabilities is also portrayed in Figure 5. While the minor permeability has a small absolute range, it has a larger percentage range than the major permeability. The surprisingly large dispersions ($3 < K\ max < 14$) observed are a consequence of the dependence of flow upon the cube of aperture, a mechanism clarifying, qualitatively at this time, the large observed variations in measured permeability in jointed rocks.

The dispersion decreases for larger samples, as the Central Limit Theorem predicts (Mood and Graybill, p. 149). Figures 6 and 7, then 8 and 9 are repetitions of the procedure using 100 and 500 conduits, respectively. Increases of sample size are accompanied by changes in slope of the frequency curves. Note also the change in plotting scale used, a feature built into the computer program to take best advantage of the dimensions of the graph. The principal axes are also better defined for larger samples concentrated within about 10 degrees of arc and 5 degrees of arc for the 100 and 500-element samples, respectively. The median value undergoes a progressive shift as sample size increases, as shown in the summary permeability plot, Figure 3. To see why, imagine the distribution of one of the principal permeabilities, if the samples were of size 1.0. It would reflect closely the assumed distribution of apertures cubed, being even more skewed than the aperture population, Figure 2. The median would lie far left of the mean. Now as samples of 2, 3 or more are treated similarly, the skewness falls off rapidly (Figure 5), and for large samples, (Figure 9) asymptotically approaches normal, no matter what the aperture distribution, whereupon the median and mean are identical. Therefore, all permeabilities will be smaller for small samples than for large samples. Inspection of all such summary plots indicates that the permeability of a model jointed medium is fairly well defined if 50 conductors are included in the sample, and very well defined for 100.

Plate 2 and its continuation, Plate 3, illustrates the effect of decreasing dispersion of a single set of dispersed joints. Across the top row of figures are the joint populations for Fisher's K_f = 6 to 60, and below each, the representation of principal permeabilities for samples of size 92 to 106, varying according to equation (A-20) to maintain a sample dimension of 1035 cm for a mass of inverse specific surface 10 cm. As dispersion decreases, there is a progressive reduction of dispersion of principal axes and permeabilities, diminution of the minor permeability, better approach to normal distribution, convergence of the two highest permeabilities and a marked increase of anisotropy. Figure 2 summarizes the convergence of permeabilities, which change little in magnitude after K_f = 30. Irregularities indicated for the permeabilities on the isotropic plane are due to the sample size, for when 500 conductors are included in each, the trends are smoothed (solutions are not shown for 500). Figure 2A is a summary plot of maximum anisotropies.. Dispersion coefficients less than K_f = 6 give principal permeabilities rapidly approaching isotropy, whereas above K_f = 20, the anisotropies are quite large. The plotted range covers the usual natural joint dispersions encountered. The sheeted granite exposure shown in Figure 5-1 indicates that a single-set model has a real counterpart in nature; whether or not apertures have been well represented remains unknown.

The simplest system of dispersed joints consists of two equal orthogonal sets, represented in Plate 4. Figure 5-2 shows a rock exposure that is essentially a two-set orthogonal system. The choice of central tendencies dipping 45 degrees NW and SE is arbitrary. The stereonet plots of principal axes indicate that the central tendencies of the two sets lie on the plane of isotropy, even for small samples. The unique major axis contains the central plane of each set, in other words, lies parallel to the predominant direction of intersections. The problem of identifying two axes on a plane of isotropy, discussed above, is exemplified in Figure 3, the summary, as though there is always a small anisotropy on that plane, whereas the scatter suggests that the two lesser permeabilities converge to each other. A medium, cut by two orthogonal sets of no dispersion (parallel), must be isotropic on the plane normal to both, with permeability exactly twice that value in the direction of the intersection. Plate 4 approaches that condition.

As soon as the two sets differ, as they do in Figure 1 of Plate 5, three unique axes appear, one axis parallel to each central tendency, the major axis again coinciding with the direction of joint intersection. The first impression is of a plane of isotropy for small samples, but on closer inspection, it is seen that the circles and crosses are not evenly intermingled. At sample size 200, the axes are distant. A small difference in principal permeabilities always results in strong dispersion of axial directions along their common plane. Note that the minor axis follows the central normal to the least dispersed set, for flow components are least in that direction.

A similar result can be obtained by varying the spacing of two orthogonal sets, as shown on Plate 6. The NW set, Figure 1, is only half as frequent as the SE set. The intersection direction is still the major axis. The lesson to learn from this plate is that of the two lesser axes, the stronger lies in the plane of the more frequent set.

When two equal sets are not orthogonal, as in Figure 1 of Plate 7, the principal axes coincide with the axes of symmetry of the system: major axis on the intersection, intermediate bisecting the acute angle and the minor bisecting the obtuse angle between conduit planes (vice-versa the conduit normals).

If one of the two non-orthogonal sets is less dispersed than the other, as in Figure 1 of Plate 8, we get the same results as in Plate 7, except that the minor principal axis shifts closer to the more dispersed planes, or less dispersed normals.

The most common natural rock unit contains three sets. Figure 3-4 illustrates a remarkably perfect, persistent, orthogonal system. Three equal sets disposed orthogonally in a pseudo-cubic pattern, as shown in Figure 1 of Plate 9, result in isotropic permeability for all sample sizes. The axes are scattered over all orientations, and permeabilities converge slowly with sample size towards a single value. The significant aspect here, as in other isotropic conditions, is the randomness of axial orientation, even though each solution is slightly anisotropic.

If two orthogonal sets are equal, their normals lie on a plane of isotropy even though a third orthogonal set exists. If that third set is weaker than the other two, for instance with greater dispersion, or greater spacing as in Plate 10, then the central tendency of the weaker set is the major axis. If the extraordinary set is stronger, by reason of closer spacing or less dispersion, as in Plate 11, then that axis is the minor permeability direction. In all such orthogonal cases weak anisotropy exists, so the axes are highly variable, converging slowly with increasing sample size towards unique axes.

If all three orthogonal sets are different, by reason of different dispersions, as in Plate 12, or by different spacings, as in Plate 13, the principal axes are still parallel to the central tendencies of the sets, with major axes parallel to the normals of the weakest conductors, and minor axis parallel to the normals of the strongest. Comparison of Plates 12 and 13 shows that spacing is more important than orientation dispersion, for the axes converge to their unique orientations for smaller sample sizes if it is spacing rather than orientation dispersion that varies.

When the third set is not orthogonal to the other two orthogonal, equal sets, as in Plate 14, then the major axis lies closest to the greatest number of intersections. Inspection of Figure 1 reveals an axis in the NW quadrant containing the central plane of the vertical set and bisecting the central planes of the horizontal and 45 degree SE set, so this is the major axis. The minor axis is that having least intersections, in this case bisecting the angle between the two closest normals.

Three non-orthogonal but equal sets are disposed at the same angle from each other in Figure 1 of Plate 15, appearing as though they belonged to a single, dispersed set. The resulting directional permeability has the symmetry of a single set, developing a plane of isotropy and a unique minor axis symmetrically centered between the three normals.

<u>Estimating principal directions from field data</u>

A general case could easily be modeled, but to no advantage. Any field data not fitting these special cases would serve as a general example. Figure 1 of Plate 26 (Page) is a stereonet

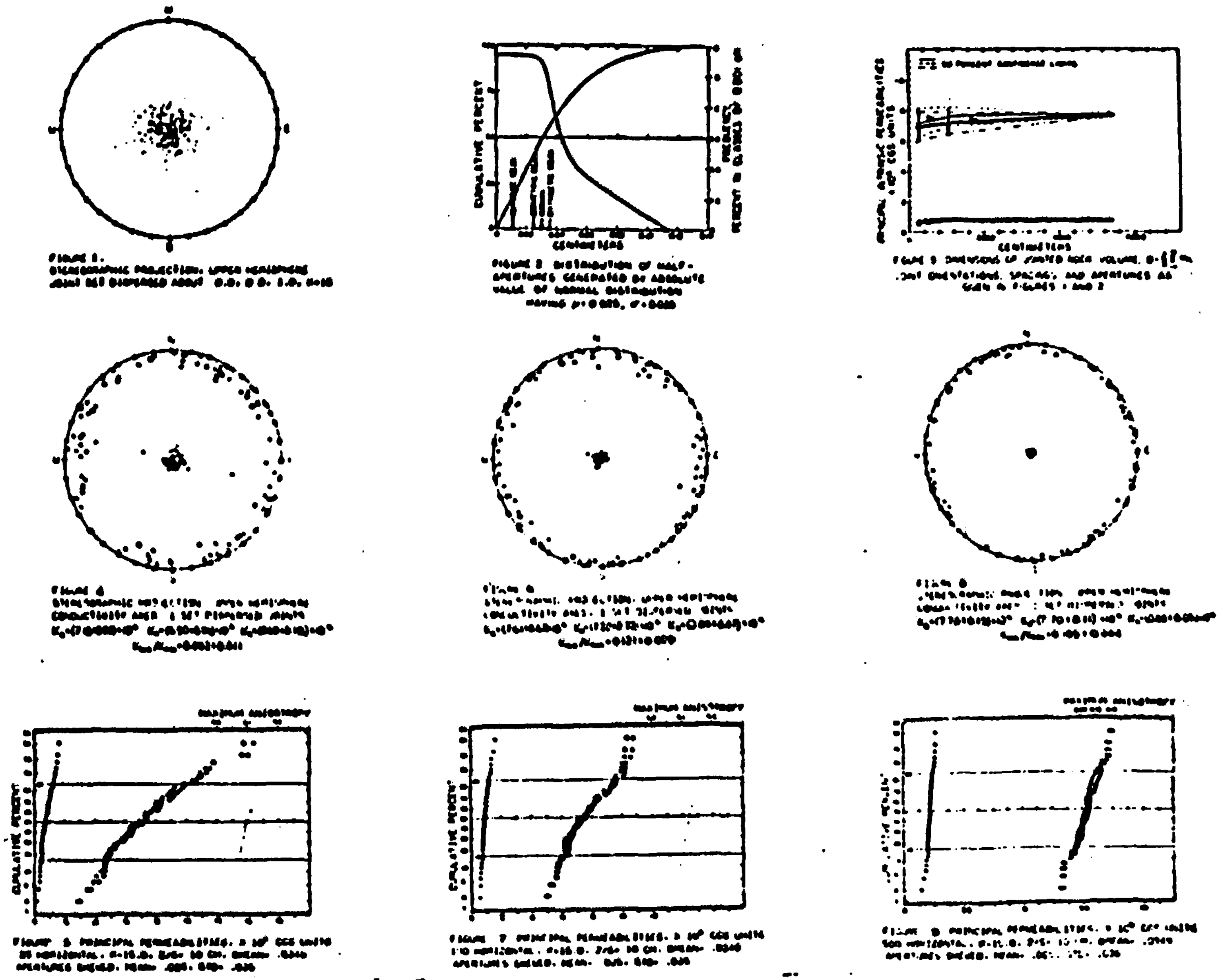

PLATE 1

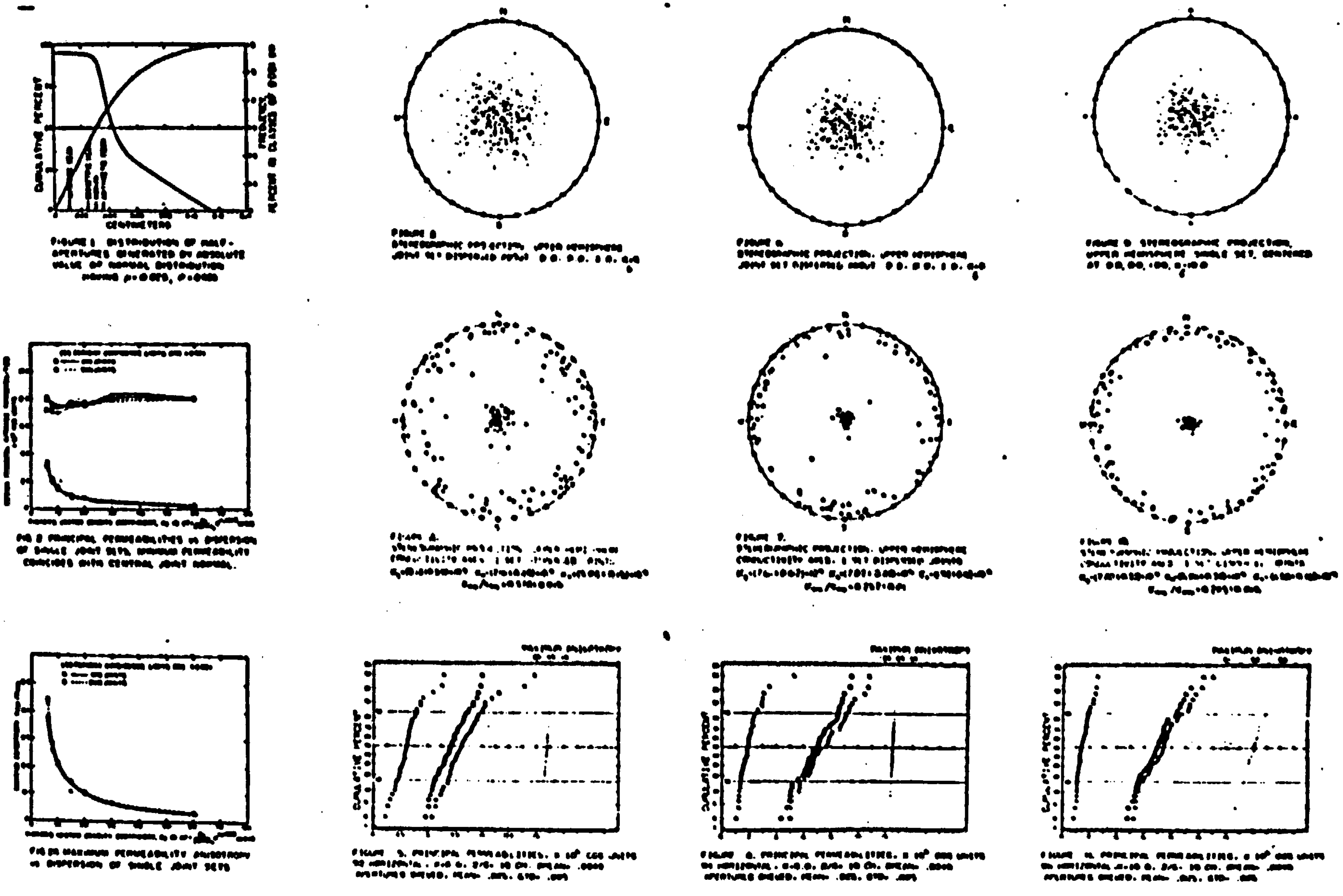

PLATE 2

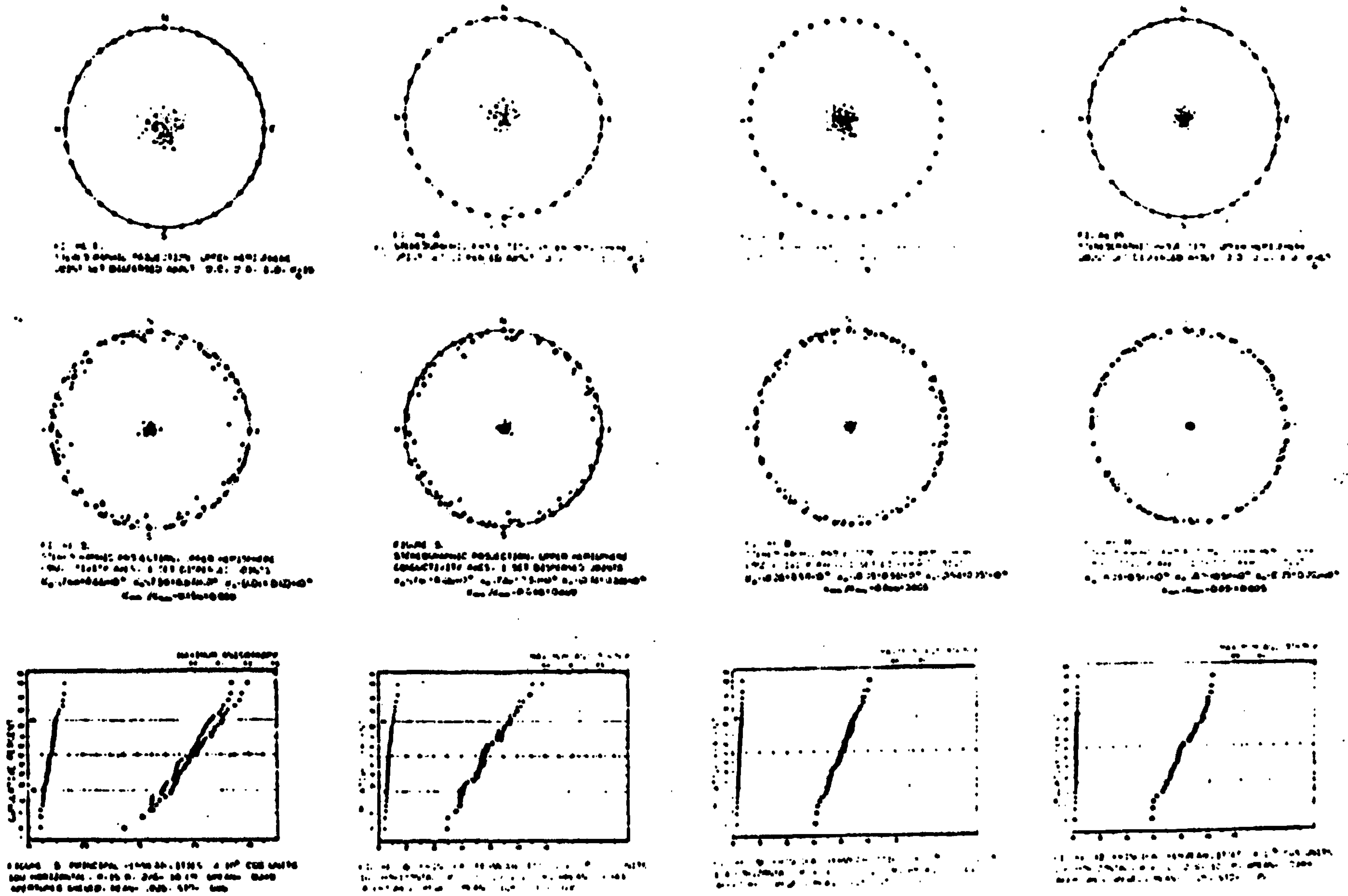

PLATE 3

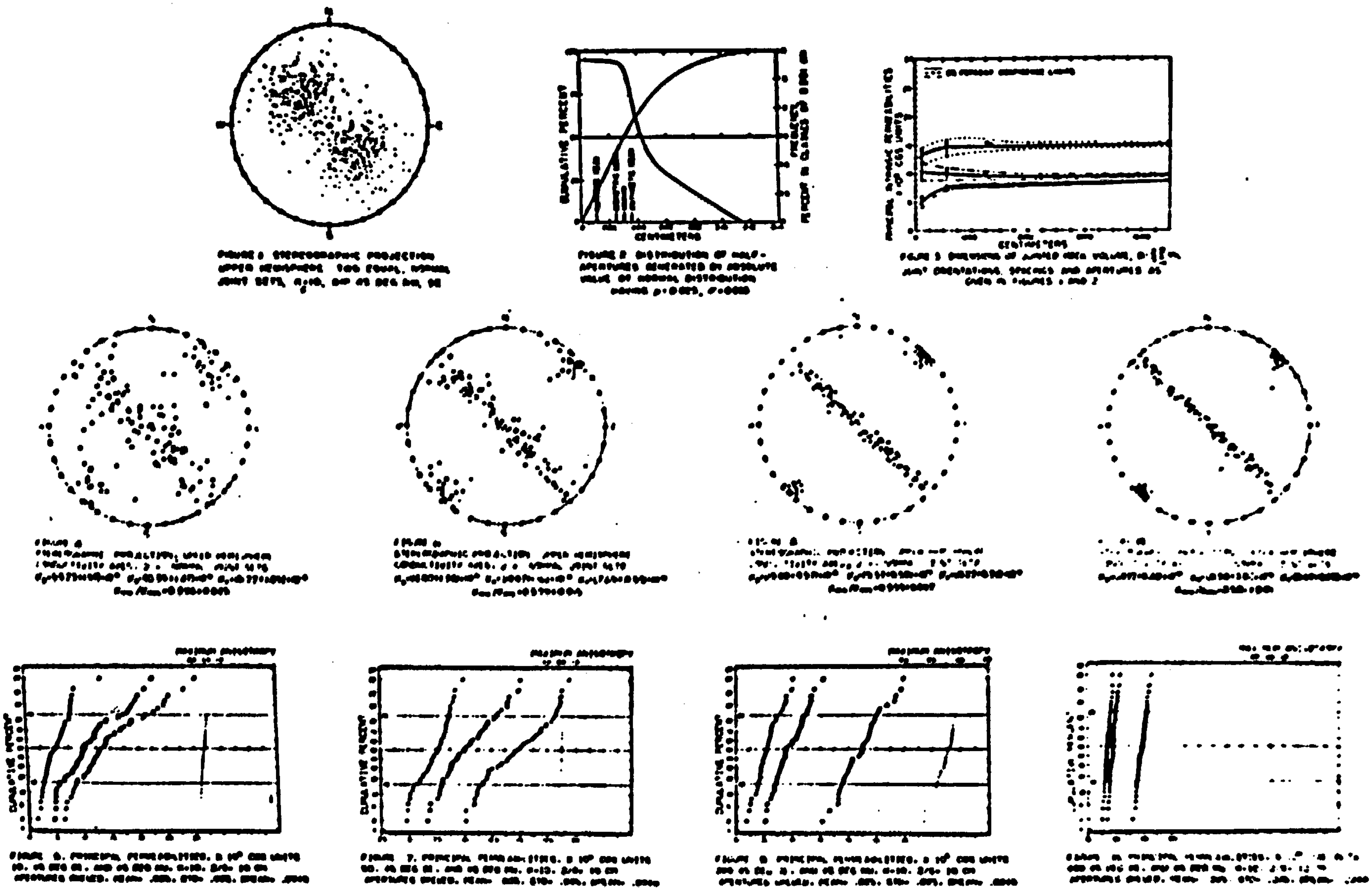

PLATE 4

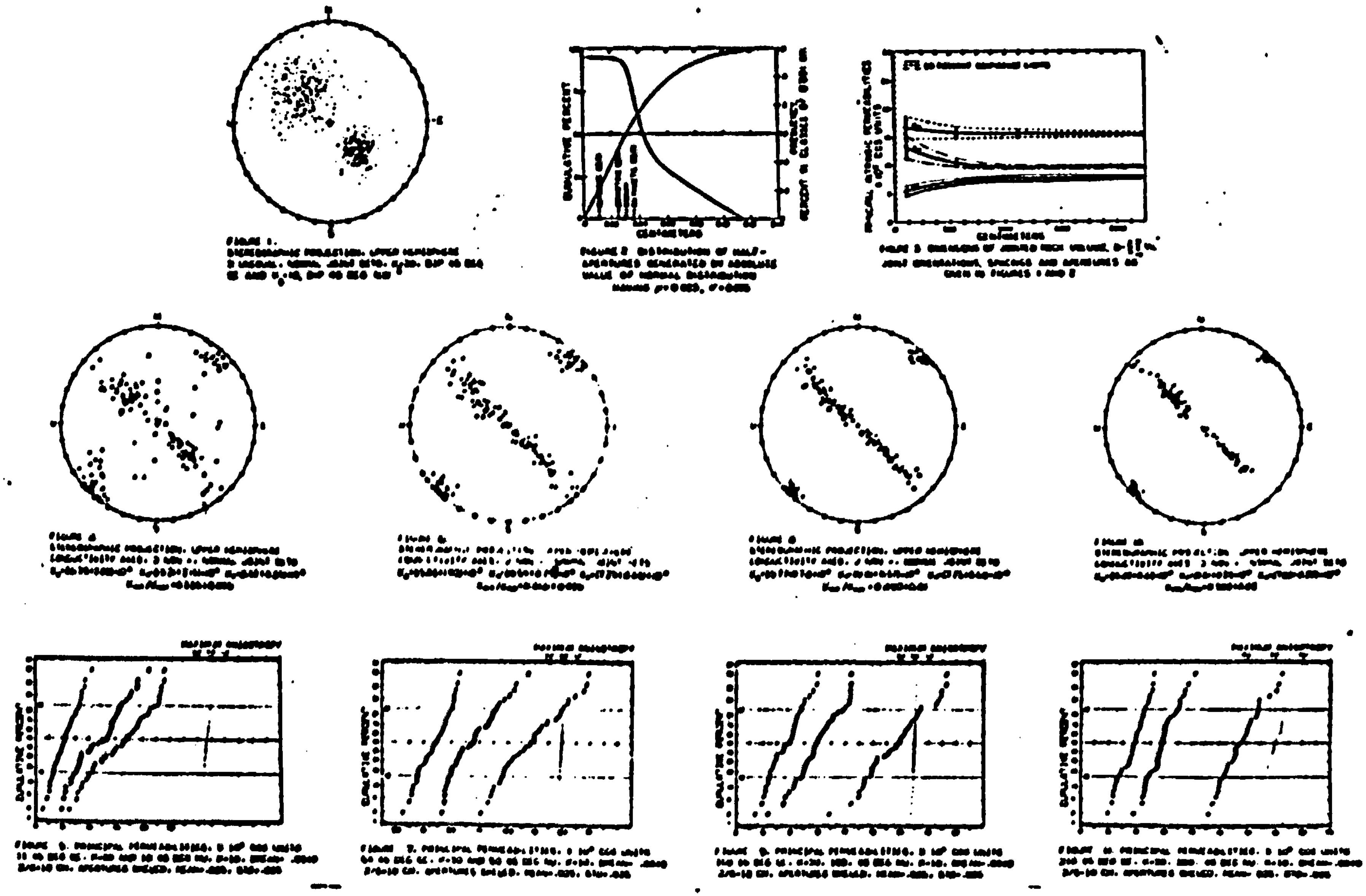

PLATE 5

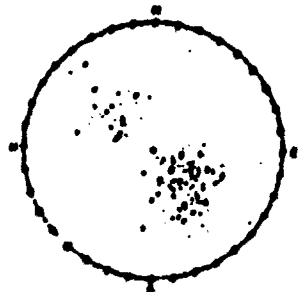

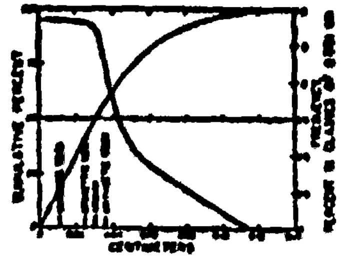

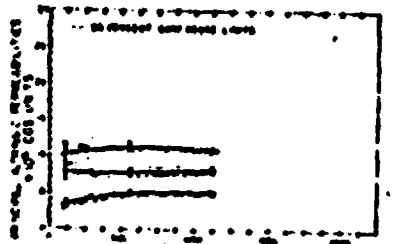

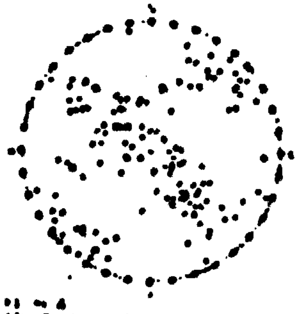

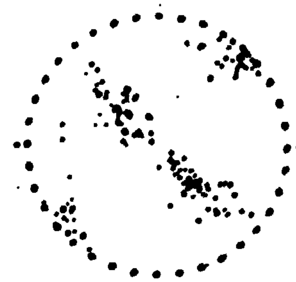

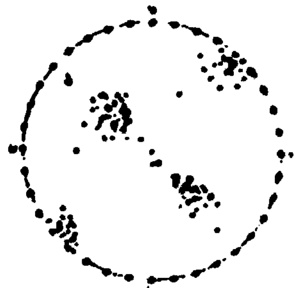

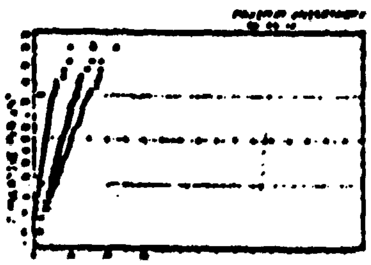

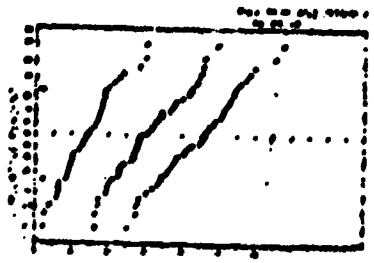

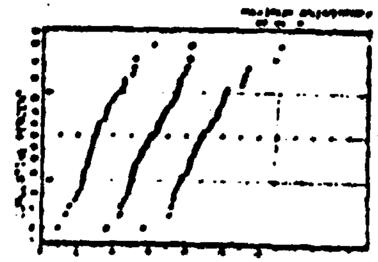

PLATE 6

PLATE 7

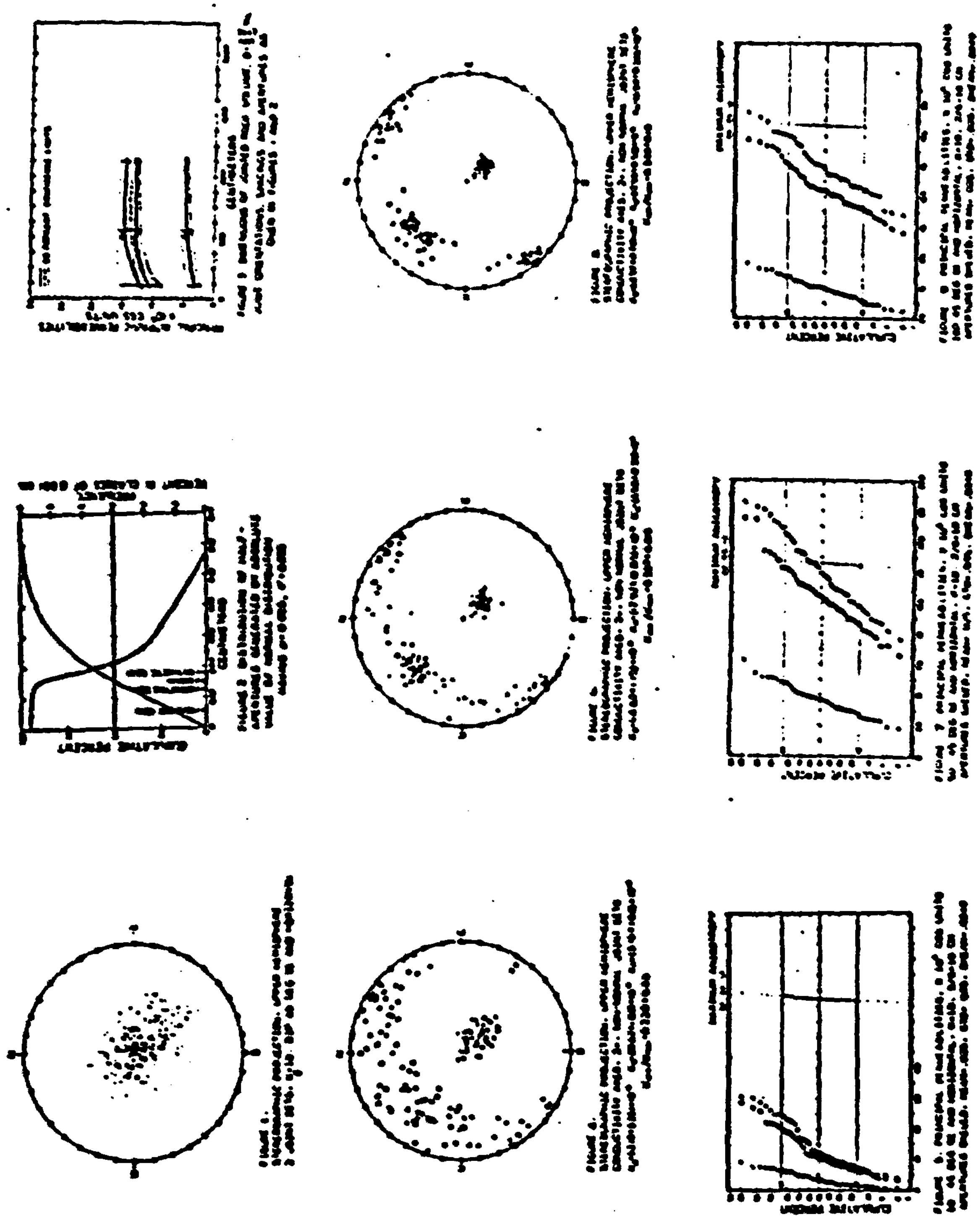

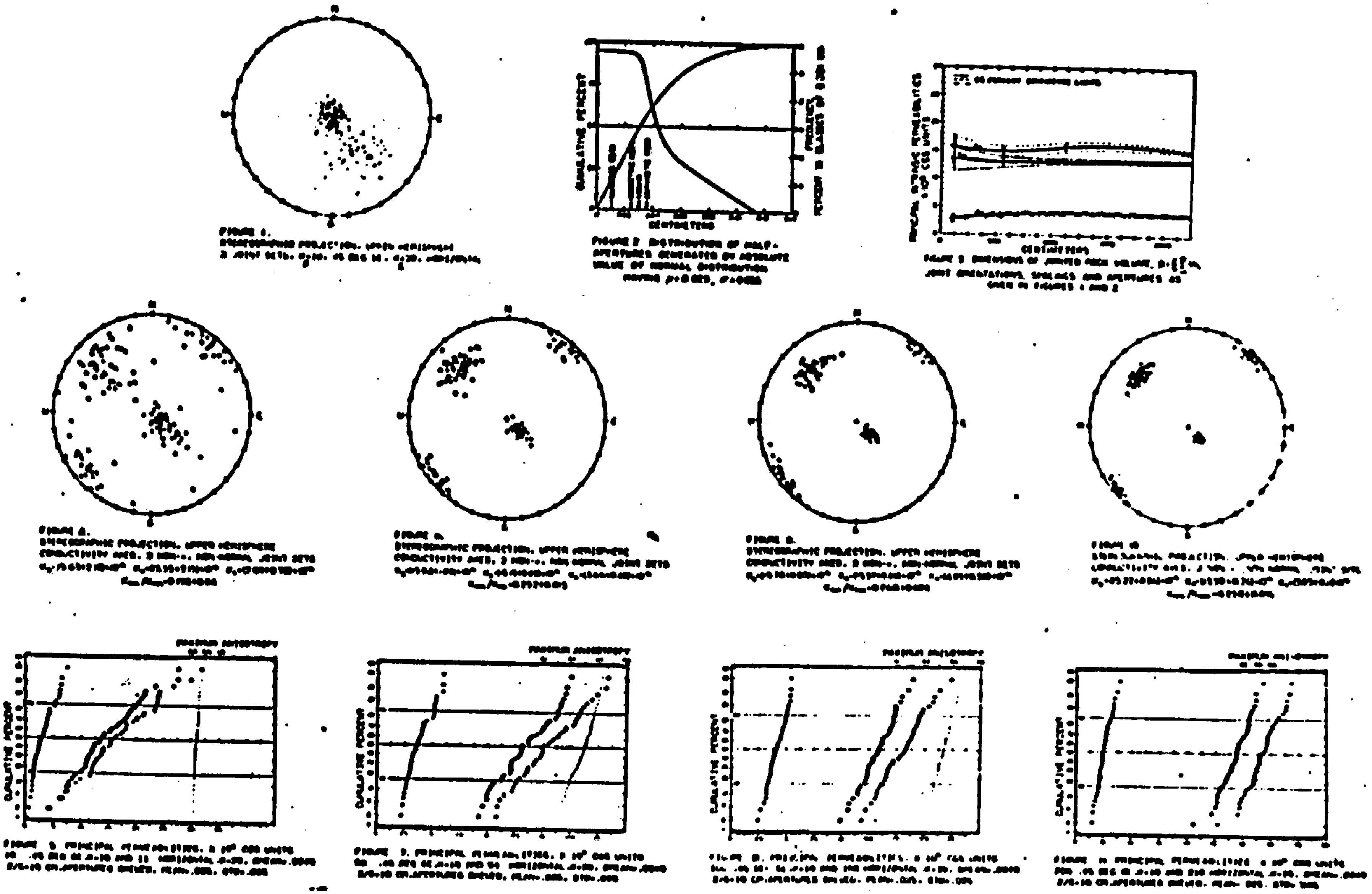

PLATE 8

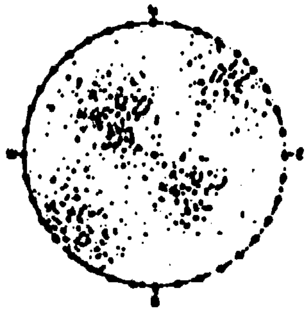

FIGURE 1. STEREOGRAPHIC PROJECTION, UPPER HEMISPHERE [illegible]

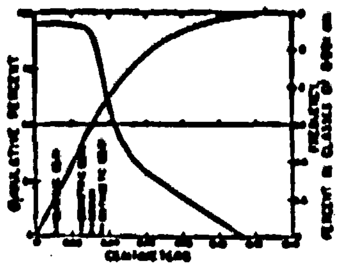

FIGURE 2. DISTRIBUTION OF HALF-APERTURES GENERATED BY ABSOLUTE VALUE OF NORMAL DISTRIBUTION [illegible]

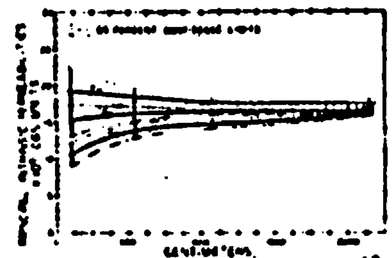

FIGURE 3 [illegible]

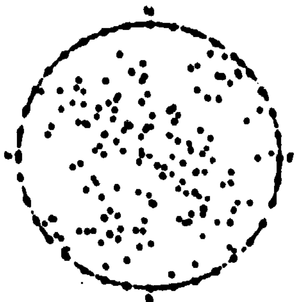

FIGURE 4. [illegible]

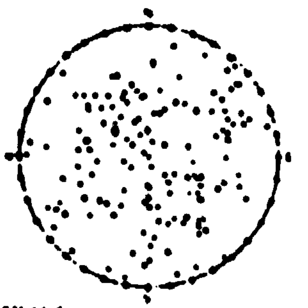

FIGURE 6. STEREOGRAPHIC PROJECTION, UPPER HEMISPHERE [illegible]

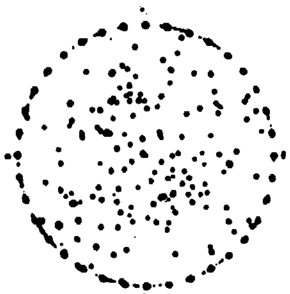

FIGURE 8. [illegible]

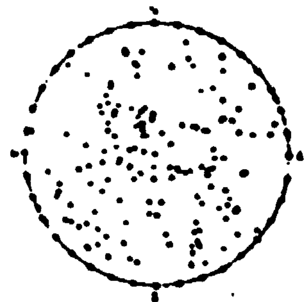

FIGURE 10. STEREOGRAPHIC PROJECTION, UPPER HEMISPHERE [illegible]

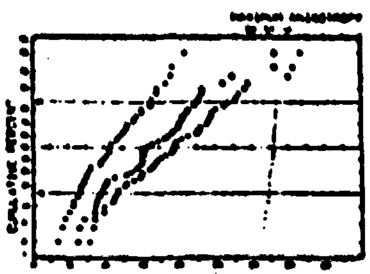

FIGURE 5. PRINCIPAL PERMEABILITIES [illegible]

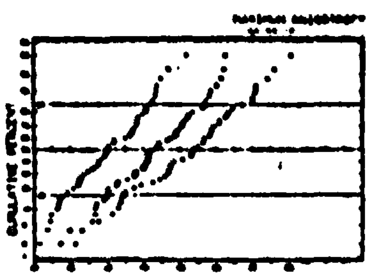

FIGURE 7. PRINCIPAL PERMEABILITIES [illegible]

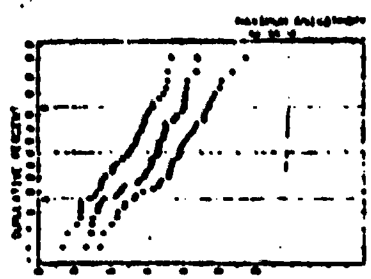

FIGURE 9. PRINCIPAL PERMEABILITIES [illegible]

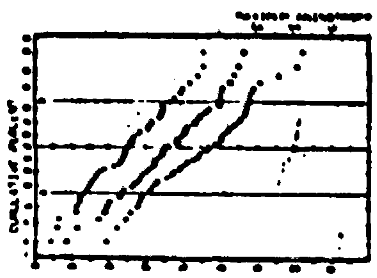

FIGURE 11. PRINCIPAL PERMEABILITIES [illegible]

PLATE 9

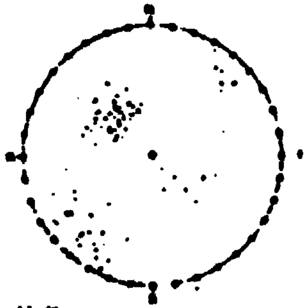

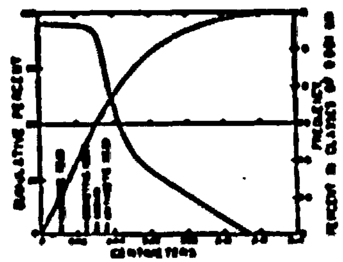

FIGURE 2 DISTRIBUTION OF HALF-APERTURES GENERATED BY ABSOLUTE VALUE OF NORMAL DISTRIBUTION

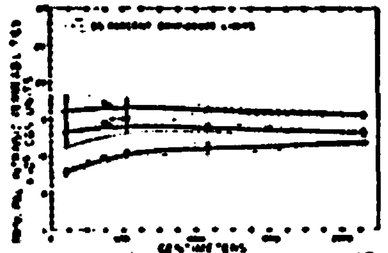

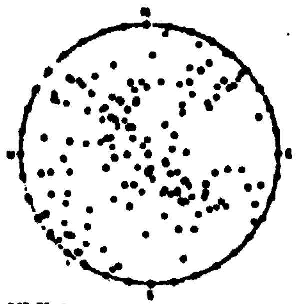

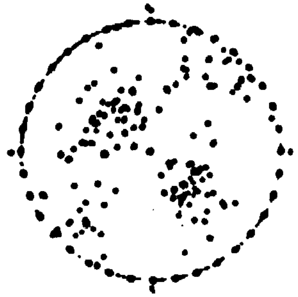

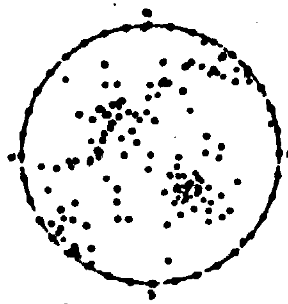

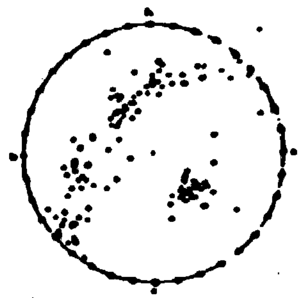

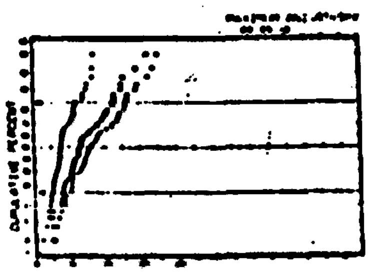

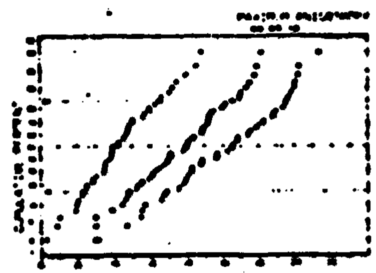

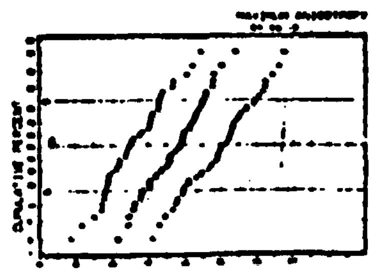

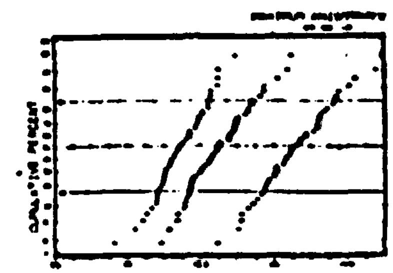

PLATE 10

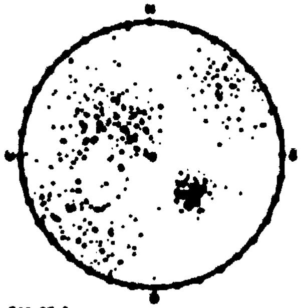

FIGURE 1.
STEREOGRAPHIC PROJECTION, UPPER HEMISPHERE [illegible]

FIGURE 2. DISTRIBUTION OF HALF-APERTURES GENERATED BY ABSOLUTE VALUE OF NORMAL DISTRIBUTION [illegible]

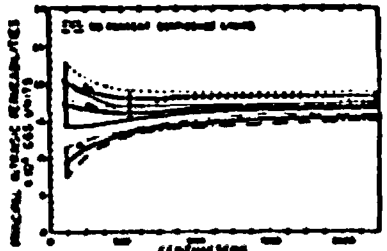

FIGURE 3. DIMENSIONS OF JOINTED ROCK VOLUME [illegible] JOINT ORIENTATIONS, SPACINGS AND APERTURES AS GIVEN IN FIGURES 1 AND 2

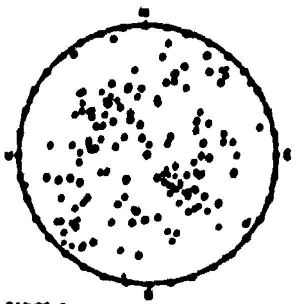

FIGURE 4.
STEREOGRAPHIC PROJECTION, UPPER HEMISPHERE [illegible]

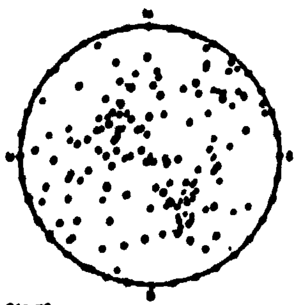

FIGURE 6.
STEREOGRAPHIC PROJECTION, UPPER HEMISPHERE [illegible]

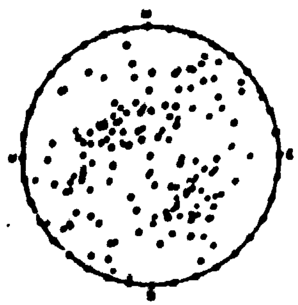

FIGURE 8.
STEREOGRAPHIC PROJECTION, UPPER HEMISPHERE [illegible]

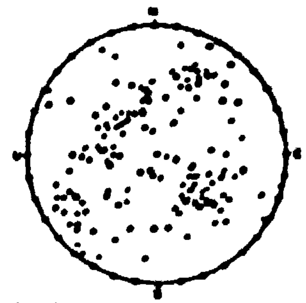

FIGURE 10.
STEREOGRAPHIC PROJECTION, UPPER HEMISPHERE [illegible]

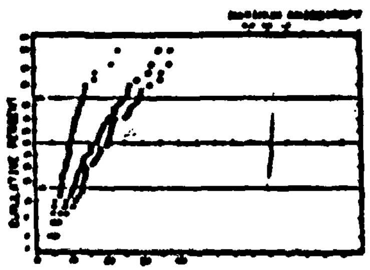

FIGURE 5. PRINCIPAL CONDUCTIVITIES [illegible]

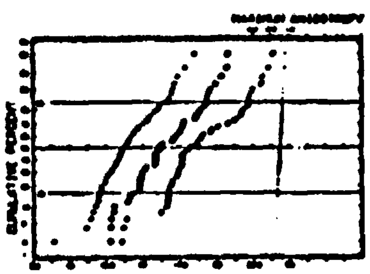

FIGURE 7. PRINCIPAL CONDUCTIVITIES [illegible]

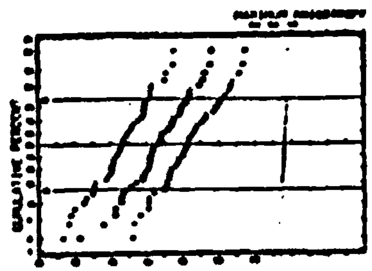

FIGURE 9. PRINCIPAL CONDUCTIVITIES [illegible]

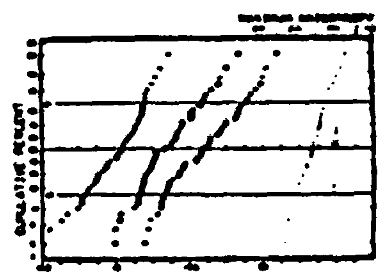

FIGURE 11. PRINCIPAL CONDUCTIVITIES [illegible]

PLATE 11

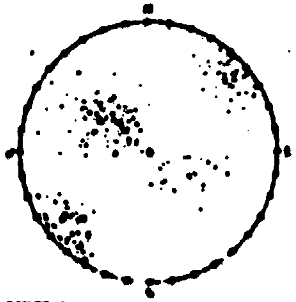

[illegible]

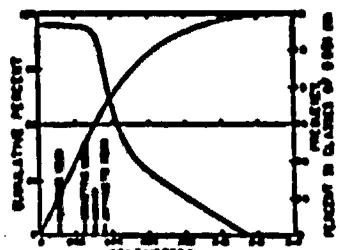

[illegible]

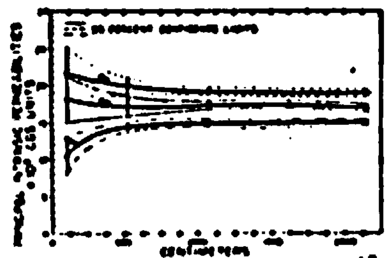

[illegible]

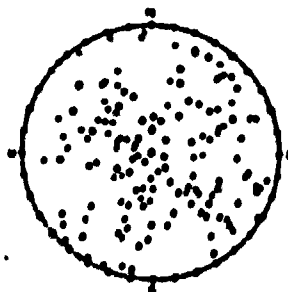

[illegible]

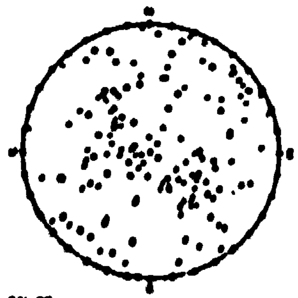

[illegible]

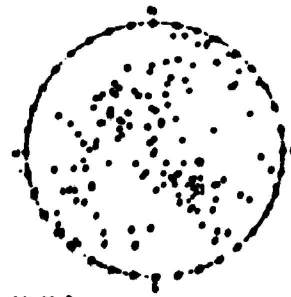

[illegible]

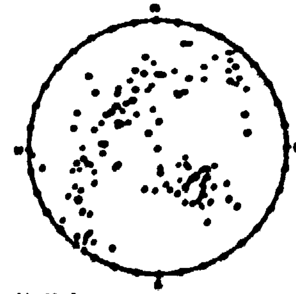

[illegible]

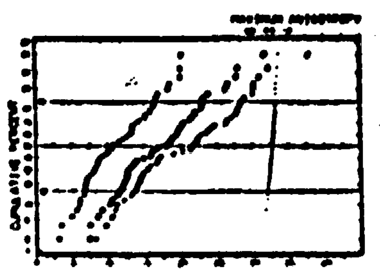

[illegible]

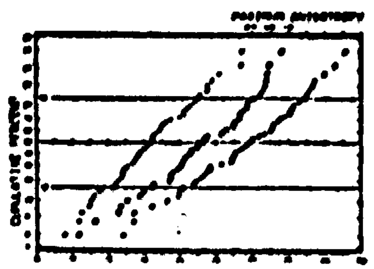

[illegible]

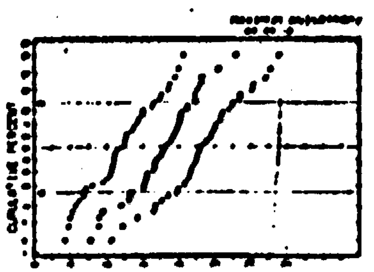

[illegible]

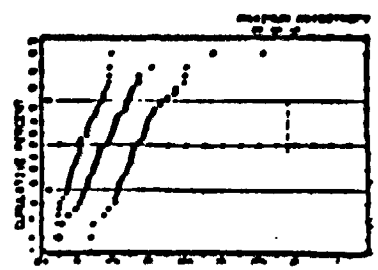

[illegible]

PLATE 12

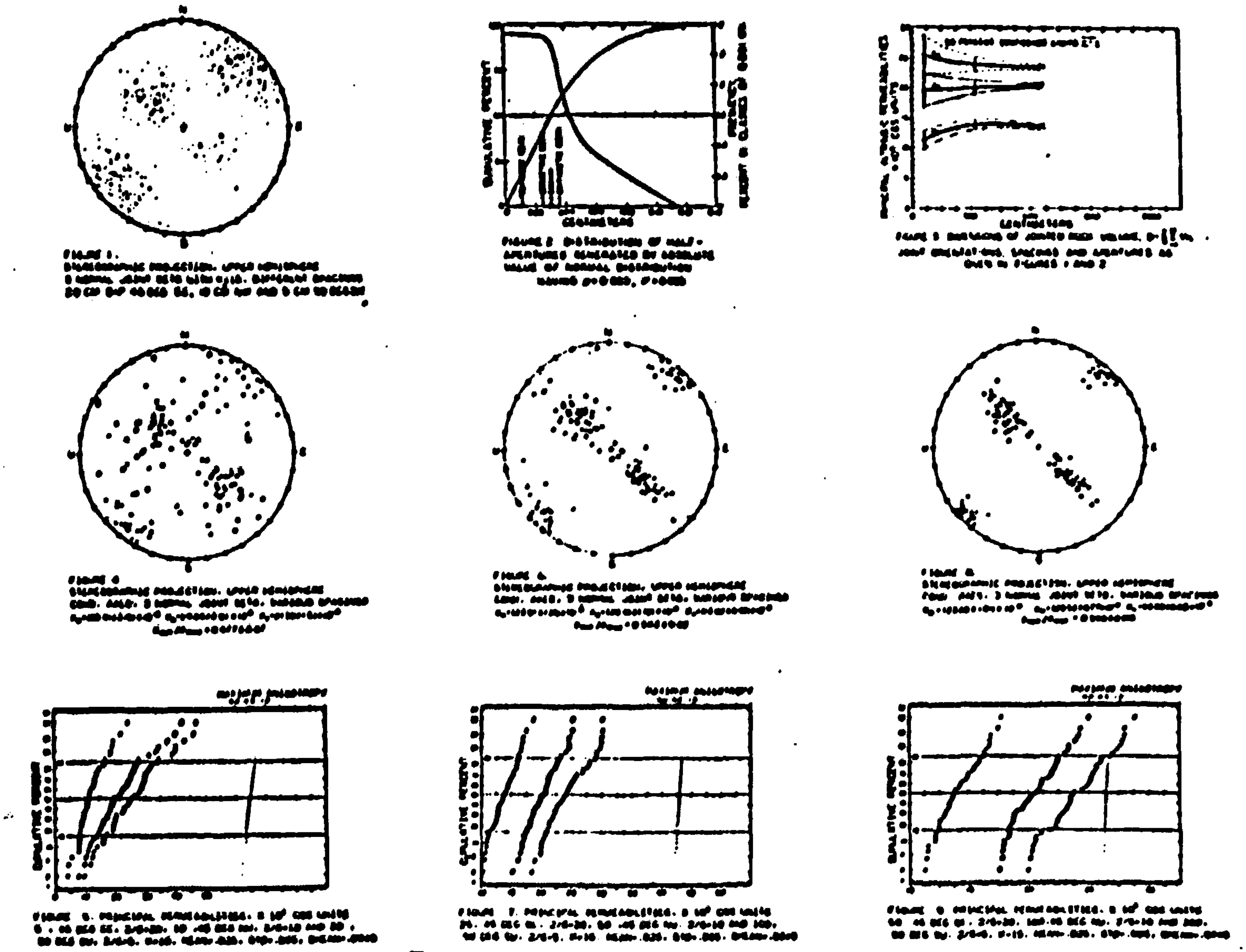

PLATE 13

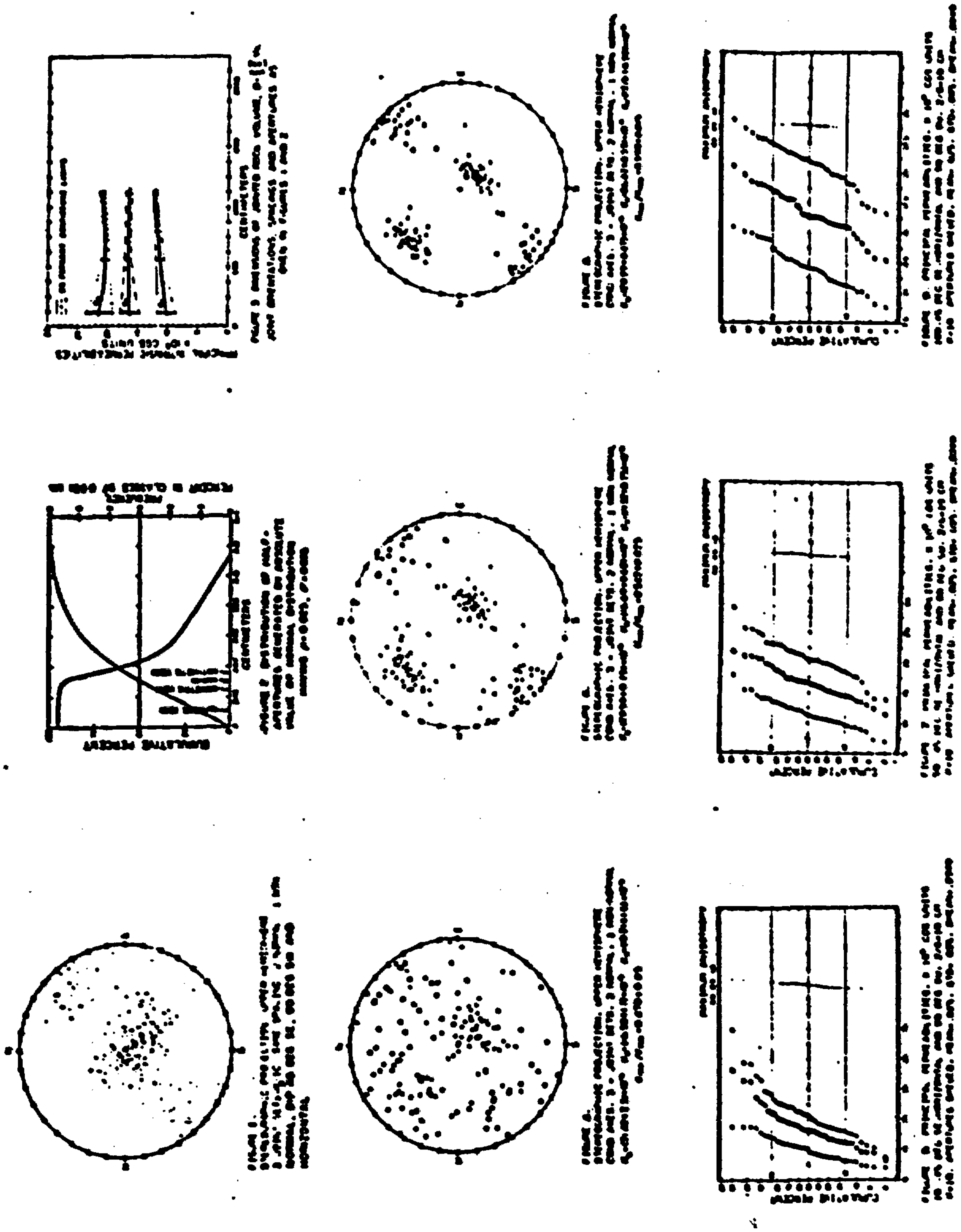

PLATE 15

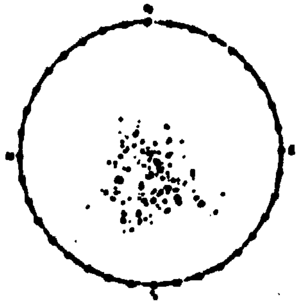

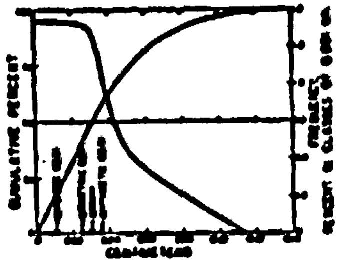

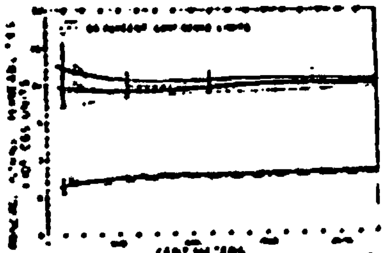

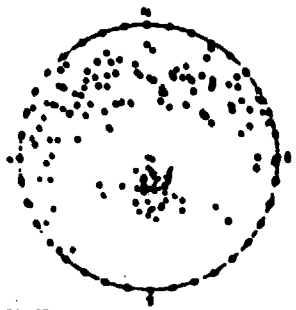

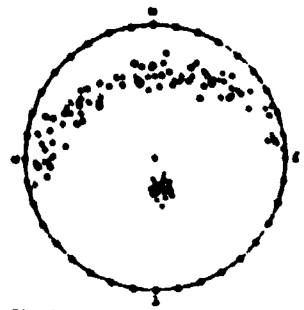

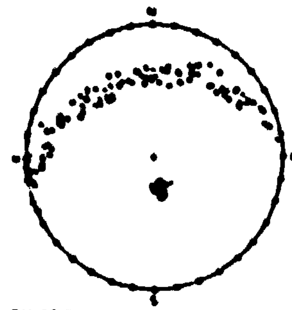

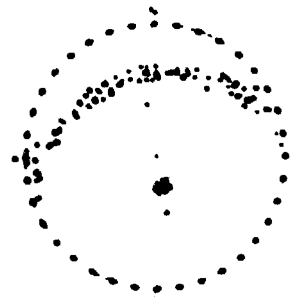

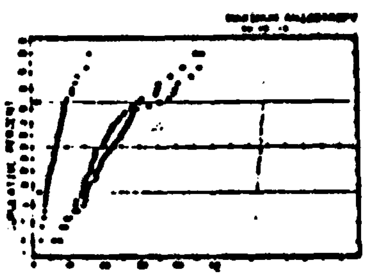

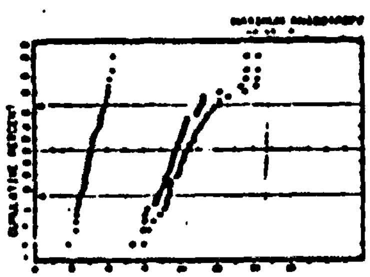

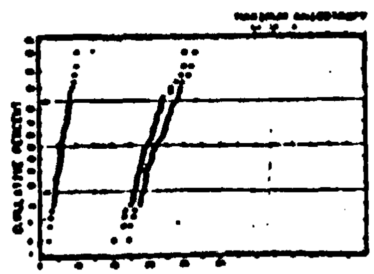

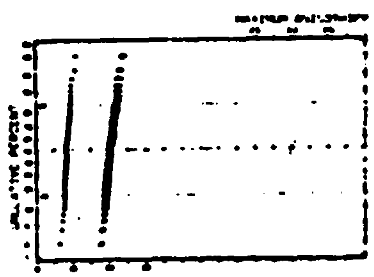

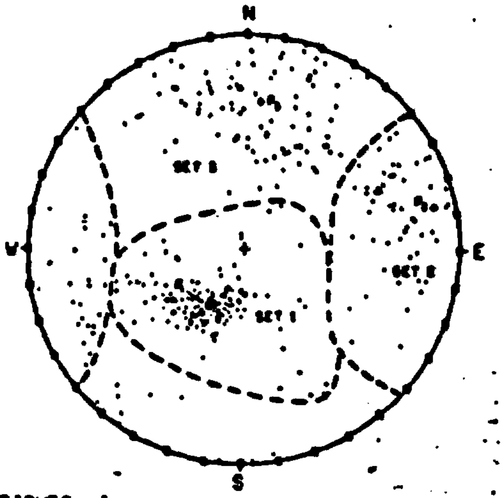

FIGURE 1.
STEREOGRAPHIC PROJECTION, UPPER HEMISPHERE
DWR OROVILLE, LET 1, PLATE 4, JOINT PATTERN
P_1 = 04759, -0 2994, 0 8276 P_2 = -02283, 09637, 01050
P_3 = -09323, 00819, 03540
K_{f_1} = 13 0 K_{f_2} = 12 0 K_{f_3} = 9 75

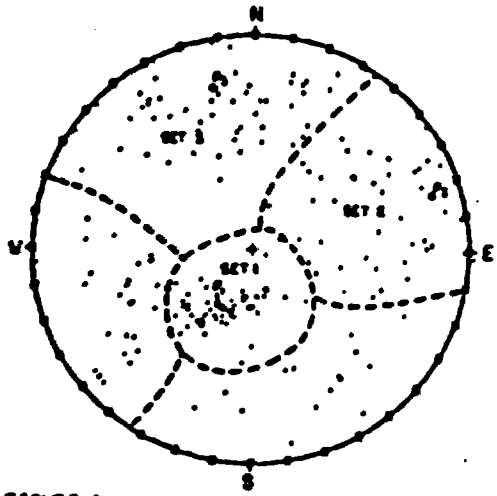

FIGURE 4.
STEREOGRAPHIC PROJECTION, UPPER HEMISPHERE
DWR PLATE 6, LET-2 LOC. JOINT PATTERN
P_1 = 0 5000, -0 2580, 0 2635, P_2 = -0 2848, 0 3856, 0 8780,
P_3 = -0 9474, -0 2463, 0 2070
K_{f_1} = 12 3 K_{f_2} = 6 0 K_{f_3} = 7 3

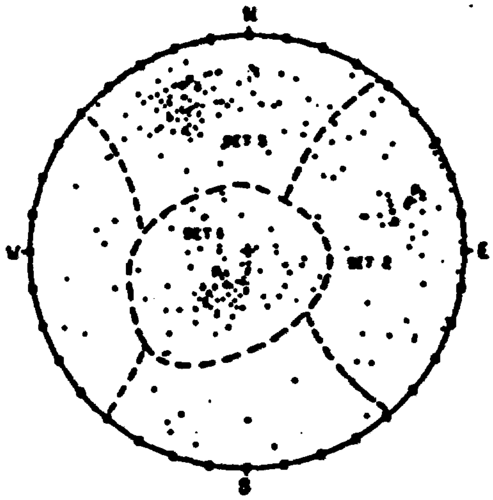

FIGURE 3.
STEREOGRAPHIC PROJECTION, UPPER HEMISPHERE
DWR OROVILLE, PLATE 10, CHANNEL JOINT PATTERN
P_1 = 0 2786, -0 1893, 0 9418, P_2 = -0 3171, 0 9186, 0 236
P_3 = -0 9176, -0 3549, 0 1790
K_{f_1} = 11 0 K_{f_2} = 12.0 K_{f_3} = 11 75

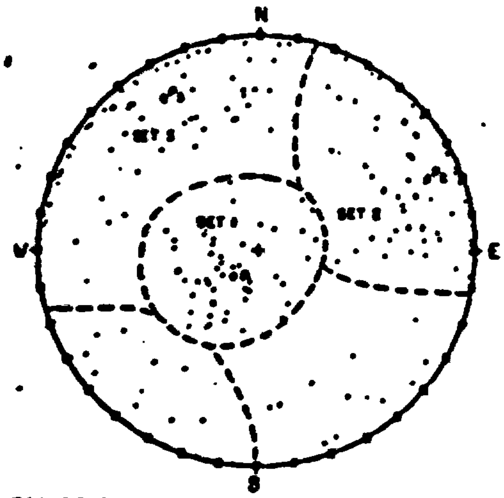

FIGURE 2.
STEREOGRAPHIC PROJECTION, UPPER HEMISPHERE
DWR PLATE 9, L. ABUT OUTCROP, JOINT PATTERN
P_1 = 0 2318, -0 2083, 0.9505, P_2 = 0.3916, 0 9003, 0 1760
P_3 = -0 8460, -0 5128, 0 1470

of joint normals replotted from Oroville Damsite exploration data (Lyons, 1960) by Subroutine REPLTI, with its parameters, namely the central tendency of each set and the vector strength, computed by Subroutine JDATA. These axes differ by several degrees from the visual estimates used by the designers of the Oroville power cavern. The axes are marked and the equivalent dispersion coefficients labeled. Figure 5-0 was used to translate vector strength to Fisher's coefficient. The angle between central tendencies are, in degrees:

Set 1 ∢ Set 2 = 72

Set 1 ∢ Set 3 = 80

Set 2 ∢ Set 3 = 71

In this non-orthogonal system, there is some symmetry, since set 2 is almost equidistant from sets 1 and 3, but it will be shown that the symmetry does not help locate the principal axes. The relationships are sketched in Figure 2 of Plate 26. Judging by the dispersions, (Figure 1) set 1 is the strongest and set 3 the weakest, but none of the sets are remarkably different. The model studies, in particular Plate 12, indicated a rather weak dependence of axes upon relative dispersion of the sets. A report on the jointing at the Oroville site (Lyons, 1961) tabulates observed properties of the three sets from tunnel exposures:

Table 5-1

Feature	Joint Set 1	Joint Set 2	Joint Set 3
Spacing, Range Average	0.02 - 5.0 1.5 ft.	0.05 - 5.0 1.2 ft.	0.05 - 4.0 1.0 ft.
Regularity	Planar	Irregular &/or curved	Curved, less commonly regular
Nature of Surface	Smooth, less commonly rough	Rough	Rough
Width Range Average	1/2 1/32 in.	1 1/32 in.	3/4 1/32 in.
Tightness	Tight	Tight, a few slightly open	Tight, a few slightly open
Staining & filling	Quartz, calcite, some iron oxide	Quartz, epidote calcite, rarely chlorite, pyrite, iron oxide	Quartz, calcite, less common iron oxide, rare epidote, chloride, pyrite
Notes	Locally well developed	Parallel with schistocity	Well developed

Some qualitative conclusions can be drawn from these observations. The effect of spacing makes set 3 strongest and 1 weakest. The factor of spacing is more influential in controlling relative strength of the sets than is the dispersion, factors which are partly compensating in this case. All other factors equal, more planar conductors are less resistent to flow than are irregular ones, but the planar joints are diagnosed as shear failures with smoother, tighter-fitting surfaces. In this case, one might conclude from the table that the tight, smooth set 1 is a poor conductor compared to sets 2 and 3. Paucity of iron-staining would be indicative of little percolation, but all sets [redacted] seem alike in this aspect. An observer cannot obtain a good measure of aperture at the exposure. A shear direction complimentary to set 1 is not evident, while the roughness, tightness, apparent aperture and irregularity of sets 2 and 3 put them in the tension joint category, probably several times as conductive as set 1. Set 3, besides, is better developed, meaning more continuous. A reasonable estimate of the permeability with respect to these sets may be

Set 1 : Set 2 : Set 3 = 2 : 5 : 6

Since it is not sets 1 and 3 that are alike, the orientation symmetry does not help. Since a minor axis lies closest to the normal of a strong conductive set, a fair estimation of the orientation of the minor axis when several sets are combined is the resultant of normals, weighted according to their estimated conductivities. Thus the resultant

$$2(\vec{1}) + 5(\vec{2}) + 6(\vec{3})$$

has direction cosines -.676, .541, .503,

the minor permeability axis shown in Figure 2 of Plate 26. The other axes are on the plane normal to the minor axis. The major axis is near to the intersection of the 2 and 3-planes, slightly towards the 1-plane, as estimated in the figure. This defines the intermediate orthogonal as well.

These axes, determined solely from the geometry of joints and with qualitative guidance from the nature of the fractures, applies only to the jointed decompressed rock near the exposed surface. Somewhat different conditions may exist in the undisturbed rock. If only surface observations are available, they must be used as guides to the undisturbed, deeper medium. If pressure-testing is being designed, as recommended in Chapter 2, surface orientations give the best available indications of principal axes. Borings usually confirm (in the writer's experience) the extrapolation of surface joint geometry to depth, but study of the core, bore-hole photographs and drill-water consumption must be maintained for continued re-evaluation of the surface-data estimate.

Spacing varies rapidly with depth in many crystalline rocks. The cost of conducting a sophisticated pressure-test program is little more than the cost of conventional methods. It seems advisable, in cases where seepage or potential distribution is critical, to augment pressure tests with data obtained by tools like the bore-hole camera to determine joint orientations, spacings and measures of large apertures.

There is available (Calif. Dept. of Water Resources, 1963) for the Oroville site the rare sort of data necessary to establish the relative conductive importance of joint sets at depth. Figure 3 of Plate 26 presents in stereographic projection the reported orientations of 84 major planar features, 77 faults, 1-25 feet wide, and 7 schistose zones up to 7 feet wide. A significant clustering of orientations occurs in the direction of set 2 of Fig. 1, Plate 26.

Insofar as 90 percent of the pumping test discharges (Thayer, 1962), could be attributed to flow in shears instead of joints, it is apparent that Fig. 3 more nearly indicates the anisotropy of the foundation as a whole than does Fig. 2 which is appropriate for near-surface (e.g. the periphery of tunnels) problems.

The major conductors of Fig. 3 fall nearly within a symmetrical single-set dispersion of $K_f \cong 15$. Plates 2 and 3 were used to estimate this dispersion. The axis of minimum permeability is inclined 23 degrees westward, having about 1/7th the permeability as exists on an isotropic plane that strikes nearly N-S and dips steeply E.

<u>The effect of sample size</u>

One of the foundations of ground-water hydrology is the assumption that intergranular porous media may be treated as continua within recognizable geologic boundaries.

The average velocity through a unit area is the vector sum of the discharges of a large number of pore openings through the unit area (Day, P. R., Lecture, University of California, Nov. 17, 1961). Though individual pore discharges are presumably variable in magnitude and direction, the mean of a large sample is the mean of the entire population, with small dispersion about the mean for successive samples (see Chapter 6).

Similar reasoning applies to fractured media (Muskat, 1949, p. 267):

> "When such fractures are of limited extent and uniformly distributed through the pay, they will give a resultant effect equivalent to that of a homogeneous porous medium. However, when they are of extended length and limited in number, they may be considered separately as linear channels."

Sands and jointed rock do not qualify in detail as continua: neither retain the same properties upon infinite subdivision. Most boundaries of intergranular flow problems include such large numbers of conductors, however, that the assumption of continuity is acceptable. But since large numbers of fractures cannot be assumed to lie within problem boundaries, an adequate number of conduits (or adequate boundary dimensions) should be specified to give the desired precision of answers.

Whether or not a discontinuous jointed rock can be treated as a continuum depends on arbitrary confidence levels one may set. The work of this chapter, in part, is to indicate the sample size required for acceptable precision in permeability prediction. Almost all flow problems lie in a region between the extremes indicated by Muskat, a region where properties are evident only after statistical manipulation. The model proposed here is a tool for simulating Nature's statistics of fractured media.

How to determine from test values the best permeability to apply to a large-scale boundary problem in jointed rock is an important and somewhat questionable problem. Petroleum engineers have studied it, with the object of extrapolating laboratory permeability data obtained from drill cores, to volumes having the dimensions of a reservoir. Warren and Price (1961) summarized the literature and presented computer model results based on the assumption that small volumes of rock possess uniform permeability and that the whole mass is composed of many such volumes having permeabilities distributed as the laboratory test values. This led them (p. 160) to the conclusion that regardless of the distribution, the overall permeability is well estimated by the geometric mean of individual measures. Jointed or fractured rock does not fit this assumption of uniform discrete blocks of different permeability. Individual planar conductors extend large distances. Some die out with distance, overlapping others that commence at an intermediate position. The important variable, continuity of conductors, therefore, urgently requires field and model investigation. Needed is a procedure for estimating overall permeability from sample permeabilities, one that lies between the methods of Warren and Price, and that of the writer.

It is felt that most jointed rock is more closely duplicated by the continuous-channel model than by the discrete-element model. The influence of discontinuities depends upon the scales involved. It could perhaps be demonstrated that if joints extend many times their spacing, the discontinuities in the array will alter the permeability very little. When extent approaches spacing, permeability may drop rapidly. Mueller (1933) and Hodgson (1961) have attempted to obtain field data on spacing. Field examination is hampered by the need to study conduits in exposures, where they are seen in only one dimension, much disturbed from their intact subsurface state.

One objective fulfilled by the model is elucidation of the dependence of permeability on sample size, or for given spacing, on volume of media between boundaries. Inspection of Figs. 3 of plates 1 to 15 show that with some geometrical fracture systems, all three principal permeabilities, minor, intermediate, and major, increase with increasing sample size. More often one or two increase while the other falls. Since it is the geometric mean of the three that serves as the isotropic permeability in discharge computations, it is logical to investigate the effect of sample size upon this effective permeability:

$$K = \sqrt[3]{K_1 K_2 K_3} .$$

Figures 5-4 and 5-5 summarize these relationships between the geometric mean (isotropic) permeability and sample size, from all computer batches, Plates 1 to 15. All model systems display increasing permeability with size, usually becoming assymptotic to an infinite sample-size value at about 200 conductors, though a few appear to increase without limit. Uncertainties within the range of the 95 percent confidence limits may explain some of the exceptions to asymptotic closure. The difference between infinite medium permeability and small sample (20 to 30 conductors) permeability varies from one system to another, and doubtless depends also on the parent distribution of apertures. Permeability changes, from small to large samples, are 5 to 25 percent of the infinite-sample values. It is concluded that whatever aperture distributions are found in nature, the infrequency of large apertures (see Chapter 6) will result in highly skewed aperture-cubed distributions. Consequently, there is a trend of increasing bulk permeability with increasing problem dimensions.

If heterogeneity is as postulated by Warren and Price (1961), with the bulk composed of individual uniform, volume elements, larger samples would give smaller permeability. Each of the 49 runs depicted in each frequency curve could be considered as the permeability of a volume element. The geometric mean of such a distribution, skewed to the right, is always less than the median or mean. (See Fig. 2 of Plate 1)

The usefulness of the median permeability for predicting flow in a single installation, such as a drill-hole in an extensive medium, has been discussed. The median is readily obtained by cumulative plotting of permeability measures (see Chapter 6).

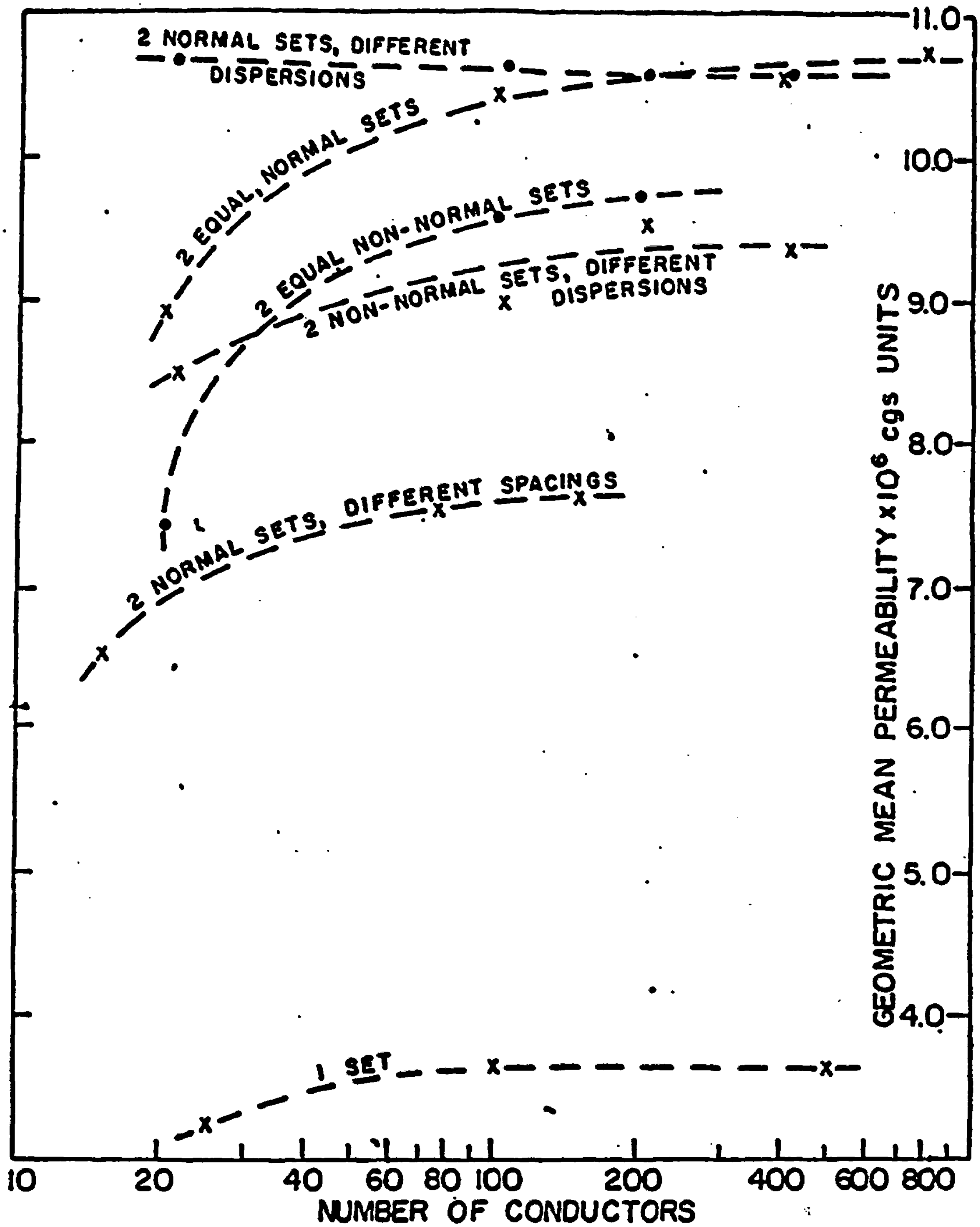

FIGURE 5-4. INCREASE OF GEOMETRIC MEAN PERMEABILITY, $\sqrt[3]{K_x K_o K_\phi}$, WITH THE NUMBERS OF CONDUCTORS IN THE MODEL. DATA DERIVED FROM ONE AND TWO-SET SYSTEMS, PLATES I AND 4-8.

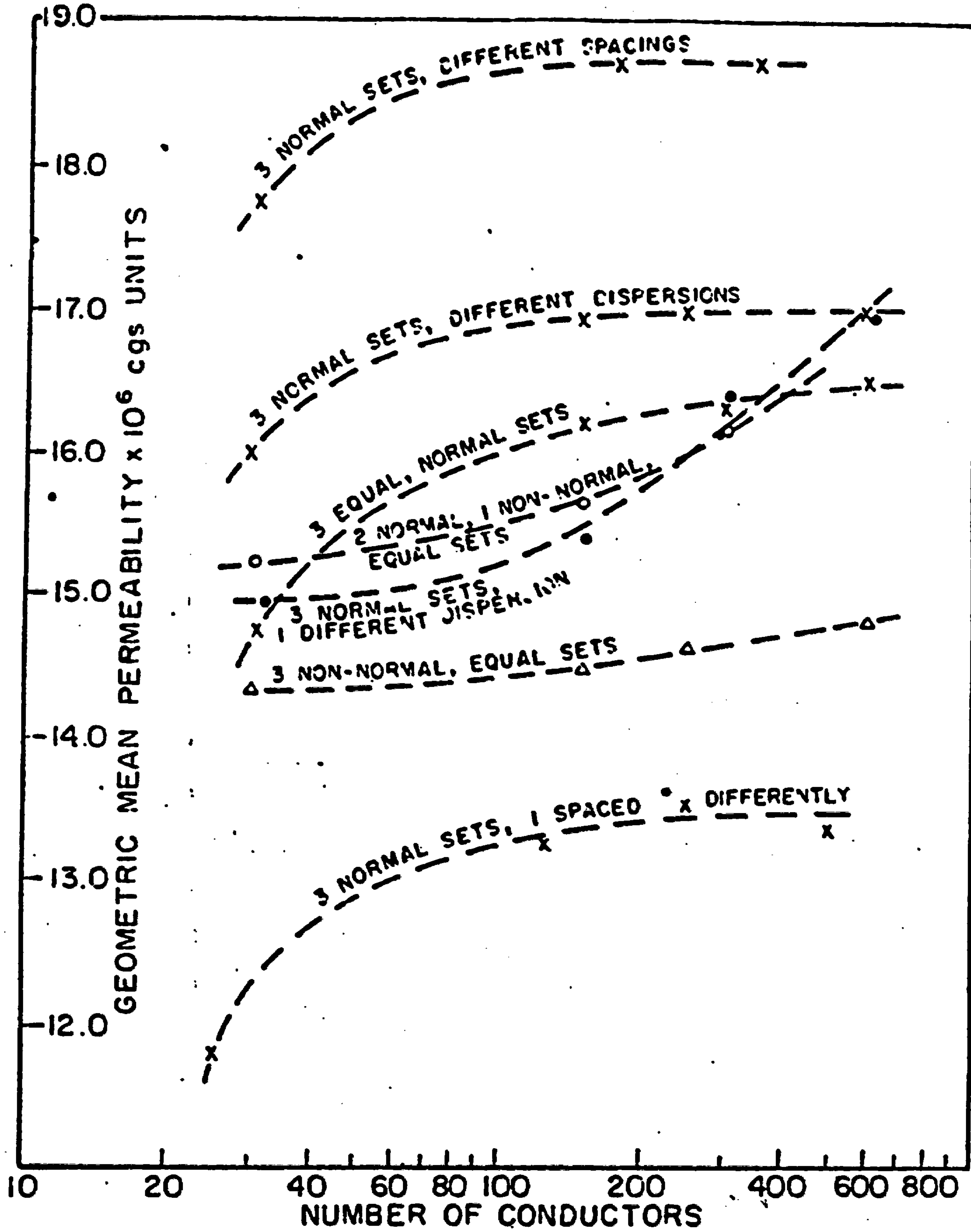

FIGURE 5-5. INCREASE OF GEOMETRIC MEAN PERMEABILITY, $\sqrt[3]{K_x K_o K_o}$, WITH THE NUMBER OF CONDUCTORS IN THE MODEL. DATA DERIVED FROM THREE SET SYSTEMS. PLATES 9 - 15.

Other parameters must be determined from the shape of the permeability distribution curves, namely the means and dispersion. All small-sample distributions shown in Plates 1 to 15 disclose considerable dispersion and skewness. The skewness developed encouraged further model study because it resembles the skewness of foundation pressure-test discharges noted by Turk (1963). Dispersion and skewness decrease for larger sample sizes in the model, as well as in the prototype (Chapter 6). Other aperture distributions than the somewhat arbitrary one employed here would indicate different rates of change of dispersion and skewness, but since little is yet known about actual distributions of apertures, further study of such rates is unwarranted.

Just as the 50th percentile point is used to estimate the population median, so too may any other point of a non-parametric distribution be used as an estimate of a percentile point of a population. Then any interval selected may be used as a measure of the population dispersion. For a normal distribution, the 16th and 84th percentile points enclose an interval equal to twice the standard deviation, centered about the mean. It is convenient to use this interval even for skewed, non-normal distributions. The 16th and 84th percentile points are scored by horizontal lines on the frequency plots of Plates 1 to 15. Figure 5-6 displays these dispersions expressed as a percentage of the median, versus the number of conductor elements.

The population of permeabilities obtained by sampling 30 or less at a time has very large dispersion, 68 percent of the measures lying within a region about the median that measures 60 to 140 percent of the median. The dispersion decreases rapidly to the range 30 to 60 percent at size 100, 20 to 40 percent at size 200, but thereafter closes very slowly, the range being 12 to 20

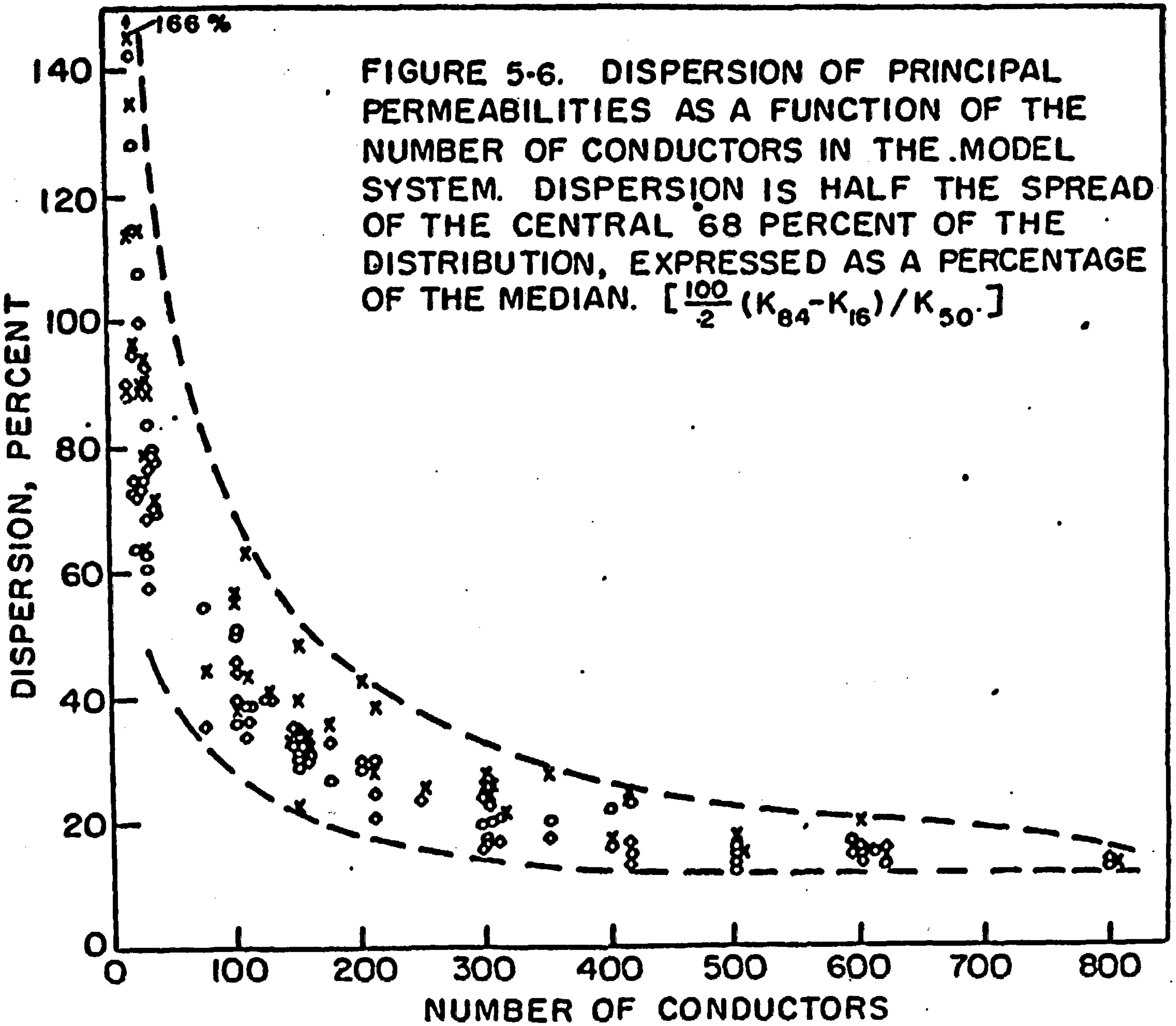

FIGURE 5-6. DISPERSION OF PRINCIPAL PERMEABILITIES AS A FUNCTION OF THE NUMBER OF CONDUCTORS IN THE MODEL SYSTEM. DISPERSION IS HALF THE SPREAD OF THE CENTRAL 68 PERCENT OF THE DISTRIBUTION, EXPRESSED AS A PERCENTAGE OF THE MEDIAN. $[\frac{100}{2}(K_{84}-K_{16})/K_{50}]$

percent with samples of size 600. The minor axis has greater percentage dispersion than the major axis. It is apparent that if reasonably accurate predictions are to be made from known aperture and geometry distributions, samples of 100 or more should be used.

Any boundary problem solution in fractured rock consists of two parts: obtaining a solution for the most likely properties, and evaluating the variations that may arise because the properties are not fixed. For the conditions modeled, the curves of dispersion define one probability limit as a function of sample size, within which 68 percent of the trials will fall. For example, if we measure permeabilities in drill holes with packers set to bracket 30 conductors, (small samples) of 3 sets, we can define a distribution curve for that sample size. If a tunnel section is to be left unlined in the same medium, with a length that will cut 300 conductors, we can use the sample permeability dispersion to estimate the dispersion in the full-size installation. First use the model curve, Fig. 5-5, to estimate the increase of the expected median according to the increase of sample size, from 30 to 300. Then use the model curve, Fig. 5-6, to find the percentage dispersion change, from size 30 to 300, and apply that percentage to the expected 300 median. Take, for example, Fig. 3 of Plate 17, Chapter 6, displaying pump test permeability data from part of the Oroville damsite, with median 5000 gallons/day and dispersion 130 percent of the median. A testing program designed on the basis of Chapter 3 would provide three such curves for the three principal permeabilities, whose geometric mean, $K = \sqrt[3]{K_a K_b K_c}$, would characterize the medium. The Oroville data can only be interpreted as isotropic. The average pressure test-length at Oroville was 60 ft., which we may assume to cut 30 conductors, on the average. Now, figure 5-5 shows how the median changes in an orthogonal joint system of three sets, not very different from the system at Oroville. The geometric mean of medians, or for this isotropic example, the median, is nearly constant above 200 conductors. The median for 300 conductors is 4.5 to 11 percent greater than at 30 conductor size, depending on the cause of anisotropy. Thus, the expected median for the tunnel section may be taken as 5400 gallons/day, an 8 percent increase predicted. The dispersion of the model medians at size 30 is about 100 percent, while at 300 it is 22 percent. A proportionate decrease for the field data would be from 130 percent at 30 to 29 percent at 300 conductors. Thus, the estimated permeability to be used in tunnel discharge computation is

$$K = \frac{Q_t}{S_j} = \frac{5400 \times 10^{-9}}{68.4(281.)1.844} = 0.19 \times 10^{-9} \text{ cgs units}$$ (see Appendix A, PTESTI),

with probability 0.68 that the experienced value will fall within the range of .13 to .24 x 10^{-9} cgs units.

The arithmetic mean, or so-called expected value, cannot be estimated by non-parametric methods. It always lies to the right of the median for these skewed distributions. But the model indicates that for numbers of conductors exceeding 100, the mean is within 10 percent of the median as distributions approach the symmetric normal.

The model-study results cannot be applied confidently to field problems until they have been well tested by measurement of geometries, prediction of anisotropies, and verification. We need enlightened assistance of all agencies equipped and financed for permeability studies on damsites, oil-fields, tunnels, leaching fields, waste-disposal or underground storage, testing these methods in all possible fractured formations. Some suggestions to method are advanced in Chapter 8. The sort of rock permeability data now being employed in civil engineering practice is analyzed in Chapter 6.

Chapter 6

FRACTURE FREQUENCIES AND APERTURES SUGGESTED BY PRESSURE TESTS IN CRYSTALLINE ROCK

Introduction

At this writing, no data is available to check the validity of the relationships between orientations, spacings, or apertures predicted by the model, but there are almost unlimited sources of in-situ rock permeability data of varied quality that can be used to substantiate at least the general shape of the permeability frequency curve, and thereby to check some of the assumptions employed in the model. This chapter undertakes an analysis of pressure-test discharges from seven damsites on crystalline rock. It interprets the data in terms of the frequency of intersected conductors, and fracture aperture distributions that may account for the observed permeabilities.

Evidence of the magnitude and variability of fractures in rock

Fracture apertures, deep within a body of rock, are not as directly measurable as are planar orientations. While orientations persist from exposed exterior to concealed interior, fracture apertures, opened by release of compression and weathering near the surface, are largely closed at depth. This is proved below by analysis of pressure tests in rock.

Still, exposures furnish qualitative indications that apertures are variable, both along the surface of a fracture, and from one individual to another. Aerial variations are indicated by fractures that pinch out at their extremities, though abutting fractures are also common (Hodgson, 1961). The dimensions of disturbed fractures at exposed faces in fresh rock (underground) are such that open ones and tight ones may be distinguished. That this is real and not apparent is suggested by the observation that water seeps out at only a few spots on rock faces excavated below the water table. The reason for this belief is demonstrated by the following analogy:

Suppose capillary tubes of equal length, but different diameter, rise above a closed reservoir and standpipe as shown, Fig. 6-1.

Initially, (a) this equipotential system will have portions below atmospheric pressure, for there will be capillary rise, depending inversely upon the diameter. Upon addition of water (b) at the standpipe, potential throughout rises by d_1, at which time the finest capillary meniscus reaches the top of its tube. All the menisci retain their relative heights and characteristic contact angles, θ_c.

Adding more water (c) raises the potential and column heights in all capillaries except the finest, because the latter can only spill by reversing the curvature of its meniscus. Rather, the first meniscus begins to flatten, until, at the moment the second column reaches the top, the first has a meniscus

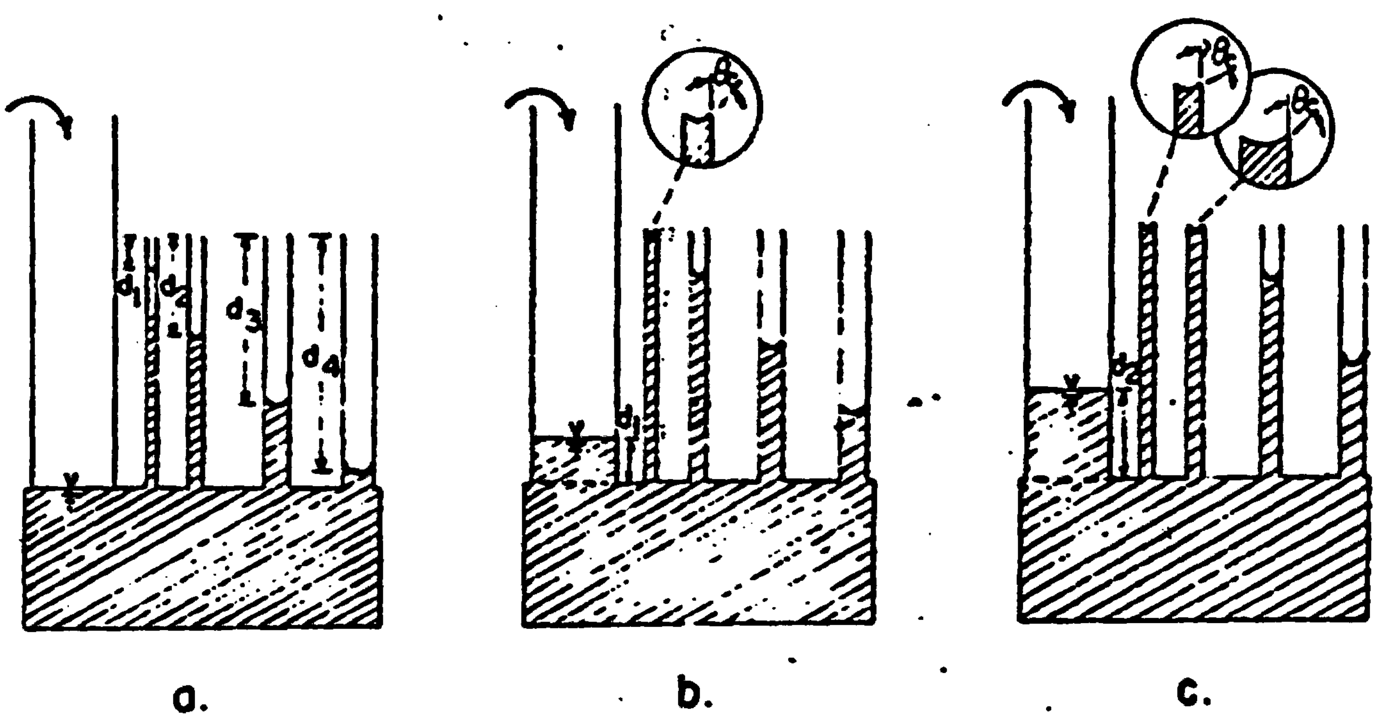

Figure 6-1. A tubular analogy of capillary fractures at a free face.

with the same curvature as the second. There is now the same potential difference across both menisci, first and second, because they have equal radii and their column heights are the same. Further filling of the standpipe raises successive columns to the top, slowly decreasing the radius of all filled capillaries. When the standpipe head reaches the level of the tops of the tubes, all menisci are flat and no tension exists anywhere in the fluid. Further filling reverses the menisci, which rise with equal convexity upward. The largest capillary therefore develops the highest meniscus. While all menisci decrease their radii of curvature, that of the largest tube obtains a minimum, a hemisphere centered on the top. Thereafter, its radius must increase, giving a drop in pressure across the meniscus. Flow from only the largest capillary therefore ensues, all others remaining saturated to their outlets.

At rock exposures, the largest aperture spills first, at its most open point. Furthermore, once the rough, exposed rock surface near the largest opening is wetted, the roughness develops capillary tension in the water film, further decreasing the potential at the aperture. The wetting may spread to the vicinity of other lesser capillaries, inducing some to flow.

A preliminary attempt to measure anisotropic conductivity of single fractures, using water as fluid in a permeameter, failed because of such capillary irregularity. Water discharged at only a few points along the periphery of the crack, as opposed to the expected continuous distribution.

In the rock beyond the decompression zone around an excavation (Talobre, 1957), there are probably variations of apertures akin to the variations evident at the face, though only pressure-tests have been made to prove it so. Direct in-situ measurement is not easily accomplished, but if the fractures could first be preserved by grout impregnation, their in-situ apertures may be exposed without much disturbance. A low-viscosity, non-particulate grout, such as AM-9 (American Cyanamid Co., undated) could be introduced at such pressures as to cause negligible wall movement. Diamond drill holes penetrating the grouted rock mass would intersect the grout fillings, whose thickness could be determined microscopically on the core, or by scanning the walls optically, or for a radioactive tracer added to the grout.

Mineral vein deposits cannot substitute for grout as preservers of in-situ apertures, because the time-pressure history of injection is unknown. "Book" quartz (Newhouse, 1942, p. 43), a slickensided, layer-upon-layer structure, indicates that some, if not most veins are filled in stages consequent to repeated fault movement.

Soviet research on fractured media (Gostop Lenin, 1962) has come to the writer's attention too late for review in this thesis. A Polish group is applying the Russian method to oil reservoir studies (P. A. Witherspoon, personal communication, 1964). On orthogonal thin-sections cut from cores of oil-producing carbonates, they measure the lengths and apertures of microscopic (~10μ) cracks. Porosity is a computed function of the sum of lengths, apertures and the area of the field of view. They find fracture porosity to be 0.1 to 0.2 percent, seldom over 1 percent in rocks whose total porosity is about 2 percent. The Poles and Soviets find 0.1 mm the maximum fracture aperture in the subsurface. The calculated porosities correlate well with the gamma-ray log, which suggests that they are measuring clay laminae, or openings due to clay expansion on unloading. Their positive correlation of fracture porosity with permeability of the pay may be because micro-fracturing is more intense where major fractures are frequent, rather than directly related.

Standardization of Pressure-test Data

A method of determining apertures indirectly has been sought, since no in-situ data are available. The hope was that if all other geometrical variables could be measured, some information about the unknown apertures might be derived from measures of permeability. The most abundant data, reflecting geometrical variations at many sites, are records of pump-tests and well discharges.

Turk (1963) and Davis and Turk (1964) have applied pump-test and water-well data to a search for systematic inhomogeneity in fractured rock. They established statistically that fractured rocks of diverse lithology decrease logarithmically in permeability as the logarithm of depth increases. Their histograms of well yield and pump-test discharge all show a characteristic shape, highly skewed to the right. The writer has replotted the data collected by Turk, plus similar data from other damsites.

Cumulative frequency distributions of discharge are used because they avoid the choice of class intervals. Before plotting, the raw data is standarized on the assumption that each test, of different length between packers, is in a medium of uniform permeability. If all test lengths and net pressures were the same, what would the discharge be? In the notation of Chapter 2,

$$Q = KSy$$

relating discharge to permeability, the shape of the piezometer, and the head, respectively. A 25-foot test length of NX hole, with 100 psi head acting, has been selected as standard, to which all other tests are reduced by

$$Q_{standard} = Q \frac{S_{standard} \; y_{standard}}{S \; y},$$

where Q is in GPM, and y is in feet, corrected to the mid-section of the test.

Hand computation is feasible for small tabulations, but for large aggregates of data, computer handling is desirable. In all, the writer analyzed 311 pump tests, using a few minutes of computer time for a job that would ordinarily be budgeted for a total of about $100,000 in labor. More refined results are obtained by Subroutines PTEST1, PTEST2A, PTEST3, and PTEST4 than customarily employed. Each program was written for somewhat differently recorded field data. The output consists of punched cards containing the raw and standardized data, so that the results can be sorted by depth zones, lengths of test section, pressures, etc. Each set of data is then fed to Subroutine DISCHG, which plots each cumulative, standardized discharge curve and computes parameters of the curve for comparative purposes. Brief program descriptions and listings are in Appendix A.

The data for Plate 17 was furnished the writer by the California Department of Water Resources (Thayer, 1962). It includes Oroville, California damsite tests from NX holes in the vicinity of the underground power cavern. The entire foundation is amphibolite. In Figures 1, 2 and 3 of Plate 17, the tests are grouped in ranges of depth below ground surface to the middle of the test length. In Figure 4, all the data of Figures 1 to 3, plus other tests outside their depth ranges, are combined.

The shape of each cumulative plot in Plate 17 is characteristic of all discharge distributions from pump tests in crystalline rock. There is usually a finite zero-frequency, a high percentage (about 70) below the mean, and a long tail. For no known reason, the mean and standard deviation are nearly equal. No common distribution function has this relationship, though the Chi-square, with two degrees of freedom, fits fairly well.

The discharges are recorded in gallons per day under the standard 100 psi, 25-foot test length in NX holes. The absolute permeability corresponding to these discharges is labeled at the top in cgs units.

Data for Plate 18 were collected by the writer at two damsites on the Merced River, California under construction for the Merced Irrigation District. Figure 1 records pressure tests in slate and meta-volcanics in NX holes drilled 45 degrees to the steep slatey cleavage, through contacts and a prominent set of flat, open and weathered joints. Figure 2 records tests in similar slate except for one high discharge obtained in a quartzose fault zone. The data for Figure 3 include tests in jointed slate, chlorite and talc schist, serpentine and silica-carbonate rock. The Merced data were furnished by Woodward-Clyde-Sherard and Associates, Inc., Oakland, California.

Plates 19 and 20 record water tests conducted routinely for placement of a grout curtain in the jointed diabase foundations of the Virginia Ranch Dam, California. The data was not collected by the writer, but previously analyzed by him for the designers, Woodward-Clyde-Sherard and Associates, Inc. All holes except the check holes completed after grouting, Figure 4 of Plate 20, were approximately 10-foot, vertical, air-driven holes. If fractures are clogged by cuttings, they do not seem to influence the shape of the discharge curves. The short length of tested holes resulted in high zero-frequencies, in spite of an apparent joint spacing of

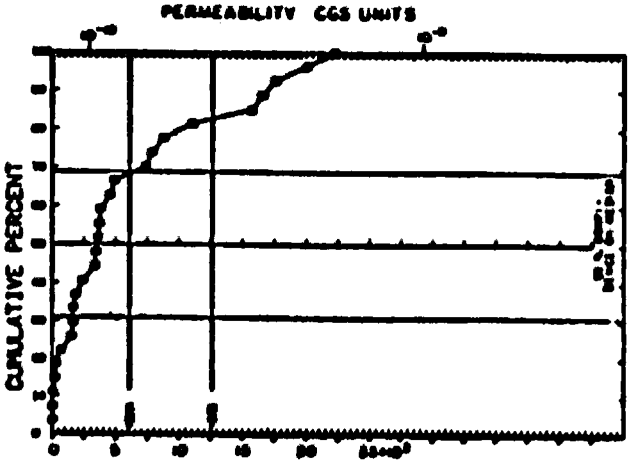

FIGURE 1 STANDARDIZED PUMP TEST DISCHARGE, GALLONS/DAY
DWR PUMP TEST DATA, LEFT ABUTMENT, OROVILLE DAM
BELOW WATER TABLE, MID-DEPTHS 100-200 FEET

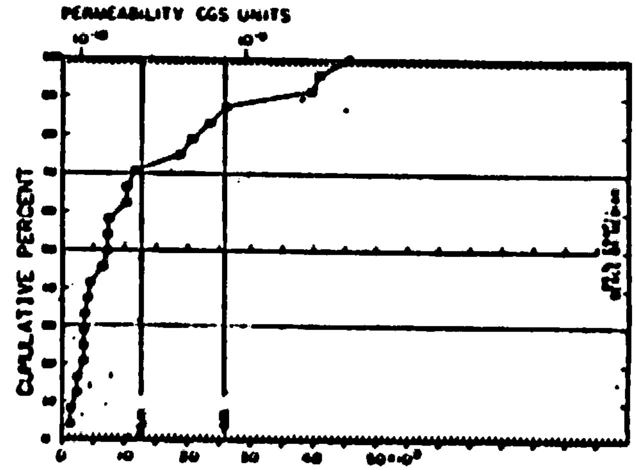

FIGURE 2 STANDARDIZED PUMP TEST DISCHARGE, GALLONS/DAY
DWR PUMP TEST DATA, LEFT ABUTMENT, OROVILLE DAM
BELOW WATER TABLE, MID-DEPTHS 200-300 FEET

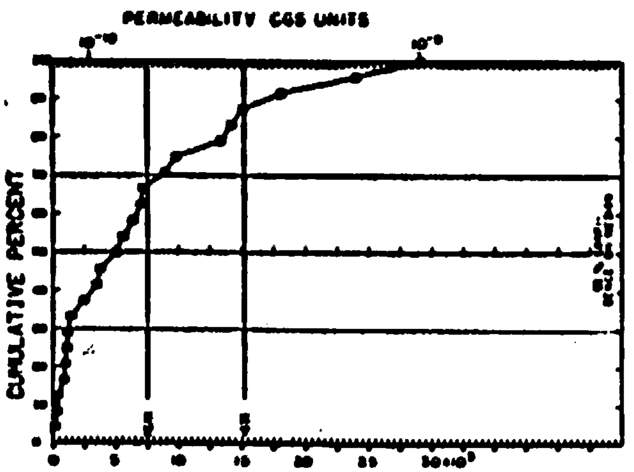

FIGURE 3 STANDARDIZED PUMP TEST DISCHARGE, GALLONS/DAY
DWR PUMP TEST DATA, LEFT ABUTMENT, OROVILLE DAM
BELOW WATER TABLE, MID-DEPTHS 300-400 FEET

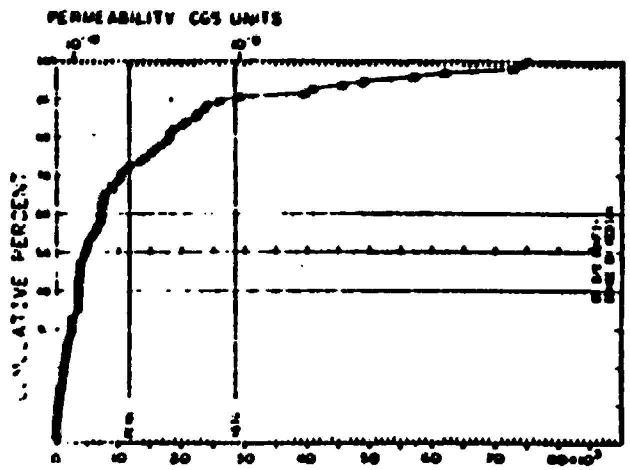

FIGURE 4 STANDARDIZED PUMP TEST DISCHARGE, GALLONS/DAY
DWR PUMP TEST DATA, LEFT ABUTMENT, OROVILLE DAM
BELOW WATER TABLE, MID-DEPTHS 55-438 FEET

PLATE 17

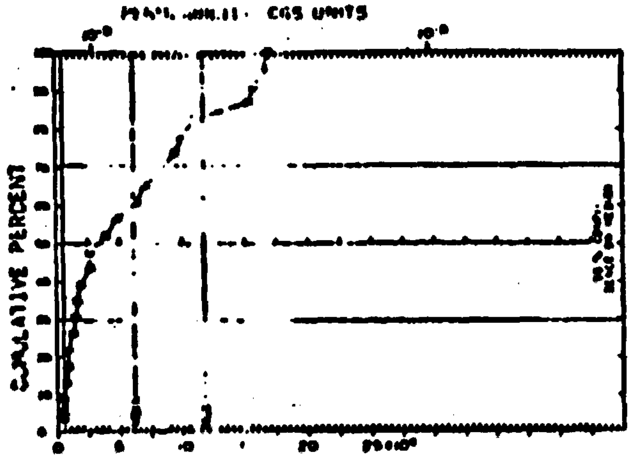

FIGURE 1 STANDARDIZED PUMP TEST DISCHARGE, GALLONS/DAY
MERCED IRR. DIST., RIGHT ABUTMENT, MCSWAIN DAM
PUMP-TESTS CONVERTED TO 25 FT, 100 PSI, RANKED DATA

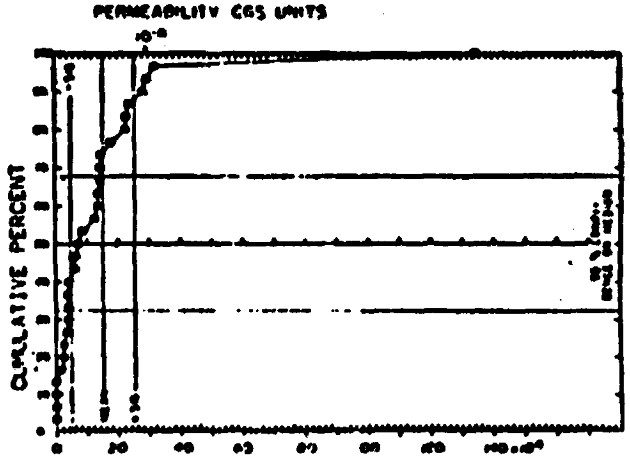

FIGURE 2 STANDARDIZED PUMP TEST DISCHARGE, GALLONS/DAY
MERCED IRR. DIST., LEFT ABUTMENT, MCSWAIN DAM
PUMP-TESTS CONVERTED TO 25 FT, 100 PSI, RANKED DATA

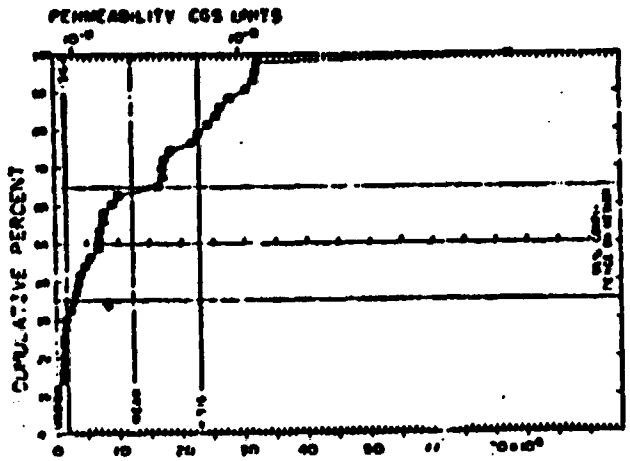

FIGURE 3 STANDARDIZED PUMP TEST DISCHARGE, GALLONS/DAY
MERCED IRR. DIST., EXCHEQUER SPILLWAY DAMSITE
PUMP-TESTS CONVERTED TO 25 FT, 100 PSI, RANKED DATA

PLATE 18

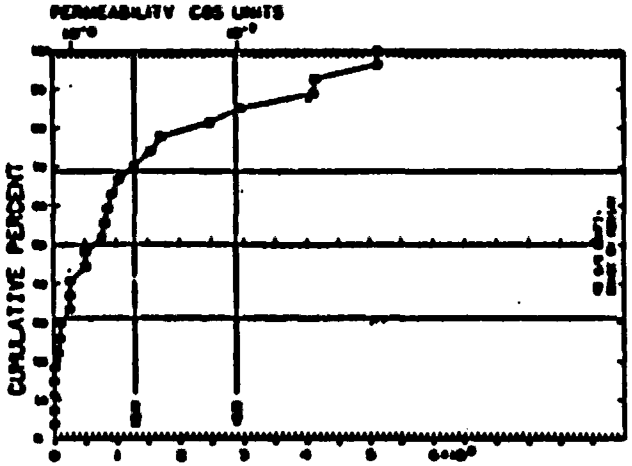

FIGURE 1 STANDARDIZED PUMP TEST DISCHARGE, GALLONS/DAY
0 TO 14.7 FOOT MID-DEPTH, LEFT ABUTMENT, GROUT CURTAIN
VIRGINIA RANCH DAM, CALIF., NX, AIR-DRIVEN HOLES

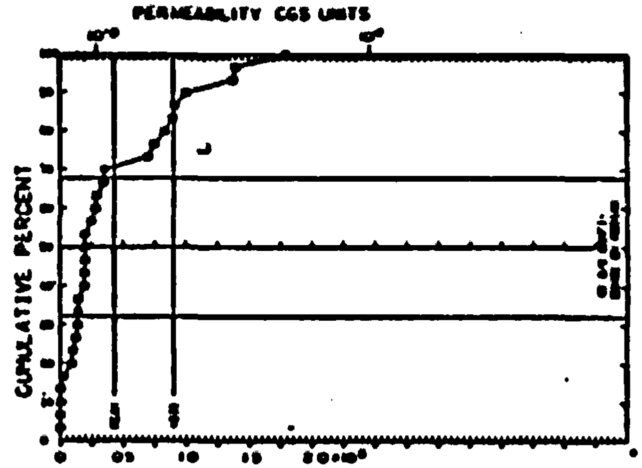

FIGURE 2 STANDARDIZED PUMP TEST DISCHARGE, GALLONS/DAY
15 TO 22 FOOT MID-DEPTH, LEFT ABUTMENT, GROUT CURTAIN
VIRGINIA RANCH DAM, CALIF., NX, AIR-DRIVEN HOLES

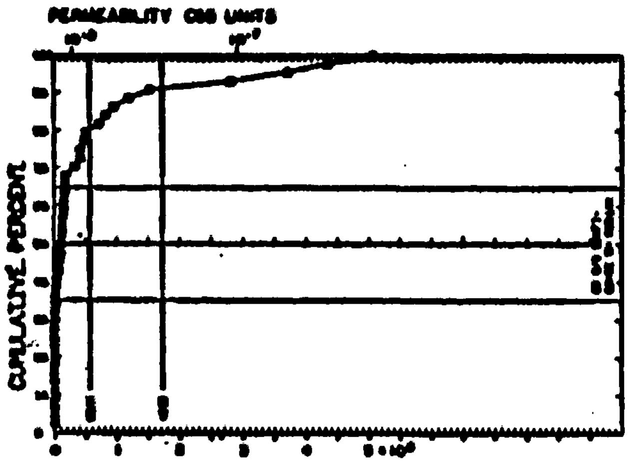

FIGURE 3 STANDARDIZED PUMP TEST DISCHARGE, GALLONS/DAY
0 TO 14.8 FOOT MID-DEPTH, CHANNEL SECTION, GROUT CURTAIN
VIRGINIA RANCH DAM, CALIF., NX, AIR-DRIVEN HOLES

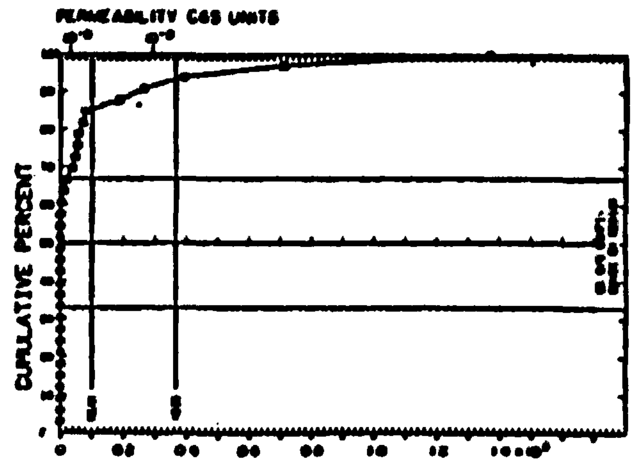

FIGURE 4 STANDARDIZED PUMP TEST DISCHARGE, GALLONS/DAY
15 TO 25.3 FOOT MID-DEPTH, CHANNEL SECTION, GROUT CURTAIN
VIRGINIA RANCH DAM, CALIF., NX, AIR-DRIVEN HOLES

PLATE 90

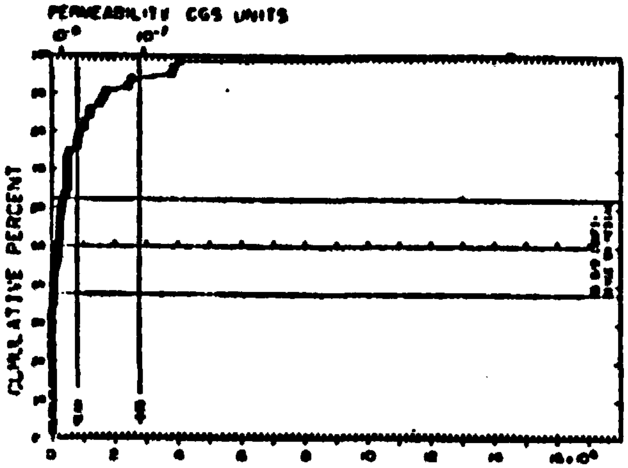

FIGURE 1. STANDARDIZED PUMP TEST DISCHARGE, GALLONS/DAY
0 TO 4.9 FOOT MID-DEPTH, RIGHT ABUTMENT, GROUT CURTAIN
VIRGINIA RANCH DAM, CALIF., NX, AIR-DRIVEN HOLES

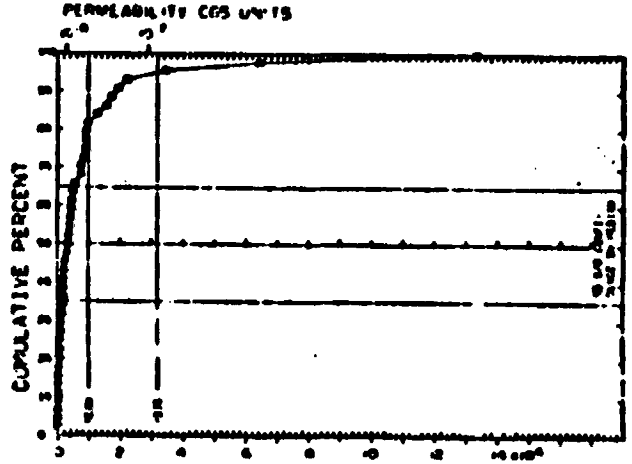

FIGURE 2. STANDARDIZED PUMP TEST DISCHARGE, GALLONS/DAY
5 TO 14.5 FOOT MID-DEPTH, RIGHT ABUTMENT, GROUT CURTAIN
VIRGINIA RANCH DAM, CALIF., NX, AIR-DRIVEN HOLES

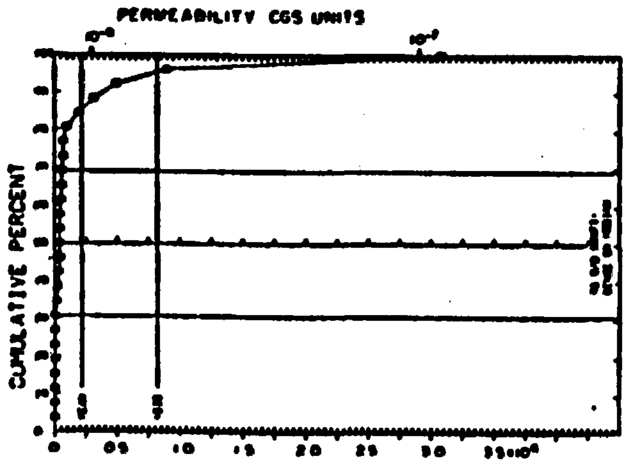

FIGURE 3. STANDARDIZED PUMP TEST DISCHARGE, GALLONS/DAY
15 TO 25.5 FOOT MID-DEPTH, RIGHT ABUTMENT, GROUT CURTAIN
VIRGINIA RANCH DAM, CALIF., NX, AIR-DRIVEN HOLES

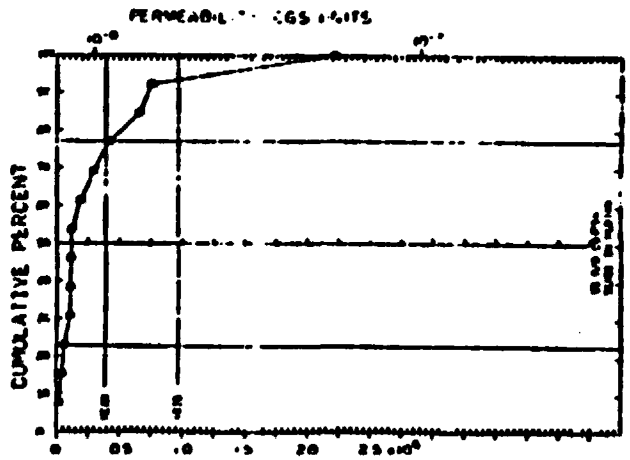

FIGURE 4. STANDARDIZED PUMP TEST DISCHARGE, GALLONS/DAY
0 TO 26 FOOT MID-DEPTH, ALL SECTIONS. CHECK HOLES AFTER GROUT
VIRGINIA RANCH DAM, CALIF., NX, AIR-DRIVEN HOLES

PLATE 20

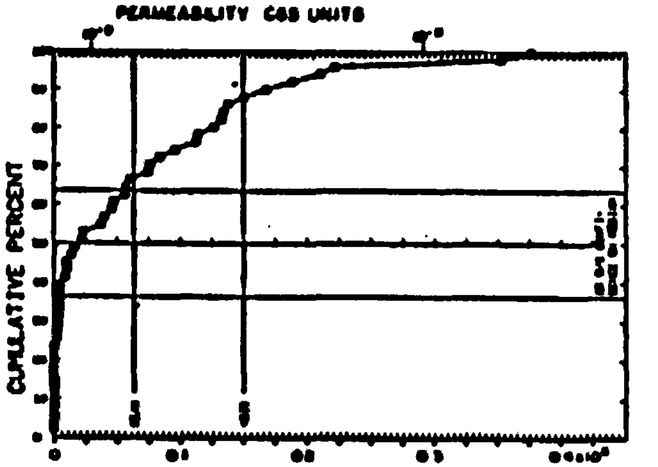

FIGURE 1 STANDARDIZED PUMP TEST DISCHARGE, GALLONS/DAY
MID-DEPTHS OF TEST SECTIONS, 0 TO 49.6 FEET
FOLSOM DAMSITE EXPLORATIONS, NX TEST HOLES

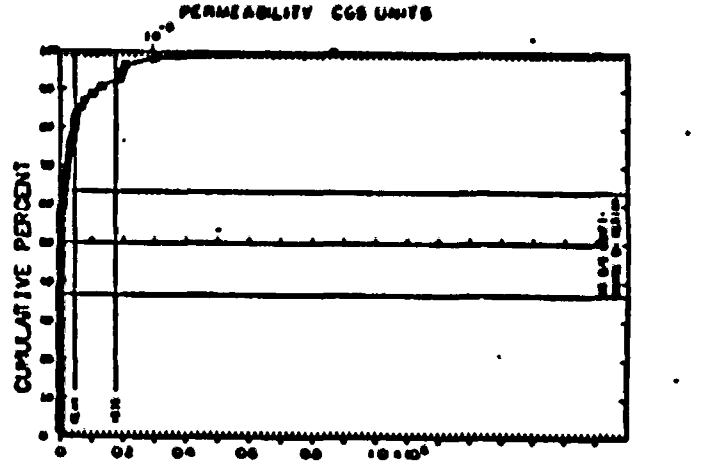

FIGURE 2 STANDARDIZED PUMP TEST DISCHARGE, GALLONS/DAY
MID-DEPTHS OF TEST SECTIONS, 50 TO 141 FEET
FOLSOM DAMSITE EXPLORATIONS, NX TEST HOLES

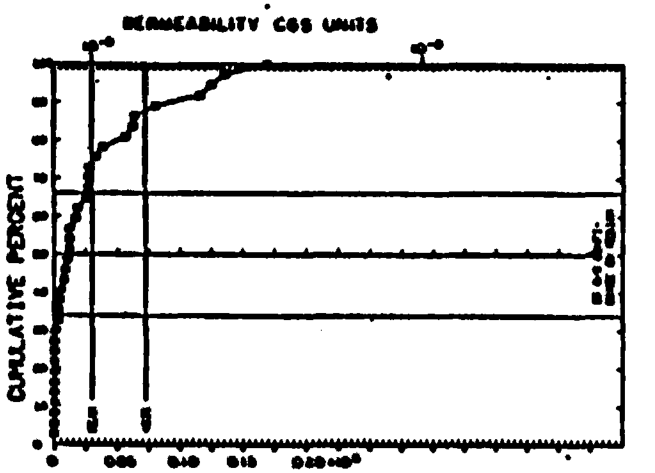

FIGURE 3 STANDARDIZED PUMP TEST DISCHARGE, GALLONS/DAY
MID-DEPTHS OF TEST SECTIONS, 0 TO 100 FEET
AUBURN DAMSITE EXPLORATIONS, NX TEST HOLES

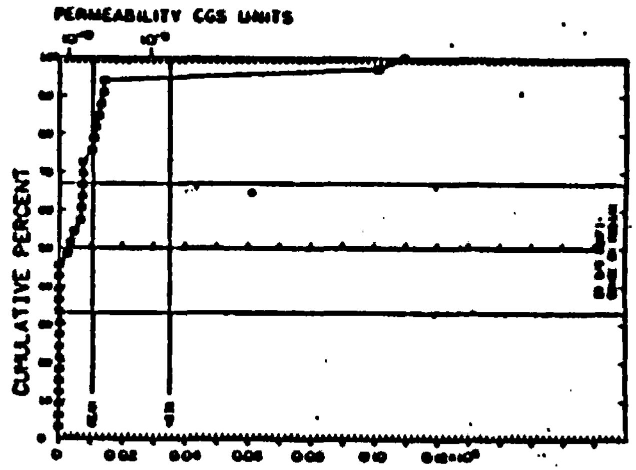

FIGURE 4 STANDARDIZED PUMP TEST DISCHARGE, GALLONS/DAY
MID-DEPTHS OF TEST SECTIONS, 100 TO 181 FEET
AUBURN DAMSITE EXPLORATIONS, NX TEST HOLES

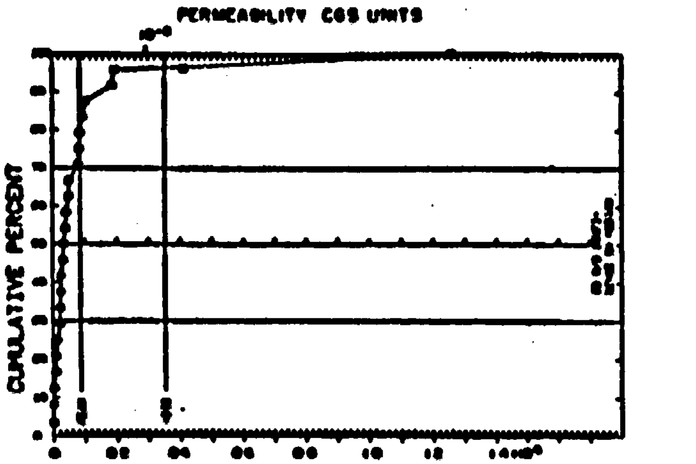

FIGURE 1. STANDARDIZED PUMP TEST DISCHARGE, GALLONS/DAY
MID-DEPTHS OF TEST SECTIONS, 0 TO 50 FEET
SPRING CREEK TUNNEL EXPLORATIONS, NX TEST HOLES

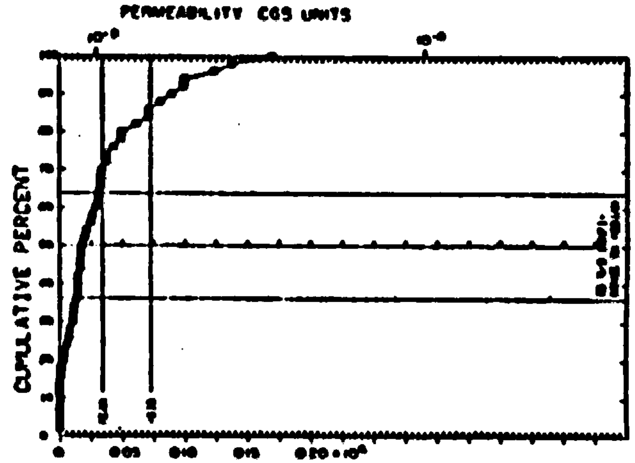

FIGURE 2 STANDARDIZED PUMP TEST DISCHARGE, GALLONS/DAY
MID-DEPTHS OF TEST SECTIONS, 50 TO 100 FEET
SPRING CREEK TUNNEL EXPLORATIONS, NX TEST HOLES

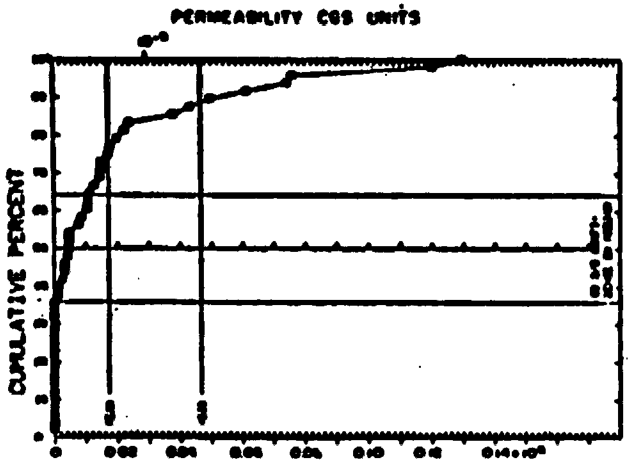

FIGURE 3 STANDARDIZED PUMP TEST DISCHARGE, GALLONS/DAY
MID-DEPTHS OF TEST SECTIONS, 100 TO 199 FEET
SPRING CREEK TUNNEL EXPLORATIONS, NX TEST HOLES

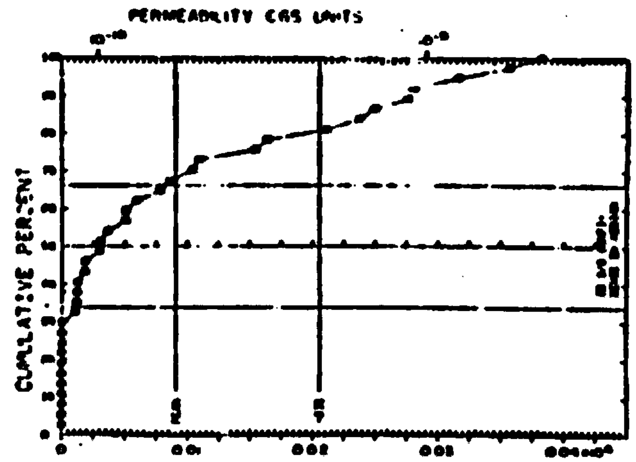

FIGURE 4. STANDARDIZED PUMP TEST DISCHARGE, GALLONS/DAY
MID-DEPTHS OF TEST SECTIONS, 200 TO 477 FEET
SPRING CREEK TUNNEL EXPLORATIONS, NX TEST HOLES

about two feet at the surface. Such standardized pressure tests serve fairly for assessing the efficiency of grouting. In this case, the check-hole curve is hardly distinguishable from the pre-grout tests, suggesting that the small volumes of neat cement emplaced blocked rather than filled the fine joint conductors. Permeability was never a problem at this site.

Data for Plates 21 and 22 were assembled by Turk (1963) from sources in the U. S. Bureau of Reclamation and U. S. Corps of Engineers, for three California sites on grano-diorite of the Sierra Nevada foothills: Folsom and Auburn damsites, and the Spring Creek Tunnel.

Implications of the Observed Discharge-Frequency Curves

The cumulative discharge skewed graphs generalize the finding of distribution of permeability, and express what is common experience to anyone who has pump-tested rock: Most flow measures are small, but unusually large ones can be expected anywhere. Turk (1963) concluded from data standardized in a different way that under given conditions, the mean yield of wells is about three times the median yield. Plates 17-22 confirm that expression of skewness for standardized tests, with means that are 2 to 4 times the median. Davis and Turk (1964) applied these findings to the practical problems of planning well systems. They concluded that the variation of yield decreases at the same logarithmic rate with depth for all rock types, including granite, slate, phyllite, schist, amphibolite, quartzite, greenstone and meta-rhyolite.

Systematically-varying inhomogeneity is not considered a factor in this paper, rather, the variable of depth is avoided when possible by classifying data according to depth zones. Variations in the permeability that arise when different samples are taken from populations of fracture orientations and apertures are considered as smaller-scale inhomogeneities than those treated by Davis and Turk, or alternatively, as variations along a surface of uniform depth below the ground surface. Such sampling inhomogeneities must also be treated statistically; in fact, the sampling problems should be understood before systematic variations are assessed.

Once it is recognized that permeability is determined by values sampled from distributions of orientations and apertures, both in the field and in the model, then there is hope of devising rational utilization of the dependent properties. A given volume of rock contains a discrete number of planar fluid conductors, but since all reasonable aperture values are possible, the entire population is continuous. Thus, permeability varies continuously also, and pumping-tests may be regarded as measures of combinations of elemental conductors, sampled from the entire distribution in just the way employed in Chapter 5. Inhomogeneity is assumed due only to the sampling process. Furthermore, we can assume for the moment that joint density in the mass is sufficiently constant that the number of conductors in a volume sampled is the same as in any other like volume.

If the above assumptions hold, then the skewness offers a clue to the distribution of fracture apertures. To see how, imagine that all fractures penetrated by a hole are parallel, and that pumpage induces flow in all of them. The total discharge would be the mean discharge of individual fractures times their number, N. The wetted bore of a reasonably-sized well is essentially an equipotential, thus, the discharge is proportional to the mean cube of apertures of all the fractures taken N at a time. Thus a frequency plot of the discharges of many wells or test-holes is proportional to the distribution of mean cubes of apertures taken N at a time. If N is known, then the mean and variance of the parent distribution of cubes can be obtained by the Central Limit Theorem. Unfortunately, it is impossible to obtain the distribution of apertures, b, from the cube root of discharge, for there is no unique distribution of b giving a known distribution of discharge, Q, where the two are related by some function

$$Q = C \Sigma b^3,$$

for $\quad b \neq (Q/C)^{1/3}.$

The Central Limit Theorem that operates to produce normal distributions in the model (Chapter 5) also operates in natural rock media to give more normal curves of smaller and smaller dispersion as the sample size increases. If exposures reveal the true joint frequency, then pump-test samples contain large numbers of conductors. An average test section at the Oroville damsite was about 60 feet long (Thayer, 1962, Table 6) and intersected about 150 joints, according to the 1.5, 1.2 and 1.0 - foot spacings reported by Lyons (1960, Table 2). Yet the curves are not normal, so the assumptions must be incorrect. Either: 1) the sample size is actually small or, 2) the population of apertures is so highly skewed that samples must be of huge size to develop normal distributions of means. If it can be established that the frequency of zero apertures must be zero, then a cumulative distribution of apertures (b), must be sigmoidal in form. In this case, one hundred or more elements, as at Oroville, constitute a large sample, whose distribution of means would be very nearly normal.

<u>Frequency of Zero-Apertures</u>

Study of intergranular pore size distributions have led petroleum engineers to the conclusion that as pore size in reservoir rocks tends to zero in the limit, their frequency must vanish (Fatt, I., personal communication, 1964). Published experimental evidence on this point is inconclusive, as indicated by capillary pressure-imbibition tests. If a minimum pore size exists in a porous material, there should be a definite limit to the amount of mercury that can be imbibed against increasing capillary pressure. A minimum pore size is indicated by data of Ritter and Drake (1945), and Drake and Ritter (1945) for diatomaceous earth, fritted glass, porcellain, porous iron and flint quartz, but other materials, such as silica-alumina gel, activated alumina or clay, Fuller's earth, bauxite, and carbon all showed continuous imbibition to at least ten thousand psi (214 Å). Continuous pore-size distributions to zero size are implied by Ritter and Drake's data, especially in such cases (silica gel) where the pressure-volume curve is linear. Foster's (1948) data, obtained from absorption isothermals for gels, are not interpretable of minimum size. Data of Purcell (1949), Burdine, Gournay and Reichertz (1950), and Engelhardt (1960, pp. 87-123) on reservoir rocks (sandstones, limestones) indicate, at most, a continuously decreasing pore volume, pore-size relationship, suggesting a zero asymptote in some size range beyond the experimental limit. No capillary imbibition tests are known to have been performed on fractured material, nor is it feasible to separate primary from secondary porosity in the microsizes (see Ritter and Drake, 1945, for definitions). The Griffith (1921) theory assumes a crack to have an elliptical cross-section approaching zero eccentricity (ratio of minor to major axes; see also Perry, 1950, p. 378). Some aspects of the theory have been verified (Perkins and Kern, 1961) but it is difficult to check the assumption of a rounded, elliptic crack extremity. Savage and Hasegawa (1964) measured with an interferometer a minimum aperture of 2 microns for cracks in glass. The practical difficulties of measuring the shape of crack extremities in opaque solids suggests that that part of the Griffith theory may never be confirmed. Observations of Griggs (1939), Brace (1963) and others already discussed, indicate initial failure by a multitude of cracks that coalesce to form a single debris-covered break, a further indication of a minimum aperture. Hodgson (1961) noted that many parallel joints of a systematic set deviate at their extremities to abut against each other like two cupped hands, fingertips to palms, thus lacking fracture termini.

In any event, the notion of a distribution of apertures implies a sampling process, such as the cracks encountered along a straight line through the medium. The probability of encountering an edge is very small. All things considered, it is concluded that the likelihood of finding a zero fracture aperture is nil. Alternative 2) is therefore rejected in favor of the argument of small sample size.

The Frequency of Conductors Intersected by Drill-Holes

In samples of equal drill-hole length, L, the number of conductors, N, must be Poisson-distributed if the conductors are random-uniform in spacial location and if the samples are very small compared to the size of the population. The appropriateness of this conclusion is illustrated by the following one-

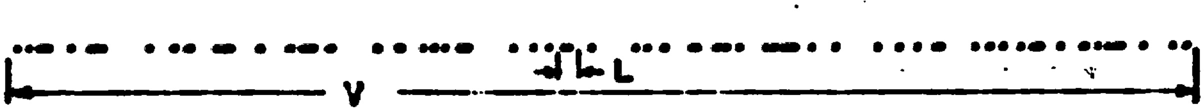

FIGURE 6-2. HYPOTHETICAL LOCATIONS OF JOINTS CROSSING A LINE, DISTRIBUTED UNIFORMLY RANDOM. T=100 POINTS, $\eta L = 5/3$.

dimensional plot of points, locating the intersection of a line and all plane conductors cutting a homogeneous volume of fractured material. For jointed rock, such a line must run essentially parallel to the ground, or be an assembly of a number of lines crossing a homogeneous layer of limited thickness. This recognizes Turk's (1963) findings of systematic depth inhomogeneity and the comparability of pumping yields for all places and formations at a given depth.

Let T be the total number of intersection points in the length V. A fracture occupies no appreciable part of the line, so we can say that there is no crowding and the occurrence of one has no effect on whether or not another occurs in any small sample, L, of the population. If the total number of conductors in V is T, then the average density η is T/V. The sample, L, a drill-hole length, for instance, may be moved along (or around) at will, including a different number of conductors, N, at various locations. The probability that N conductors (points) occur in L is given by the binomial density (Mood and Graybill, 1963, p. 71):

$$P(N) = \binom{T}{N}\left(\frac{L}{V}\right)^{N}\left(1-\frac{L}{T}\right)^{T-N}.$$

Let V and T become infinite while $\eta = T/V$ remains constant. The binomial can be rewritten:

$$P(N) = \frac{T(T-1)(T-2)\cdots(T-N+1)}{N!\,T^{N}}\left(\frac{TL}{V}\right)^{N}\left(1-\frac{TL}{TV}\right)^{T-N}$$

$$P(N) = \frac{\left(1-\frac{1}{T}\right)\left(1-\frac{2}{T}\right)\cdots\left(1-\frac{N-1}{T}\right)}{N!}(\eta L)^{N}\left(1-\frac{\eta L}{T}\right)^{T-N}.$$

As T becomes infinite, this approaches

$$P(N) = \frac{e^{-\eta L}(\eta L)^{N}}{N!},$$

the Poisson density. The expectation, or average number, is λL. P(N) is increasingly skewed for λL decreasing below 5, whereas P(N) rapidly approaches normal above 5 (Parzen, 1960, p. 246).

The observed skewness of pressure-test discharges can be accounted for if the usual sample length, L, is such that the expectation λL, is small. It will be shown that if pump test samples contain large numbers of conductors, distribution of yield would always be normal.

Some of the possible combinations of aperture and number distributions are tabulated here for clarity, with explanation following:

Table 6-1

Distributions of Discharges Under Various Sample and Aperture Conditions

Conduits in Sample		Distribution of Apertures Cubed		
		Constant	Normal	Skewed
Large Numbers	Constant	Constant	Normal	Normal
	Normal	Normal	Normal	Normal
Small Numbers	Skewed	Skewed	Skewed	Skewed
	Poisson	Poisson	Skewed	Skewed

If the conduit density is high, sample volumes will either contain conductors that vary in number from one to another, or that have the same number throughout. Normal distribution is likely but not certain. Sample size could be Gamma-distributed, Beta, or any other, though the matter is immaterial. This is because large samples, however variable the number or aperture distribution, cannot produce the skewed discharge distributions, having high zero frequencies, that are apparent from field testing.

For illustration, let us assume that the number of conductors intersected by drill-holes of the same length piercing the formation varies according to the Gaussian distribution. If all apertures are alike (constant) the discharge is distributed according to the numbers N:

$$Q \propto N b^3,$$

and if b^3 is normal, so too is the discharge. If b^3 is skewed (Chi-square would do), then closure to normalcy requires larger numbers, but the discharge would never be like those observed. The same may be said for large samples of constant size, represented in the upper row of the table. Discharges would be constant, normal, or approaching normal if apertures are constant, normal or skewed, respectively.

Aperture Distributions are Obscured

If sample sizes are small, the homogeneity assumption leads inevitibly to a Poisson distribution of sample sizes. If apertures are constant, the discharge distribution must also be Poisson. The salient feature of a Poisson distribution is that it is defined by one parameter. The one parameter, λ', is both mean and variance. The discharge plots, Plates 17 through 22, consistantly display a mean that is approximately equal to the standard deviation, instead of the variance. Accordingly, if numbers of conductors are Poisson-distributed, the apertures-cubed must be either normal or skewed. It seems impossible to follow this reasoning further, for the apertures-cubed may be attributed to any one of many possible skewed distributions of apertures, b: skewed normal, log normal, exponential, linear, Beta, Gamma, composite, etc. Distributions unbounded to the negative are impossible, thus eliminating normalcy. Truncated (at 0) or transposed forms (such as used in Chapter 5), are unlikely because a finite frequency at b=0 is not expected. Functions bounded in the larger sizes, including linear or Beta distributions, seem not to be represented in nature, where extreme openings, like the grottos at Castillon Dam (Chapter 3) are occasionally reported. Log-normal exponential or Gamma ($\alpha > 0$) distributions of apertures-cubed, are most likely, with log normalcy favored until better information is available because other natural distributions follow this law (grain-size, intergranular permeability).

Another way of viewing the discharge distribution is as the sum of distributions of many narrow classes of aperture, each taken small enough in range that less than one member, on the average, appears in any sample. The total discharge is

$$Q = N_i \, b_i^3 ,$$

wherein each N_i is distributed as a Poisson with expectation λ_i. Such a sum of Poisson's is also a Poisson with expectation

$$\lambda = \Sigma \lambda_i \qquad \text{(Parzen, 1960, p. 406).}$$

λ must be small, else the sum would be normally distributed. Unfortunately, there is no known way of finding the λ_i that would describe the entire aperture distribution.

Description of real aperture distributions, in jointed rock or other media, will depend, ultimately, upon direct measurement, perhaps down-the-hole. The practical difficulties demand, first, that other methods be exhausted. It might be possible to identify which ones are conductors, thereby fixing the number per length of hole. In Chapter 8, a method of determining λ is suggested. Then the aperture-cubed mean and variance can be ascertained, for the Central Limit Theorem (Mood and Graybill, 1963, pp. 149-152) states that the sample means of <u>any</u> distribution with finite variance σ^2, and mean μ are approximately distributed as normal variates with variance σ^2/N and mean μ, where N is the sample size. Furthermore, the discharge skewness requires that the aperture-cubes are even more skewed. Good representation of the distribution of apertures, and therefore porosity, could be obtained if the general shape were known and two parameters of each cubed distribution were measured.

One is not much better off dealing with some property of fractured media that depends on lower powers of aperture, electrical conductivity, for instance. There are as many possible distributions of b that could give a certain sum, Σb, as there are giving a sum, Σb^3.

Limitation by the Assumption of a Homogeneous Population

In application to field problems, care must be taken in defining the geological limits of a joint population, for there remains reason to doubt that fractured rock in a given depth range is homogeneous across formation boundaries, fault zones, or other major structures. While the average joint density seems uniform throughout most of a rock body, and Turk's (1963) data suggested no dependence of fracture permeability on lithology, the vicinity of a fault is often more highly fractured. The record of water flows into the Harold D. Roberts Tunnel, Colorado (Wahlstrom and Hornback, 1962), indicated that 90% of the total ingress came from about 1% of the 23 mile bore length. In such a zone, expect a normal distribution of pump-test discharges, while in the country rock expect skewed distributions, simply because of the frequency contrast.

If the homogeneity assumption is removed, the small-sample reasoning is changed but little. Suppose joints are gregarious, clustering about fault zones or characteristically bunched for some other reason. Compared to a homogeneous medium, whose con-

PLATE 23

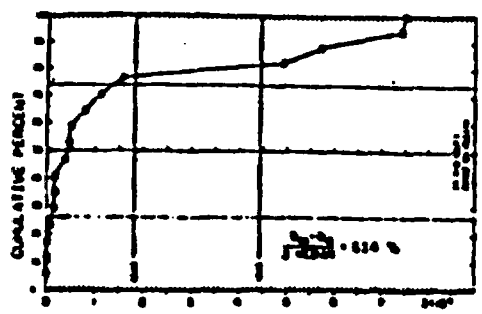

FIGURE 1 STANDARDIZED PUMP TEST DISCHARGE, GALLONS/DAY
TEST SECTIONS OF LENGTH 21 TO 87 FEET
LETS OROVILLE PUMP TESTS, MID-DEPTHS 54 TO 180 FEET

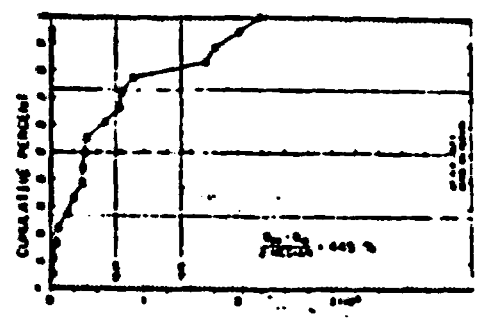

FIGURE 2 STANDARDIZED PUMP TEST DISCHARGE, GALLONS/DAY
TEST SECTIONS OF LENGTH 91 TO 121 FEET
LETS OROVILLE PUMP TESTS, MID-DEPTHS 68 TO 197 FEET

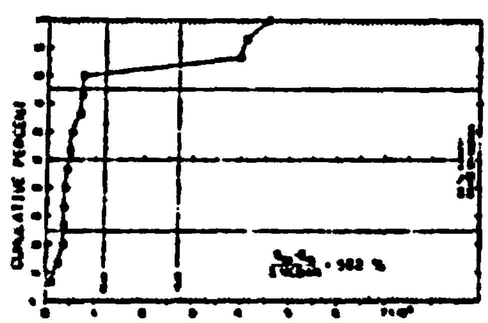

FIGURE 3 STANDARDIZED PUMP TEST DISCHARGE, GALLONS/DAY
TEST SECTIONS OF LENGTH 31 TO 51 FEET
LETS OROVILLE PUMP TESTS, MID-DEPTHS 235 TO 329 FEET

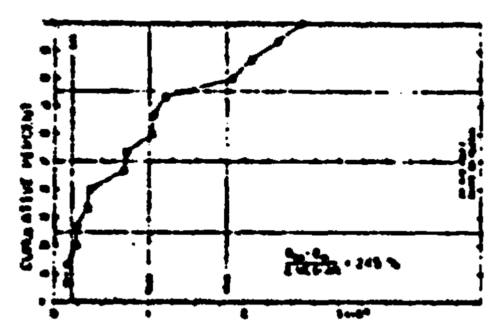

FIGURE 4 STANDARDIZED PUMP TEST DISCHARGE, GALLONS/DAY
TEST SECTIONS OF LENGTH 56 TO [illegible] FEET
LETS OROVILLE PUMP TESTS, MID-DEPTHS 213 TO 294 FEET

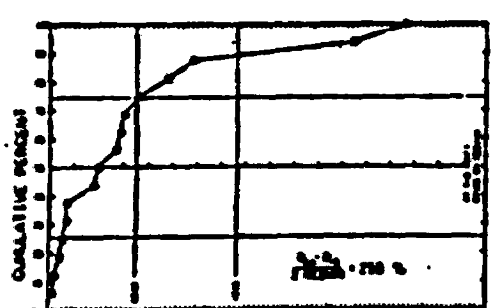

FIGURE 5 STANDARDIZED PUMP TEST DISCHARGE, GALLONS/DAY
TEST SECTIONS OF LENGTH 28 TO 54 FEET
LETS OROVILLE PUMP TESTS, MID-DEPTHS 352 TO 438 FEET

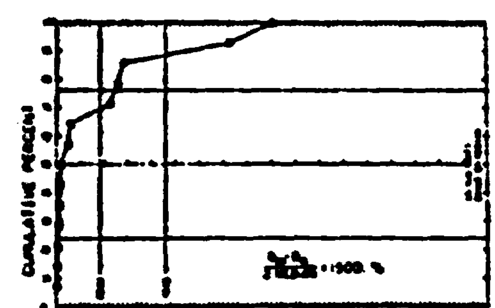

FIGURE 6 STANDARDIZED PUMP TEST DISCHARGE, GALLONS/DAY
TEST SECTIONS OF LENGTH 60 TO 112 FEET
LETS OROVILLE PUMP TESTS, MID-DEPTHS 326 TO 433 FEET

PLATE 24

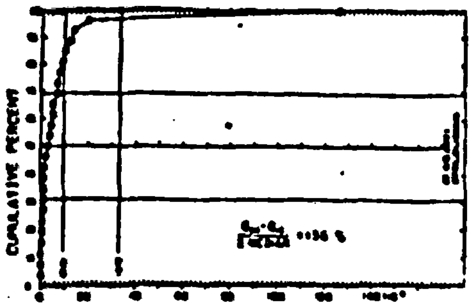

FIGURE 1 STANDARDIZED PUMP TEST DISCHARGE, GALLONS/DAY
TEST SECTIONS OF LENGTH 5 TO 10.9 FEET
SPRING CREEK TUNNEL PUMP TESTS, MID-DEPTHS 13 TO 71 FEET

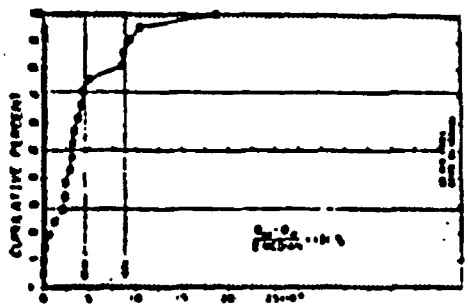

FIGURE 2 STANDARDIZED PUMP TEST DISCHARGE, GALLONS/DAY
TEST SECTIONS OF LENGTH 11 TO [illegible] FEET
SPRING CREEK TUNNEL PUMP TESTS, MID-DEPTHS 12 TO [illegible] FEET

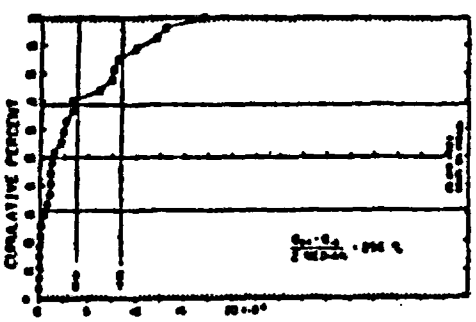

FIGURE 3 STANDARDIZED PUMP TEST DISCHARGE, GALLONS/DAY
TEST SECTIONS OF LENGTH 5 TO [illegible] FEET
SPRING CREEK TUNNEL PUMP TESTS, MID-DEPTHS 75 TO 148 FEET

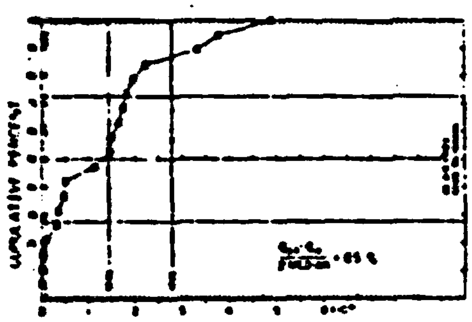

FIGURE 4 STANDARDIZED PUMP TEST DISCHARGE, GALLONS/DAY
TEST SECTIONS OF LENGTH 12 TO [illegible] FEET
SPRING CREEK TUNNEL PUMP TESTS, MID-DEPTHS 62 TO 144 FEET

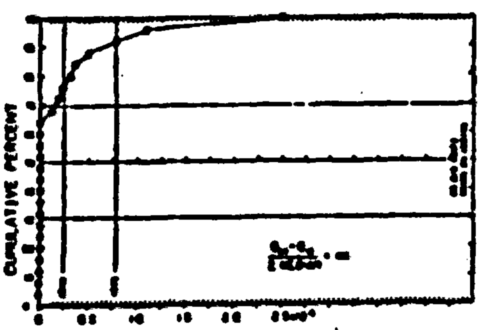

FIGURE 5 STANDARDIZED PUMP TEST DISCHARGE, GALLONS/DAY
TEST SECTIONS OF LENGTH 10 TO 12 FEET
SPRING CREEK TUNNEL PUMP TESTS, MID-DEPTHS 151 TO 395 FEET

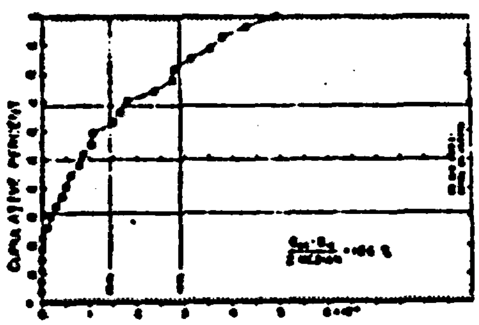

FIGURE 6 STANDARDIZED PUMP TEST DISCHARGE, GALLONS/DAY
TEST SECTIONS OF LENGTH 13 TO 34 FEET
SPRING CREEK TUNNEL PUMP TESTS, MID-DEPTHS 305 TO 477 FEET

ductors are distributed throughout the space in a uniformly random manner, expect non-uniform distributions to yield even more skewed distributions of sample size N than predicted by the Poisson Law for a given average density, μ. As shown in Table 6-1, all aperture-cubed distributions, including constant, would produce skewed discharge distributions for small samples.

Verification of Model-Predicted Relationships

Plates 23 and 24 illustrate, by regrouping data from Plates 17 and 22, the changes in discharge distributions, first with depth, and second with sample size as measured by test lengths. Horizontal rows of figures represent mid-depth intervals considered as statistically homogeneous volumes: 54 to 197 feet, 210 to 329 feet, and 334 to 448 feet at the Oroville damsite. The left-hand or odd numbered figures represent pressure test discharges for short lengths between packers, and the right hand figures for longer test lengths at the same depth.

As a test of the issue (Chapter 5) of the trend of permeability with boundary dimensions or sample size, this data fails, for in some cases the longer tests show greater mean and median permeability, and in others smaller permeability. To investigate this aspect more thoroughly, more extensive data than available should be employed, so that when one depth zone at a site is grouped according to length of test section, each group contains numerous measures.

Dispersion, expressed either by standard deviation as a percentage of the mean, or the 84 to 16 percentile range as a percentage of twice the median, decreases for the longer test lengths (Figures 1, 2, 3, 4) in accordance with the predicted effect of increased sample size (Chapter 5). But when sample sizes become very small at depth, as opposed to large and constant, (such as used in the model for Plates 1 to 15), the percentage dispersion does not necessarily decrease for longer test lengths (Plate 23, Figures 5,6) because the median or mean tends to zero.

Pump test data from the Spring Creek Tunnel site are similarly grouped in Plate 24. Dispersion decreases with increasing test lengths, in all depth ranges.

Conclusions from Pressure-test Data

It is concluded that the distribution of apertures in fractured media, or porosity, for that matter, cannot be obtained from permeability data alone. Except for direct measurement of the elements of an aperture population, the only promising approach is to determine the number of conductors. As will be shown in Chapter 7, porosity can be estimated from the frequency of fractures, together with permeability statistics. Pressure-tests alone, as currently used, are inefficient for such uses as grout take prediction. Grout take could even rise with falling permeability, so far as porosity governs it. Skewed discharge curves constitute a statistical substantiation of an oft-suspected property of jointed rock: The preponderance of the joints visible at an exposure are closed at depth, or at least, a small proportion have significance as hydraulic conductors.

Modeling Pumping Tests

To substantiate the deductions from field pumping tests, the computer model was employed to find out under what conditions would the characteristic field curves be reproduced. For this purpose, Subroutines NUMBER, PIEZO and PUMPLT were added to the program (Appendix A).

NUMBER has the purpose of selecting sample size at random from pre-computed tables of the Poisson distribution. The ex-

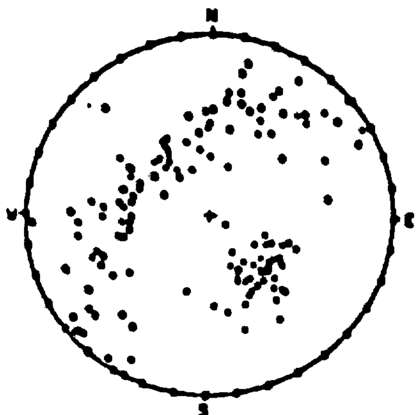

FIGURE 1.
STEREOGRAPHIC PROJECTION. UPPER HEMISPHERE
CONDUCTIVITY AXES. SINGLE SET OF JOINTS. K=10

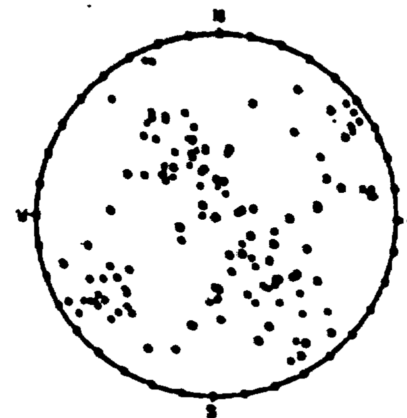

FIGURE 4.
STEREOGRAPHIC PROJECTION. UPPER HEMISPHERE
CONDUCTIVITY AXES. 2 NORMAL SETS OF JOINTS. K=20

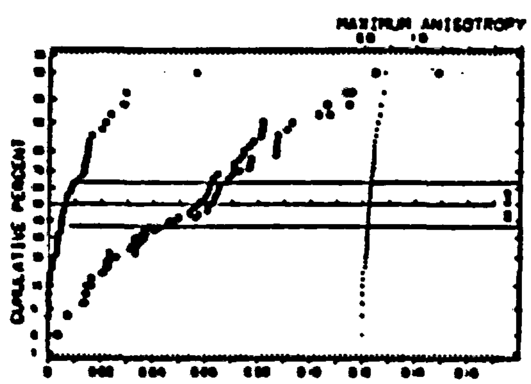

FIGURE 2. PRINCIPAL PERMEABILITIES. X 10[8] CGS UNITS
MEAN NUMBER OF 5 JOINTS. CENTERED 45 DEG SE. K=10
STANDARD DEVIATION= .005. CENTER= .025. DELTA=1120

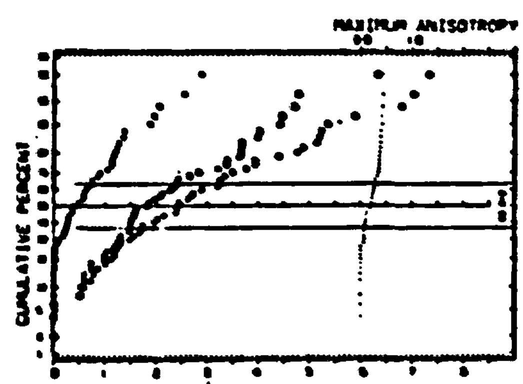

FIGURE 5. PRINCIPAL PERMEABILITIES. X 10[7] CGS UNITS
MEAN NUMBER OF 1.2 JOINT ON SE SET. 1 ON NW SET
NORMAL APERTURE DISTRIBUTION. CENTER=.025. STD=.005.DELTA=112

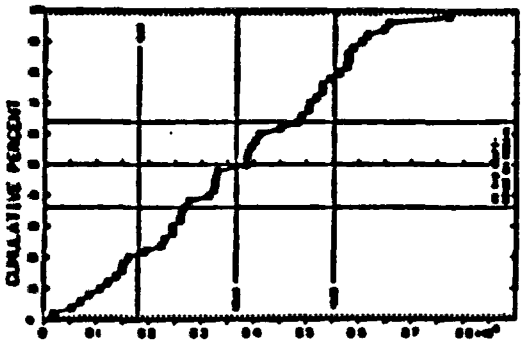

FIGURE 3. STANDARDIZED PUMP TEST DISCHARGE. GALLONS/DAY
TEST HOLE INCLINED 45 DEG SE. 25 FT LONG. 100 FT HEAD

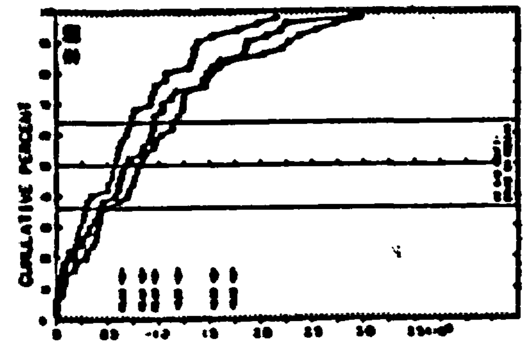

FIGURE 6. STANDARDIZED PUMP TEST DISCHARGE. GALLONS/DAY
3 ORTHOGONAL TEST HOLES. PARALLEL PRIN. AXES
NX HOLE. TEST SECTION 25 FT LONG. HEAD= 100 FT

pectation is read in with the other fixed parameters. Each time a new sample is called for, a random uniform number is generated as a probability level. NUMBER searches the table to find the sample size closest to that probability.

PIEZO duplicates the calculations described in Chapter 3, for computing the steady discharge of a cylinder drill hole, oriented in a fixed direction (read in) in a saturated infinite medium having the directional permeability computed for the sample. Each of 49 computed discharges is stored, to correspond with the 49 independent samplings of one or more given joint aperture and orientation distributions.

Subroutine PUMPLT generates a cumulative frequency plot of the discharges, in a manner analogous to the operation of FREQPL. It also computes the mean and standard deviation of discharge, marking their absissas on the graph.

When large or moderate sample sizes were used, all pump-test distribution curves proved to be normal, as predicted. Figures 1, 2 and 3 of Plate 25 display one of the many trial solutions obtained under a variety of conditions. In this case, the simulated drill hole lay parallel to the central tendency of one dispersed set of conductors. The near-equality of the mean and median discharge, and the symmetry of the cumulative curve generated indicate that if a drill hole intercepts 5 or more conductors of any size (and these apertures were quite varied), the distribution of discharges will be nearly normal.

When small samples are used, some of the samples have no conductors at all, many would have one or two, and rarely would there be as many as five. Figures 4,5 and 6 display a solution to a two-set system of conductors. Instead of one hole, three orthogonal ones have been arranged along predicted average principal axes, just as one would proceed in designing anisotropic field testing, as per Chapter 3. The expectation of joints on one set was made 0.5, the other 1.0, totaling 1.5 per sample. All the discharge curves in this case (Figure 6) are skewed, and the statistical parameters shown on each plot agree well with the observation from field data that the mean and standard deviation are of like magnitude.

Notable confirmation of the anisotropic pump test methods of Chapter 3 is that the test-hole following the axis of least permeability (X-symbols) gives the highest discharge, since it cuts across the densest set of conductors. The hole along the major permeability axis discharges least because it lies nearly parallel with both sets of conductors.

The computer model has succeeded in predicting discharge relationships similar to those in Plate 25 for aperture distributions that are normal, truncated normal, log normal, and exponential, with a wide variety of parameters for each (see Chapter 7 for aperture distributions). One, two and three-set joint systems have been studied.

Speculations on the Hydraulic and Mechanical Properties of Fine Structures

The properties of fine fractures, microjoints or fluid inclusions are not disclosed by permeability tests. The mechanical properties of rock masses are probably influenced strongly by such features, depending upon their ability to transmit pressure changes. Ellis (1906) and Dale (1923) discussed rift and grain in crystalline rocks, and identified such planes of fracture with planes of microscopic fluid inclusions. Wise (1964) recognized that the microjoints he studied are also resurrected planes of microscopic fluid inclusions. Composition and PVT relationships of the fluids of either isolated primary inclusions, or planes of secondary ones, are discussed by Roedder (1962). Wise found microjoints in granite, migmatite, gneiss, schist, amphibolite, and basalt, but best developed in the most massive rocks. Their presence may be an important universal attribute of crystalline rocks.

Wise believes that common joints developed later and "semi-independent" (p. 296) of the microjoints. This seems unlikely from Hodgson's observations (1962) that joint sets have no mutual effect upon intersection, and from Wise's own findings: At a given site there may be found a microjoint orientation not represented there in the common joints. The "unrepresented" set often appears as a common joint set nearby. The lack of a measure or property of fine fractures to define a lower size limit to common joints, or an upper limit to microjoints, leaves room for speculation that, microjoints and common joints, fluid inclusion planes, constitute a continuous, evolutionary species. The common joints may be opened microjoints, which, in turn, are predetermined by planes of fluid inclusions which formed by cementation of earlier joint planes. Joints are probably transient conductors throughout the geologic history of a rock body, repeatedly opening and resealing during tectonic and quiescent periods.

Analysis of transient pressure tests may not give evidence of the nature of fine interconnected fractures when larger ones are present, because a moving water table may mask any changes that could take place with time in a truly infinite medium.

Though the structure of water at crystal interfaces is virtually unknown (Martin, 1960), it behaves as an imperfect solid (Rosenquist, lecture at University of California, Sept. 28, 1960) capable of creep by dislocations. The strength of water decreases away from solid boundaries, absorbing (influencing) up to 10 layers (53 Å) distant from silicate minerals. Thus, water in cracks opened less than 100 Å is largely held water.

Continuous interconnected fluid films in fine fractures larger than 100 Å must come to hydraulic and physico-chemical equilibrium with nearly free ground water, if sufficient time has elapsed during steady conditions. On the other hand, unopened joints, recognized by entrapped fluid inclusions, cannot reflect the mobile hydraulic regime. Roedder (1962), says that it is easy to spot by composition, the rare fluid inclusions that have leaked. Different planes of inclusions often have different, but uniform, fluid composition, evidence that they formed at different times, and at different pressures.

Discrete inclusions and open fractures isolated by crystallization are known to contain fluids under high pressures, even in thin sections. Roedder (1962) has verified 1000 psi pressure in some containing CO_2 and brine, by observing the gas expansion upon the release of pressure. Composition and PVT relationships can be determined by heating or freezing fluid inclusions containing two or three phases, observing the changes under a microscope. Residual fluid pressures result from geologic or excavation unloading. Across the solid bridges of a plane of fluid inclusions, there must exist high tensile stresses. Furthermore, when rock is strained, the confined fluids must impose stress concentrations influencing the mechanical properties of the rock under static exterior loading, blast impact or drilling pressures. This promising line of research seems not to have been exploited.

The mechanical influence of pore fluids cannot be discounted even for pervious rocks such as sandstones, for individual grains are stressed by contained inclusions. Hydraulically closed fractures extending more than a few grain diameters are unlikely in a sandstone, but rehealed fractures, marked by planes of inclusions, constitute planes of weakness. May this account for "new" ruptures when strain might otherwise be accommodated along "old" fractures?

No pressure tests have been analysed from formations having intergranular permeability as well as fracture permeability. In Chapter 4, it was shown that intergranular permeability is superposable on fracture permeability. Therefore, in jointed sandstone, the cumulative discharge curves should shift to the right of the zero abscissa, but the skewed shape should resemble curves from crystalline rocks.

<u>Field discrimination of planar features</u>

We cannot always forecast which of the many planar features of a rock mass will prove to be hydraulic conductors. We must drill, and measure or pressure-test each joint to characterize it. The sporadic appearance of seeps at an exposed face might be accounted for by non-conductivity as well as capillarity. Certain weathered, wet joints can be identified definitely as conductors, but unweathered, apparently tight joints cannot be called non-conductors upon inspection alone. We only know that the density of conductors in a volume is small compared to the density apparent at outcrops. Instead of one conductor per foot or so, the evidence from pressure tests indicates an expectation of one to five per 100 feet. For example, at Oroville, the spacing of effective conductors may be 20, 40, or more feet, instead of inches. Pump-tests of known shears, fracture zones and schistose zones there suggested to the geologists (Thayer, 1962, p. 2) that the shears are the main conductors and that only 10 percent of the permeability is contributed by joints. The small-sample statistics of pump tests would be consistent with rejection of essentially all joints at Oroville as conductors.

A geologist should discriminate carefully the features observed on drill core: Unless a fracture changes the drill-water circulation, shows staining, decomposition, transported fillings or drusiness, it is probably a machine-break of no original consequence as a conductor. For practical foundation investigations, it is the directional and spacial statistics of the larger openings that need attention, not the small openings.

Permeability near Exposures and in Undisturbed Rock

It follows that we should look for a wholly different medium within the decompression zone surrounding an underground opening than exists in the undisturbed rock mass. If the visible joints are conductors, the decompression zone possesses relatively high permeability. Consequently, low hydraulic gradients there favor stability of the opening because the intergranular stresses are high. Leeman's observations (1958) indicate that the zone of fracturing is 4 to 25 feet thick around mine workings, the extent depending upon the time elapsed since excavation and the depth below the ground surface. Lutch (1958) measured a 4 to 10 foot thickness of fractured wall rock under similar conditions in the Witwatersrand mines. It is noteworthy that around shallow workings, the joint system reflects the rock fabric, whereas around deep workings, "ring-stress" and "slabbing" fractures (Leeman, 1958) develop more prominently, in relation to the geometry of the excavation. Permeability axes would tend to have constant orientation around shallow workings, and radial symmetry at depth.

If the computer model is given conductors distributed as the observed joints, it should serve well for predicting permeability axes in the decompressed regions of high fracture density. For similar volumes, it may fail in undisturbed rock because the boundaries encompass few significant conductors.

Figure 1 of Plate 26 shows the attitudes of measured joints replotted from data collected at the Oroville damsite (Lyons, 1960) and Figure 2 shows the axes of principal permeabilities interpreted from it by the writer's methods. This is an estimate of the directional character of rock peripheral to underground openings such as the power cavern under construction. Compare these with Figure 3, describing the major conductors of the entire foundation area (Calif. Dept. of Water Resources, 1963), a stereographic plot of faults, shears, and schistose zones. Also on this figure are the estimated permeability axes for the foundation as a whole, which may be used to analyze potential distribution in the rock between the reservoir and the vicinity of the power cavern. Whereas the analysis of exposed joint orientations and observations of the apparent spacing, texture, continuity and openness suggested that sets 2 and 3 are nearly equally conductive, (Chapter 5) the analysis of the major shears throughout the site shows that set 2 dominates., Since these shears accounted for most of the pump test discharges, set 2 at the outcrop may likewise control the anisotropy around the openings. Interpreting Figure 3 of Plate 26 as a single set with dispersion $K_s \cong 16$, leads to different anisotropy, strongest on a plane dipping steeply east, and about 1/7th as strong normal to that plane of isotropy.

The fractured zone induced by explosives and decompression around unlined tunnels seems to be of similar permeability in all hard rocks, as suggested by the decay or absorption of waterhammer (J. Barry Cooke, lecture at University of California, May

PLATE 26

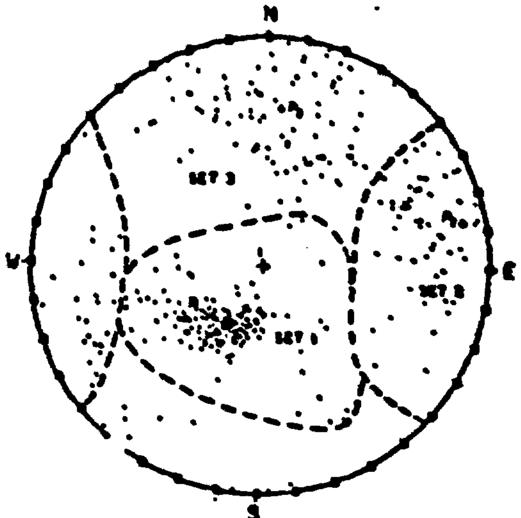

FIGURE 1
STEREOGRAPHIC PROJECTION, UPPER HEMISPHERE
DWR OROVILLE, LET-1, PLATE 4, JOINT PATTERN
P_1=0.4759, -0.2994, 0.8276 P_2=-0.2283, 0.9637, 0.1050
P_3=-0.9323, 0.0819, 0.3540
K_{P_1}=13.0 K_{P_2}=12.0 K_{P_3}=9.75

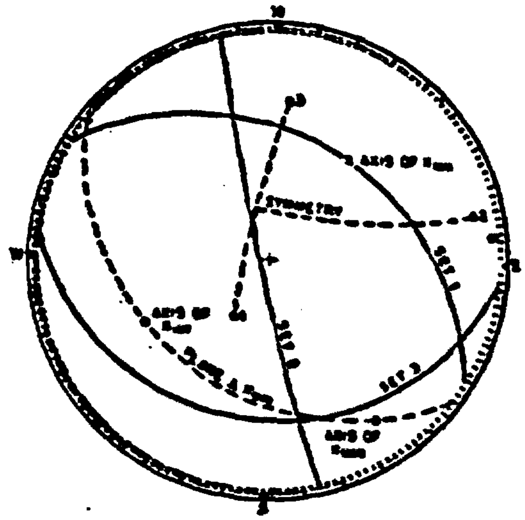

FIGURE 2 ANALYSIS OF PRINCIPAL PERMEABILITY AXES FROM JOINT GEOMETRY, OROVILLE DAMSITE, LET-1

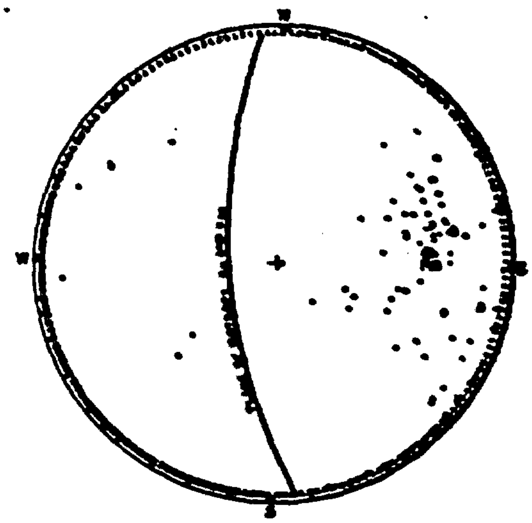

FIGURE 3 STEREONET PLOT OF NORMALS TO ALL MAJOR PLANAR STRUCTURES AT OROVILLE DAMSITE: 80 SHEARS, 1-25 FT THICK, 7 SCHISTOSE ZONES, 1-3 FT THICK, DISPERSION [illegible]

21, 1961).

<u>Sample Size Required for Acceptable Anisotropy Estimates</u>

One of the objectives of the model study was to estimate the size of sample needed to define adequately the directions of principal axes when only one sample of joints is obtained. Plates 1 to 15 of Chapter 5 show unacceptable scatter of axes when 25 or fewer elements are in the model, and principal permeabilities are too dispersed to be considered acceptable approximations of an equivalent continuum if there are less than 50. If several samples of joint orientations are made, and axes are estimated from each, the dispersion of axes will narrow the field of uncertainty. If the joint system is homogeneous, one may as well combine samplings into one sample of adequate size, say 100 joints per set.

The major planar structures at Oroville (Figure 3 of Plate 26) include about 20 shears from the vicinity of the power cavern (Thayer, 1962). For assessing the anisotropy of the undisturbed rock between the reservoir and the cavern, it is better to assimilate shears from the entire site into one sample characterizing a tectonically homogeneous medium (Figure 3), than to rely on a few random shears nearby.

Orientation of drill holes for anisotropic pump-testing should also be based on adequate samples, otherwise on combined samplings from the entire area. Geological boundaries and different joint systems may indicate that distinct areas should be tested and analyzed individually. In cases where an insufficient sample size is unavoidable, the few major conductors should be tested separately, and the boundary problem solved for those specific conductors, neglecting all minor features. Computer programs such as the TRAN (Warren, Dougherty, and Price, 1960) or others discussed by Schenck (1963), are available for solving many complicated boundary problems by relaxation and finite-difference equivalents of the diffusion or Laplace equations. Conductor planes within the boundaries, representing specific features, can be built into such models. The Oroville power cavern site is a typical situation in crystalline rock whose permeability is governed by a few shears. As an alternative to the statistical approach, solve for the potential distribution along such conduits, then apply them as boundary conditions for small-scale problems, lying wholly between major conductors. The principal axes and permeabilities of rock bodies between major conductors would be determined from joint orientations and pressure tests. Both parts of the solution would be important for design of drainage or rockwall stability. The two-stage method presupposes that major and minor conductors may be distinguished early in the exploration. It recognizes that the potential distribution and, thus, the flow, depends almost entirely upon the largest conductors, but that the local potential distribution, say in a tunnel wall, depends also on the fine structure.

An indefinite range of small-aperture fractures will undergo prolonged transient adjustment to the potentials on the major features. The oil films observed on shear surfaces in the Ain Zalah field, Persia (Daniel, 1954), indicate slow movement in many fractures that contribute little to permeability.

Since the effective conductors in crystalline rock are infrequent, some randomly-placed wells will often lack communication with the openings, so giving insignificant yield. A dry well might be made to produce by shooting or hydrofracing, especially if the well is oriented parallel to the predominant joint set. Similarly, the difference between wet and dry tunnels in crystalline rock lies not in the peripheral conductivity, but in continuity with preexisting open joints nearby.

In this chapter, we have used the notions gained by modeling fractured media to try to understand why permeability of fractured rock varies as it does, and conversely, we have conveyed interpretations from discharge data to the model for its improvement. Without more critical field data, we may not be able to learn much more. The measurement technique proposed in Chapter 2 should yield further substantiation of anisotropy and the statistics of its variations.

We have learned little about aperture distributions, and suspect that we cannot do so without direct measurement, which would be difficult.

In Chapter 4, there was presented a possible determination of porosity, assuming all apertures alike. So to see if it is really important to know the aperture distributions, Chapter 7 has been written.

Chapter 7

ESTIMATION OF POROSITY FROM THE PERMEABILITY AND GEOMETRY OF FRACTURED MEDIA

Introduction

The need for a method of estimating the secondary porosity of fractured permeable media is clear from the many practical problems depending on porosity. Porosity is reflected in storage capacity, in density, neutron absorption, thermal or electrical conductivity, elasticity, compressibility and strength. Civil and petroleum engineers could employ knowledge of fracture porosity in fluid displacement problems. There is interest in the bulk volume impregnated by a unit volume of displacing chemical grout, or in oil reservoir water flooding. Prediction of the vector average particle velocity of fluids moving in fractured media depends on a knowledge of porosity and the average macroscopic or continuum velocity.

Factors Governing Porosity

Porosity in fractured media depends upon the spatial frequency of conductors, their orientations and the distribution of their apertures. Orientation is the only readily accessible variable, but it may be the least important. The spatial frequency was found to be small and variable, as indicated in Chapter 6 by analysis of pressure tests. Even if the exact frequency is known in a given case, porosity cannot be determined precisely from permeability, because permeability depends upon the sum of cubes of aperture and the same sum could be obtained from any of many possible distribution functions.

In this chapter we have studied the influence of three different aperture distribution functions, to see if by averaging the divergent porosity values computed from many samples, an acceptable precision can be obtained.

In Chapter 6, a significant property of fractured media is established: pumping test discharge values can only be explained if the spatial frequency of conductors is small compared to frequencies disclosed in natural or excavation exposures. Something like one fracture in a hundred potential ones is effective as a water conductor in undisturbed rock. For purposes such as displacement, it is only the large openings that matter, while total fracture porosity may have a large inaccessible component. For a given permeability, a small number of conductors leads to much smaller porosity than when many occur, since discharge depends on the third power of aperture. It will be easier to identify conductors in the field than it will be to devise methods of measuring their apertures, so it will be more fruitful to measure frequencies than apertures in future research.

Computation of Porosity with Various Aperture Distributions

In Chapter 4 there was presented a set of simultaneous equations (4-28) to determine the permeability of fictitious sets of parallel conductors having the same aperture distributions as the actual orientation-dispersed sets. The porosity due to the parallel sets and that of the medium cut by dispersed sets can be estimated on the assumption that all apertures are equal. An evaluation of the errors introduced by the uniformity assumption, when apertures are actually distributed, facilitates translation of permeability into porosity.

An object of the computer model studies has been to find out how important is the form of the distribution function that defines the apertures, when orientations and spatial frequencies are known. To attain this objective, porosity is computed in two ways for any given set of geometrical variables. The first is by summing the void space per unit volume as the apertures and orientations are generated, so giving true porosity. The second method assumes uniformity, and computes an equivalent porosity from the anisotropic permeability derived from each specific sample of the aperture and orientation distributions. The frequency of conductors in the volume DELTA is taken always to be the specified Poisson expectation.

The results presented below indicate that quite acceptable estimates of secondary (fracture) porosity can be made from permeability measures, provided that the average fracture frequency is well known. According to equation(4-31), porosity depends on the number of conductors in the volume, taken to the two-thirds power.

A method of field determination of the frequency of effective joint conductors is suggested in Chapter 8, but since it remains untested, the importance of this parameter suggests that it be given priority in further research on fractured media. It has been suggested that pre-exploration grouting be used to mark conductors. Alternatively, one could use a statistical approach (Chapter 8). On the walls of tunnels or drill holes, or on recovered cores, one may identify weathered, drusy or opened fractures as conductors, as opposed to fresh fractures of relatively unlikely conductivity.

In the model, average joint frequency is specified, but each sample has a different number for the same volume, the numbers satisfying a Poisson distribution. When the average frequency is used to compute porosity from permeability (by the second method), large sampling errors are encountered in the porosity values, which are themselves, Poisson-distributed. Each of these porosity measures is compared to the actual porosity of the sample, quantities precisely known by summing the apertures, modified by their orientation (by the second method). Subroutine EQPOR, given in Appendix A, computes the porosity from the generated anisotropic permeability and constants of the orientation distributions, then discloses the ratio of computed to actual values. The average ratio is close to one. The example below follows the development of equations (4-27) to (4-31), somewhat simplified by use of only two sets of conductors with orthogonal central tendencies, so that only two simultaneous equations need be solved.

Each joint set has a Fisher's dispersion coefficient, $K_f = 20$. One has a central tendency along

$$\overset{1}{\alpha}_i = .5, .6, .7071,$$

and the other

$$\overset{2}{\alpha}_i = -.600, -.388, .699.$$

The coefficients corresponding to dispersion $K_f = 20$ (Figure 4-7) are

$$K_{max.} = c_1 K_{parallel} , \quad c_1 = .956 .$$

$$K_{min.} = c_2 K_{parallel} , \quad c_2 = .100 .$$

Nothing is known of the apertures or the number of elements included in a sample, but it is assumed that average frequencies have been deduced by some means for the medium, as well as orientations. The first set in this example has reciprocal specific surface of 2 meters, which amounts to a spacing of one conductor each 224 centimeters along the central tendency line. The second set has reciprocal specific surface of one meter, or one per 112 centimeters along its central tendency.

One of the random samples of conductors from these sets produces principal permeabilities, computed to be

$$K_{11} = 3.67 \times 10^{-9} \quad \text{cgs units}$$

$$K_{22} = 2.63 \times 10^{-9}$$

$$K_{33} = .946 \times 10^{-9}.$$

Were these data obtained in the field, principal axes would have to be approximated from the orientations of the entire joint system. Since the particular example given here is computer-generated, the direction cosines of the axes are known.

The central tendencies must be rotated to a coordinate system parallel to the principal axes, by applying the transformation

$$m_j' = a_{ij}\, m_i \ ,$$

where a_{ij} is the matrix of principal axes. The transformation is:

$$m_j' = \begin{vmatrix} .462 & -.731 & .611 \\ .688 & -.078 & -.721 \\ .567 & .678 & .468 \end{vmatrix} \begin{vmatrix} .5 \\ .5 \\ .7071 \end{vmatrix} \text{, or by } \begin{vmatrix} -.600 \\ -.388 \\ .699 \end{vmatrix} ,$$

for the first and second sets, respectively. These are:

$$\overset{1}{m_j} = .222,\ -.206,\ .953$$

$$\overset{2}{m_j} = .370,\ -.887,\ -.276.$$

Two of the possible simultaneous equations (4-28) are:

$$K_{11} = [\overset{1}{c_1} + (\overset{1}{c_2} - \overset{1}{c_1})\, \overset{1}{m_1}\, \overset{1}{m_1}]\, \overset{1}{\ell_p} + [\overset{2}{c_1} + (\overset{2}{c_2} - \overset{2}{c_1})\, \overset{2}{m_1}\, \overset{2}{m_1}]\, \overset{2}{\ell_p}$$

$$K_{22} = [\overset{1}{c_1} + (\overset{1}{c_2} - \overset{1}{c_1})\, \overset{1}{m_2}\, \overset{1}{m_2}]\, \overset{1}{\ell_p} + [\overset{2}{c_1} + (\overset{2}{c_2} - \overset{2}{c_1})\, \overset{2}{m_2}\, \overset{2}{m_2}]\, \overset{2}{\ell_p}$$

$$3.67 = [.956 - .856(.049)]\, \overset{1}{\ell_p} + [.956 - .856(.137)]\, \overset{2}{\ell_p}$$

$$2.63 = [.956 - .856(.041)]\, \overset{1}{\ell_p} + [.956 - .856(.786)]\, \overset{2}{\ell_p}$$

$$\overset{2}{\ell_p} = 1.72 \times 10^{-9}$$

$$\overset{1}{\ell_p} = 2.32 \times 10^{-9}.$$

The average aperture is obtained by:

$$b = \sqrt[3]{3 \ell_p D / 2N}$$

$$b_1 = [3(2.32)112./2(0.5)]^{1/3} = .009$$

$$b_2 = [3(1.72)112./2(1.0)]^{1/3} = .006.$$

Porosity of a set is

$$\Theta = c(3\ell_p)^{1/3}(2N/D)^{2/3},$$

where c is a correction for specific surface given in figure 4-6, relating the parallel case to the dispersed case.

$$\Theta_1 = 1.061\,[3(2.32)10^{-9}]^{1/3}[2(0.5)/112.]^{2/3} = .000087$$

$$\Theta_2 = 1.061\,[3(1.72)10^{-9}]^{1/3}[2(1.0)/112.]^{2/3} = .000125$$

The total permeability-equivalent porosity,

$$\Theta = .000212$$

could not be verified if the permeability data were obtained in the field, but since every conductor of the sample model has known aperture and orientation, a precise porosity is known, in this case:

$$\Theta_{actual} = .000390.$$

The "equivalent" porosity is .544 of the true. Other samples give a scattering of ratios, greater or less than unity.

<u>Porosity for normal, log-normal and exponential aperture distributions</u>

The porosity ratios generated by the model provide an opportunity to investigate the importance of the various distribution functions that are likely descriptions of joint aperture in real rock. Table 7-1 summarizes the results of 39 model studies of 49 samples each, employing absolute (or transposed) normal, log-normal and exponential distributions of apertures, but with all other parameters constant, such as conductor frequency and orientation dispersion. The example calculated above is one of the samples. The distribution functions describing the

TABLE [redacted] 7-1

COMPUTED PERMEABILITIES AND POROSITIES WITH VARYING APERTURE DISTRIBUTION

1.	2.	3.	4.	5.		6.	7.	8.	9.	10.
APERTURE DISTRIB.		PRINCIPAL PERMEABILITIES CGS UNITS AVERAGE OF SAMPLES				POROSITY				
μ	σ	K11	K22	K33		AVERAGE TRUE VALUE	EQUIVALENT TO PERM.	RATIO 7./6.	AVG. RATIO FROM SMPLS	STD. DEVIATION, RATIOS
ABSOLUTE VALUE (TRANSPOSED) NORMAL DISTRIBUTION										
N1=.5, N2=1.0, DELTA=112										
.005	.001	.221	.172	.052	10^{-8}	.00023	.00017	.748	.877	.483
.025	.005	.291	.231	.086	10^{-6}	.00124	.00088	.711	1.047	.980
.125	.025	.377	.295	.094	10^{-4}	.00650	.00448	.690	.791	.440
N1=5.0, N2=10.0, DELTA=1120.										
.005	.001	.138	.100	.051	10^{-8}	.00015	.00016	1.011	1.212	.580
N1=.5, N2=1.0, DELTA=112										
.005	.005	.813	.708	.111	10^{-8}	.00028	.00025	.887	.921	.583
.025	.025	.131	.116	.017	10^{-5}	.00151	.00132	.875	1.037	.685
.125	.125	.141	.122	.020	10^{-3}	.00769	.00645	.838	.968	.654
.005	.015	.876	.773	.107	10^{-8}	.00060	.00054	.899	.954	.526
.025	.075	.173	.155	.020	10^{-4}	.00361	.00308	.852	.972	.601
.125	.375	.161	.143	.019	10^{-2}	.01660	.01404	.845	.674	.304
.005	.045	.194	.173	.022	10^{-6}	.00172	.00150	.870	.924	.506
.025	.225	.418	.372	.050	10^{-3}	.01052	.00898	.853	.913	.457
.125	.125	.369	.330	.041	10^{-1}	.04730	.03962	.838	.936	.365
AVERAGE								.839	.956	
EXPONENTIAL DISTIBUTION										
N1=.5, N2=1.0, DELTA=112										
.005	.16								1.039	.35
.025	.16								1.091	.40
.125	.16								.957	.30
N1=5.0, N2=10.0, DELTA=1120.										
.125	.16								1.079	.15
N1=.5, N2=1.0, DELTA=112										
.005	1.40	.332	.268	.068	10^{-8}	.00024	.00020	.806	.943	.463
.025	1.40	.407	.347	.066	10^{-6}	.00117	.00093	.797	1.031	.828
.125	1.40	.643	.549	.100	10^{-4}	.00680	.00503	.735	1.059	.776
.005	2.70	.116	.102	.015	10^{-7}	.00029	.00028	.960	1.091	1.037
.025	2.70	.146	.133	.015	10^{-5}	.00140	.00133	.952	.902	.354
.125	2.70	.261	.232	.029	10^{-3}	.00844	.00763	.904	1.088	.684
.005	4.16	.644	.593	.052	10^{-7}	.00040	.00046	1.158	1.143	.921
.025	4.16	.846	.782	.062	10^{-5}	.00195	.00230	1.179	.979	.406
.125	4.16	.164	.149	.015	10^{-2}	.01227	.01376	1.121	1.046	.450
AVERAGE								.957	1.035	

TABLE 7-1 [redacted] (CONTINUED)

1. APERTURE DISTRIB. μ	2. σ	3. PRINCIPAL PERMEABILITIES CGS UNITS AVERAGE OF SAMPLES K11	4. K22	5. K33		6. POROSITY AVERAGE TRUE VALUE	7. EQUIVALENT TO PERM.	8. RATIO 7./6.	9. AVG. RATIO FROM SMPLS	10. STD. DEVIATION, RATIOS
LOGNORMAL DISTRIBUTION										
N1=.5, N2=1.0, DELTA=112										
.005	.06								1.122	.35
.025	.06								.851	.25
.125	.06								1.133	.35
N1=5.0, N2=10.0, DELTA=1120.										
.005	.06								1.098	.100
N1=.5, N2=1.0, DELTA=112										
.005	.50	.133	.122	.011	10^{-7}	.00030	.00027	.895	.914	.539
.025	.50	.300	.284	.018	10^{-5}	.00169	.00156	.925	.941	.476
.125	.50	.238	.217	.022	10^{-3}	.00839	.00716	.854	.829	.306
.005	1.00	.977	.970	.008	10^{-6}	.00059	.00087	1.473	.974	.497
.025	1.00	.378	.376	.002	10^{-3}	.00406	.00607	1.497	1.019	.405
.125	1.00	.138	.137	.002	10^{-4}	.01669	.02200	1.318	.994	.575
.005	1.63	.649	.649	.007	10^{-5}	.00216	.00633	2.928	1.201	1.070
.025	1.63	.320	.320	.000	10^{-6}	.02097	.04967	2.368	1.172	.524
.125	1.63	.510	.510	.000	10^{-4}	.06196	.13129	2.118	1.044	.420
AVERAGE								1.598	1.023	

aperture populations sampled are displayed in Plates 27, 28 and 29. Warren and Price, (1961, p. 158) tabulate properties of several other useful functions.

In the tables, the first column indicates the mean of apertures employed in the distributions, including .005, .025 and .125 centimeters. Standard deviations were selected to include a range of 0.2 to 10 times the mean. In this way, various degrees of skewness (the third moment was not computed) were developed, some with and some without appreciable near-zero frequencies. Subroutine APER, found in Appendix A, generates the distributions.

The transposed normal distributions, of the type employed in Chapter 5 and plates 1 to 15 therein, are derived from Caughran's (1963) generator of random normal deviates, RANDEV, (having mean zero and standard deviation 1), modified by

$$B = |\sigma(\text{RANDEV}) + \mu|,$$

where B is the half aperture,

σ is the desired standard deviation, and

μ is the desired mean. Absolute values are taken to maintain positive apertures and to introduce skewness.

Log-normal distributions (Aithchison and Brown, 1957) were formed from the Caughran random normal deviates by

$$\ln\left(\frac{B}{\mu}\right) = \sqrt{2}\,\sigma(\text{RANDEV}).$$

Exponential distributions employed a generator of random deviates, UNIRAN, uniform between 0 and 1, modified by

$$\ln\left(\frac{B}{\mu}\right) = \frac{\sigma}{2}(2[\text{UNIRAN}] - 1).$$

Tables 8-1, 2 and 3 list, in column order, the mean and dispersion measures (μ and σ , as defined in the above equations), then the principal permeabilities averaged from the 49 samples. The true porosity is computed from the actual apertures included in all 49 samples. The next column reports equivalent porosity,

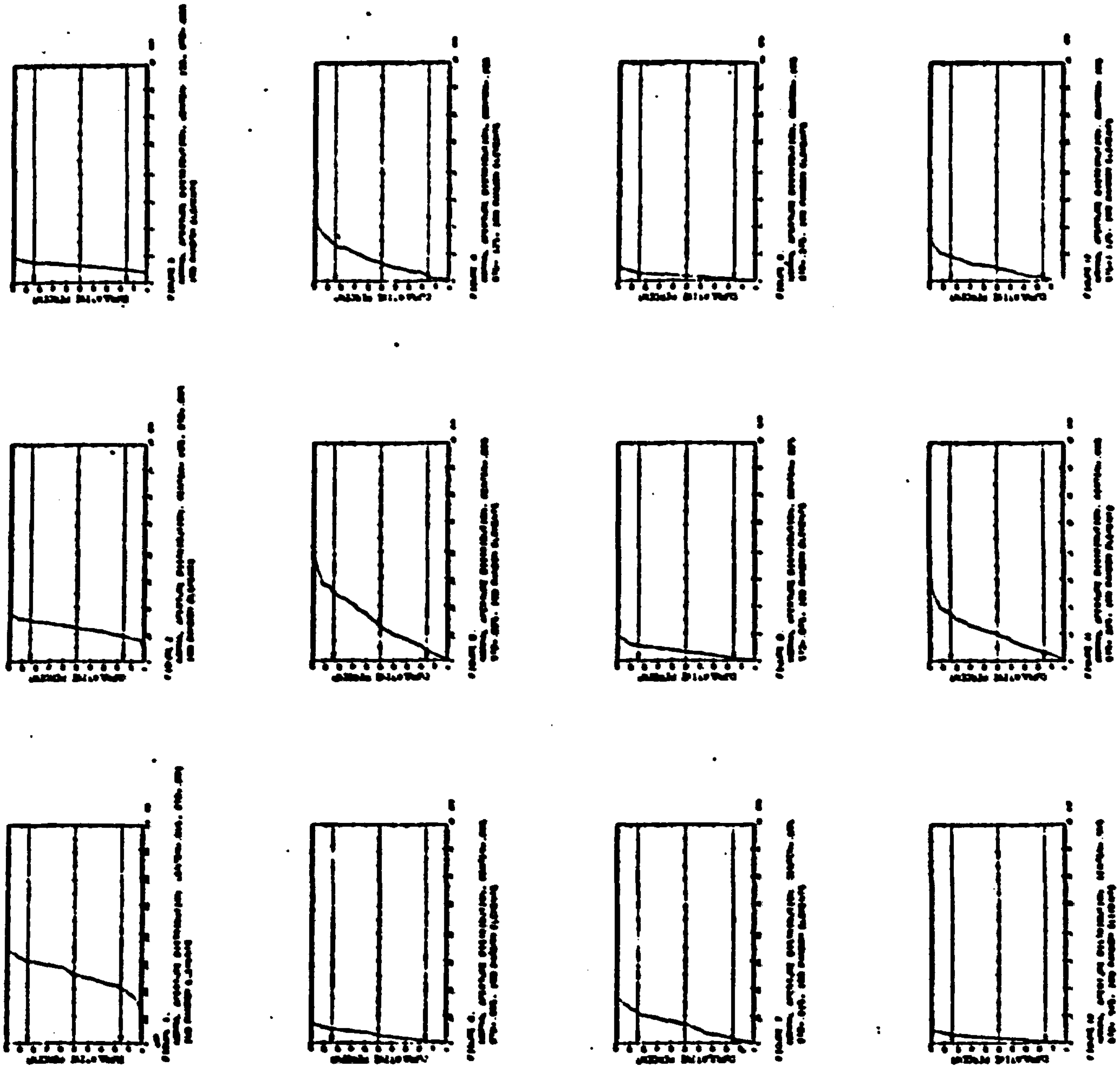

PLATE 28

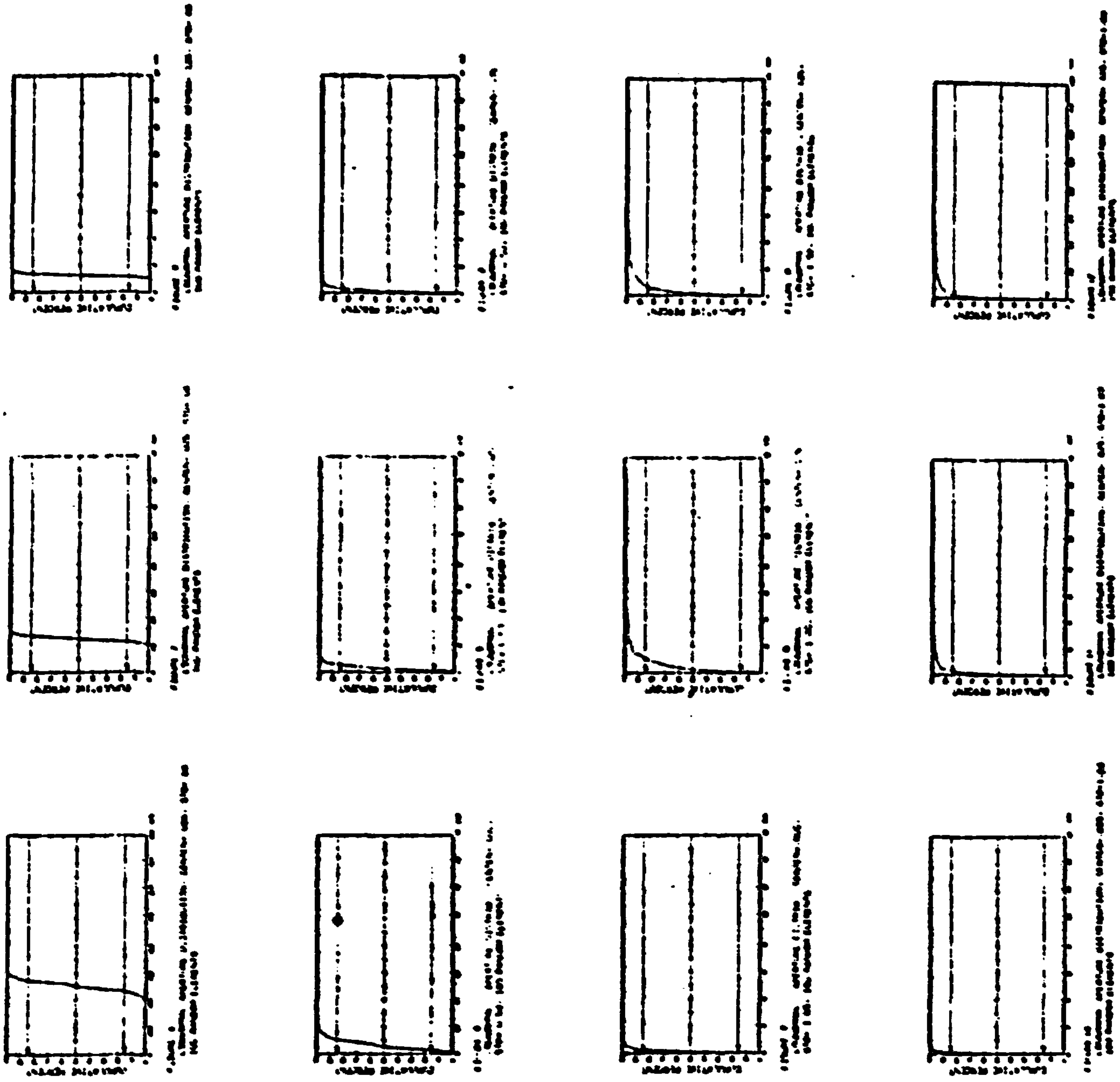

PLATE 29

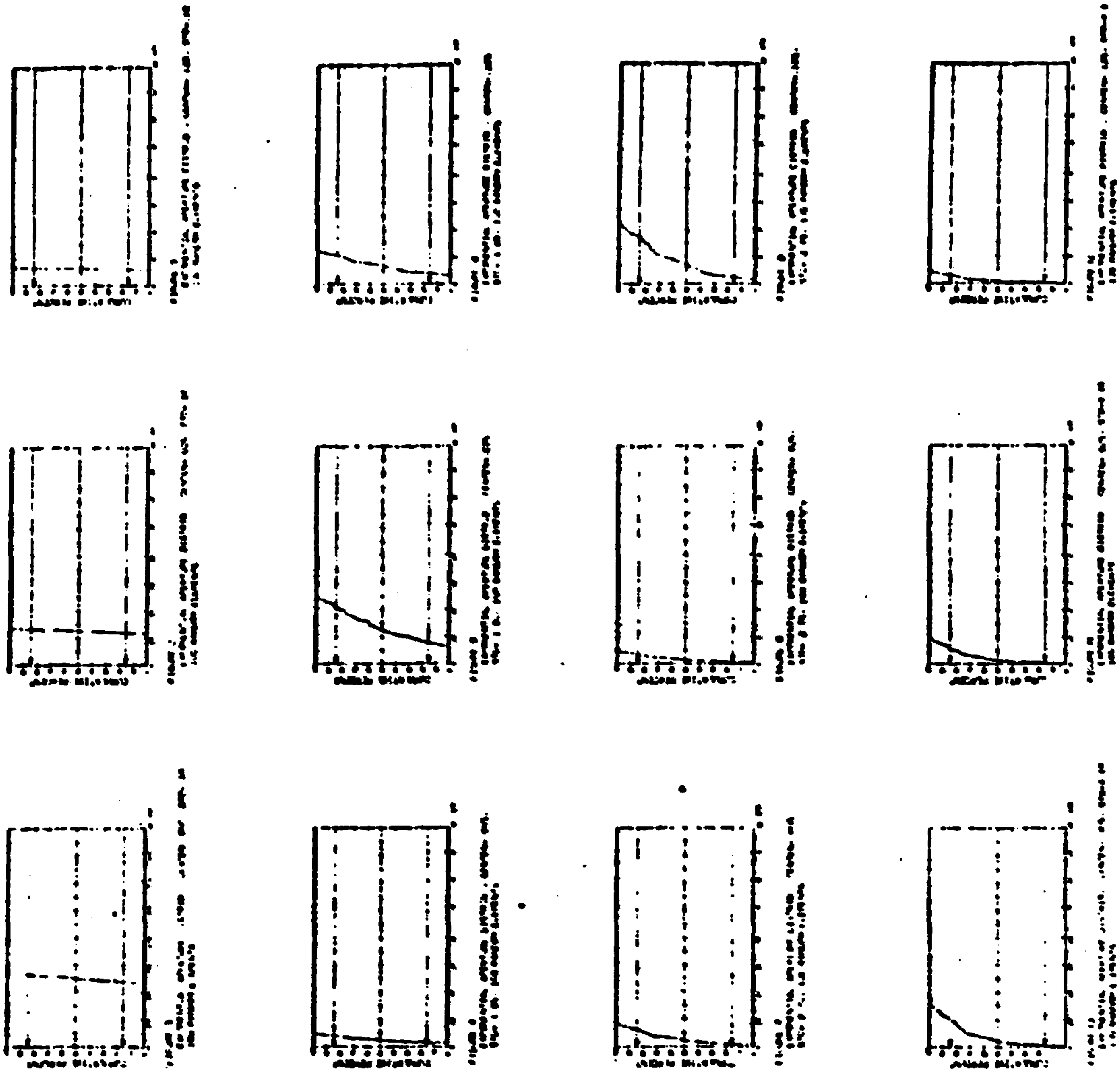

computed in Subroutine POREQ, by the same method employed in EQPOR and in the illustrative example given in this chapter, but employing the <u>average</u> permeabilities as a measure, and the central tendencies of the two joint sets as predicted principal axes. The tabulated ratios of equivalent to true porosity assess the reliability of using average permeabilities to predict the true porosity.

Porosity computed from average permeabilities ranges from 0.7 to 1.0 times the true porosity averaged over all samples from a normal distribution. The more skewed the aperture distribution, the higher becomes the ratio of computed to true porosity. This is because permeability depends on the cube, and porosity on the first power of apertures and the mean of skewed distributions increases faster for cubes when sample size increases. Note in each table the progressive increase of the ratio, as dispersion of apertures and skewness increases from top to bottom of column 8. The normal distribution is least sensitive to such changes, suggesting that if porosity is computed from average permeabilities, and this distribution is proved to represent jointed rock, then true porosity may be estimated by

$$\theta = 1.2\ (\theta_{\text{computed from average } k})$$

Porosity computed from average permeabilities ranges from .73 to 1.1 times the true porosity when exponential aperture distributions are assumed. A correction factor of 1.05 may be used to estimate true porosity.

Porosity computed from average permeabilities ranges from .85 to 2.9 times the true porosity when log-normal aperture distributions are assumed. The skewness is apparently more significant for this type than for the normal or exponential, and presumably, even greater errors might be made if skewness exceeds that studied here.

Porosity estimation from a series of anisotropic permeability measurements may be improved by calculating equivalent porosity for each permeability measure, assuming a constant fracture frequency even though it is known to vary from test to test. The individual porosity measures will be dispersed, but the average of all porosity measures approaches the true porosity for the medium as a whole, with errors of at most 10%. The next to last column of the tables reports the average porosity as a ratio to the true. The last column shows the standard deviation of the distribution of average porosity ratios, generally about 0.5.

Relative Importance of Frequency and Aperture Distribution

A porosity estimate is no better than the estimate of fracture frequency because $\Theta \propto (N/D)^{2/3}$. This emphasizes the importance of determining, either for field or research problems, which fractures observed are conductors and which are not. Suppose that a fractured rock is refractured so that a new conductor is formed, equal and parallel to every original one. Now halve the apertures of all of them, so that porosity is as before. Under the same gradient, the fractures will transmit 1/8th their original discharge. The permeability is thus 1/4 the original value, while porosity is unchanged. The results of the model studies of permeability-porosity relationships suggest that the exact form of the aperture distribution is not critical for these purposes. The insensitivity of porosity measurements to aperture distributions encourages investigation of more crucial properties of fractured rock.

The above methods of computing porosity from permeability data can, and should be field-checked. After predicting porosity from pumping tests, seek confirmation by measuring grout impregnation. The volume of rock impregnated must occupy an irregular bulbous region around an injection point. The extent of grout may be determined by a series of check holes. Only those conductors which are hydraulically effective would be grout-filled. AM-9 chemical grout would be ideal for these purposes because it has aqueous properties, while neat cement is a non-uniform fluid suspension.

Porosity determination is but one of the possible applications of the fractured-media model. Its role in defining permeability leads to useful applications where the flow of fluids or the hydraulic potential distribution is needed. Chapter 8 contains a few suggested areas of interest, and some suggestions regarding techniques of application.

Chapter 8

SUGGESTED APPLICATIONS TO FLOW AND POTENTIAL PROBLEMS

Introduction

Numerous immediate or eventually feasible applications may be anticipated, either as direct results of the theory and techniques advanced in the preceeding chapters, or consequent to logical sequels to this thesis.

The applications may be grouped into categories that are geological, petroleum engineering, civil engineering or ground water hydrologic in nature, with inevitable overlap of the categories.

Geology Problems

The origin of joints remains just as obscure as was the origin of thrust faults prior to popularization of the notion that pore fluid pressures can account for the low apparent sliding resistance of rock on rock (Hubbert and Ruby, 1959). The mechanics of rupture of materials containing confined fluids would be an even more significant contribution, not only because of its implications for initial and rejuvenated jointing, but for static and dynamic breakage in materials engineering, excavation stability, explosive or drilling technology. Dynamic aspects of tectonic structures may also be clarified by analysis of fluid potential distribution adjacent to initial failure surfaces.

Recognition that individual planar conduits may have anisotropic properties by reason of textural lineation suggests applications to ore-finding. First of all, measurement of anisotropy of individuals could discriminate faults from joints, or detect the direction of slip on faults. If conduit anisotropy proves significant, it is a further variable (with orientations, spacing and apertures), controlling the overall anisotropy of a fractured rock mass.

Anisotropy of a fractured medium may facilitate reconstruction of the history of ore implacement from migrating solutions, thereby pointing to undiscovered ore. Similarly, modern ore-forming structures that are potential producers of steam, brine and metaliferous juvenile fluids would be amenable to analysis of the fracture systems characteristic of domal structures (Wisser, 1960). Indeed, the success of such brine well operations may depend upon analysis to locate productive sites that will promote flow of juvenile waters versus meteoric waters. Knowledge of the mechanics of the doming process by vertical tectonics and fluid pressure distribution would be a by-product of singular importance to economic geology.

Mine drainage is an important engineering problem in the mineral industry. Analysis of boundary problems on the basis of isotropy should be preceeded by testing for anisotropic permeability, leading to appropriate boundary transformations.

Grouting, blasting and tunnel support technology, discussed in later paragraphs, also have applications in mining.

The design of leaching projects to exploit low grade vein deposits by injection of water and withdrawal of solutions via wells or tunnels may be improved by better knowledge of statistical permeability properties of the open vein system. Leaching-field design is a boundary problem similar to that of mine drainage. A rational prediction may be made of flow paths and available surface area, and one might detect, by pump-test methods proposed in Chapter 2, features that diminish leaching efficiency by channeling.

Petroleum Engineering Problems

Petroleum exploration may be guided in a manner analogous to ore exploration, by knowledge of the anisotropy and porosity of fractured media serving as conductors from source to reservoir, and as fracture permeability traps.

Though directional drilling for measurement of principal permeabilities is not feasible at great depths, the theory of Chapter 2 may be modified for short packer-tests conducted in the bottom of a vertical well as drilling progresses in fractured rock, thereby permitting statistical analysis of data ordinarily obscured by overall well behavior. Such tests were suggested by P. A. Witherspoon (personal communication, 1964). Tests should be complimented by study of the orientation and spacing of joints to estimate principal axes. Knowledge of reservoir anisotropy would be valuable for planning well fields. Secondary porosity estimates (Chapter 7), based on fracture permeability, would be equally useful, to predict yield and optimum production rates. Knowledge of reservoir anisotropy and porosity would contribute to the design of secondary recovery schemes, including water spreading, and combustion drive. New interest in fractured media is emerging from the application of ground water hydrology for assessing the integrity of aquifers for underground gas storage purposes (Witherspoon, Mueller and Donovan, 1962). Fractured cap rocks will eventually be tested for permeability, possibly by methods akin to those proposed here, aided by analysis of fracture geometry.

Ground Water Hydrology Problems

The importance of planar conductors in governing the hydrology of a basin may not be limited to the crystalline basement rocks, but may contribute also to the conductivity of unconsolidated basin sediments, where jointing is recognized (Plafker, 1964) but so far not introduced into conventional aquifer analysis.

fracture permeability, modified by solution enlargement, is certainly dominant in carbonate formations. Under-seepage through basement rocks is usually neglected though recognized as a limitation on calculations of basin-wide water balance. In negative groundwater areas, underlain wholly by crystalline rocks and their weathering products, fracture permeability determines well yield. The statistics of such media are important for well planning (Davis and Turk, 1964). Regional flow analysis is being employed to predict the distribution of radionuclides in ground water (Davis, 1963), moving past atomic explosion sites. These often involve fractured basement rocks of unknown anisotropy that could be estimated by the methods proposed here. Tests may establish the frequency of effective water-bearing joints, and determine which set is conductive when more than one is present. Well hydraulics in a discontinuous-anisotropic-nonhomogeneous jointed medium may be improved upon consideration of the variables governing anisotropy. The importance of sample size (Chapter 6), and well orientation (Chapter 2) with respect to principal axes (Chapter 5), may be included in a statistical analysis of yield based on media transformed according to measured anisotropy. The well-pumping test results of Lewis and Burgy (1964) showing drawdown-time curves concave upward instead of downward, more likely result from vertical inhomogeneity of the rock than from the sampling statistics treated here.

Civil Engineering Problems

The assumption of isotropy customarily made in solving boundary problems in foundation engineering can be avoided if principal permeabilities are determined and oriented in the manner suggested in Chapter 2. Whereas the anisotropy of fractured rock may be weak, as would be the case for three near-orthogonal and near-equal sets, other situations may prove highly anisotropic.

Such is the case of the apparent dominance of a single dispersed set of faults cutting the Oroville Dam foundation (Figure 3 of Plate 26). Apparent permeability measured in unoriented drill-holes in this medium is considerably in error because the E-W principal permeability is about 1/7 the other two. Furthermore, the distribution of fluid potentials obtained by the designers using an isotropic electrical analogue could be obtained more precisely after transformation. A natural-scale model was used, with contours on the reservoir bottom as one boundary and underground openings as the other, submerged in a tank of electrolyte. Drainage holes in great numbers and of similar length have been designed to perforate the wall-rocks around the power cavern. It can be seen, without graphic proof, that the transformed medium expanded E-W by a factor of $\sqrt{7}$, will have the approximately circular cylindrical opening of the machine hall expanded to an elliptic cylinder, with flow lines concentrated at the east and west walls and equipotentials crowded to these walls. Retransformed to the natural scale, the anisotropic flow net, no longer equidimensional nor orthogonal, would retain high gradients towards the walls. Only by elongating the lateral drain-holes may pore-pressure distribution be made radially symmetrical to the opening. Longer horizontal drains than vertical would improve the stability of the excavation.

Similar analysis of anisotropic permeability can be used in other potential distribution problems in hydro-engineering, including prediction of uplift distribution beneath masonary dams, and pressure distribution around penstocks or power caverns. Imperfect correlation between prediction and observation would reflect the random variations in permeability arising because the scale of the problem, the base of the dam, for instance, may be only a few times the average conductor spacing. This condition of least predictability is unfortunately the condition most critical for design, leading to the highest and most erratic pressures (Terzaghi, 1929).

The portions of unlined tunnels most sensitive to rock properties are those with shallow cover, as in the approaches to portals. Leakage and landsliding are the hazards. Portal areas where investment is concentrated (penstocks, powerhouse), are usually protected by steel linings. A more rational approach to potential distribution in these areas, made possible through improved exploration, testing and analysis, but no more costly than currently employed, would lead to safer, more economical installations.

Predictions of flow between complicated boundaries of anisotropic media must ordinarily be based on the potential distribution, i.e. the flow net. Thus, the transformation methods discussed in Chapter 1 can be advantageously applied to the prediction of foundation leakage under dams or through reservoir rims, or to estimate water loss or water make to tunnels. The storage of fluids in subterranean caverns poses analogous problems in leakage evaluation.

Underground disposal of liquid wastes, be they industrial chemical wastes, atomic refinery wastes, or undesirable fractions from geothermal wells, may gain importance as fractured media become better understood. Directional permeability and porosity are the most significant properties needed to design injection well systems and to predict displacement in an aquifer. The entire subject of dispersion of solutes in fractured media warrants study.

Transient pressures, not treated in this thesis, are often very important in engineering as well as other fields. Anisotropy plays a significant role at all times of flow, such as during pressure tests. The subject needs more research, along lines pursued by Goodman, et. al.(1964).

The loading of foundation rocks during the construction of a dam is a transient condition if the foundation permeability is so low that a series of steady-state conditions do not exist. Such may have been the case of the Waco, Texas dam failure, a foundation slide in shale (R. Bean, Lecture at University of California, June 26, 1963), where 100% excess pore pressure, in other words, full construction load, had developed in underlying shale. Though other explanations have been advanced to explain the failure, strong anisotropy in the horizontal beds could also have contributed. The expectable high lateral permeability compared to the vertical permeability would lead to low lateral gradients, extending the high pore pressures over a large slide-surface area.

A more rapid pressure transient is water-hammer in pressure tunnels. Water-hammer has never caused rock falls, even though rapid declining pressure must result in tunnelward gradients in the walls. A marked increase in fracture permeability in the disturbed decompression zone around the opening may be the factor providing safety by minimizing gradients.

Gas flow in preexisting and induced fractures around explosives detonated in rock constitute more complex hydraulic phenomena than considered here, but involve the same media. Appleby's (1940) observations that dynamited faces have the same fracture patterns as natural faces lends strength to the notion that anisotropy estimated from orientations and pump tests can also indicate the anisotropy in the field of gas expansion near a tunnel or quarry face. It follows that more efficient orientations of shot holes, or more effective spacings or patterns might be devised. The influence of jointing modifying the radial symmetry of an underground nuclear detonation might be analyzed as well.

The anisotropy of mechanical properties of fractured media may be shown ultimately to be correlative with anisotropy of fluid conductivity. Take, for instance, the possibility that a rough fracture, such as a tension joint, has high permeability compared to smooth shear joints, while its shear strength is clearly in the inverse. Developed into a working theory of rock strength, pressure testing could serve as a tool to explore the directional strength properties of rock slopes or dam abutments. Pressure potential is also an important factor in the analysis of the stability of slopes cut in fractured rock.

Foundation grouting is a subject that stands to improve by application of the proposed methods of testing, and by analysis of anisotropy and porosity. Current practices are largely empirical. The plight of the art is well voiced in discussions of deMello's (1960) paper and by similar complaints (Lambe, 1957):

"It is seldom on any grouting job that one can obtain sufficient information on the soil or rock conditions involved to assure that the grouting work will be successful. In rock grouting, for example, it is almost impossible to know in advance the degree of continuity between voids and cracks, even if these voids and cracks were originally found by core drilling at the site or by observations of seepage."

An easy answer to all rock grouting problems is not to be found in this thesis, but rather, a seemingly arduous scheme of measurement and calculation leading to answers that have only statistical validity. But variability is the well-demonstrated characteristic of the medium, and any rational approach to definition of the means and variations of the properties is more promising than refined empirical techniques (e.g. Grant, 1964).

It seems that the design of a grout curtain may take two alternative courses, the first more practical, the second more elegant: 1. If the scale of fracture spacing is on the order of a fraction of the curtain depth or dimensions of a dam, then samples of conductors cutting a grout hole will include such a number that the rock may be replaced by in equivalent continuous anisotropic medium. In this case, design should assume impregnation of all openings in certain volumes around each drill hole. Alternatively, 2. if conductors are sparse, then exploration should define the location, continuity and aperture of each plane, with grouting designed to seal individual openings to form a water-barrier by compartmentation of the foundation, rather than by impregnation of a massive curtain.

In practice, it will be rare that a suitably-located, fully-connected Virginia fence of open conduits can be designed with confidence. If effective conductors are so widely spaced that the volume of influence around a drill hole contains fewer than one open conduit per 5 feet, then no alternative exists but to use the proposed statistical approach to impregnation grouting, even though the sample size is inadequate to assure reasonable confidence in the statistical measures.

Research on grouting should approach the simplest situation first: by assuming immiscible displacement of water by AM-9 Chemical Grout (1.2 centipoises). Miscible displacement in anisotropic fractured media is apparently a dispersion problem entailing tensor relationships between the potential gradient and the movement of a diffuse front. The complications of unsaturated flow above the water-table, and the non-homogeneous fluid properties of cement grout in saturated and non-saturated media may be treated subsequently.

A more optimistic aspect of rock grouting is the implication of a favorable mobility ratio for grout in water, limiting the development of viscous fingering in single fractures if not the aggregate system of fractures. Unlike injection into sand, however, there is a decided tendency for the majority of the grout to confine its travels to one or more major openings. Suppose, for example, that two parallel fractures are grouted at once through a drill-hole crossing them, and that one has twice the aperture of the other. The large one will convey 8 times the discharge of the smaller, filling it to twice the radius. In general, the radii to frontal positions under equal gradients will be nearly proportional to the apertures (in consequence of equation 4-6). If individual planar conduits are pressure-tested by isolating them with packers, the areal distribution of individual grout fillings may be estimated. Uniformity of aperture over the area of a single fracture should be studied. Such relationships for a few prominent planar conduits in a foundation would serve as the basis for design of a grout hole pattern for a compartmentation curtain.

In the usual situation, numerous conductors of unknown character are encountered in a hole, and pressure test discharges reflect their variable apertures and numbers. Mass impregnation grouting should then be the objective, for which effective porosity is the salient variable needed to plan hole spacings, injection volumes and gellation time.

Average fracture frequency must be known to estimate porosity from numerous permeability measures by the methods outlined in Chapter 7. To determine the frequency, a method suggested is to progressively shorten the separation between packers until a fair proportion of the pressure tests yield no flow. According to the reasoning developed in Chapter 6 for non-aggregating joints, the distribution of small numbers of fractures in the uniform test length, occupying many positions down the hole, should be Poisson. One need only consult a table of the Poisson distribution (Crow and Gardner, 1959, or abbreviated tables in any good text) to ascertain the expectation giving a frequency of zero measures equal to the observed proportion of no-flow tests. For example, if 14% of a series of 10-foot-long pressure tests give no discharge, the mean number or expectation of conductors is 2.0 in ten feet. This would be the total expectation for all sets intersected by the hole, and nothing can substitute for bore-hole photography, television, or at least core inspection to apportion the total frequency to the individual sets.

Light portable pressure-testing equipment should be devised for operation by a lone geologist without tying up a drill rig, for such extensive testing as here proposed as routine will never be attractive at the cost of idle-time for conventional drilling rigs.

Average porosities of the joint sets, computed as indicated in Chapter 7, may then be utilized for estimating the rock volume grouted per unit volume of chemical grout (not cement).

The shape of a displacement front around a point source, idealized as sharp rather than diffuse, would be a sphere in an isotropic medium. In Chapter 1, it was indicated that an anisotropic medium may be transformed to isotropic. The true front position is found by retransforming after ascertaining the isotropic configuration. Thus, the front forms an ellipsoid of semi-axes:

$$r_1 : r_2 : r_3 = K_{11}^{1/2} : K_{22}^{1/2} : K_{33}^{1/2} .$$

The volume of rock impregnated is found from:

$$\frac{\text{Vol. Grout}}{\text{Porosity}} = \frac{4}{3}\pi\left(\frac{K_{11}}{K_{22}}\right)^{1/2}\left(\frac{K_{33}}{K_{22}}\right)^{1/2} R_2^3 ,$$

where R_2 is the intermediate axis of the ellipsoidal front.

$$R_2 = \left(\frac{V_g}{\theta}\,\frac{3}{4\pi}\,\frac{K_{22}}{(K_{11}K_{33})^{1/2}}\right)^{1/3}$$

$$R_1 = \left(\frac{K_{11}}{K_{22}}\right)^{1/2} R_2 \qquad (8\text{-}1)$$

$$R_3 = \left(\frac{K_{33}}{K_{22}}\right)^{1/2} R_2$$

Equations (8-1) define the shape of a bulb of grouted rock, in terms of its semi-axes along the principal directions, based on the presumption that the front maintains its smoothness as though all conduits had the same aperture. In actuality, the ellipsoidal bulb cannot be realized as it is in sand, because the number of conductors does not form an adequate statistical sample as do the numerous intergranular pores of a sediment. Rather, some large openings will be filled to several times the computed radius, while smaller ones will remain water-filled, but possibly isolated by grouted openings. The shape of any given displacement body is a random-dimensioned figure that we can define only in average terms. The conduits that extend beyond the design front will, in some cases, truncate paths of ground-water movement not otherwise intersepted, but the unsealed finer openings may leave other paths uninterrupted. It is suggested that 2 to 4 times the calculated grout volume be pumped in order to attain radii of 1.25 to 1.6 times the half-spacing between drill holes.

Unlimited improvisation is possible when anisotropy is properly determined. More efficient cut-off can be provided if it is known which joints are effective as conductors. For example, the Oroville system of three sets would conventionally be treated with vertical grout holes. Yet the evidence on Plate 26 suggests that set 2 is most significant. Since its members are near-vertical and trend up-and-down-stream, it is likely that many conduits will be missed by vertical holes. The most efficient orientation of holes would be inclined about 45° towards the west. Longer inclined holes would be required to attain design depth, but probably a lesser footage would suffice. In other circumstances, inclined curtains or novel patterns or allignments may be devised in accordance with the determined anisotropy, analysed by transformed models.

CONCLUSIONS AND RECOMMENDATIONS

There is a clear need for, and advantage in pursuing further this inquiry into the permeable properties of fractured media. Changes in the theory presented are expected upon refinement of the assumptions.

It is concluded that:

1. The laminar discharge of parallel-plate openings is proportional to the cube of aperture.
2. When roughness height exceeds the aperture, higher apparent friction must result from increased fluid-particle path lengths and decreased apertures between crystal faces inclined to the fracture plane.
3. Individual fine fractures are expected to have directional permeability, because surface textures reflect foliation of rock fabric.
4. The anisotropic permeability of intersecting aggregates of fine, rough fractures must differ from that computed as though the fractures were parallel plates.
5. When a medium contains both coarse and fine openings, it is only the coarse ones that influence anisotropy because of the discharge, aperture-cubed relationship.
6. If there is flow on each of two (or more) intersecting parallel-plate openings, there is a unique field gradient of hydraulic conductivity generally not lying in either plane, whose projectionson the planes cause the flow there and in the pores of an intergranular-conducting medium lying between the fractures.
7. One may sum the discharge components of intersecting fractures and the solid medium.
8. The discharge of a single parallel-plate opening can be expressed as a symmetric second-rank tensor, and if the conduit is

itself anisotropic, the tensor has two symmetric components.

9. The discharge of any aggregate of intersecting parallel-plate openings is a symmetric second-rank tensor.

10. A medium cut by parallel fractures has infinite anisotropy. The permeability parallel to the conductors is proportional to the average of cubes of apertures and inversely to the average spacing between conductors.

11. Specific surface serves to define the spacing of plane conductors dispersed in orientation.

12. The permeability of a dispersed set of plane conduits is a symmetric second-rank tensor, the contributing terms from each individual conduit weighted according to the inverse cosine of its inclination from the average direction.

13. If several sets of dispersed conductors exist, the frequency of each must be weighted according to ~~their~~ its specific surface and orientation dispersion.

14. The tensor-permeability of jointed, granular-porous media may be obtained by superposition of components due to the fractures and due to the permeable solids; i.e. primary and secondary permeability is cumulative if expressed tensorially.

The assumption that each parallel plate conduit is uniform over its infinite extent is obviously incorrect for real fractured media, and an assessment of the importance of discontinuties and aerial uniformity is needed. Models could be built to assess the influence of extent-to-spacing ratios, or to model fractures that "lens out." Conceivably a distribution of apertures, from one member to another, also may resemble a distribution of apertures over a single fracture area.

On the assumption of infinite uniformity it is found that:
1) The anisotropy of a single dispersed set has the symmetry of an oblate spheroid, flattening as fracture alignment improves,

and with a plane of isotropy parallel to the average conductor plane.

2) Two orthogonal sets of equal properties develop anisotropy with the symmetry of a prolate spheroid, with a maximum parallel to their intersection having twice the permeability on an isotropic plane normal to both sets.

3) Three equal, orthogonal sets form an isotropic medium.

4) Three unique principal axes occur in all cases of lower conduit-orientation symmetry, with the maximum along the most frequent direction of intersections, the least tending to lie normal to the set of greatest conductivity.

5) The principal axes of any arbitrary system of conductors can be approximated from inspection of a stereonet plot of normals.

Field pressure-test data cannot define the distribution of fracture apertures at any given site, but other lines of reasoning suggest that they must be skewed in shape. Direct aperture measurements, insitu, may be required eventually. The field data does indicate that:

1) The frequency of effective hydraulic conductors in undisturbed rock is much smaller than exposures of jointing would indicate, perhaps by a factor of 100.

2) The numbers of conductors per drill-hole length is distributed as a Poisson.

3) The expectation of the Poisson distribution at a site can be estimated from the proportion of zero-discharge pressure tests.

Current field practice does not produce measures of principal permeabilities, so a method has been devised, based on the finding that:

1) The discharge of a long cylindrical cavity is largely dependent upon the geometric mean of permeabilities normal to the

cylinder axis.

2) The three principal permeabilities can be deduced from apparent permeabilities obtained by pressure testing in three orthogonal drill-holes following principal axes.

While porosity would appear to be indeterminate if apertures cannot be assessed, an approximation assuming all apertures alike can be made from knowledge of measured principal permeabilities, frequencies and the dispersión of orientations. The model studies show that:

1) If porosity is calculated from each measure of principal permeabilities, the average is within 10 percent of the true porosity.

2) If porosity is computed from single values of principal permeabilities averaged from all measures, the error may be as much as 180 percent.

The properties of fractured media, and perhaps intergranular porous media as well, are more completely defined by numerous tests of small volumes, with statistical evaluation of results, than by single large-volume tests that average and conceal the variations.

BIBLIOGRAPHY

ABUZIED, M. 1960, FIELD METHOD OF MEASURING SOIL HYDRAULIC CONDUCTIVITY. UNPUBL. M.S. THESIS, UNIV. OF CALIF., DAVIS.

AITKEN, H. H., 1955, TABLES OF THE CUMULATIVE BINOMIAL PROBABILITY DISTRIBUTION. HARVARD UNIV. PRESS, 503 PP.

AITHCHISON,J. AND J.A. BROWN, 1957, THE LOG-NORMAL DISTRIBUTION, UNIVERSITY PRESS, CAMBRIDGE., 176 PP.

AMERICAN CYANAMID CO., UNDATED, AM-9 CHEMICAL GROUT, TECHNICAL DATA. BOUND BROOK, NEW JERSEY, 60 PP.

AMYX, J.W., D. M. BASS AND R. L. WHITING, 1960, PETROLEUM RESERVOIR ENGINEERING. MCGRAW-HILL BOOK CO., N. Y. 610 PP.

ANDERSON, A. T., 1954, DEVELOPMENT OF PETROLEUM RESERVOIRS IN FRACTURED ROCKS OF THE MONTEREY FORMATION, CALIFORNIA. UNPUBL. PH. D. THESIS, STANFORD UNIV., 108 PP., 28 PL., 2 MAPS.

ANDERSON, E. M., 1951, THE DYNAMICS OF FAULTING. OLIVER AND BOYD, EDINBURGH, 2ND ED. 206 PP.

ANDERSON, E.M. AND H. JEFFRIES, 1936, THE DYNAMICS OF THE FORMATION OF CONE-SHEETS, RING-DYKES AND CAULDRON SUBSIDENCE, WITH 'NOTE ON FRACTURE'. PROC. ROY. SOC., EDINBURGH, VOL. 56, NO. 2, PP. 128-163.

APPLEBY, A. N., 1940, JOINT PATTERNS IN HIGHLY FOLDED AND CRYSTALLINE ROCKS OF THE NEW JERSEY HIGHLANDS, BULL. GEOL. SOC. AMER.,VOL. 51.

ARNOLD, K. J., 1941, ON SPHERICAL PROBABILITY DISTRIBUTIONS. UNPUBL. PH.D. THESIS, MASS. INST. TECHN., CAMBRIDGE, MASS.

ARNOLD, M. D., H. J. GONZALES AND P.B. CRAWFORD, 1962, ESTIMATION OF RESERVOIR ANISOTROPY FROM PRODUCTIVE DATA. JOUR. PETROL. TECHN., AUGUST , PP. 909-912.

BARFIELD, E.C., J.K. GORDON, AND W.D. MOORE, 1959, AN ANALYSIS OF LARGE-SCALE FLOODING IN THE FRACTURED SPRABERRY TREND RESERVOIR. JOUR. PET. TECH. VOL. 11, NO. 4, P. 15.

BILLINGS, M. P., 1942, STRUCTURAL GEOLOGY. PRENTISS-HALL, INC., 473 PP.

BILLINGS, M. P., 1943, RING-DIKES AND THEIR ORIGIN. TRANS. NEW YORK ACAD. SCI., VOL. 5, NO. 6, PP. 131-144.

BORG, S. F., 19,3. MATRIX-TENSOR METHODS IN CONTINUUM MECHANICS. D. VAN NOSTRAND CO., NEW YORK, 313 PP.

BRACE, W. F., 1963, BRITTLE FRACTURE OF ROCKS. INT'L CONF. ON STATE OF STRESS IN THE EARTH'S CRUST, THE RAND CORP, SANTA MONICA, PP. 2-1 TO 2-1?3.

BROOKS, C. S., AND W. R. PURCELL, 1952, SURFACE AREA MEASUREMENTS ON SEDIMENTARY ROCKS. TRANS. AMER. INST. MIN. AND MET. ENG., VOL. 195,, PP. 289-296.

BRYAN, K., 1919, CLASSIFICATION OF SPRINGS. JOUR. GEOL., VOL. 27, PP. 322-561.

BURDINE, N. T., L. S. GOURNAY, AND P. P. REICHERTZ, 1950, PORE SIZE DISTRIBUTION OF PETROLEUM RESERVOIR ROCKS. TRANS. AMER. INST. MIN. AND MET. ENG., VOL. 189, PP.195-204.

BURWELL, E.B., AND B. C. MONEYMAKER, 1950, GEOLOGY IN DAM CONSTRUCTION, IN APPLICATION OF GEOLOGY TO ENGINEERING PRACTICE (BERKELEY VOL.), GEOL. SOC. AMER., PP. 11-43.

CALIFORNIA DEPT. OF WATER RESOURCES, 1959, PROCEDURES FOR ESTIMATING COSTS OF TUNNEL CONSTRUCTION. APP. C., BULL. 78, INVESTIGATION OF ALTERNATE AQUEDUCT SYSTEMS TO SERVE SO. CALIF., 73 PP.

CALIF. DEPT. OF WATER RESOURCES, 1962, ANNOTATED BIBLIOGRAPHY THROUGH 1961 ON METHODS OF DETERMINATION OF COEFFICIENTS OF TRANSMISSIBILITY AND STORAGE. UNPUBL. OFFICE REPT., SACRAMENTO, CALIF.

CALIF. DEPT. OF WATER RESOURCES, 1963, BASIC DATA COMPILATION FOR PENSTOCKS AND INTAKES, OROVILLE DAM-- GEOLOGIC EXPLORATION HOLES 218R-222R, FEB. 4.

CAMBEFORT,H.,1963, ETANCHEMENT ET CONSOLIDATION DES ROCHES. FELSMECHANIK UND INGENIEURGEOLOGIE, VOL. 1, NO. 2, PP. 134-151.

CARDWELL, W. T., AND R. L. PARSONS, 1945, AVERAGE PERMEABILITY OF HETEROGENEOUS OIL SANDS. TRANS. AMER. INST. MIN. AND MET. ENG., VOL. 160, PP. 34-42.

CARMAN, P.C., 1956, FLOW OF GASES THROUGH POROUS MEDIA. ACADEMIC PRESS, N. Y., 182 PP.

CARSLAW, H.S. AND J.C. JAEGER, 1959, CONDUCTION OF HEAT IN SOLIDS, CLARENDON PRESS, OXFORD, PP. 43-45.

CASAGRAND E, A., 1937, SEEPAGE THROUGH DAMS. NEW ENGLAND WATER WORKS ASSOC., VOL. 51, NO. 2, REPUBL. BY BOSTON SOC. CIV. ENG., CONTRIB. TO SOIL MECH., 1925-1940, PP. 295-336.

CASAGRANDE , A., 1961, CONTROL OF SEEPAGE THROUGH FOUNDATIONS AND ABUTMENTS OF DAMS . GEOTECHNIQUE, VOL. 11, NO. 3, PP. 161-181.

CAUGHRAN, J., 1963, PSEUDO-RANDOM NORMAL DEVIATE ROUTINE, GS BC DEV3, UNIV. CALIF. COMPUTER CENTER, BERKELEY.

CHIEN,C-H., 1952, RELAXATION TECHNIQUES FOR THREE-DIMENSIONAL FLOW NETS. TRANS. AMER. GEOPHYS. UNION, VOL. 33, NO. 1.

PP. 123-125.

CHILDS, E.C., AND N. C. GEORGE, 1948, INTERACTION OF WATER AND POROUS MATERIALS, SOIL GEOMETRY AND SOIL-WATER EQUILIBRIUM. DISCUSSIONS OF THE FARADAY SOC.,NO. 3, PP. 78-85.

CHILDS, E.C., AND N. C. GEORGE, 1950, THE PERMEABILITY OF POROUS MATERIALS, PROC. ROYAL SOC., LONDON, VOL. A, P. 201.

CHILDS, E.C., 1952, THE MEASUREMENT OF HYDRAULIC PERMEABILITY OF SATURATED SOIL IN SITU, I, PRINCIPLES OF A PROPOSED METHOD. PROC. ROYAL SOC. OF LONDON, VOL. 215, SEC. A., PP. 525-535.

CHILDS, E.C., 1957, THE PHYSICS OF LAND DRAINAGE, IN DRAINAGE OF AGRICULTURAL LANDS, J.N. LUTHIN, ED., AMER. SOC. AGRIC., MADISON, WISCONSIN, PP. 1-78.

CLEARY, J. M., 1959, HYDRAULIC FRACTURE THEORY, PARTS I, II AND III, CIRCULARS 251, 252, 281. ILLINOIS GEOLOGICAL SURVEY, URBANA, ILL.

COLEBROOK, C.F., 1939, TURBULENT FLOW IN PIPES, WITH PARTICULAR REFERENCE TO THE TRANSITION REGION BETWEEN THE SMOOTH AND ROUGH PIPE LAWS. JOUR. INST. CIV. ENG. , LONDON, FEB., P. 133.

COLLINS, R.E., 1961, FLOW OF FLUIDS THROUGH POROUS MATERIALS. REINHOLD PUBLISHING CO., N. Y., 270 PP.

CROW, E. L., AND R. S. GARDNER, 1959, CONFIDENCE INTERVALS FOR THE EXPECTATION OF A POISSON VARIABLE. BIOMETRIKA, VOL. 46, PP. 441-453.

CROSBY, W.O., 1881, ON THE ABSENCE OF JOINT STRUCTURE AT GREAT DEPTHS, AND ITS RELATIONS TO THE FORMS OF COARSELY CRYSTALLINE ERRUPTIVE MASSES. GEOL. MAG. (DECADE2), VOL. 8.

CROSBY, W.O., 1893, THE ORIGIN OF PARALLEL AND INTERSECTING JOINTS. AMER. GEOL., VOL. 12, PP. 368-375.

DACHLER,R., 1936, GRUNDWASSERSTRUMMUNGEN. SPRINGER, VIENNA.

DALE, T. N., AND H. E. GREGORY, 1911, THE GRANITES OF CONNECTICUT. U. S. GEOL. SURVEY BULL. 484, 137 PP.

DALE, T. N., AND H. E. GREGORY, 1923, THE COMMERCIAL GRANITES OF NEW ENGLAND. U. S. GEOL. SURVEY BULL. 738, 488 PP.

DANIEL, E. J., 1954, FRACTURED RESERVOIRS OF THE MIDDLE EAST. BULL. AMER. ASSOC. PETROL. GEOL., VOL. 38, PP. 774-815.

DAVIES, S. J., AND C. M. WHITE, 1928, AN EXPERIMANTAL STUDY OF THE FLOW OF WATER IN PIPES OF RECTANGULAR SECTION. PROC. ROY. SOC. LONDON, VOL. 119, SER. A., P. 92.

DAVIS, S. N., AND L. J. TURK, 1963A, SOME HYDROGEOLOGIC

CHARACTERISTICS OF CRYSTALLINE ROCKS. PRIVATE REPORT. HAZLETON NUCLEAR SCIENCE CORP., HNS-38.

DAVIS, S. N., 1963B, HYDROLOGIC AND GEOLOGICIC EVALUATION, NEVADA TEST SITE, INTERIM REPORT. HAZLETON NUCLEAR SCIENCE CORP., PALO ALTO, CALIF., 25 PP.

DAVIS, S. N., AND L. J. TURK, 1964, OPTIMUM DEPTH OF WELLS IN CRYSTALLINE ROCKS. GROUNDWATER, VOL. 2, NO. 2, PP. 6-11.

DE MELLO, V. F. B., 1960, SOME QUANTITATIVE INVESTIGATIONS ON CURTAIN GROUTING IN ROCK FOUNDATIONS OF EARTH DAMS . PROC. 1ST PAN-AM. CONF. ON SOIL MECH. AND FOUNDATION ENG.

DE SITTER, L. U., 1956, STRUCTURAL GEOLOGY. MCGRAW-HILL BOOK CO., NEW YORK, 552 PP.

DONN, W. L., 1958, GRAPHIC METHODS IN STRUCTURAL GEOLOGY. APPLETON-CENTURY CROFTS, 180 PP.

DRAKE, L. C., AND H. L. RITTER, 1945, MACROPORE-SIZE DISTRIBUTIONS IN SOME TYPICAL POROUS SUBSTANCES. IND. ENG. AND CHEM., ANAL. ED., VOL. 17, PP. 787-791.

DUHAMEL, J.M.C., 1832, SUR LES EQUATIONS GENERALES DE LA PROPAGATION DE LA CHALEUR DANS LE CORPS SOLIDES DONT LA CONDUCTABILITE N'EST PAS LA MEME DANS TOUS LES SENS. JOUR. ECOLE POLYT., PARIS, VOL. 13, BOOK 20, PP. 356-399.

DUSINBERRE, G.E., 1961, HEAT TRANSFER CALCULATIONS BY FINITE DIFFERENCES. INTERNATIONAL TEXTBOOK CO., SCRANTON, PA., 293 PP.

ELKINS, L. F. AND A. M. SKOV, 1960, ANISOTROPIC SPREAD OF PRESSURE TRANSIENTS DELINEATES SPRABERRY FRACTURE ORIENTATION. TRANS. AMER. INST. MIN. AND MET. ENG., VOL. 219, P. 407.

ELLIS, E.E., 1906, OCCURENCE OF WATER IN CRYSTALLINE ROCKS, IN UNDERGROUND WATER PAPERS. U.S. GEOL. SURVEY, W.S. PAPER 160, PP. 19-29.

ELLIS, E.E., 1909, GROUND WATER IN THE CRYSTALLINE ROCKS OF CONNECTICUTT. U.S. GEOL. SURVEY, W.S. PAPER 232, PP. 54-103.

ENGLEHARDT, W. VON, 1960, DER PORENRAUM DER SEDIMENTE. SPRINGER, BERLIN, 207 PP.

ESMIOL, E.E., 1957, SEEPAGE THROUGH FOUNDATIONS CONTAINING DISCONTINUITIES. JOUR. SOIL MECH. AND FOUND. ENG., AMER. SOC. CIV. ENG., VOL. 83, PROC. PAPER 1143, PP. 1-17.

EVANS, D. D., AND D. KIRKHAM, 1950, MEASUREMENT OF AIR PERMEABILITY OF SOIL IN SITU. SOIL SCI. SOC. AMER., PROC., VOL. 14, PP. 65-73.

FARMIN, R., 1937, HYPOGENE EXFOLIATION IN ROCK MASSES. JOUR. GEOL., VOL. 45, PP. 625-635.

FATT, I., 1952, STATISTICAL ANALYSIS OF QUANTITATIVE INTERPRETATION OF THE ELECTRIC LOG. UNPUBL. REPT., PROJ. 5215, CALIF. RESEARCH CORP., LA HABRA, NOV. 29, 6 PP., 14 FIGS.

FATT, I., 1956, THE NETWORK MODEL OF POROUS MEDIA. TRANS. AMER. INST. MIN. AND MET. ENG., VOL. 207, PARTS I,II, AND III, PP. 144-181.

FATT, I., 1961, INFLUENCE OF DEAD-END PORES ON RELATIVE PERMEABILITY OF POROUS MEDIA. SCIENCE, VOL. 134, PP. 1750-1751.

FELLER, W., 1960, AN INTRODUCTION TO PROBABILITY THEORY AND ITS APPLICATION, 2ND ED., VOL. I, JOHN WILEY AND SONS, NEW YORK, 461 PP.

FERRANDON, J., 1948, LES LOIS DE L'ECOULEMENT DE FILTRATION. GENIE CIVIL, VOL. 125, PP. 24-28.

FERRANDON, J., 1954, MECHANIQUE DES TERRAINS PERMEABLES. HOUILLE BLANCHE, VOL. 9, PP. 466-480.

FISHER, R. A., 1953, DISPERSION ON A SPHERE. PROC. ROYAL SOC., LONDON, SER. A., VOL. 217, PP. 295-306.

FORSCHEIMER, P., 1930, HYDRAULIK,3D. ED., TEUBNER, LEIOZIG AND BERLI

FOSTER, A.G., 1948, PORE SIZE AND PORE DISTRIBUTION. DISCUSSIONS OF THE FARADAY SOC., NO. 3, PP. 41-51.

FREVERT,R.K. AND D. KIRKHAM, 1948, A FIELD METHOD FOR MEASURING THE PERMEABILITY OF SOIL BELOW A WATER TABLE.PROC. HWY. RES. BD., VOL. 28, PP. 433-442.

FRYERS, F. J., ANC J. W. SHELDON, 1962, THE USE OF A HIGH-SPEED DIGITAL COMPUTER IN THE STUDY OF THE HYDRODYNAMICS OF GEOLOGIC BASINS,. JOUR. GEOPHYS. RES., VOL. 67, PP. 2421-2431.

GIEFER, G. J., 1963, WATER WELLS, AN ANNOTATED BIBLIOGRAPHY. WATER RES. CTR. ARCHIVES, UNIV. OF CALIF., BERKELEY, 141 PP.

GIGNOUX,M.AND R. BARBIER, 1955, GEOLOGIE DES BARRAGES ET DES AMENAGEMENTS HYDRAULIQUES. MASSON ET CIE., PARIS, 343 PP.

GILBERT, C.M., 1938, WELDED TUFF IN EASTERN CALIFORNIA. BULL. GEOL. SOC. AMER. , VOL. 49, PP. 1829-1861.

GILBERT, G. K., 1904, DOMES AND DOME STRUCTURE OF THE HIGH SIERRA. GEOL. SOC. AMER. BULL., VOL. 15, PP. 29-36.

GLOVER, R. E., 1953, FLOW FROM A TEST-HOLE LOCATED ABOVE GROUNDWATER LEVEL. IN ZANGAR, C. N., THEORY AND PROBLEMS OF WATER PERCOLATION, ENG. MONO. NO. 8, U.S. BUR. RECLAM., APP. B, PP. 69-71.

GOGUEL, J., 1945, SUR L'ORIGINE MECHANIQUE DE LA SCHIST-OSITE. BOL. SOC. GEOL. FRANCE, VOL. 5, NO. 15, PP. 519-522.

GOODMAN, R. E., 1963, THE RESOLUTION OF STRESSES IN ROCK USING STEREOGRAPHIC PROJECTION. INT. JOUR. ROCK MECH. MINING SCI., VOL. 1, PP. 93-103.

GOODMAN, R.E., D.G. MOYE, A. VAN SCHALKWYK AND I. JAVANDEL, 1964, GROUNDWATER INFLOWS DURING TUNNEL DRIVING. IN PRESS, THE ENGINEERING GEOLOGIST

GOSTOPTEKHIZAT LENIN, 1962, METODICHÉSKOE POSOBIE PO IZUCHENIYU TRESHCHINOVATOSTI GORNYKH POROD I TRESCHCHINNYCH KOMEKTOROV NEFTI I GAZA. VNIGRI VIPUSK 2.1.

GRANT, L. M., 1964, AN APPLICATION OF THE UNIT TAKE CONCEPT IN EVALUATING GROUT HOLE DRILLING METHODS. IN PRESS, THE ENGINEERING GEOLOGIST.

GREENWOOD, J. A., AND D. DURAND, 1955A, THE DISTRIBUTION OF LENGTHS AND COMPONENTS OF THE SUM OF N RANDOM UNIT VECTORS. ANN. MATH. STAT., VOL. 26, NO. 2, PP. 233-246.

GREENWOOD, J. A., AND D. DURAND, 1955B, APPROXIMATION TO THE DISTRIBUTION OF THE SUM OF COSINES OF RANDOM ANGLES.PRELIMINARY REPORT READ AT INST. OF MATH., STAT., ANN ARBOR, MICH., SEPT. 1.

GRIFFITH, A.A., 1921, PHENOMENA OF RUPTURE AND FLOW IN SOLIDS. PHILOSOPHICAL TRANS., ROYAL SOC. LONDON, SER. A., VOL. 221, P. 163.

GRIGGS, D.T., 1936, DEFORMATION OF ROCKS UNDER HIGH CON-FINING PRESSURE. JOUR. GEOL., VOL. 44, PP. 541-577.

HADDOCK, M.H., 1931, DEEP BORE HOLE SURVEYS AND PROBLEMS. MCGRAW-HILL BOOK CO., NEW YORK

HALL, W. A., 1956, AN ANALYTICAL DERIVATION OF THE DARCY ECUATION. TRANS. AMER. GEOPHYS. UNION, VOL. 37, NO. 2, PP. 185-188.

HANNA, M. A., 1934, GEOLOGY OF THE GULF COAST SALT DOMES. IN PROBLEMS OF PETR. GEOL., AMER. ASSOC. PET. GEOL., TULSA, OKLA., PP. 629-678.

HANSEN, V.E., 1952, COMPLICATED WELL PROBLEMS SOLVED BY THE MEMBRANE ANALOGY. TRANS. AMER. GEOPHYS. UNION, VOL. 33, PP.912-916

HAPPEL, J., 1959, DISCUSSION OF A PAPER BY S. IRMAY. JOUR. GEOPHYS. RES., VOL. 64, NO. 4, PP.

HELE-SHAW, H.S., 1898, INVESTIGATION OF THE NATURE OF SURFACE RESISTANCE OF WATER AND OF STREAMLINE MOTION UNDER CERTAIN EXPERIMENTAL CONDITIONS. TRANS. INST. NAVAL ARCHITECTS, VOL. 40, PP. 21-46.

HILDEBRAND, F. B., 1956, INTRODUCTION TO NUMERICAL ANALYSIS. MCGRAW-HILL BOOK CO., NEW YORK, 511 PP.

HODGSON, R. A., 1961A, CLASSIFICATION OF STRUCTURES ON JOINT SURFACES. AMER. JOUR. SCI., VOL. 259, PP. 493-502.

HODGSON, R. A., 1961B, REGIONAL STUDY OF JOINTING IN COMB RIDGE, NAVAJO MOUNTAIN AREA, ARIZONA AND UTAH. AMER. ASSOC. PETROL. GEOL. BULL., VOL. 45, PP. 1-38.

HOEL, P. G., 1947, AN INTRODUCTION TO MATHEMATICAL STATISTICS. JOHN WILEY AND SONS, NEW YORK, 331 PP.

HOLMES, C. D., 1963, TIDAL STRAIN AS A POSSIBLE CAUSE OF MICROSEIMS AND ROCK JOINTING. BULL. GEOL. SOC. AMER., VOL. 74, PP. 1411-1412.

HOWELL, J.V., 1960, GLOSSARY OF GEOLOGY AND RELATED SCIENCES, AMER. GEOL. INST., WASHINGTON, D.C., 72 PP.

HUITT, J.L., 1956, FLUID FLOW IN SIMULATED FRACTURES. JOUR. AICHE, VOL. 2, P. 259.

HUBBERT, M. K., 1956, DARCY'S LAW AND THE FIELD EQUATIONS OF THE FLOW OF UNDERGROUND FLUIDS. TRANS. AMER. INST. MIN. MET. AND PETROL. ENG. , VOL. 207, PP. 222-239.

HUBBERT, M. K., AND D. G. WILLIS, 1957, MECHANICS OF HYDRAULIC FRACTURING. TRANS. AMER. INST. MIN. MET. AND PETROL. ENG., VOL. 210, PP. 153-

HUBBERT, M. K., AND W. W. RUBY, 1959, ROLE OF FLUID PRESSURE IN MECHANICS OF OVERTHRUST FAULTING. GEOL. SOC. AMER. BULL., VOL. 70, PP. 115-166.

HVORSLEV, M. J., 1951, TIME LAG AND SOIL PERMEABILITY IN GROUND-WATER OBSERVATIONS. BULL. 36, WATERWAYS EXPER. STA., CORPS ENG. U. S. ARMY, VICKSBURG, MISS.

IRMAY, S., 1958, ON THE THEORETICAL DERIVATION OF DARCY AND FORSCHIMER FORMULAS, TRANS. AMER. GEOPHYS. UNION, VOL. 39, NO. 4., PP.

JAEGER, J. C., 1961, ROCK MECHANICS FOR HYDROPOWER ENGINEERING. WATER POWER, SEPT-OCT., PP.

JAHNS, R. H., 1943, SHEET STRUCTURE IN GRANITE, ITS ORIGIN AND USES AS A MEASURE OF GLACIAL EROSION IN NEW ENGLAND. JOUR. GEOL., VOL. 51, NO. 2, PP. 71-98.

JEFFRIES, H. AND B.S. JEFFRIES, 1956, METHODS OF NUMERICAL PHYSICS. CAMBRIDGE UNIV. PRESS, 679 PP.

JOHN, K.W., 1962, AN APPROACH TO ROCK MECHANICS. JOUR. SOIL MECH. AND FOUND. ENG., AMER. SOC. CIV. ENG., VOL. 88, PT. I, PP. 1-30.

JOHNSON, E.E., 1947, GROUND WATER. H.M. SMYTH PRINTING CO, MINNESOTA, 509 PP.

JOHNSON, W. E., AND R. V. HUGHES, 1948, DIRECTIONAL PERMEABILITY MEASUREMENTS AND THEIR SIGNIFICANCE. PRODUCER'S MONTHLY, VOL. 13, PP. 17-25.

JOHNSON, W. E., AND J. N. BRESTON, 1951, DIRECTIONAL PERMEABILITY MEASUREMENTS ON OIL SANDSTONES FROM VARIOUS STATES. PRODUCERS MONTHLY, VOL. 14, PP. 10-19.

JOHNSTON, W. D., AND E. CLOOS, 1934, STRUCTURAL HISTORY OF THE FRACTURE SYSTEMS AT GRASS VALLEY, CALIFORNIA. EC. GEOL., VOL. 29, PP. 39-54.

JONES, P.H., 1963, THE VELOCITY OF GROUNDWATER FLOW IN BASALT AQUIFERS OF THE SNAKE RIVER PLAIN, IDAHO. ABSTR. IN PROC. INT'L UNION GEOD. AND GEOPHYS., BERKELEY, CALIF, VOL. VIII, P. 140.

KING, P. B., 1948, GEOLOGY OF THE SOUTHERN GUADALUPE MOUNTAINS, TEXAS. U. S. GEOL. SURVEY PROF. PAPER NO. 215.

KIRKHAM, D., 1945, ARTIFICIAL DRAINAGE OF LAND. STREAMLINE EXPERIMENTS, THE ARTESIAN BASIN, III. TRANS. AMER. GEOPHYS. UN., VOL. 26, PP. 393-406.

KRASNOW, E., 1960, FORTRAN PROGRAM TO GENERATE PSEUDO INTEGERS IN RANDOM SEQUENCE, SHARE LISTING GS BC RANDY, COMPUTER CENTER, BERKELEY, 4 PP.

KRAUSSE, H. F. AND G. LUHRS, 1962, VORLAUFIGE MITTEILUNG UBER STATISCHE AUSWERTUNG VON GEFUGEDATEN MIT HILFE ELEKTRONISCHE RECHELANLAGEN. BERGBAUWISSENSCHAFTEN, HEFT 8, S. 190-194.

KRUMBEIN, W. C., 1954, APPLICATION OF STATISTICAL METHODS TO SEDIMENTARY ROCKS. JOUR. AMER. STAT. ASSOC., VOL. 49, PP. 51-66.

KRYNINE, D.P., AND W. R. JUDD, 1957, PRINCIPLES OF ENGINEERING GEOLOGY AND GEOTECNICS . MCGRAW-HILL BOOK CO., NEW YORK, 728 PP.

KWANTES, IN SAX, H. G., 1946, THE TECTONICS OF THE SOUTH LIMBURG COAL FIELD (ABRIDGED TRANSLATION). MED. GEOL. STICHTING (CI-1), VOL. 3.

LACHENBRUCH, A. H., 1961, DEPTH AND SPACING OF TENSION CRACKS. JOUR. GEOPHYS.RES., VOL. 66, NO. 12, PP. 4273-4292.

LAMB, H., 1932, HYDRODYNAMICS, SIXTH ED., CAMBRIDGE UNIV. PRESS, 738 PP.

LAMBE, T.W., 1957, CHEMICAL GROUTING, TASK COMMITTEE ON CHEMICAL GROUTING. JOUR. SOIL MECH. AND FOUNDATION ENG., AMER. SOC. CIVIL ENG., PAPER 1426, 106 PP.

LANDRUM, B. L. AND P. B. CRAWFORD, 1960, EFFECT OF DIRECTIONAL PERMEABILITY ON SWEEP EFFICIENCY AND PRODUCTION CAPACITY. TRANS. AMER. INST. MIN. AND MET. ENG., VOL. 219, P. 301.

LAW , J., 1944, STATISTICAL APPROACH TO THE INTERSTITIAL HETEROGENEITY OF SAND RESERVOIRS. TRANS. AMER. INST. OF MIN. AND MET. ENG. VOL. 155, P. 202.

LEE, D.B., 1948, POTENTIOMETRIC MODEL STUDIES OF FLUID FLOW IN PETROLEUM RESERVOIRS. TRANS. AMER. INST. MIN. AND MET. ENG. VOL. 174, PP. 41-66.

LEEMAN, E. R., 1958, SOME UNDERGROUND OBSERVATIONS RELATING TO THE EXTENT OF THE FRACTURE ZONE AROUND EXCAVATIONS IN SOME CENTRAL RAND MINES. ASSOC. OF MINE MANAGERS, PP. 357-384.

LEGGETT, R. F., 1962, GEOLOGY AND ENGINEERING. MCGRAW-HILL BOOK CO., NEW YORK, 2ND ED., 884 PP.

LE GRAND, H.E., 1949, SHEET STRUCTURE, A MAJOR FACTOR IN THE OCCURRENCE OF GROUND WATER IN THE GRANITES OF GEORGIA. EC. GEOL., VOL. 44, NO. 2, PP. 110-118.

LEWIS, D. C., AND R. H. BURGY, 1964, HYDRAULIC CHARACTERISTICS OF FRACTURED AND JOINTED ROCK. GROUND WATER, VOL. 2, NO. 3, PP. 4-9.

LINKWITZ,K., 1963, TERRESTRISCH-PHOTOGRAMMETRISCHE KLUFTMESSUNG. FELSMECHANIK UND INGENIEURGEOLOGIE, VOL. 1, NO. 2, PP. 152-159.

LONG, R. R., 1961, MECHANICS OF SOLIDS AND FLUIDS. PRENTISS-HALL, ENGLEWOOD CLIFFS, N. J., 156 PP.

LOUDERBACK, G. D., 1950, FAULTS AND ENGINEERING GEOLOGY, IN APPLICATION OF GEOLOGY TO ENGINEERING PRACTICE (BERKELEY VOL.), GEOL. SOC. AMER., PP. 125-150.

LUTCH, N.AND M. E. SZENDREI, 1958, THE EXPERIMENTAL DETERMINATION OF THE EXTENT AND DEGREE OF FRACTURE OF A ROCK FACE BY MEANS OF SONIC AND ULTRASONIC METHODS. THE ASSOC. OF MINE MANAGERS, SO. AFRICA, PP. 465-489.

LUTHIN, J. N., 1961, METHOD OF MEASURING SOIL HYDRAULIC CONDUCTIVITY IN SITU. NATURE, VOL. 192, PP. 383-384.

LUTHIN, J. N., AND D. KIRKHAM, 1949, A PIEZOMETRIC METHOD FOR MEASURING PERMEABILITY OF SOIL IN SITU BELOW A WATER TABLE. SOIL SCI., VOL. 68, PP. 349-358.

LYONS, M. S., 1960, PHASE IV, BASIC DATA COMPILATION, JOINT STUDY, UNDERGROUND POWER PLANT, OROVILLE DAM SITE. CALIF. DEPT. OF WATER RESOURCES, UNPUBLISHED REPT., 3 PP.,14 FIG.

MAASLAND, M., 1957, SOIL ANISOTROPY AND LAND DRAINAGE, IN DRAINAGE OF AGRICULTURAL LANDS ,J. N. LUTHIN, ED.. AMER. SOC. AGRONOMY,MADISON, WIS., PP. 216-285.

MAASLAND, M., AND D. KIRKHAM, 1955,. THEORY AND MEASUREMENT OF ANISOTROPIC AIR PERMEABILITY IN SOIL. PROC. SOIL SCI. SOC. AMER., PP. 395-400.

MARCUS, H. AND D.E. EVANSON, 1961, DIRECTIONAL PERMEABILITY IN ANISOTROPIC MEDIA. HYD. LAB., UNIV. CALIF., BERKELEY, WATER RESOURCES CENTER CONTRIB. NO. 31, 105 PP.

MARCUS, H., 1962, THE PERMEABILITY OF A SAMPLE OF AN ANISOTROPIC MEDIUM. JOUR. GEOPHYS. RES., VOL. 67, NO. 13, PP. 5215-5225.

MATTHES, F. E., 1930, GEOLOGIC HISTORY OF THE YOSEMITE VALLEY. U. S. GEOL. SURVEY, PROF. PAPER 160, 137 PP.

MEINZER, O.E., 1923, THE OCCURRENCE OF GROUND WATER IN THE US.. U.S. GEOL. SURVEY, W.S. PAPER 489, PP. 180-188.

MEINZER, O.E., 1927, LARGE SPRINGS IN THE US. U.S. GEOL. SURVEY W.S. PAPER 557, 94 PP.

MCKINSTRY, H. E., 1948, MINING GEOLOGY. PRENTISS-HALL, INC., NEW YORK, PP. 520-523.

MELTON, F. A., 1929, A RECONNAISSANCE OF THE JOINT SYSTEMS IN THE OUACHITA MOUNTAINS AND CENTRAL PLAINS OF OKLAHOMA. JOUR. GEOL., VOLS. 37-38, PP. 729-746.

MERWIN, M., 1959, 704 FORTRAN II SUBPROGRAM FOR MATRIX DIAGONALIZATION. MIT COMPUTATION CENTER AND SHARE LISTING F2 MI HDI3, 2PP., 186 SOURCE CARDS.

MEYER, H. A., ED., 1956, SYMPOSIUM ON MONTE-CARLO METHODS. JOHN WILEY AND SONS, NEW YORK, 382 PP.

MIKKO, S. M., 1956, STUDIES OF THE HYDRAULIC CONDUCTIVITY OF SOILS AND ITS MEASUREMENT.(CITED BY ABUZIED, INCOMPLETE REF.)

MILLER, E. E., AND R. D. MILLER, 1956, PHYSICAL THEORY FOR CAPILLARY FLOW PHENOMENA. JOUR. APPLIED PHYS. VOL. 27, NO. 4, PP. 324-332.

MOOD, A. M., AND F. A. GRAYBILL, 1963, INTRODUCTION TO THE THEORY OF STATISTICS. MCGRAW-HILL BOOK CO., 2ND ED., NEW YORK, 443 PP.

MOODY, J. D., AND M. J. HILL, 1956, WRENCH-FAULT TECTONICS. BULL. GEOL. SOC. AMER., VOL. 67, PP. 1207-1246.

MOYE, D. G., 1959, ROCK MECHANICS IN THE INVESTIGATION AND CONSTRUCTION OF T.1 UNDERGROUND POWER STATION, SNOWY MOUNTAINS, AUSTRALIA. CASE HIST. IN ENG. GEOL., GEOL. SOC. AMER., VOL. 3, PP. 13-44.

MULLER,L., 1933, UNTERSUCHEN UBER STATISTISCHE KLUFTMESSUNG. GEOL. UND BAU., JAHRG. 5, HEFT. 1, S.

MULLER, L.,1960, DER EINFLUSS DES BERGWASSERS AUF DIE

STANDFESTIGKEIT DER FELSWIDERLAGER VON TALSPERREN. OESTERREICHISCHE WASSERWIRTSCHAFT, HEFT. 8,Z. 9.

MULLER , L., AND J. W. KLAUS, 1963, RECENT DEVELOPMENT OF STABILITY STUDIES OF STEEP ROCK SLOPES IN EUROPE, TRANS. AMER. INST. MIN. AND MET. ENG., PREPRINT NO. 63A044.

MUSKAT, M., 1937, THE FLOW OF HOMOGENEOUS FLUIDS THROUGH POROUS MEDIA. MCGRAW-HILL, NEW YORK, REPRINTED 1946, J.W. EDWARDS CO., ANN ARBOR, MICH.

MUSKAT, M., 1948, EFFECT OF PERMEABILITY STRATIFICATION IN CYCLING OPERATIONS. TRANS. AMER. INST. OF MIN. AND MET. ENG., VOL. 160, P. 34.

MUSKAT, M., 1949, PHYSICAL PRINCIPLES OF OIL PRODUCTION. MCGRAW-HILL BOOK CO., 922 PP.

NEWHOUSE, W. H., ED., 1942, ORE DEPOSITS AS RELATED TO STRUCTURAL FEATURES. PRINCETON UNIV. PRESS, PRINCETON, N. J., 280 PP.

NEW JERSEY (DATE UNKNOWN), OCCURRENCE OF WATER IN THE TRIASSIC.... NEW JERSEY DIV. WATER POLICY AND SUPPLY, BULL. 10.

NIKURADSE, J., 1940, STROMMUNGSGESETZE IN RAUEN ROHREN. TRANSLATION IN PETROL. ENG. VOL. 11, NO. 6, P. 164.

OPSAL,F.W., 1955, ANALYSIS OF TWO- AND THREE-DIMENSIONAL GROUND WATER FLOW BY ELASTICITY ANALOGY. THE TREND IN ENGINEERING AT THE UNIV. OF WASH., VOL. 7, NO. 2, PP. 15-20.

OSBORNE, E. F., AND G. K. LOWTHER, 1936, PETROTECTONICS AT SHAWINIGAN FALLS. GEOL. SOC. AMER. BULL., VOL. 47, PP. 1343-1370.

PAGE, F., W.H. CORCORAN, W.G. SCHLINGER AND B.H. SAGE, 1952, IND. ENG. CHEM., VOL. 44, P. 419.

PARKER, J. M., 1942, REGIONAL SYSTEMATIC JOINTING IN SLIGHTLY DEFORMED SEDIMENTARY ROCKS. GEOL. SOC. AMER. BULL.,VOL. 53, PP. 381-408.

PARZEN, E., 1960, MODERN PROBABILITY THEORY AND ITS APPLICATIONS. JOHN WILEY AND SONS, NEW YORK, 464 PP.

PERKINS, T. K., AND L. R. KERN, 1961, WIDTHS OF HYDRAULIC FRACTURES. JOUR. PET. TECH., SEPT., PP. 937-949.

PERRY, J. H.,ED., 1950, CHEM. ENG. HANDBOOK, 3D. ED.. MCGRAW-HILL BOOK CO., NEW YORK, P. 378.

PINCUS, H. J., 1951, STATISTICAL METHODS APPLIED TO THE STUDY OF ROCK FRACTURES. BULL. GEOL. SOC. AMER., VOL. 62, PP. 81-130.

PINCUS, H. J., 1953, THE ANALYSIS OF AGGREGATES OF ORIENTATION DATA IN THE EARTH SCIENCES. JOUR. GEOL., VOL. 61, NO. 6, PP. 482-509.

PINCUS, H. J., 1956, SOME VECTORIAL AND ARITHMETIC OPERATIONS ON TWO-DIMENSIONAL ORIENTATIONAL VARIANTS, WITH APPLICATION TO GEOLOGICAL DATA. JOUR. GEOL., VOL. 64, PP. 535-57

PLAFKER, G., 1964,ORIENTED LAKES AND LINEAMENTS OF NORTHEASTERN BOLIVIA.BULL. GEOL. SOC. AMER., VOL. 75, NO. 6, PP.503-522.

POLUBARINOVA-KOCHINA, P. YA, 1962,THEORY OF GROUND WATER MOVEMENT. TRANS. BY J.M.R. DEWIEST, PRINCETON UNIV. PRESS, PRINCETON, N.J., 613 PP.

PRICE, N.J., 1959, MECHANICS OF JOINTING IN ROCKS. GEOL. MAG., VOL. 96, PP. 149-167.

PURCELL, W. R., 1949, CAPILLARY PRESSURES-THEIR MEASUREMENT USING MERCURY AND THE CALCULATION OF PERMEABILITY THEREFROM. TRANS. AMER. INST. MIN. AND MET. ENG., VOL. 186, PP. 39-45.

RAGGATT, H.G., 1954, MARKINGS ON JOINT SURFACES IN ANGELSEA MEMBERS OF DEMON'S BLUFF FORMATION, ANGELSEA, VICTORIA. AMER. ASSOC. PETROL. GEOL. BULL., VOL. 38, PP. 1808-1810.

REEVE, R.C. AND J.N. LUTHIN, 1957, METHODS OF MEASURING SOIL PERMEABILITY, IN DRAINAGE OF AGRICULTURAL LANDS. J.N. LUTHIN, ED. AMER. SOC. AGRONOMY, MADISON, WISC., PP. 395-445.

REYNOLDS, O., 1883,AN EXPERIMENTAL INVESTIGATION OF THE CIRCUMSTANCES WHICH DETERMINE WHETHER THE MOTION OF WATER WILL BE DIRECT OR SINUOUS, AND THE LAW OF RESISTANCE IN PARALLEL CHANNELS. PHIL. TRANS. ROY. SOC. , LONDON

RICHARDS, L. A., 1952,REPORT OF THE SUB-COMMITTEE ON PERMEABILITY AND INFILTRATION, COMMITTEE ON TERMINOLOGY. PROC. SOIL SCI. SOC. AMER., VOL. 16, PP. 85-88.

RICHARDSON, H. W., AND R. S. MAYO, 1941, PRACTICAL TUNNEL DRIVING. MCGRAW-HILL BOOK CO., NEW YORK, 436 PP.

RICHARDSON, J. T., 1948, SUMMARY OF UPLIFT PRESSURES AT BUREAU OF RECLAMATION DAMS. U.S. BUR. OF RECLAM. TECHN. MEMO. 636, P. 16.

RICHEY, J. E., 1963, GRANITE, PARTS III,IV,V,VI. WATER POWER, PP. 326-332, 378-382, 409-422, 475-481.

RIES, H., AND T. L. WATSON, 1947, ELEMENTS OF ENGINEERING GEOLOGY. JOHN WILEY AND SONS, NEW YORK, 2ND ED. 469 PP.

RITTER, H. L., AND L. C. DRAKE, 1945, PORE-SIZE DISTRIBUTION IN POROUS MATERIALS. IND. ENG. AND CHEM. , ANAL. ED. , VOL. 17, PP. 782-786.

RIVERA, R. A., 1964,FAULTS AS POSSIBLE SUPPLIERS OF GROUND WATER. UNPUBL. REPORT, MINERAL ENG. 299, UNIV. OF CALIF., BERKELEY

ROBERTS, J.C., 1961, FEATHER FRACTURE AND THE MECHANICS OF ROCK JOINTING. AMER. JOUR. SCI., VOL. 259, PP. 481-492.

ROEDDER, E., 1962, ANCIENT FLUIDS IN CRYSTALS. SCIENTIFIC AMERICAN, OCTOBER, PP. 2-11.

ROTHFUS, R. R., D. H. ARCHER, I. C. KLIMAS, K. G. SIKCHI, 1957, SIMPLIFIED FLOW CALCULATIONS FOR TUBES AND PARALLEL PLATES, AICHE JOUR., VOL. 3, P. 2?8.

ROWE, R.I., 1943, FAULTS AS A SOURCE OF WATER SUPPLY. BS THESIS IN IRRIG., UNIV. CALIF., BERKELEY.

SAMSIOE, A. E., 1931, EINFLUSS VON ROHRBRUNNEN AUF DIE BEWEGUNG DES GRUNDWASSERS. ZEITSCH. ANGEW. MATH. UND MECH., HEFT. 11, S. 124-135.

SANBORN, J. F., 1950,ENGINEERING GEOLOGY IN THE DESIGN AND CONSTRUCTION OF TUNNELS, IN APPLICATION OF GEOLOGY TO ENGINEERING PRACTICE, (BERKELEY VOL), GEOL. SOC. AMER., PP. 45-82.

SANDER, B., 1948, EINFUHRUNG IN DIE GEFUGEKUNDE DER GEOLOGISCHEN KORPER, ERSTE TEIL. ALLGEMAINE GEFUGEKUNDE UND ARBEITEN IM BEREICH HANDSTUCK BIS PROFIL. SPRINGER-VERLAG, WEIN UND INNSBRUCH, AUSTRIA

SAVAGE, J. C. AND H. S. HASEGAWA, 1964, SOME PROPERTIES OF TENSILE FRACTURES INFERRED FROM ELASTIC WAVE RADIATION. JOUR. GEOPHYS. RES., VOL. 69, NO. 10, PP. 2091-2100.

SCHEIDEGGER, A. E., 1954, DIRECTIONAL PERMEABILITY OF POROUS MEDIA TO HOMOGENEOUS FLUIDS. GEOFISICA PURA E APPLICATA, MILAN, , VOL. 30, PP. 17-26.

SCHEIDEGGER, H. E., 1958, PRINCIPLES OF GEODYNAMICS. SPRINGER-VERLAG, BERLIN, 280 PP.

SCHEIDEGGER, A. E., 1960,THE PHYSICS OF FLOW THROUGH POROUS MEDIA. THE MACMILLAN CO., NEW YORK, 313 PP.

SHELDON, P. O., 1912, SOME OBSERVATIONS AND EXPERIMENTS ON JOINT PLANES. JOUR. GEOL., VOL. 20, PP. 64-190.

SCHENCK,H.J., 1963, FORTRAN METHODS IN HEAT FLOW. THE RONALD PRESS CO., NEW YORK, 289 PP.

SIEGEL, H. O., 1950,A THEORY OF FRACTURE OF MATERIALS AND ITS APPLICATION TO GEOLOGY. AMER. GEOPHYS. UNION, TRANS., VOL. 31, PP. 611-619.

SIPLE, G.E., 1946, PROGRESS REPORT ON GROUND WATER INVESTIGATIONS IN SOUTH CAROLINA. SOIL CONS. RES., PLANNING AND DEV. BD., STATE OF SO. CAROLINA, BULL. 15, 116 PP.

SMITH, B.L., 1962, GEOLOGY OF THE JERSEY CENTRAL POWER AND LIGHT COMPANY YARD CREEK STORAGE PROJECT, NORTHERN NEW JERSEY. ABSTR. IN

GEOL. SOC. AMER. BULL., NOV. 14.

SMITH, J. D., 1958, PRODUCTION AND UTILIZATION OF GEOTHERMAL STEAM. PAPER PRESENTED TO WELLINGTON BR., NEW ZEALAND INST. OF ENG., APRIL 10, 24 PP., 4 TABLES, 14 FIG.

SMYTHE, W. R., 1939, STATIC AND DYNAMIC ELECTRICITY. MCGRAW-HILL BOOK CO., NEW YORK, 2ND. ED. PP.

SNOW, D.T., 1964, STEADY FLOW FROM CYLINDRICAL CAVITIES IN SATURATED, INFINITE ANISOTROPIC MEDIA. IN PRESS, THE ENGINEERING GEOLOGIST, 28 PP.

SOMMERFELD , A., 1947, MECHANICS OF DEFORMABLE BODIES, TRANSLATED FROM 2ND ED. BY G. KUERTI. ACADEMIC PRESS, NEW YORK, 396 PP.

SPENCER, E. W., 1959, FRACTURE PATTERNS IN THE BEARTOOTH MOUNTAINS, MONTANA AND WYOMING. GEOL. SOC. AMER. BULL., VOL. 70, NO.4, PP. 467-508.

STEWART, J. W., 1962, WATER-YIELDING POTENTIAL OF WEATHERED CRYSTALLINE ROCKS AT THE GEORGIA NUCLEAR LABORATORY. U. S. GEOL. SURVEY PROF. PAPER 450-B.

STINI, J., 1950, TUNNELBAUGEOLOGIE. SPRINGER, VIENNA, 366 PP.

STUART, W. T., 1955, PUMPING TEST EVALUATES WATER PROBLEM AT EUREKA, NEV.. MIN. ENG., VOL. 7, NO. 2, PP. 148-156.

TALOBRE, J., 1957, LA MECHANIQUE DES ROCHES. DUNOD, PARIS, 444 PP.

TAUSSKY, O., AND J. TODD, 1956, GENERATION OF PSEUDO-RANDOM NUMBERS, IN MEYER, SYMPOSIUM ON MONTE-CARLO METHODS. JOHN WILEY AND SONS, INC., NEW YORK.

TERZAGHI, K., 1925, ERDBAUMECHANIK AUF BODENPHYSICALISCHER GRUNDLAGE. DEUTECKE, LEIPZIG.

TERZAGHI, K., 1929, THE EFFECT OF MINOR GEOLOGIC DETAILS ON THE SAFETY OF DAMS. AMER. INST. OF MIN. AND MET. ENG., TECH. PUB. 215, PP.

TERZAGHI, K., 1946, ROCK DEFECTS AND LOADS ON TUNNEL SUPPORTS, IN ROCK TUNNELING WITH STEEL SUPPORTS. COMMERICAL SHEARING AND STAMPING CO., YOUNGSTOWN, OHIO, PP. 3-42.

TERZAGHI, K. AND R. PECK, 1961, SOIL MECHANICS AND ENGINEERING PRACTICE., JOHN WILEY AND SONS, NEW YORK, 566 PP.

TERZAGHI, K., 1962, DOES DAM FOUNDATION ENGINEERING REALLY LAG.. ENG. NEWS-RECORD, FEB. 15, P. 58.

TERZAGHI, K., 1962, DAM FOUNDATION ON SHEETED GRANITE. GEOTECHNIQUE, VOL. 12, NO. 3, PP. 199-208.

THAYER, D. P., 1962, INTERIM REPORT, PERMEABILITY STUDY, UNDERGROUND POWER PLANT, OROVILLE DAM. CALIF. DEPT. OF WATER RESOURCES, UNPUBLISHED REPORT, 14 P., 17 FIG. AND TABLES.

THROWER, P.H., 1963, 7090 FORTRAN II PLOT ROUTINE J6 BC XYP2, UNIV. CALIF., BERKELEY, 12 PP.

TODD, D.K., 1954, UNSTEADY FLOW IN POROUS MEDIA BY MEANS OF A HELE-SHAW VISCOUS FLUID MODEL. TRANS. AMER. GEOPHYS. UNION, VOL. 35, PP. 905-916.

TODD, D.K., 1959, GROUNDWATER HYDROLOGY, JOHN WILEY AND SONS, NEW YORK, 336 PP.

TOLMAN, C. F., 1937, GROUND WATER. MCGRAW-HILL BOOK CO., NEW YORK, 593 PP.

TOWNSEND, J. R., 1963. GROUND WATER DEVELOPMENT BY HORIZONTAL DRILLING. CALIF. ASSOC. OF ENG. GEOL., 5TH ANN. MEETING, 1962, PP. 46-51C.

TURK, J. L., 1963, THE OCCURRENCE OF GROUND WATER IN CRYSTALLINE ROCKS. STANFORD UNIV., UNPUBL. M. S. REPT., 42 PP., 26 TABLES.

TWELKER, N. H., 1958, INVESTIGATION OF SEEPAGE IN PERVIOUS ABUTMENTS OF DAMS. UNPUB. PH.D. THESIS, HARVARD UNIV.,   PP.

U. S. NAT. BUR. STANDARDS, 1951, MONTE CARLO METHOD. APPLIED MATH. SER. 12, U. S. GOVT. PRINTING OFF., WASH. D. C., 42 PP.

VERSLUYS, J., 1915, DE ONBEPAALDE VERGELIJKING DER PERMANENTE BEWEGING VAN HET GRONDWATER. VERK. GEOL.-MIJNBOUW. GENOOT. NED. EN KOLONIEN. GEOL. SERIE 1 S. 349-360.

VERSTEEG, K., 1942, JOINTING IN THE CENTRAL COAL BEDS OF OHIO. ECON. GEOL., VOL. 37, P. 305.

VERSTEEG, K., 1944, SOME STRUCTURAL FEATURES OF OHIO. JOUR. GEOL., VOL. 52, PP. 131-138.

VON ENGELN, O. D., 1961, THE FINGER LAKES REGION, ITS ORIGIN AND NATURE. CORNELL UNIV. PRESS, ITHACA, NEW YORK, 156 PP.

VREEDENBURGH, C. G. F., 1936, ON THE STEADY FLOW OF WATER PERCOLATING THROUGH SOILS WITH HOMOGENEOUS-ANISOTROPIC PERMEABILITY. PROC. INTN'L. CONF. SOIL MECH. AND FOUNDATION ENG. PP.222-225.

WAGER, L.R. , 1931, JOINTING IN THE GREAT SCAR LIMESTONE OF CRAVEN AND ITS RELATIONS TO THE TECTONICS OF THE AREA. QUART. JOUR. GEOL. SOC., LONDON, VOL. 87, PP. 392-420.

WAGER, L.R. AND W.A. DEER, 1938, A DYKE SWARM AND CRUSTAL FLEXURE IN EAST GREENLAND. GEOL. MAG., VOL. 75, PP. 39-46.

WAHLSTROM, E.E., AND V. Q. HORNBACK, 1962, GEOLOGY OF THE HAROLD

D. ROBERTS TUNNEL, COLORADO, WEST PORTAL TO STATION 468-49. BULL. GEOL. SOC. AMER., VOL. 73, NO. 12, PP. 1477-1498.

WALKER, J. E., G. A. WHAN, AND R.R. RUTHFUS, 1957, FLUID FRICTION IN NON-CIRCULAR DUCTS. AICHE JOUR., VOL. 3, P. 484.

WALTON, W. C. AND J. C. NEILL, 1963, STATISTICAL ANALYSIS OF SPECIFIC CAPACITY DATA FOR A DOLOMITE ACQUIFER. JOUR. GEOPHYS. RES., VOL. 68, NO. 8, PP. 2251-2262.

WARREN, J.E., E.L. DOUGHERTY AND H.S. PRICE, 1960, RESERVOIR SIMULATION ON A DIGITAL COMPUTER. THE DIFFERENTIAL EQUATION PROGRAM (TRAN). CALIF. RESEARCH CORP., LA HABRA, CALIF., PROJ. 5219.

WARREN, J. E., AND H. S. PRICE, 1961, FLOW IN HETEROGENEOUS POROUS MEDIA. AMER. INST. MIN. AND MET. ENG., VOL. 222, PP. 153-169.

WARREN, J.E., H.S. PRICE AND F.F. SKIBA, 1962, MISCIBLE DISPLACEMENT. THE LIQUID-LIQUID CASE. ABSTR. SPE 118, JOUR. PET. TECH., P. 883.

WATSON, G. S., 1956A, ANALYSIS OF DISPERSION ON A SPHERE. ROYAL ASTRON SOC., MONTH. NOTICES, GEOPHYS. SUPPL., VOL. 7, NO. 4, PP. 153-159.

WATSON, G. S., 1956B, A TEST FOR RANDOMNESS OF DIRECTIONS. ROYAL ASTRON. SOC., MONTH NOTICES, GEOPHYS. SUPPL., VOL. 7, NO. 4, PP. 160-161.

WATSON, G. S., AND E. J. WILLIAMS, 1956, ON THE CONSTRUCTION OF SIGNIFICANCE TESTS ON THE CIRCLE AND THE SPHERE. ROYAL ASTRON. SOC., MONTHLY NOTICES, GEOPHY. SUPPL., VOL. 7, NO. 4, ALSO, BIOMETRIKA, VOL. 43, PARTS 3 AND 4, PP. 344-352.

WATSON, T. L., 1910, GRANITES OF THE SOUTHEASTERN ATLANTIC STATES. U. S. GEOL. SURVEY, BULL. 426, 282 PP.

WHITE, D. E., E. T. ANDERSON AND D. K. GRUBBS, 1963, GEOTHERMAL BRINE WELL, MILE-DEEP DRILL HOLE MAY TAP ORE-BEARING MAGMATIC WATER AND ROCK UNDERGOING METAMORPHISM . SCIENCE, VOL. 139, NO. 3558, PP. 919-922.

WILSON, C. W., 1934, A STUDY OF THE JOINTING IN THE FIVE SPRINGS CREEK AREA, EAST OF KONE, WYOMING. JOUR. GEOL., VOL. 42, PP. 498-522.

WINGER, R. L., 1956, FIELD DETERMINATION OF HYDRAULIC CONDUCTIVITY ABOVE A WATER TABLE. OFFICE DRAINAGE AND GROUND WATER ENG. U. S. BUR. RECLAM.

WISE, D. U., 1964, MICROJOINTING IN BASEMENT, MIDDLE ROCKY MOUNTAINS OF MONTANA AND WYOMING. BULL. GEOL. SOC. AMER., VOL. 75, PP. 287-306.

WISSER, E., 1939, GEOLOGIC PARALLELS. HOG MOUNTAIN, ALABAMA, AND PARACOLES, PHILLIPINE ISLANDS. EC. GEOL., VOL. 34, NO. 3, PP. 297-323.

WISSER, E., 196C, RELATION OF ORE DEPOSITION TO DOMING IN THE NORTH AMERICAN CORDILLERA. GEOL. SOC. AMER., MEMOIR 77, 117 PP.

WITHERSPOON, P.A., T.D. MUELLER AND R.W. DONOVAN, 1962, EVALUATION OF UNDERGROUND GAS STORAGE CONDITIONS IN AQUIFERS THROUGH INVESTIGATIONS OF GROUNDWATER HYDROLOGY. JOUR. PET. TECH., MAY, PP. 555-561.

WOLK, E., 1937, ZUR KLUFTTEKTONIK DES NIEDERRHEINISCHEN HAUPT-BRAUNKOHLENFLOZES. ZEITSCHR. DEUTSCH. GEOL. GES., HEFT. 91, Z. 2, S. 109.

WOODWORTH, J. B., 1895, FEATURES OF JOINTS. SCIENCE, VOL. 2, PP. 903-904.

WOODWORTH, J. B., 1896, ON THE FRACTURE SYSTEMS OF JOINTS, WITH REMARKS ON CERTAIN GREAT FRACTURES. BOSTON SOC. NAT. HIST. PROC., VOL. 27, PP. 163-184.

WYLIE, C. R., JR., 196C, ADVANCED ENGINEERING MATHEMATICS. MCGRAW-HILL BOOK CO., NEW YORK, 2ND ED., 696 PP.

YANG, SHIH TE, 1948, ON THE PERMEABILITY OF HOMOGENEOUS ANISOTROPIC SOILS. PROC. 2ND INT. CONF. SOIL MECH. AND FOUNDATION ENG., ROTTERDAM PP. 317-320.

YOKOTA, J., 1963, EXPERIMENTAL STUDIES ON THE DESIGN OF GROUTING CURTAIN AND DRAINAGE FOR THE KUROBE NO. 4. DAM. FELSMECHANIK UND INGENIEURGEOLOGIE, VOL. 1, NO. 2 PP. 104-119.

ZAFRANI, I., AND D. K. TODD, 1963, FLOW OF CLAY SUSPENSIONS THROUGH FRACTURES. HYDRAULIC LAB., UNIV. OF CALIF., BERKELEY, 29 PP.

ZANGAR, C. N., 1953, THEORY AND PROBLEMS OF WATER PERCOLATION. ENG. MONOGRAPH 8, U. S. BUR. RECLAIM, DENVER , COLO.,, 76 PP.

ZANGAR, C. N., AND H. B. PHILLIPS, 1946, ELECTRIC ANALOGY CONDUCTIVITY TESTS FOR PERCOLATION OUT OF WELLS. MEMO TO T. P. AHRENS, U. S. BUR. RECLAM., DENVER, COLO.

ZWART, H.J., 1951, BREUKEN UND DIAKLAZEN IN ROBIN'S HOOD BAY.

APPENDIX A

COMPUTER PROGRAMS

Program Used for Orientation Studies, Chapter 5

The following program models media, containing infinite, uniform isotropic conductors in one to five dispersed sets having different, or equal aperture distributions, but constant sample size for each set. Some further comments on the operation and results obtained by this program are contained in Chapters 4 and 5.

The following description of operations, together with comment statements in the several subroutines, explains the principal features of the program. MAIN reads the basic input data cards defining the (N) joint sets, and for each set, the number of elements, M (N), the three direction cosines specifying the orientation of the central tendency CT1 (N), CT2 (N), CT3 (N), the orientation dispersion coefficient, AK (N), two parameters defining the aperture frequency distribution, STD (N), CENTER (N), and, lastly, the joint frequency is given by the sample dimension DELTA.

When all parameters of the joint sets are in storage, MAIN executes a 49-cycle loop, L, transferring to subroutine CNTROL, which computes and stores the permeability tensor. CNTROL calls two other brief subroutines, VECTOR and APER, described later, which furnish a pair of random orientations and aperture values to describe a conductor. CNTROL computes 9 tensor elements from them, as well as the median, mode, and the arithmetic, geometric and harmonic means of the aperture distribution generated for each set. As many as 5 sets may each have up to 500 joints. CNTROL also furnishes a check on the orientation distribution by computing the vector strength, (Pincus, 1953) a measure of dispersion sometimes employed in geological statistics and relatable, by Figure 5-0, to Fisher's vector dispersion coefficient K_f. Once CNTROL has obtained all the required members of a single joint set and has computed and added the tensor contributions of all conductors of the set, it repeats the procedure for other joint sets, each with distinct orientation and aperture dispersion parameters. Before transferring results to OUTPUT, CNTROL divides the summary tensor by DELTA, weighting the tensor according to the dimensions of the volume that would contain the sample. Using DELTA the same for all sets requires that the number of elements of each set be proportioned according to its specific surface and orientation dispersions, as described in Chapter 4.

OUTPUT utilizes Merwin's (1959) subprogram MI HD13 for matrix diagonalization. Two resulting 3 x 3 matrices are stored, one, the diagonal matrix of eigenvalues, (the principal permeabilities) the other, the matrix of eigenvectors, (the principal axes). The ratio of minimum to maximum eigenvalues TINSQ is stored to record the maximum anisotropy.

When all 49 independent solutions have been obtained and stored, MAIN calls, in order, STEREO and FREQPL, subroutines designed to generate point coordinates for the Cal-Comp Plotter, which draws finished ink graphs with frames, scales, labels and captions.

Subroutine STEREO displays the principal axes of all solutions on an 18 cm., upper hemisphere, conformal stereographic projection. Details of the geometry and techniques of stereographic projection of vectors may be found in Donn (1958), or Goodman (1963). A circle with 10-degree ticks frames the plot. Geographic cardinals, two lines of caption, built in, and one line of caption, read in, are lettered before data plotting starts.

Each solution furnishes 3 orthogonal vectors, identified by diamonds, circles, and crosses for the axes of maximum, intermediate and minimum permeability, respectively. The simple trigonometry converting direction cosines to x-y coordinates is in statements 22 to 13 of STEREO. Should lower hemisphere plots be desired, change the signs of components by reordering the transfers in the IF statement preceeding statement 12.

Subroutine FREQPL displays the cumulative distribution of eigenvalues, the same diamonds, circles, and crosses applying to the major, intermediate, and minor directional permeabilities of each solution. Similarly, maximum anisotropies are displayed with dots. To plot cumulatively, the 49 values of each variable are organized in ascending order of magnitude. The ordinate has the probability scale of cumulative percent, whose plot coordinates are read into the program at the beginning of MAIN. The abcissa varies from plot to plot, different scales selected to spread over most of the graph the range from least minor permeability to greatest major permeability. Integral scale factors are used to retain the usefulness of the 0.1-inch scale marks. Printed computer output permits subsequent manual labelling of the abcissa.

```
C     MAIN CONTROL PROGRAM, D.T. SNOW, DEPT. MINERAL TECHNOLOGY
CCMPUTATION OF DIRECTIONAL PERMEABILITY WITH DIFFERENT SETS OF
CCNDUCTING JOINTS HAVING DISTRIBUTED APERTURES AND ORIENTATIONS. FIFTY
CCNSECUTIVE RANDOM SAMPLES OF THE DATA GIVE THE DISTRIBUTION OF ANSWERS.
CCNTINUOUS CHANGE OF THE SAMPLE SIZE IS USED TO EVALUATE THE
CCNTINUUM-EQUIVALENT  VOLUME OF ROCK.  ALL RESULTS ARE PLOTTED.
CCMPUTED SMALL-ELEMENT TENSORS STORED FOR POSSIBLE INCLUSION IN LARGER
      DIMENSION MTOT(5),Q(3,3,50),CT1(5),CT2(5),CT3(5),AK(5),STD(5),
     1CENTEN(5),P(3,3),E(3,3),A(3),C(3),AVB(5),M(5),H(3,3),HH(3,50),
     2X(3),IQ(3),L(3,3),UU(3,3,50),AA(15),BB(4),CC(10),DD(12),FF(4),
     3GG(12),TINSQ(50),V(4),W(8),WW(2),DDD(12),EE(2),YF(15),YV(49),
     4VAVB(5,50),SUMCOS(5),COSSUM(5,50)
      COMMON DELTA,M,CT1,CT2,CT3,AK,STD,CENTEN,L,P,Q,AVB,MTOT,E,A,C,H,
     1HH,U,UU,AA,BB,CC,CD,FF,GG,TINSQ,V,W,WW,DDD,NMAX,EE,YF,YV,VAVB,
     2SUMCOS,COSSUM
      CALL FTMUPT(2,32767,606)
      REWIND 6
CCORDINATES OF PROBABILITY SCALE READ ON.
      READ 660,YF(1),YF(2),YF(3),YF(4),YF(5),YF(6),YF(7),YF(8)
      READ 660,YF(9),YF(10),YF(11),YF(12),YF(13),YF(14),YF(15)
  660 FORMAT(8F9.3)
      READ 661,YV(1),YV(2),YV(3),YV(4),YV(5),YV(6),YV(7)
      READ 661,YV(8),YV(9),YV(10),YV(11),YV(12),YV(13),YV(14)
      READ 661,YV(15),YV(16),YV(17),YV(18),YV(19),YV(20),YV(21)
      READ 661,YV(22),YV(23),YV(24),YV(25),YV(26),YV(27),YV(28)
      READ 661,YV(29),YV(30),YV(31),YV(32),YV(33),YV(34),YV(35)
      READ 661,YV(36),YV(37),YV(38),YV(39),YV(40),YV(41),YV(42)
      READ 661,YV(43),YV(44),YV(45),YV(46),YV(47),YV(48),YV(49)
  661 FORMAT(7F10.5)
CLEAR CUMULATING PARAMETERS.
  201 DO 210 N=1,5
  210 MTOT(N)=C
      N=0
      DO 292 L=1,50
      DO 202 I=1,3
      DO 202 J=1,3
  202 Q(I,J,L)=0.0
      DO 292 N=1,5
      COSSUM(N,L)=0.0
  292 VAVB(N,L)=0.0
  606 N=N+1
      READ 652,(M(N),CT1(N),CT2(N),CT3(N),AK(N),STD(N),CENTEN(N),DELTA
      PRINT 672,M(N),CT1(N),CT2(N),CT3(N),AK(N),STD(N),CENTEN(N),DELTA
  652 FORMAT(I3,F12.8,2F10.8,F5.2,3F10.5)
  672 FORMAT(I5,3F20.6,F5.2,3F15.5)
      MTOT(N)=MTOT(N)+M(N)
      IF(1-M(N)) 606,161,8
    8 NMAX=N-1
      PRINT 680,NMAX,MTOT(1),VAVB(1,1)
  680 FORMAT(2I10, F20.5)
      DO 205 L=1,50
      L=L
      CALL CNTROL
  205 CONTINUE
      CALL STEREO
```

```
      CALL FREQPL
      N=0
      GO TO 606
  161 IF(DELTA) 201,201,162
  162 CALL NOPLOT
      ENDFILE 6
      ENDFILE 6
      CALL REWUNL(6)
      CALL EXIT
      END

*     LIST
*     LABEL
*     FORTRAN
      SUBROUTINE CNTROL
      DIMENSION MTOT(5),Q(3,3,50),CT1(5),CT2(5),CT3(5),AK(5),STD(5),
     1CENTEN(5),P(3,3),E(3,3),A(3),C(3),AVB(5),M(5),H(3,3),HH(3,50),
     2X(3),IU(3),L(3,3),UU(3,3,50),AA(15),BB(4),CC(10),DD(12),FF(4),
     3GG(12),TINSQ(50),V(4),W(8),WW(2),DDD(12),EE(2),YF(15),YV(49),
     4VAVB(5,50),SUMCOS(5),COSSUM(5,50)
      COMMON DELTA,M,CT1,CT2,CT3,AK,STD,CENTEN,L,P,U,AVB,MTOT,E,A,C,H,
     1HH,U,UU,AA,BB,CC,CD,FF,GG,TINSQ,V,W,WW,DDD,NMAX,EE,YF,YV,VAVB,
     2SUMCOS,COSSUM
      DO 220 I=1,3
      DO 220 J=1,3
  220 P(I,J)=Q(I,J,L)
C COMPUTE MATRIX OF TRANSFORMATION BETWEEN ZENITH AND
C CENTRAL TENDENCY OF SET.
      DO 813 N=1,NMAX
      DENOM=SQRTF(1.0-CT2(N)*CT2(N))
      E(1,1)=CT1(N)*CT2(N)/DENOM
      E(1,2)=-DENOM
      E(1,3)=CT2(N)*CT3(N)/DENOM
      E(2,1)=CT1(N)
      E(2,2)=CT2(N)
      E(2,3)=CT3(N)
      E(3,1)=CT3(N)/DENOM
      E(3,3)=-CT1(N)/DENOM
C CONSTANTS OF DISPERSION COMPUTED.
      F1=EXPF(AK(N))
      G1=F1-EXPF(-AK(N))
      AVB(N)=VAVB(N,L)
      SUMCOS(N)=COSSUM(N,L)
C CALL A UNIFORM RANDOM NUMBER GENERATOR TO DEFINE A PROBABILITY, THEN
C COMPUTE COSINE THETA DEFINING A CIRCLE ABOUT THE CENTRAL TENDENCY AC-
C CORDING TO AK, FISHER'S COEFFICIENT OF DISPERSION OF VECTORS ON A SPHERE
C CALL AGAIN A RANDOM UNIFORM GENERATOR TO POSITION THE VECTOR ON THE
C CIRCLE.
      MM=M(N)
      DO 813 MTIMES=1,MM
      H1=F1-RANDOM(X1)*G1
      COSTH=LOGF(H1)/AK(N)
      SUMCOS(N)=SUMCOS(N)+COSTH
      SINTH=SQRTF(1.0-COSTH*COSTH)
      PHI=RANDOM(X1)*6.28318
      A(1)=SINTH*SINF(PHI)
```

```
      A(2)=COSTH
      A(3)=SINTH*COSF(PHI)
      C(1)=E(1,1)*A(1)+E(2,1)*A(2)+E(3,1)*A(3)
      C(2)=E(1,2)*A(1)+E(2,2)*A(2)
      C(3)=E(1,3)*A(1)+E(2,3)*A(2)+E(3,3)*A(3)
      IF(C(3)) 221,224,224
  221 DO 222 J=1,3
  222 C(J)=-C(J)
C CALL RANDOM NORMAL NUMBER GENERATOR AND MODIFY IT ACCORDING TO THE
C CELECTED PARAMETERS OF THE SET.
  224 B=ABSF(STD(N)*RANDEV(X1)+CENTEN(N))
      AVB(N)=AVB(N)+B
C CALCULATE PERMEABILITY OF EACH JOINT, THEN ELEMENTS OF TENSOR.
      PERM=666666.667*B**3
      EN=ABSF(COSTH)
      P(1,1)=P(1,1)+PERM*(1.0-C(1)*C(1))/EN
      P(1,2)=P(1,2)+PERM*(-C(1)*C(2))/EN
      P(1,3)=P(1,3)+PERM*(-C(1)*C(3))/EN
      P(2,2)=P(2,2)+PERM*(1.0-C(2)*C(2))/EN
      P(2,3)=P(2,3)+PERM*(-C(2)*C(3))/EN
      P(3,3)=P(3,3)+PERM*(1.0-C(3)*C(3))/EN
  813 CONTINUE
      P(2,1)=P(1,2)
      P(3,1)=P(1,3)
      P(3,2)=P(2,3)
C CAUSE APERTURE MEAN, SAMPLE SIZE AND VECTOR STRENGTH TO BE PRINTED OUT.
      DO 207 N=1,NMAX
      BAVG=AVB(N)/FLOATF(MTOT(N))
      STR=SUMCOS(N)/FLOATF(MTOT(N))
      VAVB(N,L)=AVB(N)
      COSSUM(N,L)=SUMCOS(N)
  207 PRINT 657,BAVG,MTOT(N),STR
  657 FORMAT(F20.8,I10,F20.8)
      DO 204 I=1,3
      DO 204 J=1,3
C CARRY SAMPLE TENSOR TO NEW ARRAY FOR STORAGE.
      Q(I,J,L)=P(I,J)
  204 H(I,J)=P(I,J)/DELTA
      CALL OUTPUT
      RETURN
      END


*     LIST
*     LABEL
*     FORTRAN
      SUBROUTINE STEREO
C CALCULATES COORDINATES AND PLOTS THE STEREOGRAPHIC PROJECTION OF M VE
C CTORS ON THE UPPER HEMISPHERE OF AN 18 CM NET OVERLAY
      DIMENSION MTOT(5),Q(3,3,50),CT1(5),CT2(5),CT3(5),AK(5),STD(5),
     1CENTEN(5),P(3,3),E(3,3),A(3),C(3),AVB(5),M(5),H(3,3),HH(3,50),
     2X(3),IQ(3),U(3,3),UU(3,3,50),AA(15),BB(4),CC(10),DD(12),FF(4),
     3GG(12),TINSC(50),V(4),W(8),WW(2),DDD(12),EE(2),YF(15),YV(49),
     4VAVB(5,50)
      COMMON DELTA,M,CT1,CT2,CT3,AK,STD,CENTEN,L,P,Q,AVB,MTOT,E,A,C,H,
```

```
     1HH,U,UU,AA,BB,CC,DD,FF,GG,TINSQ,V,W,WW,DDD,NMAX,EE,YF,YV,VAVB
      V(1) =3H1HN
      V(2) =3H1HS
      V(3) =3H1HW
      V(4) =3H1HE
      WW(1)=6H9HFIGU
      WW(2)=6HRE  .
      W(1)=6H42HSTE
      W(2)=6HREOGRA
      W(3)=6HPHIC P
      W(4)=6HROJECT
      W(5)=6HION, U
      W(6)=6HPPER H
      W(7)=6HEMISPH
      W(8)=3HERE
   11 CALL GRAPH (10.0,7.8,1.1)
      READ 7, (DDD(J),J=1,12)
    7 FORMAT(12A6)
CCOORDINATES AND LETTERING DONE.
      CALL XLN (0.23,0.37,3.9,0.0)
      CALL XLN (3.8,4.0,3.9,0.0)
      CALL XLN (7.43,7.57,3.9,0.0)
      CALL YLN (0.23,0.37,3.9,0.0)
      CALL YLN (3.8,4.0,3.9,0.0)
      CALL YLN (7.43,7.57,3.9,0.0)
      CALL LTR (0.12,3.80,2,1,V(1))
      CALL LTR (7.83,3.80,2,1,V(2))
      CALL LTR (4.00,0.02,2,1,V(3))
      CALL LTR (4.00,7.68,2,1,V(4))
      CALL LTR(8.2,0.0,2,1,WW)
      CALL LTR(8.6,0.0,2,1,W)
      CALL LTR (9.0,0.0,2,1,DDD)
      CALL CURVE (2,10,0,0,-3.9,10.0,-3.9,10.0,1)
      THETA=0.0
   15 PHI=THETA/57.295
      XX=3.53*COSF(PHI)
      YY=3.53*SINF(PHI)
      CALL PLOTPT(XX,YY)
      THETA =THETA + 1.0
      IF (THETA- 360.0)15,15,999
  999 DO 10 I=1,3
CHOSEN SYMBOLS ARE DIAMONDS FOR K11 AXIS, CIRCLES FOR K22 AXIS, AND
CROSSES FOR THE K33 AXIS.
      IF(I-2) 16,19,20
   16 CALL CURVE (3,1,1,0,-3.9,10.0,-3.9,10.0,1)
      GO TO 22
   19 CALL CURVE (5,1,1,0,-3.9,10.0,-3.9,10.0,1)
      GO TO 22
   20 CALL CURVE (7,1,1,0,-3.9,10.0,-3.9,10.0,1)
   22 DO 10 L=1,50
CCMPUTE X-Y COORDINATES FROM DIRECTION COSINES.
      R=3.53*SQRTF((1.0-UU(3,I,L))/(1.0+UU(3,I,L)))
      S=UU(2,I,L)/UU(1,I,L)
      XX=R/SQRTF(1.0+S*S)
      IF(UU(1,I,L))   12,13,13
   12 XX=-XX
```

```
   13 YY=XX*S
   10 CALL PLOTPT(XX,YY)
      ENDFILE6
      ENDFILE6
      RETURN
      END
*     LIST
*     LABEL
*     FORTRAN
      SUBROUTINE CUTPUT
      DIMENSION MTOT(5),Q(3,3,50),CT1(5),CT2(5),CT3(5),AK(5),STD(5),
     1CENTEN(5),P(3,3),E(3,3),A(3),C(3),AVB(5),M(5),H(3,3),HH(3,50),
     2X(3),IQ(3),U(3,3),UU(3,3,50),AA(15),BB(4),CC(10),DD(12),FF(4),
     3GG(12),TINSQ(50),V(4),W(8),WW(2),DDD(12),EE(2),YF(15),YV(49),
     4VAVB(5,50)
      COMMON DELTA,M,CT1,CT2,CT3,AK,STD,CENTEN,L,P,U,AVB,MTOT,E,A,C,H,
     1HH,U,UU,AA,BB,CC,DD,FF,GG,TINSQ,V,W,WW,DDD,NMAX,EE,YF,YV,VAVB
  758 N=3
      IEGEN=0
CCNDUCTIVITY MATRIX IS DIAGONALIZED TO GET THE PRINCIPAL
CCNDUCTIVITIES AND AXES OF THE SYSTEM CONDUCTIVITY TENSOR
      CALL HDIAG(H,N,IEGEN,U,NR)
      PRINT 817,((H(I,J),J=1,3),I=1,3)
      PRINT 817,((U(J,I),J=1,3),I=1,3)
  817 FORMAT(1P9E12.4)
CCORDINATES OF AXES PUT ON UPPER HEMISPHERE
      DO 765 I=1,3
      IF(U(3,I)) 760,765,765
  760 DO 762 J=1,3
  762 U(J,I)=-U(J,I)
  765 CONTINUE
CAUSE SOLUTION TO BE STORED FOR LATER PLOTTING.
  780 DO 783 I=1,3
      HH(I,L)=H(I,I)
      DO 783 J=1,3
  783 UU(J,I,L)=U(J,I)
      HMIN=MIN1F(HH(1,L),HH(2,L),HH(3,L))
      HMAX=MAX1F(HH(1,L),HH(2,L),HH(3,L))
      TINSQ(L)=HMIN/HMAX
      RETURN
      END


*     LIST
*     LABEL
*     FORTRAN
      SUBROUTINE FREQPL
CUMULATIVE FREQUENCY CURVES PLOTTED FOR EACH PRINCIPAL CONDUCTIVITY
CAPTIONS AND LABELS STORED.
      DIMENSION MTOT(5),Q(3,3,50),CT1(5),CT2(5),CT3(5),AK(5),STD(5),
     1CENTEN(5),P(3,3),E(3,3),A(3),C(3),AVB(5),M(5),H(3,3),HH(3,50),
     2X(3),IQ(3),U(3,3),UU(3,3,50),AA(15),BB(4),CC(10),DD(12),FF(4),
     3GG(12),TINSQ(50),V(4),W(8),WW(2),DDD(12),EE(2),YF(15),YV(49),
     4VAVB(5,50),SUMCOS(5),COSSUM(5,50)
      COMMON DELTA,M,CT1,CT2,CT3,AK,STD,CENTEN,L,P,U,AVB,MTOT,E,A,C,H,
```

```
     1HH,U,UU,AA,BB,CC,CD,FF,GG,TINSQ,V,W,WW,DDD,HMAX,EE,YF,YV,VAVB,
     2SUMCOS,COSSUM
      AA(1)=3H1H1
      AA(2)=3H1H2
      AA(3)=3H1H5
      AA(4)=4H2H10
      AA(5)=4H2H20
      AA(6)=4H2H30
      AA(7)=4H2H40
      AA(8)=4H2H50
      AA(9)=4H2H60
      AA(10)=4H2H70
      AA(11)=4H2H80
      AA(12)=4H2H90
      AA(13)=4H2H95
      AA(14)=4H2H98
      AA(15)=4H2H99
      BB(1)=6H18HCUM
      BB(2)=6HULATIV
      BB(3)=6HE PERC
      BB(4)=3HENT
      CC(1)=3H55H
      CC(2)=6HFIGURE
      CC(3)=6H    . P
      CC(4)=6HRINCIP
      CC(5)=6HAL CON
      CC(6)=6HDUCTIV
      CC(7)=6HITIES,
      CC(8)=6H X 10
      CC(9)=6H CGS U
      CC(10)=4HNITS
      EE(1)=4H2H16
      EE(2)=4H2H84
      FF(1)=6H18HMAX
      FF(2)=6HIMUM A
      FF(3)=6HNISOTR
      FF(4)=3HOPY
C     COORDINATES AND LETTERING DONE, SCALES PLOTTED.
   26 CALL GRAPH(9.0,6.0,2.5)
      CALL FRAME(0.1,0.0)
      CALL XLN(0.4,9.0,1.77,0)
      CALL XLN(0.0,9.0,3.00,0.5)
      CALL XLN(0.4,9.0,4.23,0)
      CALL XLN(5.5,9.0,6.0,0.5)
      CALL XLN(9.0,0.0,0.0,-0.5)
      DO 310 J=1,15
  310 CALL XLN(0.0,0.1,YF(J),0)
      DO 311 J=1,15
  311 CALL XLN(8.9,9.0,YF(J),0)
      DO 21 J=1,15
      YY=YF(J)-0.05
   21 CALL LTR(-0.3,YY,1,0,AA(J))
      CALL LTR(-0.5,0.7,2,1,BB)
      CALL LTR(0.1,1.72,1,0,EE(1))
      CALL LTR(0.1,4.18,1,0,EE(2))
      CALL LTR(-1.3,-1.0,2,0,CC)
```

```
      CALL LTR(5.5,6.4,2,0,FF)
      READ 7,(GG(J),J=1,12)
      CALL LTR(-0.7,-1.4,2,0,GG)
      READ 7,(DD(J),J=1,12)
      CALL LTR(-0.6,-1.8,2,0,DD)
    7 FORMAT(12A6)
CCONDUCTIVITIES AND ANISOTROPIES ARRANGED IN ASCENDING ORDER.
      DO 32 I=1,3
      DO 32 L=1,49
      LP1=L+1
      DO 32 J=LP1,50
      IF(HH(I,L)-HH(I,J)) 32,32,38
   38 TEMP=HH(I,L)
      HH(I,L)=HH(I,J)
      HH(I,J)=TEMP
   32 CONTINUE
      DO 39 L=1,49
      LP1=L+1
      DO 39 J=LP1,50
      IF(TINSQ(L)-TINSQ(J)) 39,39,40
   40 TEMP=TINSQ(L)
      TINSQ(L)=TINSQ(J)
      TINSQ(J)=TEMP
   39 CONTINUE
CCOMPUTE FACTOR TO MAKE PERMEABILITY CURVES FIT PLOT, POSITION CURVES.
      XMIN=MIN1F(HH(1,1),HH(2,1),HH(3,1))
   61 HP=1.0E-02
   62 HS=XMIN*HP
      IF(HS-1.0) 63,64,64
   63 HP=HP*10.0
      GO TO 62
   73 HP=HP/10.0
      HS=XMIN*HP
   64 XMAX=MAX1F(HH(1,50 ),HH(2,50 ),HH(3,50 ))
      HL=XMAX*HP
      IF(HL-HS-8.0) 65,65,73
   65 IF(HL-HS-0.8) 63,63,81
   81 IX=8.0/(HL-HS)
      GO TO (69,69,303,69,69,306,306,69,309,69),IX
  303 IX=2
      GO TO 69
  306 IX=5
      GO TO 69
  309 IX=8
   69 XI=IX
      HP=HP*XI
      PRINT 31,XMIN,XMAX,IX
   31 FORMAT(1P2E20.8,I4)
      IXMIN=XMIN*HP
      XMIN=IXMIN
CCOMPUTE FACTOR TO MAKE ANISOTROPY CURVE FIT PLOT, POSITION CURVE.
      TP=0.1
   92 TDIF=TP*(TINSQ(50)-TINSQ(1))
      IF(TDIF-0.2) 93,94,94
   93 TP=TP*10.0
      GO TO 92
```

```
   94 TS=TINSQ(1)*TP
  101 ITS=TS
      TS=ITS
      PRINT 31, TINSQ(1),TINSQ(50),ITS
CURVE IDENTITY ESTABLISHEDAND STANDARD DEVIATION CALCULATED
   42 DO 35 I=1,3
      HACT=HH(I,25)*1.0E-06
      DEVH=(HH(I,42)-HH(I,8))*1.0E-06
      PRINT 350,DEVH
   35 PRINT 36,HP,HACT,I,TINSQ(25)
      DEVT=TINSQ(42)-TINSQ(8)
      PRINT 350, DEVT
   36 FORMAT(1P2E20.8,I4, E20.8)
  350 FORMAT(F20.7)
CUMULATIVE FREQUENCY CURVES PLOTTED
      DO 18 I=1,3
CHOSEN SYMBOLS ARE DIAMONDS FOR K11, CIRCLES K22, CROSSES K33.
      IF(I-2) 96,99,100
   96 CALL CURVE(3,1,1,0,0.00,9.0,0.0,6.0,1)
      GO TO 289
   99 CALL CURVE(5,1,1,0,0.00,9.0,0.0,6.0,1)
      GO TO 289
  100 CALL CURVE(7,1,1,0,0.00,9.0,0.0,6.0,1)
  289 DO 17 L=1,49
      XV=HH(I,L)*HP-XMIN
   17 CALL PLOTPT(XV,YV(L))
   18 CONTINUE
      CALL CURVE(1,1,1,0,0.0,9.0,0.0,6.0,1)
      DO 217 L=1,49
      XV=TINSQ(L)*TP-TS+6.0
  217 CALL PLOTPT(XV,YV(L))
      ENDFILE 6
      ENDFILE 6
      RETURN
      END
```

Program for Model Synthesis of Pressure Tests and Computations of Porosity

The following program includes revised editions of the above-described subroutines with additional subroutines to vary the size of samples, to compute the discharge of simulated pressure tests, to plot the resulting discharges, and to compute porosity by two methods from the geometry of joints and the computed anisotropy.

Within the portions of the program that model jointed media and compute an equivalent anisotropic-continuum permeability, the principal innovation is Subroutine NUMBER. Upon first call from MAIN, NUMBER sets up a table of probabilities of obtaining certain small integral numbers (0, 1, 2, 3, 4, etc.) of conductors, calculated according to the Poisson distribution with a specified expectation (1/10 of M (N)). A separate table serves each set, so that different frequency distributions are possible.

When MAIN executes the 49-cycle L-Loop, calls to NUMBER get a random sample size from the tables. To do so, random uniform numbers are generated as probabilities, which are then matched with the closest value in the probability table, so identifying a sample size.

Subroutine VECTOR sets up a coordinate transformation on the first call, and for each subsequent call furnishes a randomly oriented vector according to the read-in direction of the central tendency, and the Fisher dispersion. One reason for separating the vector sampling from the control routine is to permit substitution of different vector subroutines. For instance, field joint orientation data could be read into storage and sampled at random, or in their entirety. This procedure was not used because there is not yet a field method for determining in-situ apertures to pair with each measured orientation.

Subroutine APER generates on each call a random number to represent the aperture of a conductor. Alternative subroutines APER listed below include transposed (absolute value) normal distributions, log-normal and exponential distributions. Other density function generators could be compiled.

Corresponding to each sampling of all the sets, there is computed the permeability tensor as described for the simpler version of the model. To test the model's ability to duplicate field pressure-test data, there is computed in PIEZO the discharge that would occur under standard conditions for three holes of specified orientation (read in at MAIN). The program duplicates the matrix manipulations derived in Chapter 3 for cylinders of arbitrary orientation in anisotropic media. Each call to PIEZO gives different results because successive samples produce media of different anisotropy. The discharges are stored for plotting after completion of the 49 samplings.

Subroutine PUMPLT differs operationally from FREQPL only in that the ordinate is arithmetic instead of probability scale, and the computed statistical parameters of the pump-discharge distribution are marked on the plot.

Subroutine EQPOR was developed to learn whether or not the average of porosities, calculated from varying permeabilities and known spacing and orientation, does or does not approach the true porosity, based on the assumption that each sample contains the average number of conductors, and that they all have the same aperture. Since the samples have numbers defined by the Poisson distribution, and apertures and orientations defined by various dispersions, the sample porosities vary by several hundred percent from the average. To compute porosity, EQPOR sets up a new coordinate system parallel to the computed (OUTPUT) principal axes, following the procedure of Chapter 4, then sets up simultaneous equations (4-28) to determine the permeability of parallel sets, kp, that would develop the same anisotropic permeability, then by (4-31), with corrections for the orientation dispersion, it computes porosity and the ratio of computed to true porosity. Unlike real media, the model porosity is precisely known because each aperture generated in APER is added in CNTROL. The program is specifically compiled for one system of joint orientations, developing the data of Table 7-1.

Subroutine POREQ does the same service of computing porosity, but does so only once per job, using the average of all 49 permeabilities and principal axes predetermined for the specific joint system. Output from POREQ is the ratio of computed to true porosity.

```
*      DECKS
*      LABEL
*      LIST
*      FORTRAN
C KIJ MAIN CONTROL PROGRAM, D.T. SNOW, DEPT. MINERAL TECHNOLOGY
CCMPUTATION OF DIRECTIONAL PERMEABILITY WITH DIFFERENT SETS, NUMBERS OF
CCNDUCTING JOINTS HAVING DISTRIBUTED APERTURES AND ORIENTATIONS. 49
CCNSECUTIVE RANDOM SAMPLES OF THE DATA GIVE THE DISTRIBUTION OF ANSWER
      DIMENSION M(5),CT1(5),CT2(5),CT3(5),AK(5),STD(5),CENTEN(5),
     1P(3,3),E(3,3),H(3,3),U(3,3),HH(3,50),X(3),IQ(3),UU(3,3,50),
     2TINSQ(5C),AVB(5),SUMCOS(5),HARM(5),GEOM(5),Z(500),A(3),C(3),
     3AA(15),BB(4),CC(10),DD(12),EE(2),FF(4),GG(12),DDD(12),V(4),W(8),
     4WW(2),YF(15),YV(49),PP(2),COSINV(5),UR(3),CUBE(5),MPTS(50,5),
     5TR(3,3),AX(3,3),QA(50,3),CA(11),GA(12),DA(12),PR(50,5),RA(11),
     6CP(4),ORHOL(3,3),FA(4),UC(3,3),YT(3),AL(3),CK(3),PORAT(50)
      COMMON M,CT1,CT2,CT3,AK,STD,CENTEN,AVB,SUMCOS,HARM,GEOM,DELTA,
     1L,P,E,A,C,H,HH,U,UU,AA,BB,CC,DD,EE,FF,GG,TINSQ,V,W,WW,DDD,NMAX,YT
     2YV,N,NON,R,Z,PP,COSINV,CN,WA,DIAM,HEAD,CUBE,MPTS,OR,CK,TR,AX,
     3QA,CA,GA,DA,MM,PR,RA,CP,FA,ORHOL,PORUS,PORTOT,PORAT,
     4H1ULT,H2ULT,H3ULT
      CALL FTMUPT(2,32767,606)
      REWIND 6
CCORDINATES OF PROBABILITY SCALE READ IN
      READ 660,(YF(I),I=1,15)
  660 FORMAT(8F9.3)
      READ 661,(YV(I),I=1,49)
  661 FORMAT(7F10.5)
CELECT HOLES IN ORDER, PARALLEL TO MINOR, INTERMEDIATE AND  MAJOR
CCNDUCTIVITY AXES. CAN THEN SCALE  PUMPPLT TO MAX DISCHARGE.
CCSINES OF THREE ORTHOGONAL TEST HOLES AND TEST CONDITIONS  READ IN.
      DO 1157 MO=1,3
 1157 READ 661,(ORHOL(MO,JO),JO=1,3),WA,DIAM,HEAD
  201 N=0
  606 N=N+1
CCNSIDER M(N)  AS 10 TIMES THE EXPECTATION OF THE POISSON DISTRIBUTION
CCNSIDERED AS THE SIZE OF SAMPLE
CT ARE THE DIRECTION COSINES OF THE CENTRAL TENDENCY OF SET VECTORS
CCEFFICIENT AK IS THE FISHER VECTOR DISPERSION, DELTA  SAMPLE LENGTH
CENTEN AND STD ARE PARAMETERS OF THE APERTURE DISTRIBUTION
      READ 652, M(N),CT1(N),CT2(N),CT3(N),AK(N),STD(N),CENTEN(N),DELTA
      PRINT 672,M(N),CT1(N),CT2(N),CT3(N),AK(N),STD(N),CENTEN(N),DELTA
  652 FORMAT(I3,F12.8,2F10.8,F5.2,3F10.5)
  672 FORMAT(I5,3F20.6,F5.2,3F15.5)
CCORDING TO M VALUES READ, EITHER COMPUTE, PICK UP NEXT JOINT SET, OR
CAN EXAMINE DELTA
      IF(1-M(N)) 606,161,8
    8 NMAX=N-1
CALL FIRST PART OF SUBROUTINE NUMBER TO SET UP A PROBABILITY ARRAY
      NON =1
      DO 2100 N=1,NMAX
      N=N
 2100 CALL NUMBER
      PORTOT=0.C
      H1ULT=0.0
      H2ULT=0.0
      H3ULT=0.0
CYCLE THROUGH 49 SEPARATE PERMEABILITY DETERMINATIONS
```

```
      DO 205 L=1,49
      L=L
CCMPUTE A FRESH TENSORIAL ANSWER EACH TIME CNTRUL IS CALLED
      CALL CNTROL
CCMPUTE PIEZOMETER DISCHARGE CORRESPONDING TO TENSOR DEVELOPED
      CALL PIEZO
CCMPUTE PUROSITY FROM PERMEABILITY
      CALL EQPUR
CUMULATE PRINCIPAL PERMEABILITIES
      H1ULT=H1ULT+H(1,1)
      H2ULT=H2ULT+H(2,2)
      H3ULT=H3ULT+H(3,3)
  205 CONTINUE
CALCULATE AVERAGE PRINCIPAL PERMEABILITIES AND POROSITIES
      H1ULT=H1ULT/49.0
      H2ULT=H2ULT/49.0
      H3ULT=H3ULT/49.0
      PRINT 2393,H1ULT,H2ULT,H3ULT
 2393 FORMAT(49H0 AVERAGE PRINCIPAL PERMEABILITIES X 10 E6 CGS = 3E20.5)
      PORUS=PORTOT/49.0
      PRINT 2394, PORUS
 2394 FORMAT(25H0 AVERAGE TRUE POROSITY= F15.5)
CCLLECTED ANSWERS DISPLAYED IN PLOTS
      CALL STEREO
      CALL FREUPL
      CALL PUMPLT
CALCULATE AVERAGE PORE RATIO, EQUIVALENT /TRUE
      TOTPOR=0.0
      DO 2375 L=1,49
 2375 TOTPOR=TOTPOR+PORAT(L)
      TOTPOR=TOTPOR/49.0
      PRINT 2395, TOTPOR
 2395 FORMAT(24H0 AVERAGE PORE RATIO =  F20.5)
CALCULATE STANDARD DEVIATION OF PORE RATIO
      DEVPOR=0.0
      DO 2376 L=1,49
 2376 DEVPOR=DEVPOR+ (TOTPOR-PORAT(L))**2
      DEVPOR=SQRTF(DEVPOR/49.0)
      PRINT 2396, DEVPOR
 2396 FORMAT(37H0 STANDARD DEVIATION OF  PORE RATIO= F25.5)
      CALL POREQ
      GO TO 201
CCORDING TO DELTA VALUE, PICK UP NEW PROBLEM OR EXIT IF DONE
  161 IF(DELTA) 201,201,162
  162 CALL NOPLOT
      ENDFILE 6
      ENDFILE 6
      CALL REWUNL(6)
      CALL EXIT
      END
```

```
•     LIST
•     LIST
•     LABEL
•     FORTRAN
      SUBROUTINE CNTROL
      DIMENSION M(5),CT1(5),CT2(5),CT3(5),AK(5),STD(5),CENTEN(5),
     1P(3,3),E(3,3),H(3,3),U(3,3),HH(3,50),X(3),IJ(3),UU(3,3,50),
     2TINSQ(50),AVB(5),SUMCOS(5),HARM(5),GEOM(5),Z(500),A(3),C(3),
     3AA(15),BB(4),CC(10),DD(12),EE(2),FF(4),GG(12),DDD(12),V(4),W(8),
     4WW(2),YF(15),YV(49),PP(2),COSINV(5),OR(3),CUBE(5),MPTS(50,5),
     5TR(3,3),AX(3,3),WA(50,3),CA(11),GA(12),DA(12),PR(50,5),RA(11),
     6CP(4),ORHOL(3,3),FA(4),UC(3,3),YT(3),AL(3),CK(3)
      COMMON M,CT1,CT2,CT3,AK,STD,CENTEN,AVB,SUMCOS,HARM,GEOM,DELTA,
     1L,P,E,A,C,H,HH,U,UU,AA,BB,CC,DD,EE,FF,GG,TINSQ,V,W,WW,DDD,NMAX,YF
     2YV,N,NON,B,Z,PP,COSINV,EN,WA,DIAM,HEAD,CUBE,MPTS,OR,CK,TR,AX,
     3QA,CA,GA,DA,MM,PR,RA,CP,FA,ORHOL,PORUS
      DO 220 I=1,3
      DO 220 J=1,3
  220 P(I,J)=0.0
      PORUS=0.0
      IF (1-L) 2912,2911,2911
 2911 MUD=0
 2912 DO 295 N=1,NMAX
      N=N
      NON=0
C CALL SUBROUTINE NUMBER TO DETERMINE SAMPLE SIZE MM FOR THIS SOLUTION
      CALL NUMBER
      IF (MM) 293,293,2111
 2111 CALL VECTOR
      AVB(N)=0.0
      CUBE(N)=0.0
      HARM(N)=0.0
      GEOM(N)=0.0
      SUMCOS(N)=0.0
      COSINV(N)=0.0
      ELEM=FLOATF(MM)
      DO 813 MTIMES=1,MM
      MTIMES=MTIMES
C CALL FOR A RANDOM JOINT ORIENTATION
      CALL VECTOR
C CALL FOR A RANDOM APERTURE TO PAIR WITH ORIENTATION
      CALL APER
C CUMULATE VOID VOLUME FOR CONDUCTORS PENETRATING THROUGH TH VOLUME
C CENTERED ABOUT THE DRILL HOLE
      PORUS=PORUS+2.0*B/ABSF(C(1)*CT1(N)+C(2)*CT2(N)+C(3)*CT3(N))
C CONTINUE INCREMENTING STATISTICAL PARAMETERS
      AVB(N)=AVB(N)+B
      GEOM(N)=GEOM(N)+LOGF(B)
      HARM(N)=HARM(N)+1.0/B
C COLLECT APERTURES IN ARRAY Z
      Z(MTIMES)=B
      B=B**3
      CUBE(N)=CUBE(N)+B
C CALCULATE PERMEABILITY OF EACH JOINT, THEN ELEMENTS OF TENSOR.
C CONSERVE SIGNIFICANCE BY RAISING  BY FACTOR OF MILLION
      PERM=666666.667*B
```

```
      P(1,1)=P(1,1)+PERM*(1.0-C(1)*C(1))/EN
      P(1,2)=P(1,2)+PERM*(-C(1)*C(2))/EN
      P(1,3)=P(1,3)+PERM*(-C(1)*C(3))/EN
      P(2,2)=P(2,2)+PERM*(1.0-C(2)*C(2))/EN
      P(2,3)=P(2,3)+PERM*(-C(2)*C(3))/EN
      P(3,3)=P(3,3)+PERM*(1.0-C(3)*C(3))/EN
  813 CONTINUE
      P(2,1)=P(1,2)
      P(3,1)=P(1,3)
      P(3,2)=P(2,3)
C     CALCULATE VECTOR STRENGTH, STATISTICAL MEANS OF APERTURE DISTRIBUTION
      BAVG=AVB(N)/ELEM
      AVCUBE=CUBE(N)/ELEM
      STR=SUMCOS(N)/ELEM
      BGEOM=EXPF(GEOM(N)/ELEM)
      BHARM=ELEM/HARM(N)
C     CAUSE APERTURE ARRAY TO BE ORDERED
      MN=MM-1
      DO 275 LL=1,MN
      LP1=LL+1
      DO 275 J=LP1,MM
      IF(Z(LL)-Z(J)) 275,275,274
  274 TEMP=Z(LL)
      Z(LL)=Z(J)
      Z(J)=TEMP
  275 CONTINUE
C     CITE MEDIAN VALUE
      MZ=MM/2
      IF(MM-2*MZ) 291,291,292
  291 BMED=(Z(MZ)+Z(MZ+1))/2.0
      GO TO 293
  292 BMED=Z(MZ+1)
C     COMPUTE MODE FROM ORDERED ARRAY AT CENTER OF DENSEST OF 50 CLASSES
  293 IF(MUD) 231,230,230
  230 IF(1-N) 231,2230,2230
C     CLASS INTERVAL ESTIMATED BY GETTING  EXTREMES OF A SAMPLE OF 25 APERTURE
 2230 BTOP=-1.0E20
      BBOT= 1.0E20
      MUD=-1
      DO 2909 I=1,25
      CALL APER
      BTOP=MAX1F(BTOP,B)
 2909 BBOT=MIN1F(BBOT,B)
      BCLASS=(BTOP-BBOT)/50.0
      PRINT 2979, BCLASS,BTOP,BBOT,B
 2979 FORMAT( 11HC INTERVAL=  4E12.5)
C     CLASS FREQUENCIES ZEROED
      DO 232 N=1,NMAX
      DO 232 LM=1,50
  232 MPTS(LM,N)=0
      BSTOP=BBOT-BCLASS/2.0
C     COUNT FREQUENCIES IN CLASSES AND ADD EACH SOLUTION
  231 BEND=BSTOP
      LM=1
      IF(MM) 2110,2110,2118
 2118 DO 285 LL=1,MM
```

```
      IF(Z(LL)-BEND ) 280,281,281
  281 LM=LM+1
      BEND=BEND+BCLASS
  280 MPTS(LM,N)=MPTS(LM,N)+1
  285 CONTINUE
C CLASSES AND FREQUENCIES PRINTED OUT FOR LAST SAMPLE ONLY
      IF (L-49) 233,234,234
  234 BEND=BSTOP
C CUMULATIVE APERTURES DISTRIBUTION MODE FOUND
      MAXDEN=0
      DO 236 LM=1,50
C CENTER ABCISA ON MIDDLE OF INTERVAL
      ABCISA=BEND-BCLASS/2.0
      PRINT 288, ABCISA,MPTS(LM,N)
  288 FORMAT(E20.5,I10)
      IF (MPTS(LM,N) -MAXDEN)  236,237,237
  237 MAXDEN=MPTS(LM,N)
      BMODE=ABCISA
  236 BEND=BEND+BCLASS
  233 COSSUM=COSINV(N)/ELEM
C CONSIDER ONLY 49TH PRINTING OF MODE TO BE CORRECT
 2110 PRINT 658
  658 FORMAT(37H0 PROPERTIES OF APERTURE DISTRIBUTION   )
      PRINT 657,MM,  STR,COSSUM,BAVG,BGEOM,BHARM,BMED,BMODE,AVCUBE
  657 FORMAT(89H0  ELEMENTS, STRENGTH, (1/C)AV,ARITH MEAN,GEOM MEAN,HARM
     1 MEAN, MEDIAN,   MODE, AVG BCUBE  /I10,7F10.6,1PE13.3)
  295 CONTINUE
C CORRECTS TENSOR ELEMENTS, WEIGHTING THEM ACCORDING TO JOINT DENSITY
      DO 204 I=1,3
      DO 204 J=1,3
  204 H(I,J)=P(I,J)/DELTA
      CALL OUTPUT
C COMPUTE AND PRINT OUT POROSITY THIS SAMPLE, VOID VOL/TOTAL VOL
      PORUS=PORUS/DELTA
      PRINT 2599, PORUS
 2599 FORMAT(23H0 POROSITY OF SAMPLE =  F10.5//)
      RETURN
      END


*     LIST
*     LABEL
*     FORTRAN
      SUBROUTINE NUMBER
      DIMENSION M(5),CT1(5),CT2(5),CT3(5),AK(5),STD(5),CENTEN(5),
     1P(3,3),E(3,3),H(3,3),U(3,3),HH(3,50),X(3),IU(3),UU(3,3,50),
     2TINSO(50),AVB(5),SUMCOS(5),HARM(5),GEOM(5),Z(500),A(3),C(3),
     3AA(15),BB(4),CC(10),DD(12),EE(2),FF(4),GG(12),DDD(12),V(4),W(8),
     4WW(2),YF(15),YV(49),PP(2),COSINV(5),OR(3),CUBE(5),MPTS(50,5),
     5TR(3,3),AX(3,3),QA(50,3),CA(11),GA(12),DA(12),PR(50,5),RA(11),
     6CP(4),ORHOL(3,3),FA(4),UC(3,3),YT(3),AL(3),CK(3)
      COMMON M,CT1,CT2,CT3,AK,STD,CENTEN,AVB,SUMCOS,HARM,GEOM,DELTA,
     1L,P,E,A,C,H,HH,U,UU,AA,BB,CC,DD,EE,FF,GG,TINSO,V,W,WW,DDD,NMAX,YF,
     2YV,N,NON,B,Z,PP,COSINV,EN,WA,DIAM,HEAD,CUBE,MPTS,OR,CK,TR,AX,
     3QA,CA,GA,DA,MM,PR,RA,CP,FA,ORHOL,PORUS
```

```
      IF (NON) 2002,2002,2000
C     CONSIDER M(N) AS 10 TIMES THE POISSON EXPECTATION FOR THE NTH SET
C     CALCULATE A SUFFICIENTLY LARGE TABLE OF PROBABILITIES OF OBTAINING
C     CERTAIN INTEGRAL NUMBERS OF JOINTS IN A SAMPLE
 2000 IMAX=(3*M(N))/10+5
      UM=M(N)
      UM=UM/10.0
      PRINT 2310,IMAX,UM
 2310 FORMAT(I40,F10.5)
C     CLASS ZERO FREQUENCY IS GIVEN BY INDEX 1, CUMULATIVE FREQUENCY 1 BY
C     CLASS INDEX 2, 2 BY 3, ETC.
      POIS=EXPF(-UM)
      PR(1,N)=POIS
      DO 2001 I=2,IMAX
      AI=I-1
      POIS=POIS*UM/AI
 2001 PR(I,N)=PR(I-1,N)+POIS
      RETURN
C     CALL A RANDOM UNIFORM NUMBER GENERATOR TO SET A PROBABILITY LEVEL
 2002 PROB=UNIRAN(X1)
C     CLOSEST CUMULATIVE PROBABILITY IN TABLE PR(I,N) DEFINES SAMPLE SIZE.
      I=1
      DIFF1=PROB
 2101 DIFF2=ABSF(PROB-PR(I,N))
      IF (DIFF2-DIFF1) 2400,2400,2102
 2400 DIFF1=DIFF2
      I=I+1
      GO TO 2101
 2102 MM=I-1
      RETURN
      END



*     LIST
*     LABEL
*     FORTRAN
      SUBROUTINE VECTOR
      DIMENSION M(5),CT1(5),CT2(5),CT3(5),AK(5),STD(5),CENTEN(5),
     1P(3,3),E(3,3),H(3,3),U(3,3),HH(3,50),X(3),IQ(3),UU(3,3,50),
     2TINSQ(50),AVB(5),SUMCOS(5),HARM(5),GEOM(5),Z(500),A(3),C(3),
     3AA(15),BB(4),CC(10),DD(12),EE(2),FF(4),GG(12),DDD(12),V(4),W(8),
     4WW(2),YF(15),YV(49),PP(2),COSINV(5),OR(3),CUBE(5),MPTS(50,5),
     5TR(3,3),AX(3,3),QA(50,3),CA(11),GA(12),DA(12),PR(50,5),RA(11),
     6CP(4),ORHOL(3,3),FA(4),UC(3,3),YT(3),AL(3),CK(3)
      COMMON M,CT1,CT2,CT3,AK,STD,CENTEN,AVB,SUMCOS,HARM,GEOM,DELTA,
     1L,P,E,A,C,H,HH,U,UU,AA,BB,CC,DD,EE,FF,GG,TINSQ,V,W,WW,DDD,NMAX,YF,
     2YV,N,NON,B,Z,PP,COSINV,EN,WA,DIAM,HEAD,CUBE,MPTS,OR,CK,TR,AX,
     3QA,CA,GA,DA,MM,PR,RA,CP,FA,ORHOL,PORUS
      IF (NON) 460,401,401
C     COMPUTE MATRIX OF TRANSFORMATION BETWEEN ZENITH AND
C     CENTRAL TENDENCY OF SET.
  401 DENOM=SQRTF(1.0-CT2(N)*CT2(N))
      E(1,1)=CT1(N)*CT2(N)/DENOM
      E(1,2)=-DENOM
      E(1,3)=CT2(N)*CT3(N)/DENOM
```

```
      E(2,1)=CT1(N)
      E(2,2)=CT2(N)
      E(2,3)=CT3(N)
      E(3,1)=CT3(N)/DENOM
      E(3,3)=-CT1(N)/DENOM
CCNSTANTS OF DISPERSION COMPUTED.
      F1=EXPF(AK(N))
      G1=F1-EXPF(-AK(N))
      NON=NON-1
      RETURN
CALL A UNIFORM RANDOM NUMBER GENERATOR TO DEFINE A PROBABILITY, THEN
CCMPUTE COSINE THETA DEFINING A CIRCLE ABOUT THE CENTRAL TENDENCY AC-
CCRDING TO AK, FISHER'S COEFFICIENT OF DISPERSION OF VECTORS ON A SPHERE
CALL AGAIN A RANDCM UNIFORM GENERATOR TO POSITION THE VECTOR ON THE
CIRCLE.
  460 H1=F1-UNIRAN(X1)*G1
      COSTH=LOGF(H1)/AK(N)
      EN=ABSF(COSTH)
      SUMCOS(N)=SUMCOS(N)+COSTH
      COSINV(N)=COSINV(N)+1.0/COSTH
      SINTH=SQRTF(1.0-COSTH*COSTH)
      PHI=UNIRAN(X1)*6.28318
      A(1)=SINTH*SINF(PHI)
      A(2)=COSTH
      A(3)=SINTH*COSF(PHI)
      C(1)=E(1,1)*A(1)+E(2,1)*A(2)+E(3,1)*A(3)
      C(2)=E(1,2)*A(1)+E(2,2)*A(2)
      C(3)=E(1,3)*A(1)+E(2,3)*A(2)+E(3,3)*A(3)
      IF(C(3)) 221,224,224
  221 DO 222 J=1,3
  222 C(J)=-C(J)
  224 RETURN
      END



*     LIST
*     LABEL
*     FORTRAN
      SUBROUTINE APER
      DIMENSION M(5),CT1(5),CT2(5),CT3(5),AK(5),STD(5),CENTEN(5),
     1P(3,3),E(3,3),H(3,3),U(3,3),HH(3,50),X(3),IQ(3),UU(3,3,50),
     2TINSQ(50),AVB(5),SUMCOS(5),HARM(5),GEOM(5),Z(500),A(3),C(3),
     3AA(15),BB(4),CC(10),DD(12),EE(2),FF(4),GG(12),DDD(12),V(4),W(8),
     4WW(2),YF(15),YV(49),PP(2),COSINV(5),OR(3),CUBE(5),MPTS(50,5),
     5TR(3,3),AX(3,3),QA(50,3),CA(11),GA(12),DA(12),PR(50,5),RA(11),
     6CP(4),ORHOL(3,3),FA(4),UC(3,3),YT(3),AL(3),CK(3)
      COMMON M,CT1,CT2,CT3,AK,STD,CENTEN,AVB,SUMCOS,HARM,GEOM,DELTA,
     1L,P,E,A,C,H,HH,U,UU,AA,BB,CC,DD,EE,FF,GG,TINSQ,V,W,WW,DDD,NMAX,YF,
     2YV,N,NON,B,Z,PP,COSINV,EN,WA,DIAM,HEAD,CUBE,MPTS,OR,CK,TR,AX,
     3QA,CA,GA,DA,MM,PR,RA,CP,FA,ORHOL,PORUS
CASE ONE, ABSOLUTE VALUE OF NORMAL DISTRIBUTION OF APERTURES
      B=ABSF(STD(N)*RANDEV(X1)+CENTEN(N))
CALL RANDOM NORMAL NUMBER GENERATOR AND MODIFY IT ACCORDING TO THE
CELECTED PARAMETERS OF THE SET.
```

```
 3001 RETURN
      END
```

CAN SUBSTITUTE ALTERNATIVE STATEMENTS AS FOLLOWS

CASE TWO, LOGNORMAL DISTRIBUTION OF APERTURES

```
      B=CENTEN(N)*EXPF(1.414*STD(N)*RANDEV(X1))
```

CASE THREE, EXPONENTIAL DISTRIBUTION OF APERTURES.

```
 3000 B=CENTEN(N)*EXPF((2.0*UNIRAN(X1)-1.0)*STD(N)/2.0)
```

CASE FOUR, LINEAR DISTRIBUTION OF APERTURES.

```
 3000 B=3.0*CENTEN(N)*(1.0-SQRTF(1.0-UNIRAN(X1)))
      IF (B-1.0) 3001,3001,3000
```

```
*     LIST
*     LABEL
*     FORTRAN
      SUBROUTINE PIEZO
C     COMPUTES THE DISCHARGE OF A PIEZOMETER OF ORIENTATION OR(I), LENGTH WA,
C     SITUATED BELOW THE WATER TABLE OPERATING UNDER HEAD. ANSWER IN GALLONS
C     PER DAY. THE SHAPE FACTOR IS OBTAINED FROM THE PRINCIPAL AXES AND THE
C     CONDUCTIVITY OF THE FICTITIOUS ISOTROPIC MEDIUM DERIVED FROM THE SAMPLE.
      DIMENSION M(5),CT1(5),CT2(5),CT3(5),AK(5),STD(5),CENTEN(5),
     1P(3,3),E(3,3),H(3,3),U(3,3),HH(3,50),X(3),IQ(3),UU(3,3,50),
     2TINSQ(50),AVB(5),SUMCOS(5),HARM(5),GEOM(5),Z(500),A(3),C(3),
     3AA(15),BB(4),CC(10),DD(12),EE(2),FF(4),GG(12),DDD(12),V(4),W(8),
     4WW(2),YF(15),YV(49),PP(2),COSINV(5),OR(3),CUBE(5),MPTS(50,5),
     5TR(3,3),AX(3,3),QA(50,3),CA(11),GA(12),DA(12),PR(50,5),RA(11),
     6CP(4),ORHOL(3,3),FA(4),UC(3,3),YT(3),AL(3),CK(3)
      COMMON M,CT1,CT2,CT3,AK,STD,CENTEN,AVB,SUMCOS,HARM,GEOM,DELTA,
     1L,P,E,A,C,H,HH,U,UU,AA,BB,CC,DD,EE,FF,GG,TINSQ,V,W,WW,DDD,NMAX,YF,
     2YV,N,NON,B,Z,PP,COSINV,EN,WA,DIAM,HEAD,CUBE,MPTS,OR,CK,TR,AX,
     3QA,CA,GA,DA,MM,PR,RA,CP,FA,ORHOL,PORUS
      DO 1105 I=1,3
 1105 CK(I)=HH(I,L)*1844.0
      DO 1159 MO=1,3
      IF (PORUS) 1192,1192,1193
 1192 SA=0.0
      GO TO 1159
 1193 DO 1158 JO=1,3
```

```
 1158 OR(JO)=ORHOL(MO,JO)
C CALCULATE ELEMENTS OF TRANSFORMATION MATRIX
      DENOM=SQRTF(1.0-OR(2)*OR(2))
      TR(1,1)=(U(1,1)*OR(1)+U(3,1)*OR(3))*OR(2)/DENOM-U(2,1)*DENOM
      TR(2,1)=(U(1,1)*OR(3)-U(3,1)*OR(1))/DENOM
      TR(3,1)=U(1,1)*OR(1)+U(2,1)*OR(2)+U(3,1)*OR(3)
      TR(1,2)=(U(1,2)*OR(1)+U(3,2)*OR(3))*OR(2)/DENOM-U(2,2)*DENOM
      TR(2,2)=(U(1,2)*OR(3)-U(3,2)*OR(1))/DENOM
      TR(3,2)=U(1,2)*OR(1)+U(2,2)*OR(2)+U(3,2)*OR(3)
      TR(1,3)=(U(1,3)*OR(1)+U(3,3)*OR(3))*OR(2)/DENOM-U(2,3)*DENOM
      TR(2,3)=(U(1,3)*OR(3)-U(3,3)*OR(1))/DENOM
      TR(3,3)=U(1,3)*OR(1)+U(2,3)*OR(2)+U(3,3)*OR(3)
C CALCULATE COMPONENTS OF PACKER TEST LENGTH , FICTITIOUS ISOTROPIC MEDIU
      YT(1)= (CK(2)/CK(1))**0.25*WA*ABSF(TR(3,1))
      YT(2)= (CK(1)/CK(2))**0.25*WA*ABSF(TR(3,2))
      YT(3)= (CK(1)*CK(2))**0.25/SQRTF(CK(3))*WA*ABSF(TR(3,3))
C COMPOSE RESULTANT LENGTH
      WI=SQRTF(YT(1)*YT(1)+YT(2)*YT(2)+YT(3)*YT(3))
      PRINT 75, WI
   75 FORMAT(F60.5)
C COSINES OF THE CYLINDRICAL AXIS ARE
      YT(1)=YT(1)/WI
      YT(2)=YT(2)/WI
      YT(3)=YT(3)/WI
C COEFFICIENT MATRIX OF ELLIPTIC SECTION IS CALCULATED
      ARSQ=(DIAM/2.0)**2
      AX(1,1)=(TR(1,1)**2+TR(2,1)**2)/ARSQ*SQRTF(CK(1)/CK(2))
      AX(1,2)=(TR(1,1)*TR(1,2)+TR(2,1)*TR(2,2))/ARSQ
      AX(1,3)=(TR(1,1)*TR(1,3)+TR(2,1)*TR(2,3))/ARSQ *SQRTF(CK(3)/CK(2))
      AX(2,2)=(TR(1,2)**2+TR(2,2)**2)/ARSQ*SQRTF(CK(2)/CK(1))
      AX(2,3)=(TR(1,2)*TR(1,3)+TR(2,2)*TR(2,3))/ARSQ *SQRTF(CK(3)/CK(1))
      AX(3,3)=(TR(1,3)**2+TR(2,3)**2)/ARSQ*CK(3)/SQRTF(CK(1)*CK(2))
C COEFFICIENTS OF ROTATED ELLIPSE COMPUTED
      IEGEN=0
      N=3
      CALL HDIAG(AX,N,IEGEN,UC,NR)
      PRINT 70,((AX(I,J),J=1,3),I=1,3)
      PRINT 70,((UC(J,I),J=1,3),I=1,3)
   70 FORMAT(9H0 ELLIPSE   1P9E12.4)
      DO 1106 LA=1,3
C CLEAR AXES OF THE RIGHT SECTION ELLIPSE
      AL(LA)=0.0
C COMPUTE NON -ZERO AXES, AL, OF OBLIQUE ELLIPSE
      IF(AX(LA,LA)-0.01)1106,1106,1104
 1104 AL(LA)=SQRTF(1.0/AX(LA,LA))
C COMPUTE  AXES OF DIRECTRIX, AL, PROJECTING OBLIQUE AXES TO  A PLANE
C CROSSING THE CYLINDER AT A RIGHT ANGLE
      AL(LA)=AL(LA)*SQRTF(1.0-(YT(1)*UC(1,LA)+YT(2)*UC(2,LA)+YT(3)*
     1UC(3,LA))**2)
 1106 CONTINUE
C COMPUTE DIAMETER OF CIRCLE OF EQUIVALENT AREA
      DO 1178 LK=1,2
      LP1=LK+1
      DO 1178 MK=LP1,3
      IF(AL(LK)-AL(MK)) 1178,1178,1177
 1177 TEMP=AL(LK)
```

```
      AL(LK)=AL(MK)
      AL(MK)=TEMP
 1178 CONTINUE
      DISU=2.0*SQRTF(AL(2)*AL(3))
CCRNWELL-GLOVER SHAPE FACTOR IS COMPUTED
      SA=6.2832*WI/LOGF(2.0*WI/DISO)
      PRINT  76,DISO,SA
   76 FORMAT(2F30.5)
CCMPUTE DISCHARGE
 1159 QA(L,MO)=SA*HEAD*SQRTF(CK(3)*SQRTF(CK(1)*CK(2)))
      PRINT 77, (CA(L,MO),MO=1,3)
   77 FORMAT(3F20.5)
      RETURN
      END


*     LIST
*     LABEL
*     FORTRAN
      SUBROUTINE CUTPUT
      DIMENSION M(5),CT1(5),CT2(5),CT3(5),AK(5),STD(5),CENTEN(5),
     1P(3,3),E(3,3),H(3,3),U(3,3),HH(3,50),X(3),IQ(3),UU(3,3,50),
     2TINSQ(50),AVB(5),SUMCOS(5),HARM(5),GEOM(5),Z(500),A(3),C(3),
     3AA(15),BB(4),CC(10),DD(12),EE(2),FF(4),GG(12),DDD(12),V(4),W(8),
     4WW(2),YF(15),YV(49),PP(2),COSINV(5),OR(3),CUBE(5),MPTS(50,5),
     5TR(3,3),AX(3,3),QA(50,3),CA(11),GA(12),DA(12),PR(50,5),RA(11),
     6CP(4),ORHOL(3,3),FA(4),UC(3,3),YT(3),AL(3),CK(3)
      COMMON M,CT1,CT2,CT3,AK,STD,CENTEN,AVB,SUMCOS,HARM,GEOM,DELTA,
     1L,P,E,A,C,H,HH,U,UU,AA,BB,CC,DD,EE,FF,GG,TINSQ,V,W,WW,DDD,NMAX,YF,
     2YV,N,NUN,B,Z,PP,COSINV,EN,WA,DIAM,HEAD,CUBE,MPTS,OR,CK,TR,AX,
     3QA,CA,GA,DA,MM,PR,RA,CP,FA,ORHOL,PORUS
  758 N=3
      IEGEN=0
CCNDUCTIVITY MATRIX IS DIAGONALIZED TO GET THE PRINCIPAL
CCNDUCTIVITIES AND AXES OF THE SYSTEM CONDUCTIVITY TENSOR
      CALL HDIAG(H,N,IEGEN,U,NR)
      PRINT 817,((H(I,J),J=1,3),I=1,3)
      PRINT 817,((U(J,I),J=1,3),I=1,3)
  817 FORMAT(1P9E12.4)
CCORDINATES OF AXES PUT ON UPPER HEMISPHERE
      DO 765 I=1,3
      IF(U(3,I)) 760,765,765
  760 DO 762 J=1,3
  762 U(J,I)=-U(J,I)
  765 CONTINUE
CAUSE SOLUTION TO BE STORED FOR LATER PLOTTING.
  780 DO 783 I=1,3
      HH(I,L)=H(I,I)
      DO 783 J=1,3
  783 UU(J,I,L)=U(J,I)
      HMIN=MIN1F(HH(1,L),HH(2,L),HH(3,L))
      HMAX=MAX1F(HH(1,L),HH(2,L),HH(3,L))
      TINSQ(L)=HMIN/HMAX
      RETURN
      END
```

```
*       LIST
*       LABEL
*       FORTRAN
        SUBROUTINE STEREO
CALCULATES COORDINATES AND PLOTS THE STEREOGRAPHIC PROJECTION OF M VE
CTORS ON THE UPPER HEMISPHERE OF AN 18 CM NET OVERLAY
        DIMENSION M(5),CT1(5),CT2(5),CT3(5),AK(5),STD(5),CENTEN(5),
       1P(3,3),E(3,3),H(3,3),U(3,3),HH(3,50),X(3),IO(3),UU(3,3,50),
       2TINSQ(50),AVB(5),SUMCOS(5),HARM(5),GFOM(5),Z(500),A(3),C(3),
       3AA(15),BB(4),CC(10),DD(12),EE(2),FF(4),GG(12),DDD(12),V(4),W(8),
       4WW(2),YF(15),YV(49),PP(2),COSINV(5),OR(3),CUBE(5),MPTS(50,5),
       5TR(3,3),AX(3,3),QA(50,3),CA(11),GA(12),DA(12),PR(50,5),RA(11),
       6CP(4),ORHOL(3,3),FA(4),UC(3,3),YT(3),AL(3),CK(3)
        COMMON M,CT1,CT2,CT3,AK,STD,CENTEN,AVB,SUMCOS,HARM,GFOM,DELTA,
       1L,P,E,A,C,H,HH,U,UU,AA,BB,CC,DD,EE,FF,GG,TINSQ,V,W,WW,DDD,NMAX,YF,
       2YV,N,NOH,R,Z,PP,COSINV,EN,WA,DIAM,HEAD,CUBE,MPTS,OR,CK,TR,AX,
       3QA,CA,GA,DA,MM,PR,RA,CP,FA,URHOL,PORUS
        V(1) =3H1HN
        V(2) =3H1HS
        V(3) =3H1HW
        V(4) =3H1HE
        WW(1)=6H9HFIGU
        WW(2)=6HRE  .
        W(1)=6H42HSTE
        W(2)=6HREOGRA
        W(3)=6HPHIC P
        W(4)=6HROJECT
        W(5)=6HION, U
        W(6)=6HPPER H
        W(7)=6HEMISPH
        W(8)=3HERE
   11 CALL GRAPH (10.0,7.8,1.1)
        READ 7, (DDD(J),J=1,12)
    7 FORMAT(12A6)
COORDINATES AND LETTERING DONE.
        CALL XLN (0.23,0.37,3.9,0.0)
        CALL XLN (3.8,4.0,3.9,0.0)
        CALL XLN (7.43,7.57,3.9,0.0)
        CALL YLN (0.23,0.37,3.9,0.0)
        CALL YLN (3.8,4.0,3.9,0.0)
        CALL YLN (7.43,7.57,3.9,0.0)
        CALL LTR (0.12,3.80,2,1,V(1))
        CALL LTR (7.83,3.80,2,1,V(2))
        CALL LTR (4.00,0.02,2,1,V(3))
        CALL LTR (4.00,7.68,2,1,V(4))
        CALL LTR(8.2,0.0,2,1,WW)
        CALL LTR(8.6,0.0,2,1,W)
        CALL LTR (9.0,0.0,2,1,DDD)
        CALL CURVE (2,10,0,0,-3.9,10.0,-3.9,10.0,1)
        THETA=0.0
COMPUTE 360 DEGREE-POINTS ON AN 18 CM CIRCLE, MARKING EVERY 10TH DEGREE
   15 PHI=THETA/57.295
```

```
      XX=3.53*COSF(PHI)
      YY=3.53*SINF(PHI)
      CALL PLOTPT(XX,YY)
      THETA =THETA + 1.0
      IF (THETA- 360.0)15,15,999
  999 DO 10 I=1,3
CHOSEN SYMBOLS ARE DIAMONDS FOR K11 AXIS, CIRCLES FOR K22 AXIS, AND
CROSSES FOR THE K33 AXIS.
      IF(I-2) 16,19,20
   16 CALL CURVE (3,1,1,0,-3.9,10.0,-3.9,10.0,1)
      GO TO 22
   19 CALL CURVE (5,1,1,0,-3.9,10.0,-3.9,10.0,1)
      GO TO 22
   20 CALL CURVE (7,1,1,0,-3.9,10.0,-3.9,10.0,1)
   22 DO 10 L=1,49
COMPUTE X-Y COORDINATES FROM DIRECTION COSINES.
      R=3.53*SQRTF((1.0-UU(3,I,L))/(1.0+UU(3,I,L)))
      S=UU(2,I,L)/UU(1,I,L)
      XX=R/SQRTF(1.0+S*S)
      IF(UU(1,I,L))    12,13,13
   12 XX=-XX
   13 YY=XX*S
   10 CALL PLOTPT(XX,YY)
      ENDFILE6
      ENDFILE6
      RETURN
      END
*     LIST
*     LABEL
*     FORTRAN
      SUBROUTINE ECPOR
      DIMENSION M(5),CT1(5),CT2(5),CT3(5),AK(5),STD(5),CENTEN(5),
     1P(3,3),L(3,3),H(3,3),U(3,3),HH(3,50),X(3),IJ(3),UU(3,3,50),
     2TINSQ(50),AVB(5),SUMCOS(5),HARM(5),GEOM(5),Z(500),A(3),C(3),
     3AA(15),BB(4),CC(10),DD(12),EE(2),FF(4),GG(12),DDD(12),V(4),W(8),
     4WW(2),YF(15),YV(49),PP(2),COSINV(5),OR(3),CUBE(5),MPTS(50,5),
     5TR(3,3),AX(3,3),JA(50,3),CA(11),GA(12),DA(12),PR(50,5),RA(11),
     6CP(4),ORHOL(3,3),FA(4),UC(3,3),YT(3),AL(3),CK(3),PORAT(50)
      COMMON M,CT1,CT2,CT3,AK,STD,CENTEN,AVB,SUMCOS,HARM,GEOM,DELTA,
     1L,P,E,A,C,H,HH,U,UU,AA,BB,CC,DD,EE,FF,GG,TINSQ,V,W,WW,DDD,NMAX,YF,
     2YV,N,NON,B,Z,PP,COSINV,EN,WA,DIAM,HEAD,CUBE,MPTS,OR,CK,TR,AX,
     3OA,CA,GA,DA,MM,PR,RA,CP,FA,ORHOL,PORUS,PORTOT,PORAT,
     4H1ULT,H2ULT,H3ULT
CCMPUTES POROSITY FROM THE PERMEABILITY ASSUMING THAT THERE ARE
CCNDUCTORS OF EACH SET EQUAL IN NUMBER TO THE  POISSON EXPECTATION
CCRRESPONDING TO M(M)/10 AND ALL WITH THE SAME APERTURE.
      IF (PORUS) 9801,9801,9809
CCEFFICIENT RATIOS BUILT IN FOR SPECIFIC DISPERSION KF= 20
 9809 CMAX1=0.9563
      CMIN2=0.0975
      COREF= 1.061
CENTRAL TENDENCY OF ONE SET AT A TIME ROTATED TO COORDINATES ALONG PRIN
CIPAL AXES
      CTN1=U(1,1)*CT1(1)+U(2,1)*CT2(1)+U(3,1)*CT3(1)
      CTN2=U(1,2)*CT1(1)+U(2,2)*CT2(1)+U(3,2)*CT3(1)
      A1C1=CMAX1+(CMIN2-CMAX1)*CTN1*CTN1
```

```
      A1C2=CMAX1+(CMIN2-CMAX1)*CTN2*CTN2
      CTN1=U(1,1)*CT1(2)+U(2,1)*CT2(2)+U(3,1)*CT3(2)
      CTN2=U(1,2)*CT1(2)+U(2,2)*CT2(2)+U(3,2)*CT3(2)
      A2C1=CMAX1+(CMIN2-CMAX1)*CTN1*CTN1
      A2C2=CMAX1+(CMIN2-CMAX1)*CTN2*CTN2
CCMPUTE PERMEABILITY OF AN EQUIVALENT PARALLEL SET , KP.
      P2K=(A2C1*H(1,1)-A1C1*H(2,2))/(A2C1*A1C2-A1C1*A2C2)
      P1K=(H(1,1)- A1C2*P2K)/A2C1
      P1K=1.0E-6*P1K
      P2K=1.0E-6*P2K
CCMPUTE POROSITY CF  DISPERSED SETS HAVING UNIFORM APERTURE.
      GMN1=M(1)
      GMN2=M(2)
      POREQ=CUREF*(3.0*P1K)**0.333*(0.2*GMN1 /DELTA)**0.667+
     1       CUREF*(3.0*P2K)**0.333*(0.2*GMN2 /DELTA)**0.667
      PORAT(L)=POREQ/PORUS
      PRINT 9805,POREQ,PORAT(L)
 9805 FORMAT(56H0 POROSITY EQUIVALENT TO PERM, RATIO TO TRUE POROSITY =
     1 2F10.5)
      PORTOT=PORTOT+PORUS
 9801 RETURN
      END


*     LIST
*     LABEL
*     FORTRAN
      SUBROUTINE FREQPL
CUMULATIVE FREQUENCY CURVES PLOTTED FOR EACH PRINCIPAL CONDUCTIVITY
CAPTIONS AND LABELS STORED.
      DIMENSION M(5),CT1(5),CT2(5),CT3(5),AK(5),STD(5),CENTEN(5),
     1P(3,3),E(3,3),H(3,3),U(3,3),HH(3,50),X(3),IQ(3),UU(3,3,50),
     2TINSQ(50),AVB(5),SUMCOS(5),HARM(5),GEOM(5),Z(500),A(3),C(3),
     3AA(15),BB(4),CC(10),DD(12),EE(2),FF(4),GG(12),DDD(12),V(4),W(8),
     4WW(2),YF(15),YV(49),PP(2),COSINV(5),UR(3),CUBE(5),MPTS(50,5),
     5TR(3,3),AX(3,3),QA(50,3),CA(11),GA(12),DA(12),PR(50,5),RA(11),
     6CP(4),ORHOL(3,3),FA(4),UC(3,3),YT(3),AL(3),CK(3)
      COMMON M,CT1,CT2,CT3,AK,STD,CENTEN,AVB,SUMCOS,HARM,GEOM,DELTA,
     1L,P,E,A,C,H,HH,U,UU,AA,BB,CC,DD,EE,FF,GG,TINSQ,V,W,WW,DDD,NMAX,YF,
     2YV,N,NON,B,Z,PP,COSINV,EN,WA,DIAM,HEAD,CUBE,MPTS,QR,CK,TR,AX,
     3QA,CA,GA,DA,MM,PR,RA,CP,FA,ORHOL,PORUS
      AA(1)=3H1H1
      AA(2)=3H1H2
      AA(3)=3H1H5
      AA(4)=4H2H10
      AA(5)=4H2H20
      AA(6)=4H2H30
      AA(7)=4H2H40
      AA(8)=4H2H50
      AA(9)=4H2H60
      AA(10)=4H2H70
      AA(11)=4H2H80
      AA(12)=4H2H90
      AA(13)=4H2H95
```

```
      AA(14)=4H2H98
      AA(15)=4H2H99
      BB(1)=6H18HCUM
      BB(2)=6HULATIV
      BB(3)=6HE PERC
      BB(4)=3HENT
      CC(1)=3H55H
      CC(2)=6HFIGURE
      CC(3)=6H    . P
      CC(4)=6HRINCIP
      CC(5)=6HAL PER
      CC(6)=6HMEABIL
      CC(7)=6HITIES,
      CC(8)=6H X 10
      CC(9)=6H CGS U
      CC(10)=4HNITS
      FF(1)=6H18HMAX
      FF(2)=6HIMUM A
      FF(3)=6HNISCTR
      FF(4)=3HOPY
      PP(1)=6H6H95 0
      PP(2)=2H/0
C COORDINATES AND LETTERING DONE, SCALES PLOTTED.
   26 CALL GRAPH(9.0,6.0,2.5)
      CALL FRAME(0.1,0.0)
      CALL XLN(0.4,9.0,2.57,0)
      CALL XLN(0.0,8.5,3.00,0.5)
      CALL XLN(0.4,9.0,3.43,0)
      CALL XLN(5.5,9.0,6.0,0.5)
      CALL XLN(9.0,0.0,0.0,-0.5)
      DO 310 J=1,15
  310 CALL XLN(0.0,0.1,YF(J),0)
      DO 311 J=1,15
  311 CALL XLN(8.9,9.0,YF(J),0)
      DO 21 J=1,15
      YY=YF(J)-0.05
   21 CALL LTR(-0.3,YY,1,0,AA(J))
      CALL LTR(-0.5,0.7,2,1,BB)
      CALL LTR(-1.3,-1.0,2,0,CC)
      CALL LTR(5.5,6.4,2,0,FF)
      CALL LTR(8.8,2.7,1,1,PP)
      READ 7,(GG(J),J=1,12)
      CALL LTR(-0.7,-1.4,2,0,GG)
      READ 7,(DD(J),J=1,12)
      CALL LTR(-0.6,-1.8,2,0,DD)
    7 FORMAT(12A6)
C CONDUCTIVITIES AND ANISOTROPIES ARRANGED IN ASCENDING ORDER.
      DO 32 I=1,3
      DO 32 L=1,48
      LP1=L+1
      DO 32 J=LP1,49
      IF(HH(I,L)-HH(I,J)) 32,32,38
   38 TEMP=HH(I,L)
      HH(I,L)=HH(I,J)
      HH(I,J)=TEMP
   32 CONTINUE
```

```
      DO 39 L=1,48
      LP1=L+1
      DO 39 J=LP1,49
      IF(TINSQ(L)-TINSQ(J)) 39,39,40
   40 TEMP=TINSQ(L)
      TINSQ(L)=TINSQ(J)
      TINSQ(J)=TEMP
   39 CONTINUE
C COMPUTE FACTOR TO MAKE PERMEABILITY CURVES FIT PLOT, POSITION CURVES.
      XMIN=MIN1F(HH(1,1),HH(2,1),HH(3,1))
   61 HP=1.0E-02
   62 HS=XMIN*HP
      IF(1.0E-38 -HS) 60,64,64
   60 IF(HS-1.0) 63,64,64
   63 HP=HP*10.0
      GO TO 62
   73 HP=HP/10.0
      HS=XMIN*HP
   64 XMAX=MAX1F(HH(1,49 ),HH(2,49 ),HH(3,49 ))
      HL=XMAX*HP
      IF(HL-HS-8.0) 65,65,73
   65 IF(HL-HS-0.8) 63,63,81
   81 IX=8.0/(HL-HS)
      GO TO (69,69,303,69,69,306,306,69,309,69),IX
  303 IX=2
      GO TO 69
  306 IX=5
      GO TO 69
  309 IX=8
   69 XI=IX
      HP=HP*XI
      PRINT 31,XMIN,XMAX,IX
   31 FORMAT(1P2E20.8,I4)
      IXMIN=XMIN*HP
      XMIN=IXMIN
C COMPUTE FACTOR TO MAKE ANISOTROPY CURVE FIT PLOT, POSITION CURVE.
      TP=0.1
   92 TDIF=TP*(TINSQ(49)-TINSQ(1))
      IF(TDIF-0.2) 93,94,94
   93 TP=TP*10.0
      GO TO 92
   94 TS=TINSQ(1)*TP
  101 ITS=TS
      TS=ITS
      PRINT 31, TINSQ(1),TINSQ(49),ITS
C CURVE IDENTITY ESTABLISHED
   42 DO 35 I=1,3
      HACT=HH(I,25)*1.0E-06
C COMPUTE AND PRINT 95 PERCENT CONFIDENCE INTERVAL ON MEDIAN AND MAX ANISC
      DEVH=(HH(I,32)-HH(I,17))*1.0E-06/2.0
      PRINT 350,DEVH
   35 PRINT 36,HP,HACT,I,TINSQ(25)
      DEVT=TINSQ(32)-TINSQ(17)/2.0
      PRINT 350, DEVT
   36 FORMAT(1P2E20.8,I4, E20.8)
  350 FORMAT(1PE20.6)
```

```
CUMULATIVE FREQUENCY CURVES PLOTTED
      DO 18 I=1,3
CHOSEN SYMBOLS ARE DIAMONDS FOR K11, CIRCLES K22, CROSSES K33.
      IF(I-2) 96,99,100
   96 CALL CURVE(3,1,1,0,0.00,9.0,0.0,6.0,1)
      GO TO 289
   99 CALL CURVE(5,1,1,0,0.00,9.0,C.0,6.0,1)
      GO TO 289
  100 CALL CURVE(7,1,1,0,0.00,9.0,0.0,6.0,1)
  289 DO 17 L=1,49
      XV=HH(I,L)*HP-XMIN
   17 CALL PLOTPT(XV,YV(L))
   18 CONTINUE
      CALL CURVE(1,1,1,0,0.0,9.0,0.0,6.C,1)
      DO 217 L=1,49
      XV=TINSQ(L)*TP-TS+6.0
  217 CALL PLOTPT(XV,YV(L))
      ENDFILE 6
      ENDFILE 6
      RETURN
      END


*     LIST
*     LABEL
*     FORTRAN
      SUBROUTINE PUMPLT
      DIMENSION M(5),CT1(5),CT2(5),CT3(5),AK(5),STD(5),CENTEN(5),
     1P(3,3),E(3,3),H(3,3),U(3,3),HH(3,50),X(3),IQ(3),UU(3,3,50),
     2TINSQ(50),AVB(5),SUMCOS(5),HARM(5),GEOM(5),Z(500),A(3),C(3),
     3AA(15),BB(4),CC(10),DD(12),EE(2),FF(4),GG(12),DDD(12),V(4),W(8),
     4WW(2),YF(15),YV(49),PP(2),COSINV(5),OR(3),CUBE(5),MPTS(50,5),
     5TR(3,3),AX(3,3),QA(50,3),CA(11),GA(12),DA(12),PR(50,5),RA(11),
     6CP(4),ORHOL(3,3),FA(4),UC(3,3),YT(3),AL(3),CK(3)
      COMMON M,CT1,CT2,CT3,AK,STD,CENTEN,AVB,SUMCOS,HARM,GEOM,DELTA,
     1L,P,E,A,C,H,HH,U,UU,AA,BB,CC,DD,EE,FF,GG,TINSQ,V,W,WW,DDD,NMAX,YF,
     2YV,N,NON,B,Z,PP,COSINV,EN,WA,DIAM,HEAD,CUBE,MPTS,OR,CK,TR,AX,
     3QA,CA,GA,DA,MM,PR,RA,CP,FA,ORHOL,PORUS
CUMULATIVE DISTRIBUTION OF PUMP TEST DISCHARGES PLOTTED
      RA(1)=3H1H0
      RA(2)=4H2H10
      RA(3)=4H2H20
      RA(4)=4H2H30
      RA(5)=4H2H40
      RA(6)=4H2H50
      RA(7)=4H2H60
      RA(8)=4H2H70
      RA(9)=4H2H80
      RA(10)=4H2H90
      RA(11)=5H3H100
      EE(1)=6H4H-SIG
      EE(2)=6H4H+SIG
      EE(3)=6H4HMEAN
      FA(1)=3H16H
      FA(2)=6H95 C/D
```

```
      FA(3)=6H CONFI
      FA(4)=1H-
      CP(1)=3H19H
      CP(2)=6H DENCE
      CP(3)=6H ON ME
      CP(4)=4HDIAN
      CA(1)=3H53H
      CA(2)=6HFIGURE
      CA(3)=6H    ST
      CA(4)=6HANDARD
      CA(5)=6HIZED P
      CA(6)=6HUMP TE
      CA(7)=6HST DIS
      CA(8)=6HCHARGE
      CA(9)=6H, GALL
      CA(10)=6HONS/DA
      CA(11)=1HY
CCOORDINATES AND LETTERING, SCALES DONE
      CALL GRAPH(9.0,6.0,2.5)
      CALL FRAME(0.1,0.6)
      CALL XLN(0.0,8.5,3.00,0.5)
      CALL XLN(9.0,0.0,0.0,-0.5)
      CALL XLN (0.0,9.0,2.16,0)
      CALL XLN (0.0,9.0,3.84,0)
      YY=-0.05
      DO 21 J=1,11
      CALL LTR(-0.3,YY,1,0,RA(J))
   21 YY=YY+0.6
      CALL LTR(-0.5,0.7,2,1,BB)
      CALL LTR(-1.3,-1.0,2,0,CA)
      CALL LTR (8.65,1.95,1,1,FA)
      CALL LTR (8.85,1.85,1,1,CP)
      READ 7,(GA(J),J=1,12)
      CALL LTR(-0.7,-1.4,2,0,GA)
      READ 7,(DA(J),J=1,12)
      CALL LTR(-0.6,-1.8,2,0,DA)
    7 FORMAT(12A6)
      DO 1017 MO=1,3
CCOMPUTED TEST DISCHARGES ORDERED, ASCENDING
      DO 1239 L=1,48
      LP1=L+1
      DO 1239 J=LP1,49
      IF(QA(L,MO)-QA(J,MO)) 1239,1239,1240
 1240 TEMP=QA(L,MO)
      QA(L,MO)=QA(J,MO)
      QA(J,MO)=TEMP
 1239 CONTINUE
CCUMULATIVE CURVE FITTED TO PLOT DIMENSIONS
      IF(MO-1) 1061,1061,1176
 1061 HP=1.0E-02
 1062 HS=QA(1,MO)*HP
      IF(1.0E-35-HS) 1060,1064,1064
 1060 IF(HS-1.0) 1063,1064,1064
 1063 HP=HP*10.0
      GO TO 1062
 1073 HP=HP/10.0
```

```
      HS=QA(1,MO)*HP
 1064 HL=QA(49,MO)*HP
      IF(HL-HS-8.C) 1065,1065,1073
 1065 IF(HL-HS-C.8) 1C63,1063,1081
 1081 IX=8.0/(HL-HS)
      GO TO (1069,1069,1303,1303,1069,1306,1306,1306,1306,1069),IX
 1303 IX=2
      GO TO 1069
 1306 IX=5
 1069 XI=IX
      HP=HP*XI
      PRINT 31, QA(1,MO),QA(49,MO),IX
   31 FORMAT(1P2E20.8,I4)
      IXQ=QA(1,MO)*HP
      QMIN=IXQ
CCMPUTE 95 PERCENT  CONFIDENCE INTERVAL ON MEDIAN Q
 1176 CONQ=(QA(32,MO)-QA(17,MO))/2.0
CCMPUTE MEAN
      QMEAN=QA(1,MO)
      DO 1070 K=2,49
 1070 QMEAN=QMEAN+QA(K,MO)
      QMEAN=QMEAN/49.0
CCMPUTE STANDARD DEVIATION OF DISCHARGE
      DEVQ=0.0
      DO 2500 K=1,49
 2500 DEVQ=DEVQ+(QMEAN-QA(K,MO))**2
      DEVQ=SQRTF(DEVQ/49.0)
      PRINT 1033
 1033 FORMAT(55H DISCHARGE MEAN, MEDIAN , STD DEV, 95 PERCENT ON MEDIAN)
      PRINT 1034, QMEAN, QA(25,MO),DEVQ,CONQ
 1034 FORMAT(//1P4E12.4)
CUMULATIVE FREQUENCY CURVES PLOTTED
CHOSEN AXES ARE DIAMONDS FOR K11 AXIS HOLE,, CIRCLES FOR K22 AXIS HOLE,
CROSSES FOR K33 AXIS HOLE
      IF(MO-2) 1171,1172,1173
 1171 CALL CURVE (7,1,0,0,0.0,9.0,0.0,6.0,1)
      GO TO 1174
 1172 CALL CURVE (5,1,0,0,0.0,9.0,0.0,6.0,1)
      GO TO 1174
 1173 CALL CURVE (3,1,0,0,0.0,9.0,0.0,6.0,1)
 1174 YZ=0.12
      DO 1177 L=1,49
      XQ=QA(L,MO)*HP-QMIN
      CALL PLOTPT (XQ,YZ)
 1177 YZ=YZ+0.12
CROSSES, CIRCLES AND DIAMONDS MARKED ON APPROPRIATE MEAN AND STD DEV LIN
      IF(MO-2) 1181,1182,1183
 1181 CALL CURVE(7,1,1,0,0.0,9.0,0.0,6.0,1)
      GO TO 1184
 1182 CALL CURVE(5,1,1,0,0.0,9.0,0.0,6.0,1)
      GO TO 1184
 1183 CALL CURVE(3,1,1,0,0.0,9.0,0.0,6.0,1)
 1184 XMEAN=QMEAN*HP-QMIN
      XSIGMM=(QMEAN-DEVQ)*HP-QMIN
      XSIGPM=(QMEAN+DEVQ)*HP-QMIN
      IF (XSIGMM) 2517,2517,2518
```

```
 2518 CALL YLN(5.0,5.3,XSIGMM,0)
      CALL PLOTPT(XSIGMM,5.15)
      XSIGMM=XSIGMM+0.05
      CALL LTR (XSIGMM,5.35,1,1,EE(1))
 2517 CALL YLN (0.7,1.0,XSIGPM,0)
      CALL YLN(0.7,1.0,XMEAN,0)
      CALL PLOTPT(XSIGPM,0.85)
      CALL PLOTPT(XMEAN, 0.85)
      XMEAN=XMEAN+0.05
      XSIGPM=XSIGPM+0.05
      CALL LTR (XSIGPM,0.20,1,1,EE(2))
      CALL LTR(XMEAN, 0.20,1,1,EE(3))
 1017 CONTINUE
      ENDFILE6
      ENDFILE6
      RETURN
      END


*     LIST
*     LABEL
*     FORTRAN
      SUBROUTINE  POREQ
      DIMENSION M(5),CT1(5),CT2(5),CT3(5),AK(5),STD(5),CENTEN(5),
     1P(3,3),E(3,3),H(3,3),U(3,3),HH(3,50),X(3),IQ(3),UU(3,3,50),
     2TINSQ(50),AVB(5),SUMCOS(5),HARM(5),GEOM(5),Z(500),A(3),C(3),
     3AA(15),BB(4),CC(10),DD(12),EE(2),FF(4),GG(12),DDD(12),V(4),W(8),
     4WW(2),YF(15),YV(49),PP(2),COSINV(5),OR(3),CUBE(5),MPTS(50,5),
     5TR(3,3),AX(3,3),QA(50,3),CA(11),GA(12),DA(12),PR(50,5),RA(11),
     6CP(4),ORHOL(3,3),FA(4),UC(3,3),YT(3),AL(3),CK(3),PORAT(50)
      COMMON M,CT1,CT2,CT3,AK,STD,CENTEN,AVB,SUMCOS,HARM,GEOM,DELTA,
     1L,P,E,A,C,H,HH,U,UU,AA,BB,CC,DD,EE,FF,GG,TINSQ,V,W,WW,DDD,NMAX,YF,
     2YV,N,NON,B,Z,PP,COSINV,CN,WA,DIAM,HEAD,CUBE,MPTS,OR,CK,TR,AK,
     3QA,CA,GA,DA,MM,PR,RA,CP,FA,ORHOL,PORUS,PORTOT,PORAT,
     4H1ULT,H2ULT,H3ULT
CCMPUTES POROSITY FROM THE PERMEABILITY ASSUMING THAT THERE ARE
CCNDUCTORS OF EACH SET EQUAL IN NUMBER TO THE  POISSON EXPECTATIO
CCRRESPONDING TO M(N)/10 AND ALL WITH THE SAME APERTURE.
      IF(PORUS) 8801,8801,8809
CCEFFICIENT RATIOS BUILT IN FOR SPECIFIC DISPERSION KF= 20
 8809 CMAX1=0.9560
      CMIN2=0.0975
      COREF= 1.061
CENTRAL TENDENCY OF ONE SET AT A TIME ROTATED TO COORDINATES ALONG PRIN
CIPAL AXES
      CTN1=ORHOL(3,1)*CT1(1)+ORHOL(3,2)*CT2(1)+ORHOL(3,3)*CT3(1)
      CTN2=ORHOL(2,1)*CT1(1)+ORHOL(2,2)*CT2(1)+ORHOL(2,3)*CT3(1)
      A1C1=CMAX1+(CMIN2-CMAX1)*CTN1*CTN1
      A1C2=CMAX1+(CMIN2-CMAX1)*CTN2*CTN2
      CTN1=ORHOL(3,1)*CT1(2)+ORHOL(3,2)*CT2(2)+ORHOL(3,3)*CT3(2)
      CTN2=ORHOL(2,1)*CT1(2)+ORHOL(2,2)*CT2(2)+ORHOL(2,3)*CT3(2)
      A2C1=CMAX1+(CMIN2-CMAX1)*CTN1*CTN1
      A2C2=CMAX1+(CMIN2-CMAX1)*CTN2*CTN2
CCMPUTE PERMEABILITY OF AN EQUIVALENT PARALLEL SET , KP.
      P2K=(A2C1*H1ULT -A1C1*H2ULT )/(A2C1*A1C2-A1C1*A2C2)
```

```
      P1K=(H1ULT - A1C2*P2K)/A2C1
      P1K=1.0E-6*P1K
      P2K=1.0E-6*P2K
CCMPUTE POROSITY CF  DISPERSED SETS HAVING UNIFORM APERTURE.
      GMN1=M(1)
      GMN2=M(2)
      POREQ=COREF*(3.0*P1K)**0.333*(0.2*GMN1 /DELTA)**0.667+
     1      COREF*(3.0*P2K)**0.333*(0.2*GMN2 /DELTA)**0.667
      PORAT(50)=POREQ/PORUS
      PRINT 8805,POREQ,PORAT(50)
 8805 FORMAT(56H0 POROSITY EQUIV MEDIUM  PERM, RATIO TO TRUE POROSITY =
     1 2F10.5)
 8801 RETURN
      END
```

Auxiliary Program VECGEN, Generating Vector Dispersions

Synthetic data are generated by VECGEN just as is done by VECTOR. First, VECGEN computes elements of a matrix to transform a vector from coordinates including the central tendency of a set as axis, to coordinates including the geographic vertical as axis. Coefficients depending upon the specified Fisher's K_f operate on a random uniform number to define a probability, then the central angle corresponding to that probability and dispersion is computed. The location on the circle of equal probability is specified by another random uniform number between zero and 2π. The resulting vector is then transformed to geographic axes about the specified central tendency. Up to 500 vectors can be produced, stored, printed and punched for reuse or plotting by STEREO.

Auxiliary Program REPLT 1 for Reproducing Stereonets of Field Orientation Data

The wide variety of vectoral display used by other authors to represent joint orientations has necessitated several programs to manipulate punch-card data produced on the Gerber Digitizer. Strike and dip data could also be programmed for digitizing into useful form. While only conformal nets are used here, the plotting program could be modified to produce equal-area plots.

REPLT 1 reads Gerber Digitizer punched cards of fixed-point X and Y coordinates relative to an origin at the SW of center, distant $\sqrt{2}$ times the original plot radius. The program rescales the coordinates to the desired size, and computes direction cosines of the vectors represented. Each is assigned a uniform random number for later shuffling. The direction cosines of the central tendency are computed, also the vector strength and coefficient of specific surface, c.

Subroutine REPLT-2 processed the Oroville data given in Plate 16. In addition to Gerber coordinates on input cards, each point may be identified by the set of joints to which it belongs. The radius and the computed angles in the projection are then converted to direction cosines, and punched on cards for manual sorting and decisions of which vector belongs to what set. The readied deck of orientations can be resubmitted for analysis of parameters by JDATA.

```
*     PACK
*     LIST
*     LABEL
*     FORTRAN
C     UNIT VECTORS DISPERSED ON A SPHERE ACCORDING TO FISHERS EQUATION AR
CCMPUTED, THEIR DENSITY BEING  F=E TO THE K COS THETA .THE PROGRAM GIVES
CCSINES OF EACH VECTOR, PRINTED AND PUNCHED OUT AFTER TRANSFORMATION TO TI
CENTRAL TENDENCY GIVEN IN THE INPUT .
      DIMENSION A(3), B(3), C(3), E(3,3)
      READ 54, AK,N
   54 FORMAT (F10.5,I10)
      PRINT 55,AK
   55 FORMAT (26H0 DISPERSION COEFFICIENT K  /F10.5)
      READ 51,(B(I), I=1,3)
   51 FORMAT (3F15.5)
      PRINT 57, (B(I), I=1,3)
   57 FORMAT (40H0 DIRECTION COSINES OF CENTRAL TENDENCY  //3F15.5)
      DENOM=SQRTF(1.0-B(2)*B(2))
      E(1,1)=B(1)*B(2)/DENOM
      E(1,2)=-DENOM
      E(1,3)=B(2)*B(3)/DENOM
      E(2,1)=B(1)
      E(2,2)=B(2)
      E(2,3)=B(3)
      E(3,1)=B(3)/DENOM
      E(3,3)=-B(1)/DENOM
      PRINT 60,((E(I,J), I=1,3),J=1,3)
   60 FORMAT (31H0 TRANSFORMATION FACTORS E(I,J)  //(3F20.15))
      PRINT 52
   52 FORMAT(101H0 DIRECTION COSINES OF POLES OF PLANES DISPERSED ABOUT
     1B           AZIMUTH AND HADE EQUIVALENTS        //)
      F=EXPF(AK)
      G=F-EXPF(-AK)
      STR=0.0
      DO 31 I=1,N
      P=RANDOM(X)
      H=F-P*G
      COSTH=LOGF(H)/AK
      SINTH = SQRTF(1.0- COSTH*COSTH)
      PHI=RANDOM(X)*6.28318
      STR=STR+COSTH
      A(1)=SINTH*SINF(PHI)
      A(2)=COSTH
      A(3)=SINTH*COSF(PHI)
      C(1)=E(1,1)*A(1)+E(2,1)*A(2)+E(3,1)*A(3)
      C(2)=E(1,2)*A(1)+E(2,2)*A(2)
      C(3)=E(1,3)*A(1)+E(2,3)*A(2)+E(3,3)*A(3)
      IF (C(3)) 21,24,24
   21 DO 22 J=1,3
   22 C(J) = -C(J)
   24 PUNCH 53,(C(J),J=1,3),I
   53 FORMAT(3F20.7,15X,I5)
      ANGLE = ATAN2F(C(2),C(1))
      AZIM = 180.0 -57.295 * ANGLE
      HADE = 57.295 *ATANF(SQRTF(1.0-C(3)*C(3))/C(3))
      PRINT 58,(C(I), I=1,3), AZIM, HADE
   58 FORMAT(3F20.8, F23.5, F12.5)
```

```
   31 CONTINUE
      AN=N
      STR=STR/AN
      PRINT 61,STR
   61 FORMAT(17HO VECTOR STRENGTH  // F10.6)
   33 CALL EXIT
      END
*     LIST
*     LABEL
*     FORTRAN
      SUBROUTINE REPLT1
CCNVERTS STERLOPLOTS TO DIGITAL FORM, COMPUTES DISTRIBUTION PARAMETERS
      DIMENSION U(3,1000)
      COMMON U,M,MTOT
CCRRECT DATA---IHEM=1 IF UPPER, =-1 IF LOWER HEMISPHERE PLOT MEASURED
CCRRECT SCALE--- D=DIAMETER IN INCHES NET MEASURED, M=NUMBER OF POINTS
    9 READ 10, IHEM,D,M
      IF(M) 70,70,7
   10 FORMAT(I10,F10.8,I10)
CCNVERT GERBER COORDINATES TO FLOATPOINT
    7 M1=MTOT + 1
      MM=MTOT+M
      DO 37, I=M1,MM
      READ 11,IY,IT
   11 FORMAT(2I10)
      X=IT
      Y=IY
CHANGE TO SCALE OF NEW PLOT, ORIGIN AT CENTER
      X=(X/100.0-D/2.0)*7.05/D
      Y=(Y/100.0-D/2.0)*7.05/D
      IF(IHEM) 2,3,3
    2 X=-X
      Y=-Y
    3 XSQ=X*X
      YSQ=Y*Y
      PSQ=4.0*(XSQ+YSQ)/(D*D)
      U(3,I)=(1.0-PSQ)/(1.0+PSQ)
      IF (X) 25,35,25
   25 U(2,I)=SQRTF((1.0-U(3,I)*U(3,I))/(1.0+YSQ/XSQ))
      YOP=-Y
      THETA=ATAN2F(X,YOP)
      IF (THETA) 32,35,31
   32 U(2,I)=-U(2,I)
   31 U(1,I)=YOP*U(2,I)/X
      GO TO 37
   35 U(2,I)=0.0
      U(1,I)=SQRTF(1.0-U(3,I)*U(3,I))
      IF (Y) 37,37,36
   36 U(1,I)=-U(1,I)
   37 CONTINUE
      DO 38, I=M1,MM
      RAND = RANDOM(X)
      IRAND = RAND*500.0
      L=I-MTOT
   38 PUNCH 12,(U(J,I),J=1,3),IRAND,L
   12 FORMAT(3F20.8,I12,I8)
```

```
CALCULATE DIRECTION COSINES OF  CENTRAL TENDENCY
      V1=0.0
      V2=0.0
      V3=0.0
      DO 58, I=M1,MM
CONVERT EACH VECTOR BY DOUBLING ITS ANGLE WITH THE 3-AXIS,
CENTERING THERE THE EXPANSION FROM HEMI- TO SPHEREICAL DISTRIBUTION
COMPONENTS ADDED
      V1=V1+U(1,I)
      V2=V2+U(2,I)
   58 V3=V3+2.0*U(3,I)*U(3,I)-1.0
CALCULATE AVERAGE DIRECTION COSINES
      AM = M
      V1=V1/AM
      V2=V2/AM
      V3=V3/AM
CONVERT DISTRIBUTION BACK TO HEMISPHERICAL DISTRIBUTION
      V3=SQRTF((1.0+V3)/2.0)
COMPUTE VECTOR STRENGTH TO CORRELATE WITH FISHERS K
      STR=0.0
COEFFICIENT DETERMINING SPECIFIC SURFACE AND DISTANCE FOR THE SAMPLE
      C=0.0
      DO 68, I=M1,MM
      ANG=U(1,I)*V1+U(2,I)*V2+U(3,I)*V3
      STR=STR+ANG
      C=C+1.0/ANG
      STR=STR/AM
   68 C=C/AM
      PRINT 13,V1,V2,V3,M,STR,C
   13 FORMAT(3F15.5,I5,2F15.8)
      MTOT=MTOT+M
      GO TO 9
   70 RETURN
      END
*     PACK
*     LIST
*     LABEL
*     FORTRAN
      SUBROUTINE REPLT2
CONVERTS DEPT WATER RESOURCES POLAR JOINT PLOT TO NORMAL STEREONET
      DIMENSION U(3,1000)
      COMMON U,M,MTOT,DIN
CORRECTS SCALE, DIN=OUTER, DOUT =OUTER DIAMETER , M= NUMBER OF POINTS
CORRECT DATA---IHEM=1 IF UPPER, =-1 IF LOWER HEMISPHERE PLOT MEASURED
CONVERT GERBER COORDINATES TO FLOATPOINT AND TRANSFORM TO NEW COORDINATE
COLUMN 30 WILL CONTAIN 0 IF IT IS DOUBTLESS WHICH SET A JOINT IS
CONTAINED IN, OR A 1, 2, OR 3, ETC. IF ASSIGNED TO THAT SET , BUT
CORRESPONDENCE IS DOUBTFUL
    9 READ 10, IHEM, DIN, DOUT, M
   10 FORMAT(I10,2F10.5,I10)
      IF(M) 70,70,7
    7 M1=MTOT+1
      MM=MTOT+M
      DO 37  I=M1,MM
      READ 11,IY,IX, IQUEST
   11 FORMAT(3I10)
```

```
      XX=DOUT/2.0-FLOATF(IY)/100.0
      YY=-DOUT/2.0+FLOATF(IX)/100.0
      ANGL=ATAN2F(YY,XX)
      R=SQRTF(YY*YY+XX*XX)-DIN/2.0
      PHI=3.14159*R/(DOUT-DIN)
C CALCULATE DIRECTION COSINES OF EACH VECTOR
      U(3,I)=COSF(PHI)
      U1I=COSF(ANGL)
      RATIO=SINF(ANGL)/U1I
      U(1,I)=SQRTF((1.0-U(3,I)*U(3,I))/(1.0+RATIO*RATIO))
      IF(U1I) 98,99,99
   98 U(1,I)=-U(1,I)
   99 U(2,I)=U(1,I)*RATIO
      IF(IHEM) 101,101,102
  101 U(3,I)=-U(3,I)
      U(2,I)=-U(2,I)
      U(1,I)=-U(1,I)
  102 PUNCH 12, (U(J,I),J=1,3),I,IQUEST
C CAN SORT FOR 1, 2, 3, ETC,  TO REMOVE  QUESTIONABLE CARDS AND REPLACE
C CORRECTLY IN SET  INDICATED BY STEREONET. M IS ALSO CHANGED.
   12 FORMAT(3F20.8,I12,I8)
   37 CONTINUE
      MTOT=MTOT+M
      GO TO 9
   70 RETURN
      END
```

Determining Central Tendencies and Dispersions of Field Orientation Data

Subroutine JDATA determines parameters of a vector dispersion. The discomforting aspect of many plots of dispersion is that they are split between the upper and lower hemispheres, leaving many of the two-headed vector orientations ambiguous. In this case the centroid of the dispersion is obscure. JDATA therefore transforms them all so that the estimated centroid is at the zenith with all elements around it. The resultant vector is retransformed to the original system and reported as the central tendency. Using components of the vectors, the strength (Chapter 6) and the coefficient of specific surface, c, are computed. Fisher's dispersion is related to these parameters by Figures 5-9 and Figure 6-6. Each punched output card giving direction cosinesalso has a random number assigned by the permutator (without substitutions) 3C RANDY (Krasnow, 1960), a subroutine initialized by the input number XLAST.

```
*       LIST
*       LABEL
*       FORTRAN
CJDATA    D T SNOW, DEPT OF MINL TECH MAY 1964
CCMPUTES CENTRAL TENDENCY OF JOINT SETS, VECTOR STRENGTH AND SPACING
CCEFFICIENTS. RANDOMIZES SEQUENCE OF JOINTS IN OUTPUT DECK OF DIRECTION
CCSINES.
      DIMENSION U(3,1000),L1(1010),L2(1010),A(3,3),B(3)
      READ 14, XLAST
   14 FORMAT(O15)
      MTOT = 0
CCSINES OF ESTIMATED CENTRAL TENDENCY AND  NUMBER OF JOINTS IN SET READ
    9 READ 10, M,(B(I),I=1,3)
   10 FORMAT(I10,3F20.7)
      IF(M) 70,70,7
    7 M1=MTOT + 1
      MM=MTOT+M
CUMULATING PAREMATERS ZEROED
      STR=0.0
      C=0.0
      V1=0.0
      V2=0.0
      V3=0.0
      AM=FLOATF(M)
      CALL SETRAN(L1,L2,M)
      CALL GENRAN(M,M,0.0,XLAST)
CCMPUTE TRANSFORMATION MATRIX
      DENOM=SQRTF(1.0-B(2)*B(2))
      A(1,1)=B(3)/DENOM
      A(1,3)=-B(1)/DENOM
      A(2,1)=B(1)*B(2)/DENOM
      A(2,2)=-DENOM
      A(2,3)=B(2)*B(3)/DENOM
      A(3,1)=B(1)
      A(3,2)=B(2)
      A(3,3)=B(3)
CCSINES OF VECTORS READ
      DO 37 I=M1,MM
      READ 12, (U(J,I),J=1,3)
   12 FORMAT(3F20.8)
CCNVERT EACH VECTOR TO COORDINATES HAVING B AT 3-AXIS
      VT1=A(1,1)*U(1,I)+A(1,3)*U(3,I)
      VT2=A(2,1)*U(1,I)+A(2,2)*U(2,I)+A(2,3)*U(3,I)
      VT3=A(3,1)*U(1,I)+A(3,2)*U(2,I)+A(3,3)*U(3,I)
CHOOSE ONLY UPPER HEMISPHERE ENDS
      IF (VT3) 21,24,24
   21 VT1=-VT1
      VT2=-VT2
      VT3=-VT3
CUMULATE COMPONENTS
   24 V1=V1+VT1
      V2=V2+VT2
      V3=V3+VT3
   37 CONTINUE
CALCULATE DIRECTION COSINES OF CENTRAL TENDENCY, THE RESULTANT DIRECTION
      VMAG=SQRTF(V1*V1+V2*V2+V3*V3)
      VT1=V1/VMAG
```

```
      VT2=V2/VMAG
      VT3=V3/VMAG
CCNVERT CENTRAL TENDENCY BACK TO ORIGINAL COORDINATE SYSTEM
      V1=A(1,1)*VT1+A(2,1)*VT2+A(3,1)*VT3
      V2=A(2,2)*VT2+A(3,2)*VT3
      V3=A(1,3)*VT1+A(2,3)*VT2+A(3,3)*VT3
      IF (VT3) 41,44,44
   41 VT1=-VT1
      VT2=-VT2
      VT3=-VT3
CCMPUTE ANGLES EACH VECTOR MAKES WITH THE CENTRAL TENDENCY, ALSO
CCEFFICIENT DETERMINING SPECIFIC SURFACE AND DISTANCE FOR THE SAMPLE
   44 DO 58 I=M1,MM
CALL RANDUM PERMUTATOR TO LABEL EACH CARD
      KL=I-M1+1
      K=L1(KL)+1
      PUNCH 15, (L(J,I),J=1,3),I,K
   15 FORMAT(3F20.8,I12,I8)
      ANG=ABSF(U(1,I)*V1+U(2,I)*V2+U(3,I)*V3)
      STR=STR+ANG
   58 C=C+1.0/ANG
      STR=STR/AM
      C=C/AM
      PRINT 13,V1,V2,V3,STR,C
   13 FORMAT(87H0                                   CENTRAL TENDENCY
     1        VECTOR STRENGTH     C   //3F20.5,F15.4,F18.4)
      MTOT=MTOT+M
      GO TO 9
   70 PUNCH 14, XLAST
      END
      DATA
```

Subroutine STEREO has a MAIN program that reads in the data, produced by REPLT-1, JDATA, VECGEN or others. Subroutine STEREO converts direction cosines from Cartesian coordinates by applying to each vector the transformation to a right-hand system having + z upward.

$$X = \frac{D\sqrt{(1-C_3)(1+C_3)}}{2\sqrt{1+(C_2/C_1)^2}} \quad , \quad Y = (C_2/C_1)\,X$$

D is the desired plot diameter, and C_i are the direction cosines of any vector. This makes a conformal net, the poles of vectors on the upper hemisphere projected to the horizontal plane along lines to the lower pole of the sphere. Built-in functions of Subroutine SYM2, for the Cal-Comp Plotter (Thrower, 1963) are essential for all plotting routines used here.

```
*       LIST
*       LABEL
*       FORTRAN
C       MAIN CONTROL PROGRAM
        DIMENSION U(3,1000),V(4),W(10), DDD(12)
        COMMON U,M
        REWIND6
   21   READ 51,M
   51   FORMAT(I4)
        IF(M)  11,11,22
   22   DO 765 I=1,M
        READ 52, (U(J,I),J=1,3)
   52   FORMAT(3F20.7)
        IF (U(3,I)) 760,765,765
  760   DO 762 J=1,3
  762   U(J,I)=-U(J,I)
  765   CONTINUE
        CALL STEREO
        GO TO 21
   11   CALL NDPLOT
        ENDFILE6
        CALL REWUNL(6)
        CALL EXIT
        END

*       PACK
*       TAPE 85, REEL 1156, WRITE, PLOT
*       LIST
*       LABEL
*       FORTRAN
        SUBROUTINE STEREO
C       PLOTS THE STEREOGRAPHIC PROJECTION OF M VECTORS ON THE UPPER
C       HEMISPHERE OF AN 18 CM NET OVERLAY.
        DIMENSION U(3,1000),V(4),W(10), DDD(12),WW(2)
        COMMON U,M
        V(1) =3H1HN
        V(2) =3H1HS
        V(3) =3H1HW
        V(4) =3H1HE
        WW(1)=6H9HFIGU
        WW(2)=6HRE  .
        W(1)=6H42HSTE
        W(2)=6HREOGRA
        W(3)=6HPHIC P
        W(4)=6HROJECT
        W(5)=6HION, U
        W(6)=6HPPER H
        W(7)=6HEMISPH
        W(8)=3HERE
    1   CALL GRAPH (1).0,7.8,1.1)
        READ 7, (DDD(J),J=1,12)
    7   FORMAT(12A6)
        CALL XLN (0.23,0.37,3.9,0.0)
        CALL XLN (3.8,4.0,3.9,0.0)
        CALL XLN (7.43,7.57,3.9,0.0)
        CALL YLN (0.23,0.37,3.9,0.0)
        CALL YLN (3.8,4.0,3.9,0.0)
```

```
      CALL YLN (7.43,7.57,3.9,0.0)
      CALL LTR (0.12,3.85,2,1,V(1))
      CALL LTR (7.83,3.80,2,1,V(2))
      CALL LTR (4.00,0.02,2,1,V(3))
      CALL LTR (4.00,7.68,2,1,V(4))
      CALL LTR(8.2,0.0,2,1,WW)
      CALL LTR(8.6,0.0,2,1,W)
      CALL LTR (9.0,0.0,2,1,DDD)
      CALL CURVE (2,10,0,0,-3.9,10.0,-3.9,10.0,1)
      THETA=0.0
    5 PHI=THETA/57.295
      X=3.53 * COSF(PHI)
      Y= 3.53 * SINF(PHI)
      CALL PLOTPT (X,Y)
      THETA =THETA + 1.0
      IF (THETA- 360.0) 5,5,6
    6 CALL CURVE (1,1,1,0,-3.9,10.0,-3.9,10.0,1)
      DO 10 I=1,M
      R=3.53*SQRTF((1.0-U(3,I))/(1.0+U(3,I)))
      S=U(2,I)/U(1,I)
      X=R/SQRTF(1.0+S*S)
      IF(U(1,I)) 2,3,3
    2 X=-X
    3 Y=X*S
   10 CALL PLOTPT(X,Y)
      ENDFILE6
      RETURN
      END
```

Generation of Aperture Populations

BKGEN produces punch cards of the elements of sample size N according to the two parameters read in. As shown, it is for normal distributions, but has also been used for log normal, exponential and linear distributions. It computes the mean value of the generated numbers.

Plotting Aperture Distributions

Subroutine FREQPL, a modification of the same-named program that plots cumulative permeabilities, plots apertures or any other aggregate of numbers. FREQPL ranks all the data in ascending order, fits the curve to the dimensions of the frame, and plots points and a line between points to record the discharges. Plates 27 to 29 were made with this program.

```
*       PACK
*       LIST
*       LABEL
*       FORTRAN
CCMPUTE N RANDOM NORMAL DEVIATES OF STANDARD DEVIATION STD AND MEAN
CENTEN BY APPLYING BC DEV3
        READ 51, N, STD, CENTEN
     51 FORMAT(I20, 2F20.5)
        PRINT 52
     52 FORMAT(56H0            NUMBER OF ELEMENTS  STANDARD DEVIATION    MEAN
       1  //)
        PRINT 51, N, STD, CENTEN
        PRINT 53
     53 FORMAT(26H0 ELEMENTS OF DISTRIBUTION  //)
        C=0.0
        DO 10 I=1,N
        A=ABSF(STD*RANDEV(X)+CENTEN)
        PRINT 54, A
     54 FORMAT(F20.8)
        C=C+A
     10 PUNCH 55,A,I
     55 FORMAT(F20.9,55X,I5)
        BN=N
        AMEAN=C/BN
        PRINT 56,AMEAN
     56 FORMAT(14H0 SAMPLE MEAN /F20.9)
        CALL EXIT
        END
C       MAIN CONTROL PROGRAM
        DIMENSION H(1000),AA(11),BB(4),CC(10),EE(2),FF(9),GG(12),DD(12),
       1CCC(2)
        COMMON H,M
        REWIND6
     21 READ 51,M
     51 FORMAT(I4)
        IF(M)  11,11,22
     22 DO 765 I=1,M
    765 READ 55,H(I)
     55 FORMAT(F20.7)
        CALL FREUPL
        GO TO 21
     11 CALL NDPLOT
        ENDFILE6
        CALL REWUNL(6)
        CALL EXIT
        END



*       DECKS
*       LIST
*       LABEL
*       FORTRAN
        DIMENSION H(1000),AA(11),BB(4),CC(10),EE(2),FF(9),GG(12),DD(12),
       1CCC(2)
        COMMON H,M
```

```
      REWIND6
      HTOT=0.0
   21 READ 51,M,STD,CENTEN
   51 FORMAT(I3,37X,2F10.5)
      IF(M) 11,11,22
   22 DO 765 I=1,M
CASE THREE, EXPONENTIAL DISTRIBUTION OF APERTURES
      H(I)=CENTEN*EXPF((2.0*UNIRAN(X1)-1.0)*STD/2.0)
  765 HTOT=HTOT+H(I)
      AM=M
      HTOT=HTOT/AM
      PRINT 155, HTOT
  155 FORMAT(F25.6)
      CALL FREQPL
      PRINT 99,H(1),H(M)
   99 FORMAT(2F30.8)
      GO TO 21
   11 CALL NDPLOT
      ENDFILE6
      CALL REWUNL(6)
      CALL EXIT
      END


*     LIST
*     LABEL
*     FORTRAN
      SUBROUTINE FREQPL
      DIMENSION H(1000),AA(11),BB(4),CC(10),EE(2),FF(9),GG(12),DD(12),
     1CCC(2)
      COMMON H,M
C     PLOTS CUMULATIVE FREQUENCY CURVES FOR EACH PRINCIPAL CONDUCTIVITY
      AA(1)=3H1H0
      AA(2)=4H2H10
      AA(3)=4H2H20
      AA(4)=4H2H30
      AA(5)=4H2H40
      AA(6)=4H2H50
      AA(7)=4H2H60
      AA(8)=4H2H70
      AA(9)=4H2H80
      AA(10)=4H2H90
      AA(11)=5H3H100
      BB(1)=6H18HCUM
      BB(2)=6HULATIV
      BB(3)=6HE PERC
      BB(4)=3HENT
      CC(1)=6H9HFIGU
      CC(2)=6HRE
      EE(1)=4H2H16
      EE(2)=4H2H84
      FF(1)=3H1H0
      FF(2)=3H1H2
      FF(3)=3H1H4
      FF(4)=3H1H6
```

```
      FF(5)=3H1H8
      FF(6)=4H2H10
      FF(7)=4H2H12
      FF(8)=4H2H14
      FF(9)=4H2H16
    6 CALL GRAPH ( 8.0,5.0,3.5)
      CALL FRAME (0.1,0.5)
      CALL XLN(0.0, 8.0,0.78,0)
      CALL XLN (0.0, 8.0,2.50,0.5)
      CALL XLN (0.0, 8.0,4.22,0)
      Y=-0.05
      DO 1 J=1,11
      CALL LTR (-0.3,Y,1,0,AA(J))
    1 Y=Y+0.5
      CALL LTR (-0.5,0.7,2,1,BB)
      CALL LTR (0.1,0.73,1,0,EE(1))
      CALL LTR (0.1,4.17,1,0,EE(2))
      CALL LTR (-0.6,-1.0,2,0,CC)
      READ 7,(GG(J),J=1,12)
    7 FORMAT(12A6)
      CALL LTR (0.0,-1.4,2,0,GG)
      READ 7,(DD(J),J=1,12)
      CALL LTR( 0.0,-1.8,2,0,DD)
      X=-0.05
      DO 2 I=1,5
      CALL LTR (X,-0.2,1,0,FF(I))
    2 X=X+1.0
      X=X+0.05
      DO 3 I=6,9
      CALL LTR (X,-0.2,1,0,FF(I))
    3 X=X+1.0
    4 CALL CURVE (0,0,0,0,0.0,10.0,0.0,5.0,1)
      MM=M-1
      DO 12 I=1,MM
      IP1=I+1
      DO 12 J=IP1,M
      IF(H(I)-H(J)) 12,12,13
   13 TEMP=H(I)
      H(I)=H(J)
      H(J)=TEMP
   12 CONTINUE
      HP=1.0E 00
   16 HT=H(1)*HP
      IF(HT-1.0) 14,15,15
   14 HP=10.0*HP
      GO TO 16
   15 HM=H(M)*HP
      IF(HM-8.0) 18,18,19
   19 HP=HP/10.0
      GO TO 15
   18 MED=M/2
      PRINT 11,HP,H(MED)
   11 FORMAT(1P2E20.8)
      AM=M
      YINC=5.0/AM
      Y=YINC
```

```
      DO 17 I=1,M
      X=H(I)*HP/2.0
      CALL PLOTPT (X,Y)
   17 Y=Y+YINC
      ENDFILE6
      RETURN
      END
```

Standardizing and Analyzing Pressure Test Discharges

Subroutine PTEST1 reads input cards containing the angle of inclination of the drill hole, the inclined depth to the top and bottom, the discharge in GPM and the pressure in psi at the mid-depth. It then computes the length, depth to mid-section, and the head, assuming saturation to the test depth only. The Glover-Cornwell, long-piezometer shape factor is obtained, and the standardized discharge computed, i.e., that which would have occured under 100 psi. and length 25 feet of NX hole. The mid-depth and discharge of each test is printed in the output. This program served to reduce the Merced River damsite tests, wherein the water table was low.

Subroutine PTEST2A processes discharges recorded in GPM, pressure in psi., and the inclined lengths to the packers. The depth to the water table is used to establish the net head. Since the Oroville damsite data, for which the routine was designed, often employed a fixed lower packer, and a moving upper packer, additional measures are obtained by subtracting discharges and lengths of successive overlapping stages (statement 101 and following).

Subroutine PTEST3 resembles PTEST1. In addition to the collar-pressure-discharge-data the grout take data available was incorporated in the program, preserving it for possible future use.

Subroutine PTEST4 differs from PTEST1 only in that pressures were recorded at the collar, so had to be corrected to the mid-depth and according to the water table. Spring Creek, Folsom and Auburn damsite data were calculated by PTEST4.

```
*     LIST
*     LABEL
*     FORTRAN
CPTEST  DAVID T. SNOW, DEPT. MINL TECH, JUL 64, STATISTICS PUMPTESTS
      DIMENSION QA(500),DMID(500),AA(11),HB(4),CA(11),EE(2),GA(12),
     1DA(12)
      COMMON M,QA
CCUNT OF CARDS READ
      READ 1,M
    1 FORMAT(I3)
      PRINT 4
    4 FORMAT(/30H  STD DISCHARGE    MID-DEPTH     //)
CARD FOR EACH PUMP TEST READ
      DO 100 N=1,M
      READ 2,ANGLE,DINTOP,DINBOT,QO,PRESS
    2 FORMAT(5F10.3)
CALCULATE LENGTH WA OF TEST SECTION, SHAPE FACTOR,HEAD IN FEET
      WA=DINBOT-DINTOP
      SO=6.283*WA/LOGF(8.0*WA)
      HO=2.31*PRESS
CCMPUTE DISCHARGE GAL/DAY THAT WOULD OCCUR IN 25 FT LENGTH UNDER 100 PS
      QA(N)=15780.0*QO/(SO*HO)*1440.0
CCMPUTE MID-DEPTH OF TEST SECTION
      DMID(N)=(DINTOP+WA/2.0)*SINF(ANGLE*0.01745)
      PRINT 3,QA(N),DMID(N)
    3 FORMAT(2F15.1)
  100 CONTINUE
      CALL DISCHG
      CALL  NDPLOT
      ENDFILE6
      ENDFILE6
      CALL REWUNL(6)
      END
```

```
*     LIST
*     LABEL
*     FORTRAN
CPTEST2 DAVID T. SNOW, DEPT. MINL TECH, JUL 64, STATISTICS PUMPTESTS
      DIMENSION QA(500),DMID(500),AA(11),BB(4),CA(11),EE(2),GA(12),
     1DA(12),DINTOP(500),DINBOT(500),QT(500),PRESS(500),ANGLE(500),
     2WTDEEP(500)
      COMMON M,QA
CCUNT OF CARDS READ
    5 READ 1,M
    1 FORMAT(I3)
      IF(M) 160,160,150
  150 PRINT 4
    4 FORMAT( 30H0 STD DISCHARGE    MID-DEPTH     //)
CARD FOR EACH PUMP TEST READ
      DO 100 N=1,M
      READ 2,ANGLE(N),WTDEEP(N),DINTOP(N),DINBOT(N),QT(N),PRESS(N)
    2 FORMAT(6F10.3)
  100 CONTINUE
CALCULATE LENGTH WA OF TEST SECTION, SHAPE FACTOR,HEAD IN FEET
```

```
CALC. NET LENGTH AND DISCHARGE WHEN UPPER PACKER IS MOVED, LOWER FIXED
      DO 200 N=1,M
      IF(PRESS(N)-PRESS(N+1)) 110,101,110
  101 IF(DINBOT(N)-DINBOT(N+1)) 110,102,110
  102 WA=DINTOP(N+1)-DINTOP(N)
      QO=QT(N)-QT(N+1)
      GO TO 121
  110 WA=DINBOT(N)-DINTOP(N)
      QO=QT(N)
  121 SO=6.283*WA/LOGF(8.0*WA)
      HO=2.31*PRESS(N)+WTDEEP(N)
CCMPUTE DISCHARGE GAL/DAY THAT WOULD OCCUR IN 25 FT LENGTH UNDER 100 PSI
      QA(N)=15780.0*QO/(SO*HO)*1440.0
CCMPUTE MID-DEPTH OF TEST SECTION
      DMID(N)=(DINTOP(N)+WA/2.0)*SINF(ANGLE(N)*0.01745)
      PUNCH 3,QA(N),DMID(N),WA,N
    3 FORMAT(3F15.1,32X,I3)
  200 CONTINUE
      GO TO 5
  160 M=M
      END
*     DATA


*     LIST
*     LABEL
*     FORTRAN
CPTEST3ADAVID T. SNOW, DEPT. MINL TECH, JUL 64, VIRG. R. DATA
      DIMENSION QA(500),DMID(500),SACKS(500),WA(500)
CCUNT OF CARDS READ
    5 READ 1,M
    1 FORMAT(I3)
      IF(M) 7,7,6
    6 PRINT 4
    4 FORMAT(50H0  STD DISCHARGE   MID-DEPTH  SACKS GROUT/FT          //)
CARD FOR EACH PUMP TEST READ
      DO 100 N=1,M
      READ 2,ANGLE,DINTOP,DINBOT,QO,PRESS,TIME ,GROUT
    2 FORMAT(7F10.3)
CALCULATE LENGTH WA OF TEST SECTION, SHAPE FACTOR,HEAD IN FEET
      WT=DINBOT-DINTOP
      SO=6.283*WT/LOGF(8.0*WT)
      HO=2.31*PRESS
CCMPUTE DISCHARGE GAL/DAY THAT WOULD OCCUR IN 25 FT LENGTH UNDER 100 PSI
      QA(N)=118000.0*QO/(SO*HO)*1440.0
CCMPUTE MID-DEPTH OF TEST SECTION
      DMID(N)=(DINTOP+WT/2.0)*SINF(ANGLE*0.01745)
      SACKS(N)=GROUT/WT
      WA(N)=WT
      PRINT 3,QA(N),DMID(N),SACKS(N),WA(N)
      PUNCH 3,QA(N),DMID(N),SACKS(N),WA(N)
    3 FORMAT(4F15.1)
  100 CONTINUE
      GO TO 5
```

```
    7 M=M
      END

*     LIST
*     LABEL
*     FORTRAN
CPTEST4 DAVID T. SNOW, DEPT. MINL TECH, JUL 64, STATISTICS PUMPTESTS
      DIMENSION QA(500),DMID(500)
CCUNT OF CARDS READ
      READ 1,M
    1 FORMAT(I3)
      IF(M) 10,10,12
   12 PRINT 4
    4 FORMAT(/30H  STD DISCHARGE    MID-DEPTH     //)
CARD FOR EACH PUMP TEST READ
      DO 100 N=1,M
      READ 2,ANGLE,DINTOP,DINBOT,QO,PRESS
    2 FORMAT(5F10.3)
CALCULATE LENGTH WA OF TEST SECTION, SHAPE FACTOR,HEAD IN FEET
      WA=DINBOT-DINTOP
      SO=6.283*WA/LOGF(8.0*WA)
CCMPUTE MID-DEPTH OF TEST SECTION
      DMID(N)=(DINTOP+WA/2.0)*SINF(ANGLE*0.01745)
      HO=2.31*PRESS+DMID(N)
CCMPUTE DISCHARGE GAL/DAY THAT WOULD OCCUR IN 25 FT LENGTH UNDER 100 PSI
      QA(N)=15780.0*QO/(SO*HO)*1440.0
      PRINT 3,QA(N),DMID(N)
      PUNCH 3,QA(N),DMID(N)
    3 FORMAT(2F15.1)
  100 CONTINUE
   10 M=M
      END
*     DATA
```

Plotting Cumulative Pressure-Test Discharge Curves

Subroutine DISCHARGE, with its MAIN program for data input and repetitive calls for additional plots, was used to present the standardized discharges from PTEST. The operation and finished product differs in some respect from that of FREQPL. The 95% confidence limits about the median are computed by the normal approximation to the binomial, and plotted as horizontal lines on the graph. The mean and standard deviation of the discharges is computed, printed, and also plotted as vertical lines on the graph. The actual confidence range intersected by the cumulative curve of discharge is computed and printed out in the output. The entire curve, with all its points fitted to the plot, is then drawn.

```
*      PACK
*      ERROR DUMP
*      LIST
*      LABEL
*      FORTRAN
       DIMENSION QA(500),DMID(500),AA(11),BB(4),CA(11),EE(3),GA(12),
      1DA(12),QPTS(5),PTS(5), FREQ(100),FF(4),GG(4),NC(50)
       COMMON M,QA,T
     5 READ 1,M
     1 FORMAT(I3)
     3 IF(M) 11,11,6
     6 READ 2, (QA(N),N=1,M)
     2 FORMAT(F15.5)
       CALL DISCHG
       GO TO 5
    11 CALL  NDPLOT
       ENDFILE6
       ENDFILE6
       CALL REWUNL(6)
       CALL EXIT
       END
```

```
*      LIST
*      LABEL
*      FORTRAN
       SUBROUTINE DISCHG
       DIMENSION QA(500),DMID(500),AA(11),BB(4),CA(11),EE(3),GA(12),
      1DA(12),QPTS(5),PTS(5), FREQ(100),FF(4),GG(4),NC(50)
       COMMON M,QA,T
CUMULATIVE DISTRIBUTION OF PUMP TEST DISCHARGES PLOTTED
       AA(1)=3H1H0
       AA(2)=4H2H10
       AA(3)=4H2H20
       AA(4)=4H2H30
       AA(5)=4H2H40
       AA(6)=4H2H50
       AA(7)=4H2H60
       AA(8)=4H2H70
       AA(9)=4H2H80
       AA(10)=4H2H90
       AA(11)=5H3H100
       BB(1)=6H18HCUM
       BB(2)=6HULATIV
       BB(3)=6HE PERC
       BB(4)=3HENT
       CA(1)=3H58H
       CA(2)=6HFIGURE
       CA(3)=6H    ST
       CA(4)=6HANDARD
       CA(5)=6HIZED P
```

```
      CA(6)=6HUMP TE
      CA(7)=6HST CIS
      CA(8)=6HCHARGE
      CA(9)=6H, GALL
      CA(10)=6HONS/DA
      CA(11)=1HY
      EE(1)=6H4H-SIG
      EE(2)=6H4H+SIG
      EE(3)=6H4HMEAN
      FF(1)=3H16H
      FF(2)=6H95 C/O
      FF(3)=6H CONFI
      FF(4)=1H-
      GG(1)=3H19H
      GG(2)=6H DENCE
      GG(3)=6H CN ME
      GG(4)=4HDIAN
C CONFIDENCE (95 PERCENT) INTERVAL ABOUT MEDIAN, NON-PARAMETRIC METHOD
C COMPUTED FROM NORMAL APPROXIMATION TO THE BINOMIAL DISTRIBUTION
      AM=M
      PEACH=100.0/AM
      CONF=0.98*SQRTF(AM)*PEACH
C COORDINATES OF THESE LIMITS ARE
      CONFDN=3.0-0.06*CONF
      CONFUP=3.0+0.06*CONF
C COMPUTE MEAN
      T=QA(1)
      DO 1070 K=2,M
 1070 T=T+QA(K)
      QMEAN=T/AM
C COMPUTE STANDARD DEVIATION OF DISCHARGE
      DEVQ=0.0
      DO 300 K=1,M
  300 DEVQ=DEVQ+(QMEAN-QA(K))**2
      DEVQ=SQRTF(DEVQ/AM)
C COORDINATES OF DEVIATIONS
      SIGPLM=QMEAN+DEVQ
      SIGMIN=QMEAN-DEVQ
C COORDINATES AND LETTERING, SCALES DONE
      CALL GRAPH(9.0,6.0,2.5)
      CALL FRAME(0.1,0.6)
      CALL XLN(9.0,0.0,0.0,-0.5)
      CALL XLN (0.0,9.0,CONFDN,0)
      CALL XLN(0.0,8.5,3.00,0.5)
      CALL XLN (0.0,9.0,CONFUP,0)
      Y=-0.05
      DO 21 J=1,11
      CALL LTR(-0.3,Y ,1,0,AA(J))
   21 Y=Y+0.6
      CALL LTR(-0.5,0.7,2,1,BB)
      CALL LTR(-1.3,-1.0,2,0,CA)
      CALL LTR (8.65,1.95,1,1,FF)
      CALL LTR (8.85,1.85,1,1,GG)
      READ 7,(GA(J),J=1,12)
      CALL LTR(-0.7,-1.4,2,0,GA)
      READ 7,(DA(J),J=1,12)
```

```
      CALL LTR(-0.7,-1.8,2.0,DA)
    7 FORMAT(12A6)
CCMPUTED TEST DISCHARGES ORDERED, ASCENDING
      MIS=M-1
      DO 1239 L=1,MIS
      LP1=L+1
      DO 1239 J=LP1,M
      IF(QA(L)-QA(J)) 1239,1239,1240
 1240 TEMP=QA(L)
      QA(L)=QA(J)
      QA(J)=TEMP
 1239 CONTINUE
CUMULATIVE CURVE FITTED TO PLOT DIMENSIONS
 1061 HP=1.0E-08
 1064 HL=QA(M )*HP
      IF(HL-0.8) 1063,1063,1081
 1063 HP=HP*10.0
      GO TO 1064
 1081 IX=8.0/ HL
      GO TO (1069,1069,1303,1303,1069,1306,1306,1306,1306,1069),IX
 1303 IX=2
      GO TO 1069
 1306 IX=5
 1069 XI=IX
      HP=HP*XI
      PRINT 31, QA(1),QA(M ),IX
   31 FORMAT(1P2E20.8,I4)
CCMPUTE M-TILES, PTS(I)=LOWER 95 CONF LIMIT, MEDIAN, UPPER CONF LIMIT
      PTS(1)=50.0-CONF
      PTS(2)=50.0
      PTS(3)=50.0+CONF
      PNUM=1.0001
      DO 1150 I=1,3
 1099 PLUM=PEACH*PNUM
      IF(PLUM-PTS(I)) 1100,1101,1101
 1100 MB4P=PNUM
      PNUM=PNUM+1.0
      GO TO 1099
 1101 MP=PNUM
      QPTS(I)=QA(MP)-(PLUM-PTS(I))/PEACH*(QA(MP)-QA(MB4P))
 1150 CONTINUE
      PRINT 1149, SIGMIM,(QPTS(I),I=1,3),SIGPLM
 1149 FORMAT(50H0  -DEVQ    LOW CONF    MEDIAN   UP CONF  . +DEVQ   //
     15F10.2///)
CCMPUTE CONFIDENCE RANGE ABOUT MEDIAN
      CONQ=(QPTS(3)-QPTS(1))/2.0
      PRINT 1033
 1033 FORMAT(55H DISCHARGE MEAN, MEDIAN , STD DEV, 95 PERCENT ON MEDIAN)
      PRINT 1034, QMEAN, QPTS(2) ,DEVQ,CONQ
 1034 FORMAT(  1P4E12.4)
CUMULATIVE FREQUENCY CURVE PLOTTED
      CALL CURVE (4,1,0,0,0.0,9.0,0.0,6.0,1)
      YINC=6.0/AM
      YV=YINC
      DO 1017 L=1,M
      XQ=QA(L)*HP
```

```
      CALL PLOTPT (XQ,YV)
      YV=YV+YINC
 1017 CONTINUE
      XSIGMM=SIGMIM*HP
      XMEAN=QMEAN*HP
      XSIGPM=SIGPLM*HP
      IF(XSIGMM) 707,707,708
  708 CALL YLN (0.0,5.3,XSIGMM,0)
      XSIGMM=XSIGMM+0.05
      CALL LTR (XSIGMM,5.35,1,1,EE(1))
  707 CALL YLN (0.7,6.0,XSIGPM,0)
      CALL YLN(0.7,6.0,XMEAN,0)
      XMEAN=XMEAN+0.05
      XSIGPM=XSIGPM+0.05
      CALL LTR (XSIGPM,0.20,1,1,EE(2))
      CALL LTR(XMEAN, 0.20,1,1,EE(3))
      ENDFILE6
      ENDFILE6
      RETURN
      END

      DATA
```

Natural fractures in rock depart from the assumption of smooth parallel-plate openings used in the model. A great deal of theoretical and experimental work remains to be done before exhausting the important subject of the hydraulics of a single fracture whose roughness exceeds the displacement of its sides.

Huitt (1956), gives the equation for parallel plate Poiseuille flow:

$$Q = \frac{\Delta P g_c b W_f^3}{12 \mu l_f}$$

where Q is discharge,

b is the breadth,

W_f is the width (full aperture) of fractures,

μ is viscosity,

l_f is the length

and g_c is a mass-force conversion factor, all of which are in cgs units.

There is abundant confirmation that friction is linear with respect to velocity in rough planar conduits, provided that velocity is low (Huitt, 1956; Walker, Whan and Rothfus, 1957; Rothfus, Archer, Klimas and Sikchi, 1957). The Reynolds (1883) number serves as a criterion:

$$R_e = \frac{2 W_f U \rho}{\mu} \qquad \text{(Huitt, p. 259)}$$

U is the velocity in this expression. Experimental work indicates that laminar flow is maintained below $R_e = 1800$. Davies and White (1928) also obtained this value, nearly the same as Hele-Shaw's (1897, cited by Todd, 1959) critical number of 2000 (by the above definition of R_e). For instance, if water at 50°F flows under a unit gradient, laminar conditions will exist in all fractures of less than 0.16 cm aperture. The model results reported in this paper may be considered applicable to fractures up to, say 5 mm, depending on boundary conditions. Constancy of the Fanning friction factor:

$$f = \frac{\Delta p \, g_c W_f}{l_1 \rho U^2}$$

at a value

$$f = 24/R_e$$

characterizes the laminar range. The friction factor is a proportionality constant between the head loss per unit length along the flow, to the velocity head per unit aperture. Above critical velocity, f approaches a constant value for a given roughness height, (a/r), where a is the arithmetic mean elevation of protuberances and r is pipe radius or half fracture-aperture, whereas Huitt found that friction is independent of roughness height in the laminar range.

Though high-velocity flows in fractures are not considered in the present study, there are natural circumstances, such as solution-enlarged joints in carbonate rocks, or in large fractures near test-holes in any rocks, where friction exceeds that given by the equation above. Huitt's data indicates friction factors for rough fractures about 1.5 times those for pipes (Nikuradse, 1960; and Colebrook, 1939). Davies and White's data span the range of R_e = 60 to 4500, and that of Page, et al. (1952), from 7000 to 60,000. Hopf (1923, cited by Page) gave an empirical relationship between the friction factor at high Reynolds numbers and the relative roughness:

$$f = 0.04 \, (a/r)^{0.314}$$

In all these studies, the roughness heights considered are considerably less than unity. Huitt formed his rough conduits by cementing uniformly-graded sands onto shellacked steel surfaces.

Hopf used a variety of naturally-rough materials for his conductor boundaries. In no known study has a true cast-in-mold configuration been used to make z/r greatly exceed 1. Rock joints, and most other fractures fail to meet the necessary conditions for Poiseuille flow, which Lamb (1932) says is valid provided that $dW_f/d\ell_f$ is small, and if W_f is small compared to the curvature. The writer's experimental work on the conductivity of tight fractures has remained too incomplete for inclusion with the analytical results presented here, in spite of two year's efforts to obtain valid results from an air permeameter. The reason for continued concern for the aperture-conductivity relationship in real fractures is that if the irregularities are of the same, or greater magnitude than the relative displacement of the boundaries, then the path length greatly exceeds the overall particle translation, and apertures are reduced according to the inclination of micro-faces on the irregularities. Directional properties of the roughness (texture) may result in anisotropy of individual fractures.

A PARALLEL PLATE MODEL OF FRACTURED PERMEABLE MEDIA

1978

SNOW

M. Voegele

8.3.1.2.3.1

SNOW DAVID T

DEGREE DATE: 1965

65-8250

SNOW, David Tunison, 1930-
A PARALLEL PLATE MODEL OF FRACTURED PERMEABLE MEDIA.

University of California, Berkeley, Ph.D., 1965
Engineering, hydraulic

University Microfilms, Inc., Ann Arbor, Michigan

8.3.1.2.3.1.7

o Dudley, W.W., Jr., and D.T. Oakley, 1988. Agreement between NNWSI Technical Project Officer, Los Alamos National Laboratory, and NNWSI Technical Project Officer, United States Geological Survey, Regarding the Cooperative Conduct of Tracer Studies.

o Gelhar, L.W., 1982. "Analysis of Two-Well Tracer Tests with Pulse Input," RHO-BW-CR-131 P, Rockwell Hanford Operations, Basalt Waste Isolation Project, Richland, WA.

o Kelley, V.A., J.P. Pickens, M. Reeves, and R.L. Beauheim, 1987. "Double-Porosity Tracer-Test Analysis for Interpretation of the Fracture Characteristics of a Dolomite Formation," Solving Ground Water Problems with Models, proceedings of the National Water Well Association Conference, Feb. 10-12, 1987, Denver, CO.

o Polzer, W.L., and H.R. Fuentes, 1987, "The Use of a Heterogeneity-Based Isotherm to Interpret the Transport of Reactive Radionuclides in Volcanic Tuff Media," Los Alamos National Laboratory Report LA-UR-87-2901, Los Alamos, NM.

o Robertson, J.B., P.S. Huyskorn, T.D. Wadsworth, and J.E. Buckley, 1987. "Design and Analysis of Deep Two-Well Tracer Tests," Hydrogeologic, Inc., Herndon, VA.

o Robinson, B.A., 1987. "Predictive Modeling of in Situ Retardation of Reactive Tracers During C-Well Testing," Nevada Nuclear Waste Storage Investigations Milestone No. R487, Los Alamos National Laboratory.

2081

AGREEMENT BETWEEN
NNWSI Technical Project Officer, LOS ALAMOS NATIONAL LABORATORY
AND
NNWSI Technical Project Officer, UNITED STATES GEOLOGICAL SURVEY
REGARDING THE COOPERATIVE CONDUCT OF TRACER STUDIES

I. As participating agencies in the Nevada Nuclear Waste Storage Investigations, the Los Alamos National Laboratory (LANL) and the U. S. Geological Survey (USGS) are conducting mutually supportive tests at and near Yucca Mountain, Nevada. These tests, referred to as "tracer tests" contribute to meeting the following NNWSI programmatic responsibilities of the participants:

A. The USGS responsibilities under Work Breakdown Structure (WBS) 1.2.3.3, Hydrology, to define the pathways, mechanisms, fluxes, particle velocities, and coefficients of dispersion of ground-water flow at and in the vicinity of Yucca Mountain;

B. the LANL responsibilities under WBS 1.2.3.4, Geochemistry, to define the potential for movement of radionuclides in various physical and chemical forms from the sites of potential nuclear-waste emplacement at Yucca Mountain to environs that might be accessible to man.

II. The Technical Project Officer (TPO) of LANL and the TPO of the USGS agree that successful and timely completion of these investigations require: (a) the joint use of existing and future boreholes penetrating the saturated ground-water system at and in the vicinity of Yucca Mountain, particularly at the site designated UE25c; (b) cooperation in the planning and design of tests, including their sequence, to assure that the information required by both agencies can be acquired in as timely a fashion as possible; (c) that data and other information resulting from the tests be freely exchanged between LANL and USGS when needed as part of the technical basis for evaluation or development of plans.

III. In order to assure meeting of the program requirements stated in (II) above, the parties further agree to the following provisions:

A. The USGS is designated as the lead agency, and LANL as the supporting agency, for tests designed primarily to define hydrologic parameters, including hydraulic tests and the use of non-reactive (conservative) chemical or physical tracers to determine flow paths, particle velocities, and coefficients of dispersion.

8.3.1.2.3.1

B. LANL is designated as the lead agency, and USGS as the supporting agency, for tests designed primarily to determine the rates of movement (or of retardation) of radionuclides, including the use of reactive (non-conservative) tracers, or to evaluate the retarding effect of such potential phenomena as matrix diffusion.

C. The responsibilities and rights of the lead agency include:

1. Assume full responsibility to plan, conduct, and analyze tests for which it is responsible.

2. Assign and implement quality-assurance (QA) levels that are commensurate with the requirements of the supporting agency and the joint USGS/LANL objectives and responsibilities.

3. Provide the supporting agency the opportunity to review and comment on plans, including QA level assignments and technical procedures.

4. Inform the supporting agency of changes of plans or delays that could affect the overall testing effort.

5. Make all data available to the supporting agency in a timely fashion. Data availability to the supporting agency will be scheduled as a Level-3 milestone by the originating agency.

6. Have first right to publish or otherwise release the data, analysis (including modeling), and interpretations for tests for which it is responsible, subject to the conditions in Section III.E below.

7. Provide the supporting agency the opportunity to review and comment on all manuscripts pertaining to the tracer studies and intended for release or publication.

D. The responsibilities and rights of the supporting agency include:

1. Through ongoing dialogue and review of plans and previous results, provide to the lead agency ideas, concepts, or suggestions concerning planned tests.

2. Review and comment on quality-level assignments and technical procedures for activities affecting the usefulness of test results that are important to other joint tests or analyses.

3. May observe tests and, if mutually agreed upon, may directly support the lead agency's planning, testing, and analyses.

4. May not release data nor publish analyses or results prior to the release and publication by the lead agency, except as is provided in section III.E below.

E. Publication or other release by the originating agency of information needed for reference by the other in its publications will be scheduled as a level 2 (NNWSI Project Manager controlled) milestone. When the milestone is three or more months overdue, as referenced to the latest due date approved by the NNWSI Change Control Board, the using agency may use and present those unreleased data, but not interpretations, that are necessary to support its own analyses and interpretations. Such data will be referenced to the unpublished files of the originating agency and to the individual who provided the data. The originating agency or individuals are not obligated to reference the using agency in subsequent presentations or uses of the data.

IV. This agreement shall remain in effect until cancelled in writing by either of the parties hereto, their superiors, or their successors.

W. W. Dudley, Jr.
Date 4/2/86
William W. Dudley, Jr.
NNWSI Technical Project Officer
U. S. Geological Survey

Date
Donald T. Oakley
NNWSI Technical Project Officer
Los Alamos National Laboratory

CONSEIL INTERNATIONAL DES UNIONS SCIENTIFIQUES
INTERNATIONAL COUNCIL OF SCIENTIFIC UNIONS

UNION GÉODÉSIQUE ET GÉOPHYSIQUE INTERNATIONALE
INTERNATIONAL UNION OF GEODESY AND GEOPHYSICS

Bulletin of the International Association of Scientific Hydrology

Bulletin de l'Association Internationale d'Hydrologie Scientifique

XII^{e} Année N° 1

MARS 1967
MARCH 1967

Published on behalf of
THE INTERNATIONAL ASSOCIATION OF SCIENTIFIC HYDROLOGY

DETERMINATION OF THE VERTICAL AND HORIZONTAL PERMEABILITIES OF FRACTURED WATER BEARING FORMATION

Dr. Eng. Kamal F. SAAD *

Desert Institute, Mataria, Cairo, UAR

Résumé

On peut considérer les formations aquifères fracturées comme des aquifères anisotropes. Lorsqu s'agit de fractures horizontales, la perméabilité horizontale correspond aux propriétés de transmissivi des fractures et la perméabilité verticale est celle de la roche mère. Au contraire, lorsqu'il s'agit fractures verticales, la perméabilité verticale correspond aux propriétés de transmissivité des fractur et la perméabilité horizontale caractérise la roche mère. Autrement dit, on considère que la roche mè est isotrope. Le présent travail vise à déterminer les perméabilites verticale et horizontale des roch fracturées, aussi bien que leur capacité de réserve, par l'étude des données des essais de pompage. procédé employé est fondé sur la méthode de la double pente (Saad *et al.*, 1964). De plus, la magnitu des perméabilités verticale et horizontale peut fournir des indices sur les réseaux de fractures si l'e connaît la facilité de l'écoulement dans chaque direction.

Abstract

Fractured water bearing formation may be considered as an anisotropic aquifer. That is the perm ability through the fractures will be different from that of the original parent formation. In the prese paper, the values of both the vertical and horizontal permeabilities as well as the storage coefficient ha been determined through analysis of the pumping test data. The permeability in one of these two directio represents that of the fractures having the same direction, while the other characterizes the transmitti property of the parent formation. The procedure of analysis is based on the double slope metho Saad *et al.* (1965) through analysis of the modified solution of the nonsteady flow toward a well partial penetrating the fractured water bearing formation. It can also be concluded that knowledge of t magnitude of the permeabilities in both directions may indicate the pattern and trend of the fractur

Introduction

Anisotropic permeability of water bearing formation is a result of many reasons. Among the are the presence of fractures, with a certain pattern, in previous aquifer such as limesto Consequently the permeability through the fractures is different and usually higher from that the parent formation. The fractures may have either a horizontal or a vertical trend (Fig. 1) a thus they are represented hydraulically by the horizontal or the vertical permeability respective The permeability in the other direction represents the transmitting property of the parent wat bearing formation.

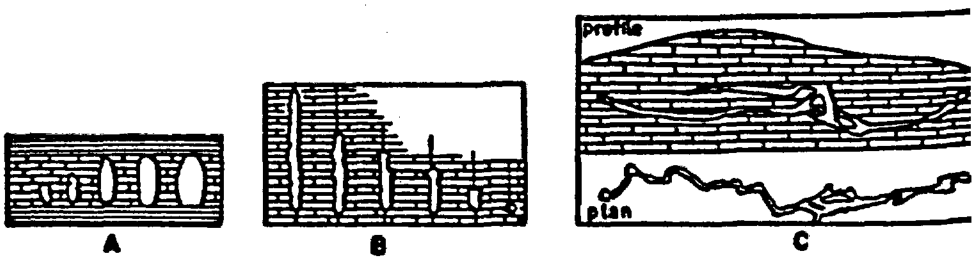

Fig. 1 — Cross section of fractured rock. A and B: Vertical fracture. C: Horizontal fracture.

* UNESCO Expert to the Republic of Mali, "Direction de l'Hydraulique", Bamako.

In practice, it frequently happens that the producing wells do not penetrate completely the fractured formation from which they are pumping. This is rather due to many technical reasons, among these are the large thickness of the fractured bed or the wide fracture openings. In both cases, drilling operation may be either expensive or impractical for large depths for excessive loss of mud circulation and other difficulties. For this, producing wells drilled in fractured water bearing formation, are usually partially penetrating the equifer.

The purpose of the present paper is to determine the permeability of both the fractures and the parent formation. These parameters as well as the storage coefficient can be determined through analysis of the pumping test data, recordes from a partially penetrating observation well, where the pumped well itself does not reach the bottom of the fractured formation. It is assumed that the fractures are either horizontal or vertical and that the storage coefficient remains constant in the whole region.

The procedure of analysis is based on the double slope method, Saad *et al*, (1965), and on the modified solution of the nonsteady flow toward a partially penetrating well, Hantush, 1961, to account for anisotropy, Muskat, 1937.

THEORY

The average drawdown (s) in an observation well, where the screens in both the pumped and the observation wells extend for the whole length of each well, and that both are partially penetrating a water bearing formation, Figure 2, has been found by Hantush, (1961) as follows:

$$s = Q/4\pi K_r b\left[W(u) + (4b^2/\pi^2 d d') \sum_{n=1}^{\infty} (1/n^2) K_0(n\pi r/b)(\sin n\pi d'/b)(\sin n\pi d'/b)\right] \qquad (1)$$

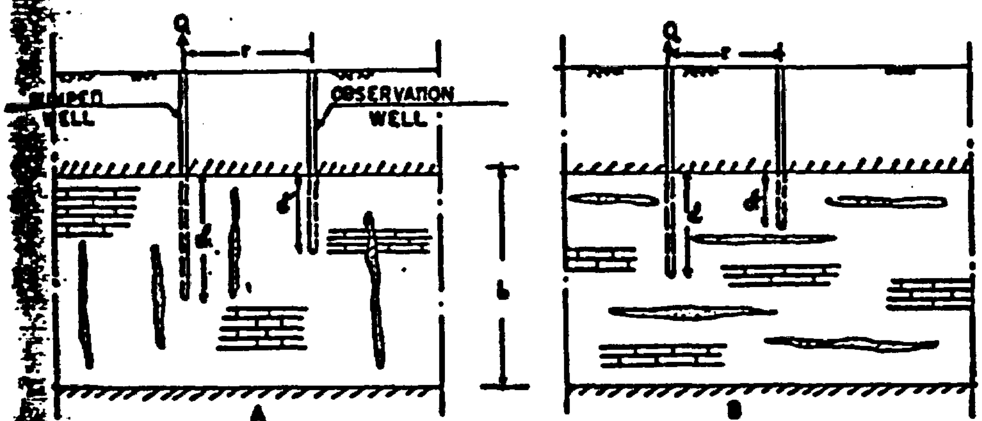

Fig. 2 — Diagrammatic representation of a well tapping fractured rock.
A: Vertical fracture. B: Horizontal fracture.

Equation (1), can be modified, to account for anisotropic permeability resulting from the presence of fractures, by multiplying the term (r/b) by $(K_z/K_r)^{1/2}$, Muskat, (1937). Thus Equation (1), will reduce to:

$$s = Q/4\pi K_r b\left[W(u) + (4b^2/\pi^2 d d') \sum_{n=1}^{\infty} 1/n^2 K_0\{(n\pi r/b)(K_z/K_r)^{1/2}\} (\sin n\pi d/b) (\sin n\pi d'/b)\right] \qquad (2)$$

Equation (2) shows that the rate of changes of the average drawdown behaves as of radial toward a well fully penetrating an aquifer.

For the determination of the hydraulic coefficients K_r and K_z, the duoble slope Saad *et al.* (1965), can be used. The procedure of the mathematical analysis is outli... follows:

i) differantiating (s) in Equation (2) with respect to $\log_e t$

$$ds/d(\ln t) = \frac{2.30\,Q}{4\pi K_r b} e^{-u} = m \qquad (3)$$

ii) differantiating (m) in Equation (3) with respect to $\ln t$

$$dm/d(\ln t) = \frac{(2.30)^2 Q}{4\pi K_r b} u\, e^{-u} = m' \qquad (4)$$

iii) the double slope function $f(u) = m'/m$, can be found

$$f(u) = m'/m = 2.30u \qquad (5)$$

Equations (5), (3), and the relationship ($u = r^2 S/4K_r bt$) and the data of pumping test, ... enable determining K_r and S, as will be shown later. The value of (K_z), can also be found in the terms in the summation form appearing in Equation (2), can be evaluated. For this, Equation (2) can be put in the following forms:

$$A = \sum_{n=1}^{\infty} (1/n^2) K_0\{(n\pi r/b)(K_z/K_r)^{1/2}\}$$

$$(\sin n\pi d/b)(\sin n\pi d'/b) \qquad (6)$$

Where

$$A = \left[\frac{s}{Q/4\pi K_r b} - W(u)\right](\pi^2 dd'/4b^2) \qquad (7)$$

Equation (6), can be further reduced to the form of Fourrier series by multiplying both sides by ($\sin(x)dx$), where ($x = \pi d'/b$), and integrating between the limits 0 and π

$$\int_0^{\pi} A \sin(x)dx = \int^{\pi} \sum_{n=1}^{\infty} (1/n^2) K_0\{(n\pi r/b)(K_z/K_r)^{1/2}\}(\sin nx)(\sin x)dx \qquad (7)$$

Using the following two identities:

$$\int \sin(nx) . \sin(mx)dx = \frac{\sin(n-m)x}{2(n-m)} - \frac{\sin(n+m)x}{2(n+m)} \qquad (8)$$

and

$$\int \{\sin(nx)\}^2 dx = (x/2) - \frac{\sin(2nx)}{4n} \qquad (9)$$

it can be shown easily that all the terms in the summation form in Equation (7) will tend to zero except when $n = 1$. Therefore Equation (7) will reduce finally to:

$$\int_0^{\pi} A \sin(x)dx = (\pi/2) K_0[((\pi r/b) K_z/K_r)^{1/2}] \sin(\pi d/b) = 2A \qquad (10)$$

given.
..., the fo...

i) Draw the ...
curve).
ii) Choose several p...
may be more accura...
or in other words when ...
iii) Plot on the same semi-log p...
iv) Select few points on the (m—l...
point, per cycle.
v) Knowing (m) and (m') at each
at each point, and find the cor...
vi) Using Equation (3) with know...
vii) Using the relationship ($u = r$...
viii) Steps from v to vii, may be re...
However the computed values
deviation is a result of improp...
ix) Choose any point on the (s—l...
x) Compute the value of (u) at th...
from tables of the well functio...
xi) Using Equation (11), the value
value of (K_r/K_z), can be foun...
xii) Knowing (K_r), determine the v...

A...

b aquifer thickness (L).
d depth of penetration of the
d' depth of penetration of the
$K_0(x)$ the zero-order modified Be...
or Dweight (1958).
K_r horizontal permeability rad...
K_z vertical permeability (L^3T)...
m slope of the tangent at an...
m' slope of the tangent at any ...
Q constant well discharge (L...
r distance between the pump...
s average drawdown in an o...
S storage coefficient or stora...
t time since pumping started
u relation $r^2 S/4K_r bt$.
$W(u) = \int_u^\infty (e^{-x}/x)\,dx$ = well func...

$$K_0[(\pi r/b(K_z/K_r)^{1/2}] = (4A/\pi)\ \mathrm{cosec}\,(\pi d/b)) \tag{11}$$

APPLICATION

For determining the hydraulic properties of both the fractured and parent formation, i.e., the vertical and horizontal permeability and the storage coefficient from the data of the pumping test, the following procedure can be applied:

i) Draw the drawdown-time curve on semilog. paper, with the time on the log scale ($S-\log t$ curve).
ii) Choose several points on the curve and measure the slope (m), per cycle at each point. It may be more accurate if the chosen points comprise the latest portion of the original curve, or in other words when the time is large.
iii) Plot on the same semi-log paper the measured slopes (m) versus $\log t$.
iv) Select few points on the ($m-\log t$) curve and measure the slope (m') of the tangent at each point, per cycle.
v) Knowing (m) and (m') at each time, find the double slope function $f(u)$, using Equation (5) at each point, and find the corresponding value of (u).
vi) Using Equation (3) with known values of (u), (Q), (b) and (m), determine the value of K_r.
vii) Using the relationship ($u = r_r S/4K_r bt$), compute the value of S.
viii) Steps from v to vii, may be repeated for other values of (m'), at different values of time. However the computed values of (K_r) and (S), should be the same at each point. Any deviation is a result of improper measurements of (m) or (m').
ix) Choose any point on the ($s-\log t$) curve and record its coordinates.
x) Compute the value of (u) at that particular point and find its corresponding value of $W(u)$, from tables of the well function, Wenzel, (1937).
xi) Using Equation (11), the value of $K_0[(r/b)(K_z/K_r)^{1/2}]$, can be calculated. From which the value of (K_r/K_z), can be found, using the tables of the modified Bessel function $K_0(x)$.
xii) Knowing (K_r), determine the value of (K_z).

APPENDIX – NOTATION

b aquifer thickness (L).
d depth of penetration of the pumped well (L).
l depth of penetration of the observation well (L).
$K_0(x)$ the zero-order modified Bessel function of the second kind, tabulated, Watson (1944) or Dweight (1958).
K_r horizontal permeability radially from the well (L/T).
K_z vertical permeability (L^3T).
m slope of the tangent at any point on the drawdown-time curve ($s-\log t$) (L/cycle).
m' slope of the tangent at any point on the drawdonw-slope-time curve ($m-\log t$) (L/cycle).
Q constant well discharge (L^3/T).
r distance between the pumped and the observation wells (L).
s average drawdown in an observation well partially penetrating the aquifer (L).
S storage coefficient or storativity.
t time since pumping started (T).
u relation $r^2S/4K_rbt$.
$W(u) = \int_u^\infty (e^{-u}/u)\,dx$ = well function of (u), tabulated by Wenzel (1942).

REFERENCES

BATEMAN, N. (1954). Bateman Manuscript Project, McGraw-Hill Book Co., New York.

CHURCHILL, R.V. (1958). Operational Mathematics. McGraw-Hill Book.

DWIGHT, H.B. (1958) Mathematical Tables. Dover Publ. Inc., New York.

EDWIN, P.W. (1946). Field Methods for Determining vertical permeability and aquifer anisotropy. *U.S. Geol. Survey*, Paper 501-D.

HANTUSH, M.S. (1957). Nonsteady Flow to a well partially penetrating an infinite leaky aquifer, *Proc. Iraqi Sc. Soc.*, no. 1.

HANTUSH, M.S. (1961). Aquifer tests on partially penetrating wells. *Amer. Soc. Civil Eng.*, New York

HANTUSH, M.S. (1961). Drawdown around a partially penetrating well. *Amer. Soc. Civil Eng.*, New York

MUSKAT, M. (1937). Flow of Homogeneous Fluids Through Porous media. McGraw-Hill Book Co., New York.

SAAD, K.F. (1960). Nonsteady Flow Toward Wells which partially penetrate thick artesian aquifers. *Bull. Inst. Desert, Egypt*, t. VIII; no. 1 (1958).

SAAD, K.F. (1960). Analysis of data from pumping wells partially penetrating artesian aquifers. *Bull. Inst. Desert, Egypt*, t. VIII; no. 1, (1958).

SAAD, K.F., A. SHUKRY and A. BALIGH (1965) Double slope method for pumping test analysis. *Amer. Soc. Civil Eng.*,

THEIS, C.V. (1935). The Relation Between the Lowering of the Piezometric Surface and Duration of Discharge well using ground water storage. *Trans. Am. Geophysic Union.*

TOLMAN, C.F. (1937). Ground Water. McGraw-Hill Book Co., New York.

WATSON, G.N. (1944). Theory of Bessel Function. Macmillan Co., New York.

L'HYDRO
DANS LES

Laboratoire d'hyd

SOMMAIRE

Dans les dunes modernes du litto
Celle-ci enfonce ses racines dans la ro
période historique. Ils sont essentiell
sans parler un sol. Aucun horizon péd
sont inexistants. La porosité et la pe
et intense comme le montre l'étude

I. INTRODUCTION

A) *Objet de l'étude*

Dans les bas-fonds placés
relativement proche de la surface d
que dans d'autres zones non encaiss
La répartition de ces « lettes maigre
représente un réel danger pour l'e
les causes. Ceci nous a amené à ab

L'humidité su sol, ses réserves en
sur les racines, la transpiration du

B) *Généralités*

1. *Ensemble des mesures et expé*

L'étude a eu lieu le long du cord
du Porge à 10 km au Nord du B
hydrogéologique complète.

De nombreuses analyses chimiq
sable. Certaines d'entre elles porte

Des appareils enregistreurs Rich
phréatique et de la température du

La balance de torsion, de précis
l'étude de la transpiration du pin m

De nombreux forages et sondag

L'ensemble de ce travail a été effe
Les moyens mis en œuvre et le tem
d'aboutir à la précision la plus satis

2. *Conditions écologiques général*

Les dunes sont de formation trè
mise en place. Il y a eu triage mécani
La méthode de séparation par le bro
la profondeur, que le sable contien
essentiellement quartzeux.

Le climat est de type océanique

La température moyenne annuel
moyenne de 749 mm.

8.3.1.2.3.1.7

- Dudley, W.W., Jr., and D.T. Oakley, 1988. Agreement between NNWSI Technical Project Officer, Los Alamos National Laboratory, and NNWSI Technical Project Officer, United States Geological Survey, Regarding the Cooperative Conduct of Tracer Studies.

- Gelhar, L.W., 1982. "Analysis of Two-Well Tracer Tests with Pulse Input," RHO-BW-CR-131 P, Rockwell Hanford Operations, Basalt Waste Isolation Project, Richland, WA.

- Kelley, V.A., J.P. Pickens, M. Reeves, and R.L. Beauheim, 1987. "Double-Porosity Tracer-Test Analysis for Interpretation of the Fracture Characteristics of a Dolomite Formation," Solving Ground Water Problems with Models, proceedings of the National Water Well Association Conference, Feb. 10-12, 1987, Denver, CO.

- Polzer, W.L., and H.R. Fuentes, 1987, "The Use of a Heterogeneity-Based Isotherm to Interpret the Transport of Reactive Radionuclides in Volcanic Tuff Media," Los Alamos National Laboratory Report LA-UR-87-2901, Los Alamos, NM.

- Robertson, J.B., P.S. Huyskorn, T.D. Wadsworth, and J.E. Buckley, 1987. "Design and Analysis of Deep Two-Well Tracer Tests," Hydrogeologic, Inc., Herndon, VA.

- Robinson, B.A., 1987. "Predictive Modeling of in Situ Retardation of Reactive Tracers During C-Well Testing," Nevada Nuclear Waste Storage Investigations Milestone No. R487, Los Alamos National Laboratory.

8.3.1.2.3.1